

Magneto-structural characterization of polynuclear complexes with supramolecular architectures

DISSERTATION

zur Erlangung des akademischen Grades doctor rerum naturalium

(Dr. rer. nat.)

vorgelegt dem Rat der Chemisch-Geowissenschaftlichen Fakultät
der Friedrich-Schiller-Universität Jena

von M. Sc. Adrian Eugeniu Ion

geboren am 31.07.1977

in Răcari-Dâmbovița, Romania

Gutachter

1. Prof. Dr. W. Plass
2. Prof. Dr. M. Westerhausen

Tag der öffentlichen Verteidigung: 25. September 2006

”The most beautiful thing we can experience is the mysterious.
It is the source of all true art and science.” Albert Einstein

La steaua care a răsărit
E o cale atât de lungă
Că mii de ani i-au trebuit
Luminii să ne-ajungă.
Mihai Eminescu

In memory of an extraordinary Professor who has the merits of my achievements,

Prof. Dr. Ovidiu Maior

and also to an unforgettable advisor

Ms. Marcela Rovinaru.

Acknowledgements

I would like to thank my supervisor, Prof. Dr. Winfried Plass, for giving me the opportunity to work in this interesting field and for his advises during my research.

Special appreciation and "uncountable" thanks to my "future wife" (hopefully) Dr. Simona Nica for supporting me always and especially for fruitful scientific conversations, although sometimes annoying. My deepest appreciation and gratitude my dear Oltean.

Special gratitude to my undergraduate research supervisor Prof. Dr. Ovidiu Maior and my direct advisor at that time, Ms. Marcela Rovinaru (Bucharest University, Romania) to whom I also dedicate my thesis. Both were my primary educators and I am profoundly indebted for the training they, among others implemented into me.

My sincere gratitude and special thanks goes to a wonderful Professor, Marius Andruh. All my deepest appreciation and particular thanks for memorable time and discussions that we had here, in Jena.

Lots of thanks to Dr. Andrew Hall and Dr. Ioana Pera for nice friendship. Thank you for beers, wines and the nice time spent together, both in Germany and in Romania. See you know in UK.

I also thank to my colleagues for the nice atmosphere and nice parties where we had fun together. Special thanks to Eike T. Spielberg for theoretical calculations performed for my second chapter. Lots of thanks to my students, Stefany Hoenig and Nicole Herzer for fruitful work during their "Forschungspraktikum"

Lots of thanks to a special person, Dr. Helmar Görls for measuring my X-ray crystal structures and for his high sense of humor. And because he knows, I will like to thank him for nice "uberaschung"s that he brought to me all the time, except for the dates on Monday mornings. Thank you very much.

I would like to thank Crista Felbel who measured the SQUID for my samples and also for trying to understand my very bad German language. Many thanks also to EPR team for measurements.

The grants for research are vital and without money research does not exist. Therefore, I would like to thank to DFG who granted this programm.

Aș dori sa mulțumesc părinților mei pentru iubirea lor și sprijinul acordat pe parcursul perioadelor mele de studiu. De asemenea mii de multumiri surorii mele, Raluca. Domnilor "Baba si Butoi" le doresc sanatate maxima și le mulțumesc pentru dragostea lor.

Domnul *Director*, Marian Ionică și soția sa-Bety, se fac de asemenea responsabili pentru o lungă si frumoasă prietenie. Ca urmare este momentul sa le mulțumesc pentru acest lucru și să ne vedem cu bine in România.

Doamnei Elena Zamfirescu, profesoara mea de chimie din Liceul Teoretic-Titu, mulțumiri pentru "primii pași pe drumul" chimiei.

Nu, în ultimul rand, aș dori sa multumesc colegilor mei de la "Laboratorul de toxicologie" pentru "bunăvointa" lor de a ma "integra" in grup.

Outline of the thesis

Coordination chemistry constitute a common ground for molecular magnetism and bioinspired chemistry. The topic of *molecular magnetism* and supramolecular assemblies are the focus of this thesis. Summarily, the thesis describes the supramolecular organization of homo- and heteropolynuclear complexes, containing different paramagnetic centers, going from d-block metal ions to combination of d-f spin carriers topologies. These polynuclear complexes have been structurally and spectroscopically characterized, and partly magnetostructural correlations have been performed.

The work is divided into seven chapters. The first chapter comprises a brief introduction into phenomenon of magnetism and contains relevant example of molecular magnetic compounds that have been described in last decades.

The second chapter is concerned with the synthesis, characterization and magnetostructural studies of antiferromagnetically coupled aza-metallacrown compounds with iron(III) ions as constituting metal centers. It has to be mentioned here that metallacrown, as a general class of coordination compounds, are the inorganic analogs of organic crown- and aza-crown ethers. Trinuclear and tetranuclear Fe(III) complexes have been isolated *via* self-assembly reaction between N-imidazol-2-yl-salicyloyl hydrazide and $\text{FeX}_3 \cdot x\text{H}_2\text{O}$ salts. The topology of the resulting complexes is based on iron-diazine bridged metal centers, with each Fe(III) ion in distorted octahedral environment. Each ligand molecule acts as bis-nucleating pentadentate system, accommodating two different iron ions. The coordination sphere of the metal ion is completed by halide and pseudo-halides (azide, thiocyanate), respectively which act as monodentate anionic ligands. The interesting feature of the chapter is the self-organization of the trinuclear Fe(III) complex which contains the thiocyanate anion ligand. This complex is re-assembled in basic media to a tetranuclear [2+2]-grid Fe(III) compound. All iron(III) complexes showed an antiferromagnetic coupling interaction for which the magnitude is strongly dependent upon torsion metal-bridging units.

The third chapter presents homonuclear Ni(II) and Co(III) complexes constructed using three-fold tridentate tris(2-hydroxybenzylidene)triaminoguanidine derivatives ligands. The influence of used co-ligands in the resulting self-organization of the oligomeric

d-metal complexes will be also presented. Although the strategy upon which these complexes were synthesized is a rational one, the serendipity plays also a key-role in the organization of the molecules. Firstly, the trinuclear Ni(II) complexes are re-organizing in presence of an outer metal ions to form pentanuclear Ni(II) complexes, independently of the used co-ligand moieties. The magnetism of this series of homonuclear Ni(II) complexes is characterized by antiferromagnetic exchange interaction between the constituting nickel(II) ions with different ground spin state of the Ni₃^{II}-core. The supramolecular arrangement in the solid state is dominated by π - π -stacking and hydrogen bonding interaction with the highlight of a honeycomb architecture which contains void-channels formed along the a crystallographic axis. In addition, a trinuclear Co(III)-complex formed through "in situ" oxidation of the starting Co(II) salt will be also described.

In the fourth chapter serendipity plays the key-role in the isolation of oxygen-bridged homonuclear Fe(III) and Cu(II) complexes. Dinuclear Fe(III)-complexes with oxo- and alkoxy-bridge have been structurally and spectroscopically characterized. Although the oligomeric units are based on simple dinuclear iron(III)-entities, one-dimensional polymers formed *via* hydrogen bonding interaction have been observed. These complexes are characterized by strong antiferromagnetic interaction transmitted by the oxygen-containing bridges. The last part of the chapter is focused on self-assembly formed dinuclear and trinuclear Cu(II) complexes with [2-(2-dimethylamino-ethylimino)-methyl]-phenol ligands. While the trinuclear Cu(II)-complex contains a partial cubane-like Cu₃O₄-core formed by phenoxy and hydroxy-bridges, the dinuclear Cu(II) complex formed with methoxy-derivative of the [2-(2-dimethylamino-ethylimino)-methyl]-phenol ligand comprises only one Cu–O(Ph)–Cu bridge. These structural arrangements are vital for the magnetic properties which vary from ferromagnetic coupled copper(II) centers in trinuclear complex to weak antiferromagnetic coupled copper spins in the dinuclear complex.

The fifth and the sixth chapters discuss the building up of heteropolynuclear complexes based on "complex-as-ligand" strategy. In chapter five trinuclear copper(II)-cobalt(II) complex with oxamate-derivative bridging and supporting ligand will be presented. Oxamide and oxamate-based ligands function as good transmitters of the magnetic interaction due to a good overlap of the magnetic orbitals of the spin carriers mediated by these bridging units.

The sixth chapter is based on heteronuclear copper-lanthanide topology and is divided into two subchapters. The first one comprises rare examples of one-dimensional Cu(II)-Ln(III) complexes based on compartmental salen-type ligands and pyrazine-2,3-dicarboxylic acid bridges. The supramolecular architecture is represented by zigzag alternating [Cu-Ln]-tectons, resulting in formation of coordination polymers. The magnetic interaction is determined by the constituting lanthanide ions and vary from antiferromagnetic one-dimensional chains for praseodymium to europium containing coordination polymers. For the other lanthanide-ion containing one-dimensional chains, the magnetism is dominated by ferromagnetic interaction. The interpretation of the magnetic properties of copper-gadolinium chain showed that the pyrazine 2,3-dicarboxylic bridge does not transmit very well the magnetic interaction along the 1-D polymeric structure. The second subchapter describes the synthesis and structural characterization of trinuclear copper-lanthanide complexes based on the same salen-like supporting ligand and salicylic acid bridge. The high spin trinuclear [Cu₂Gd]-complex showed a ferromagnetic interaction with a spin ground state $S = 9/2$. For all the other lanthanide-containing complexes, an antiferromagnetic interaction is to be expected.

Contents

1	Introduction	9
1.1	Brief history of magnetism	9
1.2	Basic theoretical background of magnetism	14
1.3	State of art	19
2	Novel tri- and tetranuclear iron azacrown clusters	23
2.1	Synthesis and spectroscopic characterization	25
2.2	Structural studies	29
2.3	Magnetic properties	45
2.4	Ni(II)-complexes with N-imidazol-2-yl-salicyloyl hydrazide ligand	50
2.5	Conclusions and future perspectives	52
2.6	Experimental Part	55
3	Triaminoguanidine derivatives as supports to construct magnetic assemblies	59
3.1	Trinuclear Ni(II)-complexes based on "triaminoguanidine"-ligand and 2,2'-bipyridine coligand	63
3.2	Pentanuclear Ni(II)-complex based on "triaminoguanidine"-ligand and 2,2'-bipyridine coligands	76
3.3	Trinuclear Ni(II)-complex based on "triaminoguanidine"-ligands and 2,4,6-tris(2-pyridyl)-1,3,5-triazine coligands	82
3.3.1	Trinuclear Ni(II)-complexes formed with tptz coligand and tris(5-bromo-2-hydroxy-salicylidene)triaminoguanidine ligand	83

3.4	Pentanuclear Ni(II)-complexes formed with tptz coligand and tris(5-bromo-2-hydroxy-salicylidene)triaminoguanidine ligand	89
3.5	Trinuclear Ni(II)-complexes based on tris(3-methoxy-2-hydroxy-salicylidene)-triaminoguanidine ligand and tptz coligands	96
3.6	Conclusions	107
3.7	Trinuclear Co(III)-complexes with tris(3-methoxy-2-hydroxy-salicylidene)-triaminoguanidine ligand	108
3.8	Future perspectives	111
3.9	Experimental Part	113
4	Polynuclear oxo-bridged d-metal complexes	118
4.1	Dinuclear oxo-bridged Fe(III)-complex with N,N'-ethylene-bis(pyridoxylidene-iminato) ligand	120
4.1.1	Magnetic properties of homodinuclear μ_2 -oxo bridged Fe(III) complex	123
4.2	Dinuclear oxygen-bridged Fe(III)-complex with N-salicylidene-2-bis(2-hydroxy-ethyl)amino)ethylamine ligand	125
4.2.1	Magnetic properties	130
4.3	Trinuclear copper complex with partial cubane-like core	133
4.3.1	Magnetic properties	136
4.4	Dinuclear phenoxo-bridged copper complex	138
4.4.1	Magnetic properties	141
4.5	Conclusions	142
4.6	Experimental Part	144
5	Polynuclear oxamate-bridged d-metal complexes	146
5.1	Mononuclear Cu(II)-complex based on oxamate-derivative ligand	148
5.2	Oxamate-bridged trinuclear [Cu ₂ Co]-complex	152
5.2.1	Magnetic properties	155
5.3	Conclusions and future perspectives	157
5.4	Experimental Part	160

6	Novel heterometallic 3d-4f complexes	163
6.1	1-D chains based on copper-lanthanide topology	174
6.1.1	Magnetic properties of the Cu ^{II} -Ln ^{III} 1-D chains	187
6.2	Trinuclear Cu ₂ ^{II} -Ln ^{III} complexes	200
6.2.1	Magnetic properties of [Cu ₂ ^{II} -Ln ^{III}] trinuclear complexes	211
6.3	Conclusions and future perspectives	218
6.4	Experimental Part	232
7	Conclusions	238

Chapter 1

Introduction

1.1 Brief history of magnetism

Magnets play an important role in our daily lives and are to be found in a large number of electronic devices that are surrounding us, ongoing from telephone, loudspeakers, microphones or video to data storage devices, motors, generators, medical devices, magnetic separators and the list can go on and on.¹

The phenomenon of magnetism dates from ancient times and has been firstly discovered by Greeks and later used by Chinese to create the "south pointing" compass. Initially, the attractive power of lodestone which is rich in magnetite (an iron rich oxide mineral) led to a plethora of myths on going from the soul possession of the stone to the "bone" of Haroeri (the grand sone of the goddess of the earth) in the ancient Egyptian belief.² Since these early times however, advances and understanding of the magnetism phenomenon has been greatly influenced by many peoples over many years. It was firstly Petrus de Maricourt in twelve century who identified that magnets have two poles labeled by him as north and south. He also observed that breaking a magnet leads not to its destruction but, to two magnets. Years later, in sixteen century, Dr. William Gilbert devoted a huge scientific activity to stop the growing trove of myths and superstitions regarding the magnetism phenomenon. He made an unprecedented revelation by deducing that the earth itself is a magnet and he prepared the first man-made magnet based on iron metal.³

Ulterior advances and understanding into the phenomenon of magnetism have been influenced by pivotal contributions from M. Faraday, A. M. Ampere and H. C. Øersted who established the connectivity between electricity and magnetism whereas, later Maxwell made the connection among the two phenomena and predicted the electromagnetic waves.⁴

With Maxwell's equations, classical electromagnetism was complete, but the ferromagnetism remained still a mystery. The question "why an iron bar does not melt when high amperian currents pass through" persisted until 1907 when the French physicist P. Weiss developed the theory of ferromagnetism based on the assumption that the interaction between magnetic molecules could be described empirically considering an internal molecular field. This new discovery was still elusive and the fundamental aspects of magnetism were to be understood only by quantum mechanics which explains that the key role of magnetic behavior is the electron spin.⁴ The number, vicinity and coupling among spins dictate the overall magnetic behavior. The magnetic susceptibility of isolated spins obeys the Curie law (page 16). When spins are brought together, they frequently oppose each other with the resulting magnetic susceptibility lower than the sum of the independent spins, phenomenon known as antiferromagnetic coupling. Instead, when the alignment of the spins enhance the value of magnetic susceptibility, the coupling is ferromagnetic.^{1,5}

Traditional magnetic materials are prepared at very high temperatures using metallurgical methodologies. These materials are atom-based magnets which means that their active spins are located on the atomic orbitals of the constituting metal ions.⁶ These classical magnets are two- or three-dimensional arrays of inorganic atoms, composed of transition metals and/or lanthanide metal containing spin units.^{6,7} Modern alloys comprising Sm-Co (SmCo_5), Nd-Fe-B and Sm-Fe-nitride are commercially available and used especially in applications where miniaturization is an important design criteria. The disadvantage of these magnets is represented by their high cost.

Therefore, the research to develop new magnetic materials has been known a raising interest. This has led to a new field of research called molecular magnetism of which purpose is to design molecular based magnets with bulk magnetism. In this phenomenon, the spins in a solid, align in the same direction to result a net magnetic moment.⁸ This

class of magnetic materials can no longer be synthesized in metallurgical manner because the molecular magnets comprise purely organic and organic/inorganic hybrid materials for which high temperature conditions usually inhibit their formation.⁸ In addition, the field of molecular magnetism is an interdisciplinary area of research with chemists and physicists collaborating closely with the stated goal to design, synthesize and characterize the magnetic properties of molecular based materials. Conversely to classical magnets, the molecular based magnets exhibit different Curie temperature T_c (temperature above which a magnetic material loses its magnetic properties in a ferromagnetic materials) and in addition, a better control over its magnetic characteristics due to a easily processed strategy.⁷ Moreover, a combination of magnetic properties with mechanical, electrical and/or optical properties will allow synthesis of multi-functional materials. In order to design materials with interesting bulk magnetic properties is necessary to understand how such a magnetism arises in samples. A complete understanding of this phenomenon has not yet been formulated, however new phenomena associated with these mesoscopic systems have been developed and comprise: macroscopic quantum tunneling, quantum hysteresis, magnetoresistance and magnetocaloric effects to name a few.⁹

A plethora of molecular magnetic materials have been reported for which interesting magnetic properties have been found.¹⁰ One of the exciting aspect of molecular magnetism was represented by pure organic compounds capable of possessing magnetic properties in addition to their specific organic reactivity.¹¹⁻¹³ The most representative examples of organic compounds that posses strong magnetic interaction are the radical class from which the nitronyl-nitroxide and dithiadiazolyl radicals have been extensively studied (Figure 1.1). The nitroxide derivatives are a group of molecules which contains NO-functionality with unpaired electrons in π^* orbital.¹⁴ This is stabilized by presence of bulky groups which do not allow the molecules to interact in order to dimerise. Its phenyl-derivatives have been also synthesized and it has been reported to order as weak bulk ferromagnet at relatively low T_c values. The dithiadiazolyl radical has also exhibited ferromagnetic interaction with T_c value of 36 K.¹³ An exciting feature of the organic radical compounds comes from their association with transition metals and/or rare earth ions. Single chain magnets have been isolated combining phenyl-nitroxide radical derivatives with hexafluoroacetylacetonate salts of anisotropic metal ions, i.e Co^{2+}

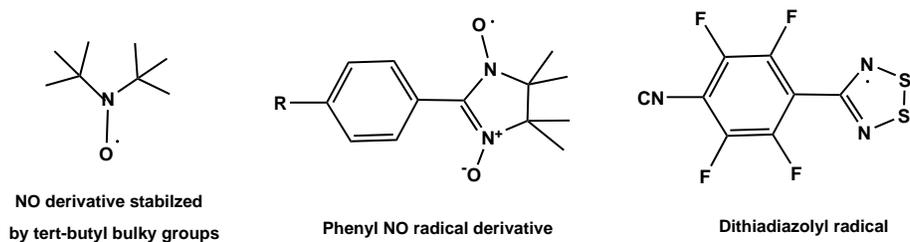
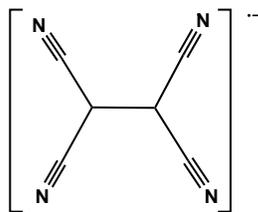


Figure 1.1: Selected organic radical molecules which exhibit ferromagnetic interaction.

and Dy^{3+} ion.^{15,16} Single chain magnets (SCM) exhibit bulk ferromagnetic interaction of one-dimensional coordination polymers.

Another representative example for this class of molecular magnetic materials based on mixed organic radical-transition metal ions is the ferromagnet reported by Miller *et al* using tetracyanoethylene (TCNE) radical.¹⁷ This new radical ion possesses four nitrogen atoms which can bind to various metal ions forming extended networks. The metallocene-radical complex of type $[\text{Fe}(\text{C}_5\text{Me}_5)_2][\text{TCNE}]$ ordered in 3-D arrangement with a T_c value of 4.8 K, whereas the vanadium-[TCNE] complex showed a $T_c = 400$ K.^{6,17,18}

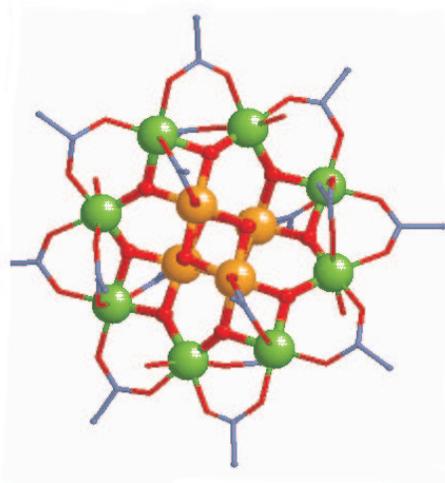


tetracyanoethylene radical

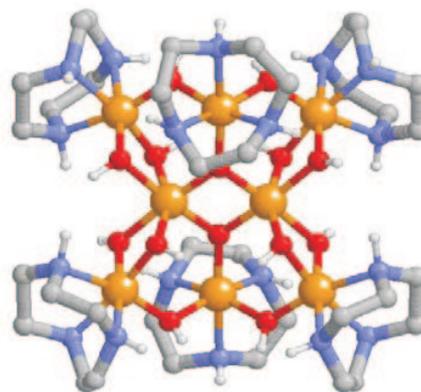
Another category of molecular magnetic materials that should be briefly introduced is based upon Prussian Blue analogs compounds.¹⁹ The Prussian blue compound is a pure inorganic mixed valence $\text{Fe}^{III}/\text{Fe}^{II}$ cyanide salt of type $\text{Fe}_4^{III}[\text{Fe}^{II}(\text{CN})_6]_3 \cdot 15\text{H}_2\text{O}$ with long range ferromagnetic ordering at $T_c = 5.6$ K.^{20,21} Other similar d-transition metal cyanide complexes have isolated and magnetically investigated. Depending on the used metal ion, their magnetic behavior varies from three dimensional ferromagnets or antiferromagnets to ferrimagnetic behavior.²¹ These pure inorganic compounds are more similar to classical magnets due to variations in properties achieved by incorporating different metal ions, rather than modification of the organic ligands as usually happens

in molecular magnetic materials. Nonetheless, the Prussian blue family are considered molecular due to their synthesis methodology which assembles the molecular chemistry, rather than solid-state chemistry. In addition, the cyanide ligands may function as bridges between d-complex entities resulting in one-dimensional single chain magnets as previously mentioned for the organic radical-metal complexes compounds.²²

The molecular magnetism has been fueled by the discovery of single molecule magnet (SMM) discovered firstly in 1993 by Sessoli *et al.*^{23,24} This inorganic cluster, synthesized firstly in Poland by Lis²⁵ and extensively studied in the early 1990s. The molecular structure contains oxo-bridged Mn(III) and Mn(IV) centers wrapped around by acetate ligands and this is abbreviated as Mn₁₂Ac. This inorganic cluster served as classical framework to understand the quantum properties of magnets, especially the quantum tunneling of the magnetization.⁹ The bulk magnetic property is truly due the individual molecule and not to long range interactions. Since these molecules are bistable, in the sense that they can be magnetized in two directions, application in data storage devices of Mn₁₂Ac was proposed.⁹ Every molecule can be considered as a bit of data with the bulk of this material capable of information density calculated to be three to four times higher than what is currently possible.²⁶ Another representative example of single molecule magnet is represented by Fe₈-inorganic cluster (shown below) which also showed slow relaxation of magnetization and hysteresis loop, two characteristic properties for a material to function as small magnet.^{26,27}



Mn₁₂Ac single molecule magnet



Fe₈ single molecule magnet

1.2 Basic theoretical background of magnetism

The magnetism behavior of the molecular magnetic material is described from two points of view: the magnetic characteristics on the atomic or ion level and as cooperative magnetism phenomenon. On the atomic or ion level there exist two fundamental types of magnetism: diamagnetism and paramagnetism.^{5,10}

A *diamagnetic behavior* of ions or atoms appears when molecular or atomic orbitals contain paired electrons and the substance is repulsed out of an applied magnetic field. With the exception of hydrogen radical, all atomic or molecular materials exhibit some diamagnetic behavior. This observed effect is temperature independent and the strength of the interaction is roughly proportional to the molecular weight of the material.

Conversely, *paramagnetism* is characterized by attraction of a substance into an applied magnetic field and this behavior arises from interaction between the magnetic field and unpaired electrons in atomic or molecular orbitals. Typically, paramagnetic species contain one or more unpaired electrons, and the strength of paramagnetism is temperature dependent. However, some substances also exhibit temperature independent paramagnetism (TIP) that arises from coupling between the magnetic ground-state and non-thermally populated excited states.

Bulk magnetic behavior of the molecular magnetic materials is characterized by cooperative magnetism. This arises from magnetic interactions between paramagnetic atoms or molecules and can lead to magnetic or non-magnetic materials depending on how adjacent magnetic spins align with each other. The magnetic interactions occur in three dimensions and the type and strength of these interaction can be defined for each dimension. In cases where different magnetic interactions are observed due to dimensionality, the material is characterized by the strongest one. Bulk magnetic behavior of a material can be described by four major classes of magnetism: paramagnetism, antiferromagnetism, ferromagnetism and ferrimagnetism. These magnetic behavior is determined by the interaction pathway of adjacent magnetic moments at absolute zero.

If no alignment of adjacent magnetic moments occur at zero absolute, the material is called *paramagnet* (Figure 1.2, pictogramm a). This phenomenon appears when individual electron spin is unaffected by its neighbors and the spins of the material are

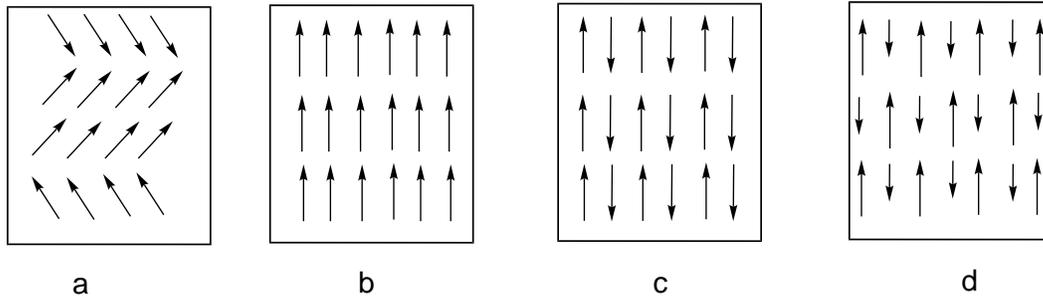


Figure 1.2: The alignment of the magnetic moments at absolute zero. No alignment of the adjacent magnetic moments in paramagnets (a). Ferromagnets (b) exhibit a parallel alignment of the adjacent magnetic moments. Antiferromagnets show an antiparallel orientation of the adjacent magnetic moments (c). The d pictogramm shows the antiparallel orientation of adjacent magnetic moments of different strength in ferrimagnets.

easily aligned by an applied magnetic field. However, the alignment is very weak and vanishes upon removal of the magnetic field when the system relaxes back to a random distribution of magnetic moments.

Ferromagnetism is a result of parallel ordering of adjacent magnetic spins that yields large net magnetic moment (Figure 1.2, pictogramm b). This alignment of the magnetic spins is more rare and unlike paramagnets, ferromagnets exhibit a net magnetic moment in the absence of an applied magnetic field.

Antiferromagnetism is a consequence of antiparallel alignment of magnetic spins resulting in no net magnetic moment (Figure 1.2, pictogramm c). At absolute zero, antiferromagnets exhibit a diamagnetic response to an applied magnetic field. This magnetic behavior is most commonly observed bulk magnetism and long-range antiferromagnetism is even exhibited by materials that order local ferromagnetically.

Ferrimagnetism is a special case of antiferromagnetic behavior where the material consists of lattice of rigidly alternating spins of different magnitude. The adjacent magnetic spins align parallel as in antiferromagnetism, but because of different magnitudes, the resulting material possess a net magnetic moment in the absence of the applied magnetic field (Figure 1.2, pictogramm d). This magnetic behavior appears in [Mn–Cu], [Co–Cu] systems.^{28,29}

Magnetic interactions are typically characterized by their responses to variations in temperature and applied magnetic field. Each of these classes of magnetism, described above, has a characteristic response to temperature and applied magnetic field used to determine the type and strength of the magnetic interaction in a molecular material. The temperature dependence magnetic behavior of a molecular magnetic material is described by Curie law, whereas the field dependence of the magnetism is described by Brillouin function.

The Curie law describes the temperature dependence of the magnetic susceptibility for an ideal paramagnet.

$$\chi_M = \frac{N\mu_\beta^2 g^2}{3kT} S(S+1)$$

where χ_M is molar magnetic susceptibility, N is Avogadro's number, g- the Landé factor, μ_β is the Bohr magneton and k is the Boltzman constant. The magnetic susceptibility is defined as the quantitative measure of the response of a material to an applied magnetic field.

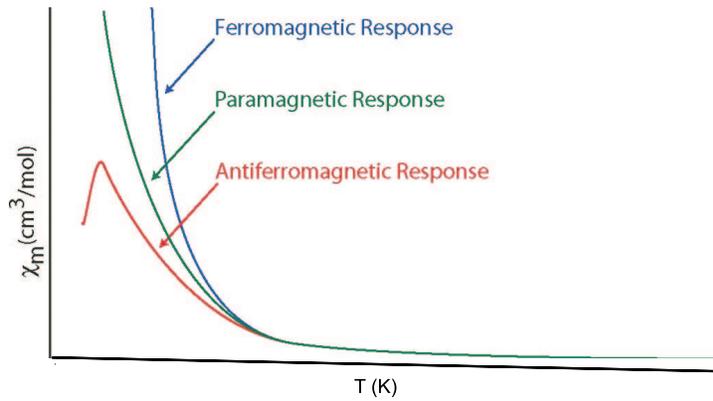
This equation can be reduced to:

$$\chi_M = \frac{C}{T - \theta}$$

called Curie-Weiss law, where C is the Currie constant and θ the Weiss constant. A positive sign of the θ value is characteristic for ferromagnetic coupling of the magnetic spins, whereas the negative sign describes an atiferromagnetic alignment of the magnetic spins.

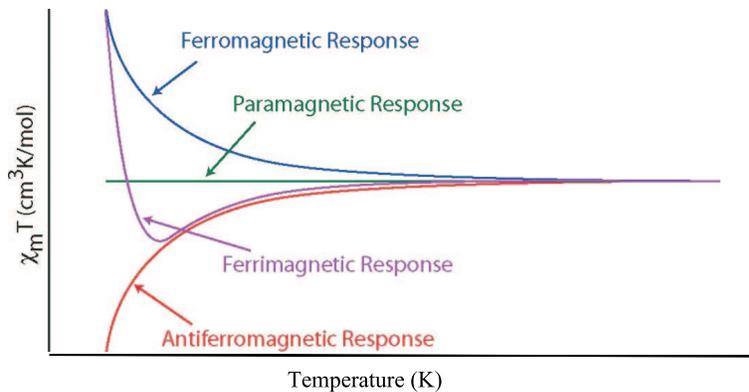
All magnetic materials behave as paramagnets at high temperature, because the thermal energy over comes the alignment of the spins. Typically the magnetic behavior of magnetic materials is carried out by examining the temperature dependence of susceptibility, the susceptibility temperature product and thermal dependence of inverse susceptibility. Each of these analysis provide slightly different information about the bulk magnetism of the material.

From the plots of thermal variation of magnetic susceptibility is in general difficult to determine the type of magnetic interaction. The most useful information can be obtained for antiferromagnetic materials which exhibit a maximum at low temperature.



The higher the temperature value at which the maximum is observed, the stronger the antiferromagnetic interaction. The shape of the maximum suggests the dimensionality of interactions, with one and two dimensional antiferromagnets marked by a rounded maximum, while a sharp maximum appears for three dimensional antiferromagnetism.

The most informative plot is the thermal variation of the temperature-magnetic susceptibility product. For a true paramagnetic material, the response is a straight line, whereas variations of the $\chi_M T$ values in the low temperature range differ from antiferromagnets to ferromagnets to ferrimagnets. At high temperatures, the $\chi_M T$ product vary little or remains unvaried due to the effective paramagnetic behavior of magnetic materials. On lowering the temperature, ferromagnetic materials display an upward deviation from the curve for an ideal paramagnet, whereas the antiferromagnetic interactions display downward curvature with decreasing temperature values. For ferrimagnetic materials, the $\chi_M T$ vs T curve present a slight downward curvature and then increases in the low temperature range.



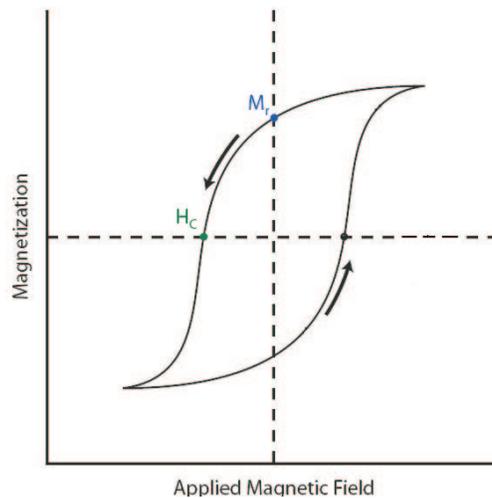
The Brillouin function describes the magnetization of a magnetic material at certain temperature. In practice it is used to determine the spin ground state of molecular magnets by varying applied magnetic field at constant temperature. The function has the following form:

$$M = Ng\mu_{\beta}SB_S(y)$$

$$B_S(y) = \frac{2S+1}{2S} \coth\left(\frac{2S+1}{2S}y\right) - \frac{1}{2S} \coth\left(\frac{1}{2S}y\right)$$

$$y = \frac{g\mu_{\beta}SH}{kT}$$

One of the most distinctive feature of materials with bulk magnetism is represented by hysteresis. This effect is observed for ferromagnetic and ferrimagnetic materials below their critical temperature and, is determined by magnetization measurements as function of an applied field. This behavior is defined by two distinctive points: remnant magnetization (M_r) and coercive field (H_c). Remnant magnetization is obtained by applying and removing large magnetic field and represents the extent to which a bulk magnetic material exhibits spontaneous magnetism. The coercive field is the magnetic field required to bring the magnetization of a sample to zero. Materials with low coercive fields ($< 1\text{G}$) are called "soft" magnets, while materials with high coercive fields ($> 500\text{G}$) are termed "hard" magnets.^{5,10}



1.3 State of art

The design of novel magnetic materials is a focusing area of research. While the ferro- and ferrimagnets may be useful materials for device design, the antiferromagnetic interaction observed in molecular magnetic material has also its apport in understanding the physical background of magnetism. Two main approaches have been involved in the attempts to isolate organic-inorganic hybrid materials. This are based on "self-assembly" process and rational design based on "complex as ligand" strategy. Both approaches led to interesting magnetic materials. Self-assembly is the most efficient approach in supramolecular chemistry and paved the field of crystal engineering which is interrelated to material science. Even though the oligomeric units are isolated following a rational strategy, their organization in solid state is hard to be predicted. Crown ethers and the corresponding aza-crown ethers are a class of organic compounds important in molecular recognition. The combination between the two types of organic compounds, namely cryptates play an important role in ion transport through membranes. The inorganic analogous class of crown ether have been reported as recognition agents, with 15-metallacrown-5 copper and nickel derivatives encapsulating lanthanide ions.³⁰ While the metallacrown compounds have been extensively studied, the corresponding aza-crown metal complexes have received less attention. Hence, the second chapter of the thesis will be focused on magneto-structural characterization of Fe(III)-complexes formed by self-assembly process between Schiff base N-imidazolyl-salicyloyl hydrazide ligand and iron(III) salts. The polydentate nature of the ligand system allowed development of rare examples of 12-azacrown-iron compounds and in addition a first example of trinuclear iron complexes in which the presence of μ_3 -bridged mode of oxygen atom³¹ is not present. The influence of the surroundings of the iron center towards magnetic interaction in the resulting complexes was also investigated. Self-assembly approach to design novel magnetic materials have been reported by Thompson *et al.*³² for hydrazide-based ligands and the resulting magnetic interaction is dictated by the torsion metal-diazine-bridging angles, varying from ferromagnetic to antiferromagnetic behavior. An eloquent example of self-assembled isolated complex will be described in Chapter 4 and comprises a ferromagnetic homonuclear Cu(II) complex with partial-cubane core. Cubane-like structural core in inorganic-organic

hybrids is a peculiar case of accidental orthogonality occurring as a consequence of 90° orientation of the magnetic orbitals. The strict orthogonality orientation of the magnetic orbitals has been reported only for V^{IV} - Cu^{II} , Ni^{II} - Cr^{III} and Fe^{III} - Cu^{II} couple systems, whereas the number of accidental orthogonality comprises other d-transition metal ions as well.¹⁰

Nevertheless, the most challenging area of research comprises the isolation of pre-defined coordination compounds. Hence, three-fold tridentate triaminoguanidine-based Schiff base ligands have been employed as organic-support to isolate Ni(II) complexes. From the magnetochemistry point of view, this polydentate system with C_3 symmetry is versatile because it may yield trinuclear metal-complexes with a resulting non-zero spin ground state when capping ligand are employed to complete the coordination sphere of the metal ions.³³⁻⁴⁰ The judicious selection of capping ligand systems may give the opportunity to obtain interesting supramolecular assemblies by self-organization of trinuclear complex unit in solid state through non-covalent interactions. Hence, 2,2'-bipyridine (bipy) and 2,4,6-tris(2-pyridyl)-1,3,5-triazine (tptz) have been employed as co-ligands in order to avoid the uncontrolled polymerization of polynuclear complexes. The triangular antiferromagnetically ordered magnetic spins play a key-role in molecular magnetism owing to their capacity to show magnetic frustration mechanism. In a triangular arrangement of the spins, it is impossible to obtain an antiparallel alignment of spins, such that all of them will interact antiferromagnetically. This has been termed as spin frustration^{10,41} since if two spins are align antiparallel, the third spin cannot be aligned antiferromagnetically with both of the spins (Figure 1.3).

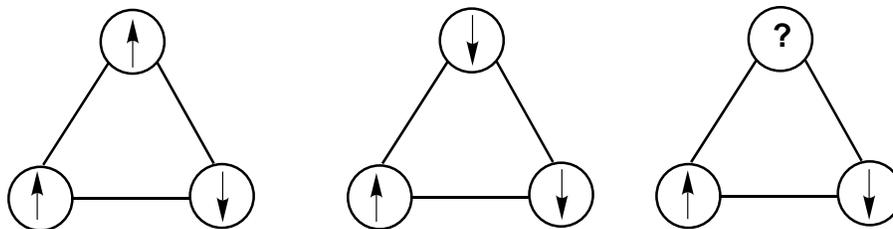


Figure 1.3: Illustration of spin frustration mechanism.

The synthetic organization of paramagnetic centers into close-spaced arrays with strong magnetic interaction mediated by the chosen bridges is still a challenge for inor-

ganic chemists. Cyanide has been proved to be useful in this regard and orthogonality connected metal orbitals and long range ferromagnetic ordering was achieved. The optimal close organization of paramagnetic centers within extended bridged structures with very short metal-metal contact has been achieved with single atom bridging unit, i.e. oxygen-based bridges. An extended organic bridge that offers a good overlap of the magnetic orbitals is based on oxalic acid and its oxamide and oxamate-derivatives. Oxalate-bridged dinuclear copper(II) complex has been found to be strongly antiferromagnetically coupled of order of magnitude of $J = - 384.5 \text{ cm}^{-1}$, although the paramagnetic centers are relatively well-separated metal by a distance of 514 pm.¹⁰ The disadvantage of the oxalate dianion is represented by uncontrolled polymerization effects, hence oxamide and oxamate-derivatives are more adequate bridging units. The strong electron donating capability of the nitrogen amide in the above mentioned derivatives, accounts for greater stability of the resulting metal complexes when compared with oxalate. Moreover, the lower electronegativity of the nitrogen atoms in oxamide and oxamate dianions allows a stronger magnetic interaction in polynuclear complexes and the polynuclear complexes are suitable candidates for designing molecular ferrimagnets. Based on these consideration, a novel mononuclear Cu(II) anion complex has been involved as molecular brick to isolate heterotrimeric [Cu₂Co]-complex. The high anisotropic metal ions are desirable paramagnetic centers in design of new ferromagnetic materials. Besides the strict orthogonality that conduct to a ferromagnetic coupling of the paramagnetic centers in a magnetic material, another example of ferromagnet is represented by Cu^{II}-Gd^{III} couple. Although the number of oligo-heterodinuclear d- transition metal-gadolinium complexes have been reported, the number of polymeric architecture with d-f topology is rather scarce. One-dimensional polymers which may function as single chain magnets are highly desirable since they can have possible applications such as nanowires. A rational approach, based on "complex as ligand" strategy will be described in Chapter 6. Starting from compartmental salen-type organic ligands, one dimensional [Cu(OMesalen)Ln(NO₃)(Pyr(COO)₂)]_n·(DMF)_n compounds will be described. The anisotropic lanthanide ions, i.e dysprosium and terbium containing compounds have been described to posses interesting magnetic behavior with lanthanide-containing complexes reported as magnet-like behavior.

Evaluation of the magnetic behavior of complexes described herein has been performed for isotropic exchange interaction based on the corresponding spin-Hamiltonian, generally represented as:

$$\hat{H} = - \sum J_{ij} S_i S_j$$

where the sum represents the over all pairwise interactions of intensity J_{ij} between S_i and S_j spins of molecules. This model of the isotropic interactions between the spins carriers is based on concept of magnetic orbitals and overlaps densities between pairs of such orbitals and allows the analyze of the spin coupling. In molecular magnetism, the magnetic behavior concerns not only the local spins associated with metal ions, but also the molecular spins associated with open-shell molecular units as a whole. The mathematical methods for calculating the magnetic susceptibilities in polynuclear complexes is based upon vector coupling method formulated by Kambe.⁴²

Chapter 2

Novel tri- and tetranuclear iron azacrown clusters

The concept of supramolecular architectures being self-assembled from simple components that are carefully designed, has been attracted considerable attention becoming a challenging area of research.⁴³⁻⁴⁵ Self-assembly reactions between transition-metal salts and polydentate ligands have lead to a large variety of interesting assemblies that include helicates,⁴⁶ cage,^{47,48} ladders,^{49,50} rocks⁵¹ and grids.^{50,52} The versatility of this process has also been supported by the interesting properties and wide range of applications of the resulting metal-based assemblies, including magnetic,^{53,54} electronic⁵⁵ and optical⁵⁶ features. Among other compounds, metallamacrocycles have been received a special attention due to the fact that this class of molecular materials is relevant to a variety of modern chemistry including catalysis,⁵⁷ sensors,⁵⁸ molecular recognition^{59,60} and chiral buildings blocks for one, two, and tree-dimensional solids.⁶¹⁻⁶³ Examples of metallamacrocycles include metallacrowns,^{30,64,65} molecular squares,⁶⁶⁻⁶⁸ metallahelicates,^{69,70} metal-lacryptates and metallacryptands⁷¹⁻⁷⁴ as well as metalacalixarenes.^{75,76} Metallacrowns (MC) exhibit a cyclic structure analog to crown ethers with transition metal ions and nitrogen atoms replacing the methylene carbon of the corresponding organic structure (Figure 2.1). The resulting assemblies contain $-[M-N-O]-n$ repeating units and there are in general constructed by using ketonoximic acids⁷⁷⁻⁷⁹ and/or hydroxamic acid, such as salicylhydroxamic acid (H_3shi)^{65,80-83} and β -alanine hydroxamic acid.⁸⁴

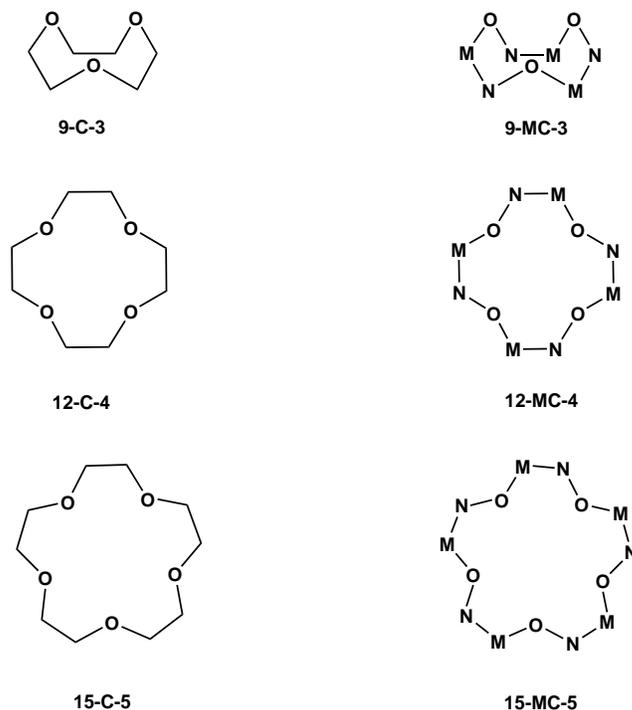


Figure 2.1: Schematic representation of the analogy between organic crown-ether (C) topologies and corresponding metallacrown (MC) inorganic compounds taken from reference.³⁰

One advantage of the metallacrown structural topology is in general represented by the fact that many metal centers are placed in close proximity and they can be exploited for a variety of applications. Metallacrown compounds are an example of molecular class which exhibits selective recognitions of cations^{80,85} and anions^{86,87} and in addition they can display interesting magnetic properties.⁸⁸ Azametallacrowns are a particular case of metallacrown compounds with the main differences staid by the repeating units in which the oxygen atom has been replaced by nitrogen atom, resulting in $-[M-N-N]-n$ repeating fragments. The most frequently occurring structural motif of the azametallacrown derivatives is represented by hydrazide-based supporting ligands.⁸⁹⁻⁹² The chelation capacity of a broad range of hydrazide based ligands has lead to interesting supramolecular assemblies^{93,94} including metal helicates structures,⁹⁵ pin-wheel clusters⁹⁶ as well as extended one- and two-dimensional metal complexes.⁹⁷ Azametallacrown compounds based on hydrazide topology comprise in general an even number of metal ions and it starts

from six and range up to twelve metal ions.^{89–92,98–101} This shows that a direct prediction of the resulting polynuclear structure is still an opened challenge. Nonetheless, the knowledge about trinuclear iron-azacrown compounds is rather scarce and the existing reports of trinuclear iron(III) ions have been focused on oxo- and/or hydroxy-bridged Fe(III) centers. Hence the magnetostructural characterization of rare examples of trinuclear Fe(III)-azametallacrown represent the focus of this chapter. A complete serie of neutral trinuclear iron complexes with mixed ligand composition of type [9-MC-3](L)₃ (L is Cl⁻, NNN⁻ and NCS⁻ end-on bound ligands) have been synthesized and magnetically investigated. These complexes represent very rare examples of trinuclear azametallacrown complexes and they are also the first example of trinuclear iron complexes in which the presence of μ_3 -bridged mode of oxygen atom³¹ is not present. The three compounds maintain the same structural motif with remark that the coordination sphere of iron atoms is changed. When thiocyanate has been used as pseudohalide source, the trinuclear iron-aza compound showed the ability to encapsulate nitrate anion acting as *host-guest* system. Finally this last 9-membered azametallacrown complex can support a ring size expansion to form a tetranuclear azametallacrown complex of type [2+2] grid compound in which the chirality of the iron atoms in the molecular structure alternates between the Λ and Δ form.

2.1 Synthesis and spectroscopic characterization

The Schiff base ligand, derived from the condensation reaction of imidazole-2-carboxaldehyde and salicyloyl hydrazide, reacts stoichiometrically with iron(III) salts to form trinuclear iron complexes in which [-Fe-N-N-]₃ linkage has been observed. These azametallacrown compounds present an neutral character since chloride and/or pseudohalide were used as coligands. The chosen organic system behaves as chelate and bridging ligand, acting as pentadentate dianionic coordination support. A schematic representation of the coordination mode of the used Schiff base ligand is depicted in Figure 2.2.

Stoichiometric reaction between H₂imsalhy ligand and FeCl₃ in presence of one equivalent of base resulted in the formation through self-assembly reaction of the trinuclear iron complex [Fe(imsalhy)(Cl)]₃·3CH₃OH (**1**). Replacement of FeCl₃ with other

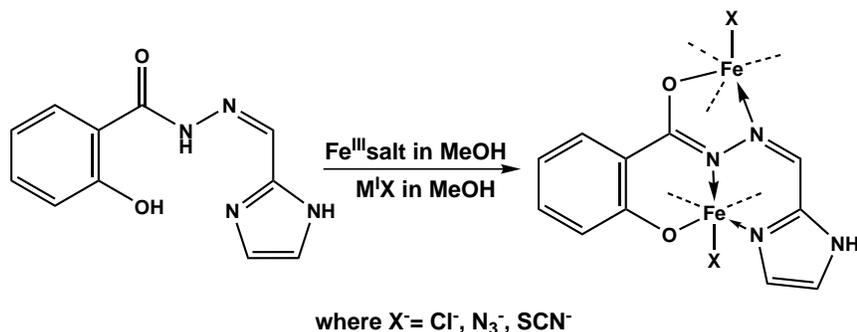


Figure 2.2: Schematic representation of the coordination mode of H₂imsalhy ligand.

salt, i.e. Fe(NO₃)₃ and use of pseudohalides, such as azide and thiocyanate afforded the neutral trinuclear iron complexes with N₃⁻ ([Fe(imsalhy)(N₃)]₃·3.5DMF (**2**) and NCS⁻ ([Fe(imsalhy)(NCS)]₃·(H₃imsalhy)·(NO₃)·H₂O·4.25CH₃OH (**3**) acting as monodentate coligands at each metal center (Figure 2.3). All these compounds are analogs of the organic azacrown compounds and therefore by analogy their nomenclature can be defined as 9-MC-3 complexes, where MC is the abbreviation for metallacrown. Any attempt to transform the *in situ* formed trinuclear iron complex **1** in the azide (**2**) or isothiocyanate (**3**) derivatives failed. Instead, when potassium thiocyanate has been used as source of pseudohalide, a tetranuclear iron complex [Fe(imsalhy)(NCS)]₄·4CH₃OH (**4**) has been isolated. Alternatively, the last complex can be also isolated through self-assembly reaction using equimolecular amounts of the Schiff base ligand and iron chloride salt in presence of an excess of base, namely two equivalents of sodium hydroxide (Figure 2.3).

The formation of these complexes was confirmed by IR spectroscopy which shows stretching vibrations characteristic to the supporting ligand as well as specific stretching vibrations of the coligands. The IR spectrum of the free ligand H₂imsalhy shows stretching bands at 1665 and 3213 cm⁻¹ attributed to C=O and phenolate vibrations, respectively. The IR spectra of the polynuclear iron complexes showed no such stretching vibrations consisting with the enolization of the hydrazide functionality and deprotonation of phenolate group upon iron coordination. This is also confirmed by 638-673 cm⁻¹ vibrations attributed to the M–O linkage and 506-583 cm⁻¹ vibrations assigned to M–N linkage. The IR spectra of all four iron complexes shows a strong stretching vibration in the region 1595-1600 cm⁻¹ specific for –C=N–N=C– functionality. In addition

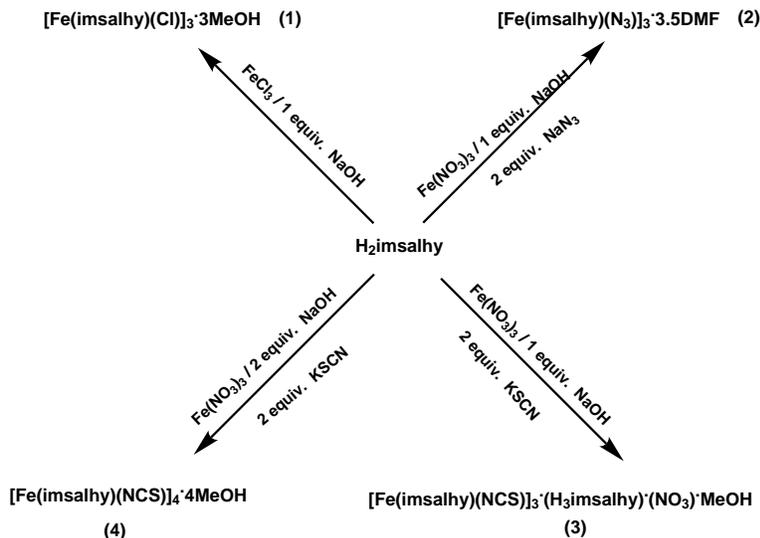


Figure 2.3: Scheme representing the synthesis of the polynuclear iron complexes.

strong stretching vibrations revealing the presence of the pseudohalides were detected at 2059 cm^{-1} in complex **2** ($\nu\text{ N}_3^-$) and 2040 and 2049 cm^{-1} attributed to NCS coordinated stretching vibration¹⁰² in complex **3** and **4**, respectively.¹⁰³ Stretching vibrations near 2050 cm^{-1} are considered typical for isothiocyanate form (N - coordination), while thiocyanate coordination (S - coordinated form) gives a stretching vibration near 2100 cm^{-1} .¹⁰⁴

The integrity of the complexes in solution has been established by electronic spectroscopy and mass spectroscopy. The UV-Vis spectrum of the free ligand $\text{H}_2\text{imalsly}$ recorded in methanol solution display absorption maxima at 240 and 326 nm . The electronic spectra for the iron clusters are quite similar, showing absorption maxima at $246\text{-}257$, $319\text{-}324$, $508\text{-}519\text{ nm}$ (See experimental part). While the first two maxima are similar to the one detected for the electronic transitions in the free ligand, the $508\text{-}519\text{ nm}$ absorption maxima are tentatively attributed to d-d transition of the $\text{Fe}(\text{III})$ ions in the ligand field. The UV-Vis spectra of the two isothiocyanate-containing iron complexes have been also recorded in solid form using BaSO_4 . There is a good agreement between solution UV-Vis spectra and the corresponding solid ones (see experimental part) which agree well with the integrity of the complexes in solution. Moreover, fast atom bombardment ionization (FAB) in methanol solution in a 3-nitrobenzyl alcohol matrix gave

molecular ion peaks at 851.0 m/e associated to the trinuclear iron core- $[\text{Fe}(\text{imsalhy})]_3^-$ for each azametallacrown complex that have been measured. FAB-MS spectrum of complex **1** containing peaks with mass-to-charge ratios corresponding to one, two and three chloride ions associated with the trinuclear iron core are observed (see Experimental part) with the intact ion peak at 958 m/e corresponding to $[\text{Fe}(\text{imsalhy})\text{Cl}]_3$. Similar patterns of peaks corresponding to mass-to-charge ratios that contain one, two and three isothiocyanate ions associated with the $[\text{Fe}(\text{imsalhy})]_3^-$ core are observed for complex **3** solution by FAB-MS. FAB-MS spectrum of **4** contains also peaks with mass-to-charge ratio corresponding to one more iron associated to previous detected trinuclear core- $[\text{Fe}(\text{imsalhy})]_3^-$ and additionally the 1139 m/e ion peak corresponding to $[\text{Fe}(\text{imsalhy})]_4^{4-}$, respectively. Therefore, it can be concluded through UV-Vis and FAB-MS spectral data that these complexes retain their structure in solution. Moreover, the herein presented polynuclear iron complexes are also stable at high temperatures. In instance, thermogravimetric measurement, performed on complex **3** shows a multistage weight losses of 27% in the temperature range 30-300 °C. This total loss corresponds to a calculated mass of 371.8 g which is around the molecular weight of the four water molecules, the free ligand molecule and the encapsulated nitrate anion. The tetranuclear iron complex **4** shows also a loss in weight of around 9.4% in the temperature range 30-143 °C. This amount of weight loss corresponds to the calculated mass of four methanol solvent molecules (128 g). Further heating up to 300 °C cause a loss of 6.1% corresponding to a calculated mass of 75 g. This last loss might be generated by pyrolysis of the isothiocyanate functionality to the corresponding CS_2 under high temperature conditions. All four iron complexes crystallize with solvent molecules with methanol being the frequent present solvent. The elemental analyze results agrees in the majority of the cases with water molecules instead of methanol molecules. Probably, the atmospheric water molecules exchange the crystallographic found methanol solvent molecules. Similar situation has been reported for a hexanuclear manganese cluster were the observed exchange of methanol with water molecules has been confirmed by paramagnetically shifted ^1H NMR spectroscopy.⁹⁸ The easy replacement of the solvent is also obvious by crystallographic determination of molecular structure for complex **1** in different solvent solutions, when methanol have been replaced by the used reaction solvents, i.e ethanol and dimethylformamide.

2.2 Structural studies

[Fe(imsalhy)(Cl)]₃·3CH₃OH (**1**). The azametallacrown complex **1** consists of a trinuclear iron core and presents a neutral character since the 3+ charge of the metal centers is balanced by the oxygen atoms of the diprotonated ligand and the chloride ligand. Molecular structure determination of complex **1** is depicted in Figure 2.6, whereas selected bond lengths and angles are listed in Table 2.1. The diprotonated pentacoordinated imidazolyl hydrazide ligand bridges two neighboring iron atoms through its hydrazide group resulting in a triangular iron core linked by three N–N bridge. The first iron atom is coordinated in the tridentate pocket of the ligand through phenolate oxygen atom (O1), the hydrazide and imidazole nitrogen atoms (N1 and N3) (Figure 2.4) with the bite angles of around 84.6° (O1–Fe–N1) and 82.1° (N3–Fe–N1), whereas the other imine nitrogen atom N2 and the iminolate oxygen atom O3 binds an adjacent iron atom with the bite angle of 72.5° (O2–Fe–N2). Each iron atom is six-coordinated in a N₃O₂Cl environment with the sixth coordination site occupied by the chloride ligands (Figure 2.6) in a bond distance of 229.6 pm.

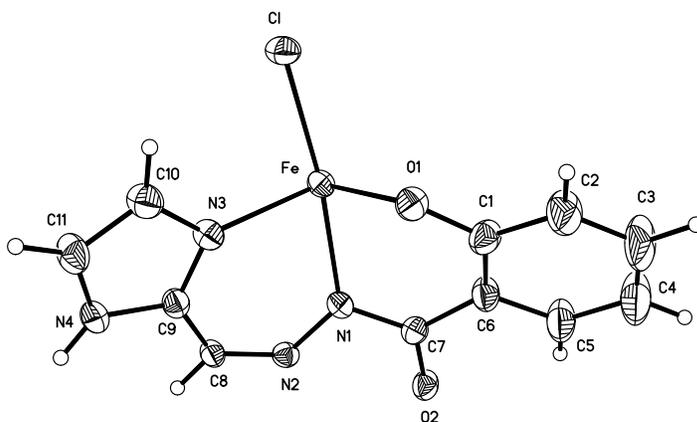


Figure 2.4: Asymmetric unit cell of the molecular structure of complex [Fe(imsalhy)(Cl)]₃·3CH₃OH (**1**). Thermal ellipsoids of non-hydrogen atoms are drawn at 50% probability.

The organization found in complex **1** results in a 9-membered trinuclear core with an $-\text{[Fe-N-N-Fe]}-$ repeating unit (Figure 2.5) as the first example of a 9-azametallacrown-3 compound. Similar trinuclear 9-MC-3 compounds have been reported for vanadium^{64,81} and other d-metal containing compounds^{77,82,83} but with the repeating unit consisting

Table 2.1: Selected bond lengths (pm) and angles ($^{\circ}$) for complex **1**.

Fe–O1	191.5(3)	Fe–N2	221.2(3)
Fe–O2	202.3(3)	Fe–Cl	229.63(9)
Fe–N3	210.7(3)	N1–C7	135.2(5)
Fe–N1	212.2(3)	N1–N2	138.1(4)
O1–Fe–O2	88.04(12)	N3–Fe–N1	82.07(12)
O1–Fe–N3	108.13(12)	N3–Fe–N2	90.06(11)
O1–Fe–N1	84.61(11)	N3–Fe–Cl	91.03(9)
O1–Fe–N2	158.04(12)	N2–N1–Fe	127.7(2)
O1–Fe–Cl	98.52(8)	N2–Fe–Cl	93.21(8)
O2–Fe–N3	161.93(11)	N1–Fe–N2	85.89(11)
O2–Fe–N2	72.51(11)	N1–N2–Fe	114.1(2)
O2–Fe–Cl	94.56(9)	N1–Fe–Cl	173.03(8)

of N–O group³⁰ whereas the reports of iron based azametallacrown complexes contain at least 18-membered core motif.¹⁰⁵

All iron atoms in complex **1** are in a distorted octahedral environment with the neighboring Fe \cdots Fe interatomic distances of 509.8 pm and interatomic Fe \cdots Fe \cdots Fe angle of 60° , value characteristic for an equilateral triangle. The Fe \cdots Fe separation is slightly longer than that of classical Fe(III)-MC-3 complexes based on salicylhydroximate⁸⁰ (484.8 pm) and longer than that found in even nuclear membered iron azacrowns of 487.2–490.6 pm in octanuclear⁹⁰ and 488.1 pm in hexanuclear¹⁰⁰ iron azametallacrowns. In complex **1** the three iron atoms are crystallographically identical with Fe–N–N–Fe torsion angle of 150° and the N–Fe–N–N torsion angle of 82.1° . The C7–O2 and C7–N1 bond lengths in the ligand fragments are around 126.0 and 135.3 pm, respectively. These bond lengths are similar to corresponding ones reported for d-metal complexes based on iminolate form of the hydrazide containing ligands.^{100,105} The Fe–N_{hydrazide} (212.2 pm) and Fe–N_{imidazole} (210.6 pm) bond lengths are significantly shorter than the Fe–N_{imine} bond lengths (221.4 pm). This difference is possibly due to the bridging nature of the ligand and the rigidity of the tridentate pocket of the organic system.

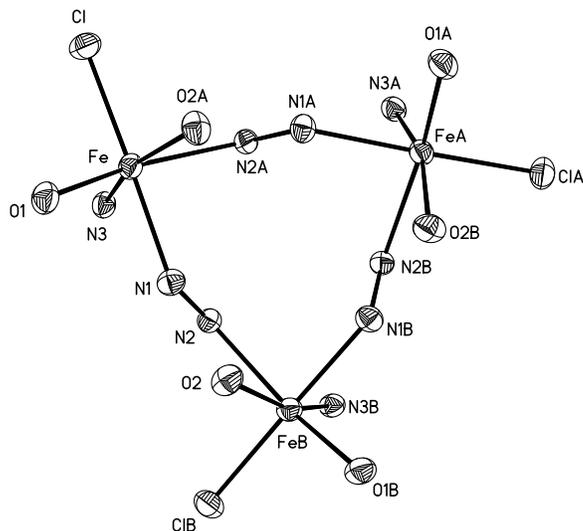


Figure 2.5: Representation of the structural core motif of complex $[\text{Fe}(\text{imsalhy})(\text{Cl})]_3 \cdot 3\text{CH}_3\text{OH}$ (**1**) showing the 9-membered 3-iron aza ring.

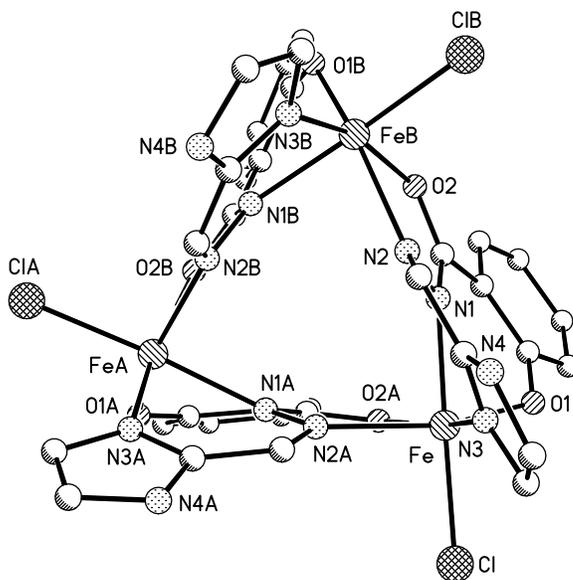


Figure 2.6: Molecular structure and numbering scheme of the coordinated heteroatoms in complex $[\text{Fe}(\text{imsalhy})(\text{Cl})]_3 \cdot 3\text{CH}_3\text{OH}$ (**1**). Hydrogen atoms and solvent molecules have been omitted for clarity.

The trinuclear iron complex **1** crystallizes in the rhombohedral $R\bar{3}c$ space group with a centrosymmetric point placed in the middle of the cavity. The Fe–O (phenolate

and iminolate oxygen atoms) bond distances of around 191 and 201 pm are similar with reported corresponding bond lengths in polynuclear iron complexes.^{90,100} Complex **1** contains lattice methanol molecules which forms hydrogen bonds with the phenolate oxygen atom (O1M···O1 279.3 pm) of the trinuclear Fe(III) entity. In addition the protonated imidazole moiety is also hydrogen bonded to neighboring solvent molecules (O1M···N4 277.7 pm). These lattice methanol molecules can be easily replaced by other solvent molecules according with the used reaction media. For example, performing the same reaction stoichiometry in ethanol lead to **1**·3EtOH (Figure 2.7). The trinuclear iron core remains unchanged, presenting the same symmetry as previously described. The Fe···Fe separation of 509.8 pm is very close to above described complex, as well as the Fe–N–N–Fe torsion angle of 150°. Small difference has been observed for N–Fe–N–N torsion angle which is 79.81°, around 2° smaller than that of **1**·3MeOH complex but within the error range of measurements. The ethanol molecules are in hydrogen bonding interaction with the imidazole moiety through protonated NH group of around 269.9 pm (N···OEt).

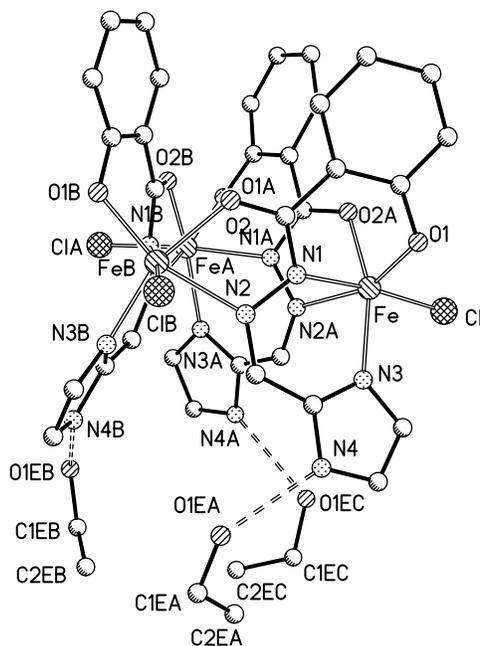


Figure 2.7: Molecular structure and selected numbering scheme of complex **1**·3EtOH. Hydrogen atoms have been omitted for clarity. Dashed lines represent hydrogen bonding interactions.

[Fe(imsalhy)(N₃)]₃·3.5DMF (**2**). The molecular structure of the neutral complex **2** is depicted in Figure 2.8, and selected bond lengths and angles are listed in Table 2.2. The three six-coordinated Fe(III) centers are bridged through hydrazide nitrogen atoms in a similar fashion as described for complex **1**. The trinuclear iron complex **2** crystallizes in the triclinic space group P1 with the same 9-MC-3 motif with three Fe(III) membered ring, three ligand molecules while the chloride ligands have been replaced with the azide anions. All iron atoms are in a distorted octahedral N₄O₂ environment. The H₂imsalhy ligand coordinates in the same fashion as previously described, namely it bridges two iron atoms providing a three chelate donor set to one iron atom through the phenolate oxygen O(1), hydrazide nitrogen N(1) and nitrogen N(3) atoms from the imidazole ring, while the second diazine nitrogen N(2) and the iminolate oxygen atom O(2) are bonded to another iron atom.

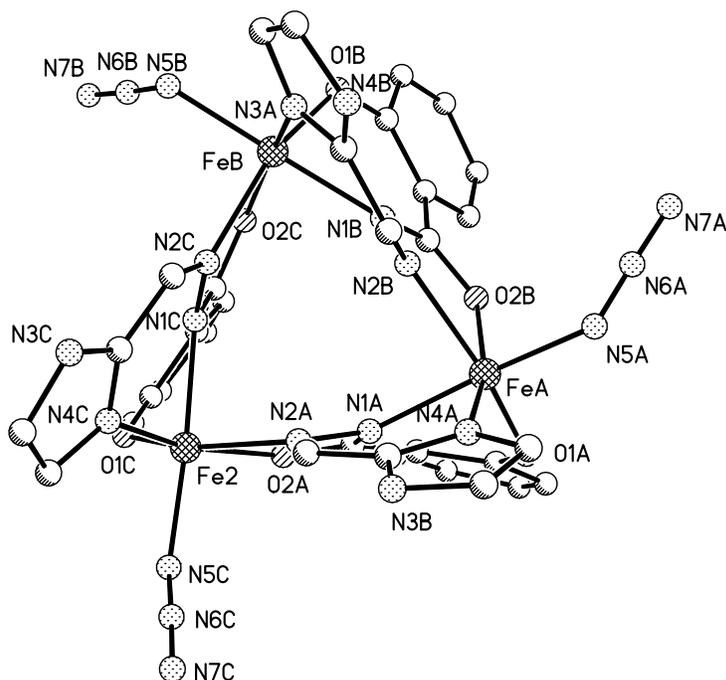


Figure 2.8: Molecular structure and selected numbering scheme of complex [Fe(imsalhy)(N₃)]₃·3.5DMF (**2**). Hydrogen atoms and solvent molecules have been omitted for clarity.

At this point it should be noted that in this case the centrosymmetric structure of compound **1** is not found in complex **2**. In the last case the iron atoms are located at the vertex of a scalene triangle with the interatomic distances raising from 506.5-510.9 pm.

Table 2.2: Selected bond lengths (pm) and angles ($^{\circ}$) for complex **2**.

FeA–O1A	189.3(3)	FeB–O1B	189.3(3)	Fe2–O1C	189.8(3)
FeA–O2B	202.6(3)	FeB–O2C	201.4(3)	Fe2–O2A	202.4(3)
FeA–N1A	213.1(3)	FeB–N1B	212.4(3)	Fe2–N1C	212.2(3)
FeA–N2B	222.7(3)	FeB–N2C	222.6(3)	Fe2–N2A	224.1(3)
FeA–N4A	208.8(3)	FeB–N3A	208.6(4)	Fe2–N4C	211.1(4)
FeA–N5A	199.4(4)	FeB–N5B	201.6(4)	Fe2–N5C	198.4(4)
N1A–C7A	134.1(5)	N1B–C7B	134.6(5)	N1C–C7C	135.1(5)
N1A–N2A	138.1(4)	N1B–N2B	139.2(4)	N1C–N2C	138.5(4)
O2A–C7A	127.4(5)	O2B–C7B	127.1(5)	O2C–C7C	127.9(4)
O1A–FeA–O2B	89.55(12)	O1B–FeB–O2C	90.19(12)	O1C–Fe2–O2A	89.27(12)
O1A–FeA–N1A	84.08(13)	O1B–FeB–N1B	84.41(12)	O1C–Fe2–N1C	84.81(12)
O1A–FeA–N2B	157.71(13)	O1B–FeB–N2C	159.84(12)	O1C–Fe2–N2A	158.72(12)
O1A–FeA–N4A	107.43(13)	O1B–FeB–N3A	106.18(13)	O1C–Fe2–N4C	108.47(13)
O1A–FeA–N5A	99.29(17)	O1B–FeB–N5B	100.43(14)	O1C–Fe2–N5C	97.05(15)
O2B–FeA–N1A	93.81(12)	O2C–FeB–N1B	92.86(12)	O2A–Fe2–N1C	89.74(12)
O2B–FeA–N2B	71.84(12)	O2C–FeB–N2C	72.69(11)	O2A–Fe2–N2A	71.98(11)
O2B–FeA–N4A	162.13(13)	O2C–FeB–N5B	94.61(14)	O2A–Fe2–N4C	159.58(12)
N1A–FeA–N2B	85.03(12)	N1B–FeB–N2C	85.89(12)	N1C–Fe2–N2A	85.11(12)
N4A–FeA–N1A	82.77(13)	O2C–FeB–N3A	162.26(12)	N4C–Fe2–N1C	82.13(12)
N4A–FeA–N2B	90.37(13)	N3A–FeB–N2C	89.91(13)	N4C–Fe2–N2A	88.62(13)
N5A–FeA–O2B	95.14(14)	N5B–FeB–N3A	89.20(16)	N5C–Fe2–O2A	96.14(16)
N5A–FeA–N1A	170.45(15)	N5B–FeB–N1B	171.07(15)	N5C–Fe2–N1C	173.84(16)
N5A–FeA–N2B	94.61(16)	N5B–FeB–N2C	91.68(14)	N5C–Fe2–N2A	94.96(15)
N1B–N2B–FeA	113.9(2)	N1C–N2C–FeB	113.9(2)	N5C–Fe2–N4C	91.71(16)
N2A–N1A–FeA	128.7(2)	N3A–FeB–N1B	82.22(14)	N2C–N1C–Fe2	127.6(2)

To each iron atoms is bound an azide ligand into a bent fashion with a torsion angle in the range 119,3 - 133,3°. This monodentate ligand is almost linear with N-N-N angles of 176.7, 177.3 and 178.0°, respectively. The Fe-N_{azide} bond distance range between 198.1 and 201.9 pm, distances similar with reported end-on bound azide to iron center,¹⁰⁶ but significantly shorter than reported distances for μ -bridged azide ligand.¹⁰⁷ The diprotonated form of the ligand, therefore the presence of the iminolate form of the hydrazide functionality is illustrated by C7-O2 bond distances of around 127 pm and further confirmed by the considerable double bond character of the C7-N1 bonds of around 134 pm. These values are similar to previous bond distances found in complex **1**. The other Fe-O (phenolate and iminolate oxygen atoms), as well as Fe-N (imine, hydrazide and imidazole nitrogen atoms) are within expected bond lengths and similar with the corresponding ones found in complex **1**. Selected bond lengths and angles for complex **2** are listed in Table 2. Complex **2** crystalizes with 3.5 molecules of DMF as solvent of crystallization, which are in hydrogen bonding contact with the protonated NH group of the imidazole moiety (N_{imidazole}-O_{DMF} = 263.2 - 267.6 pm).

[[Fe(imsalhy)(NCS)]₃·(H₃imsalhy)·(NO₃)·0.5H₂O·4.25CH₃OH (3). The new trinuclear iron complex contains a 9-membered aza ring similar to that previously described for complexes **1** and **2**, respectively. Three ligand molecules are directly coordinating the iron atoms in one five-membered and two six-membered chelate rings (Figure 2.2) which forms an N₃O₂ environment around each iron center. The sixth coordination site of each metal center is now occupied by the isothiocyanate ligands, that bound in monodentate fashion in a bond distance that range from 198.1 to 199.5 pm, significantly shorter than that reported for mononuclear Fe-NCS systems.^{103,108} The isothiocyanate ligand coordinates almost linear with Fe-N-C angles within the range 163-176°.

Complex **3** crystalizes in the P-1 space group with three crystallographically distinct iron atoms which form an propeller triangle with the interatomic Fe···Fe distance in the range 502.2-507.1 pm, values close to previous found in complex **2**. The connectivity around the ring consisting of Fe-N-N linkage is similar with previous herein described trinuclear iron complexes, with torsion angles of 149.7-151.2° for Fe-N-N-Fe and 78.2-82.4° for N-Fe-N-N, respectively. All the other bond distances, i.e. Fe-O and Fe-N are similar and within reported similar bond lengths. Selected bond lengths and angles in

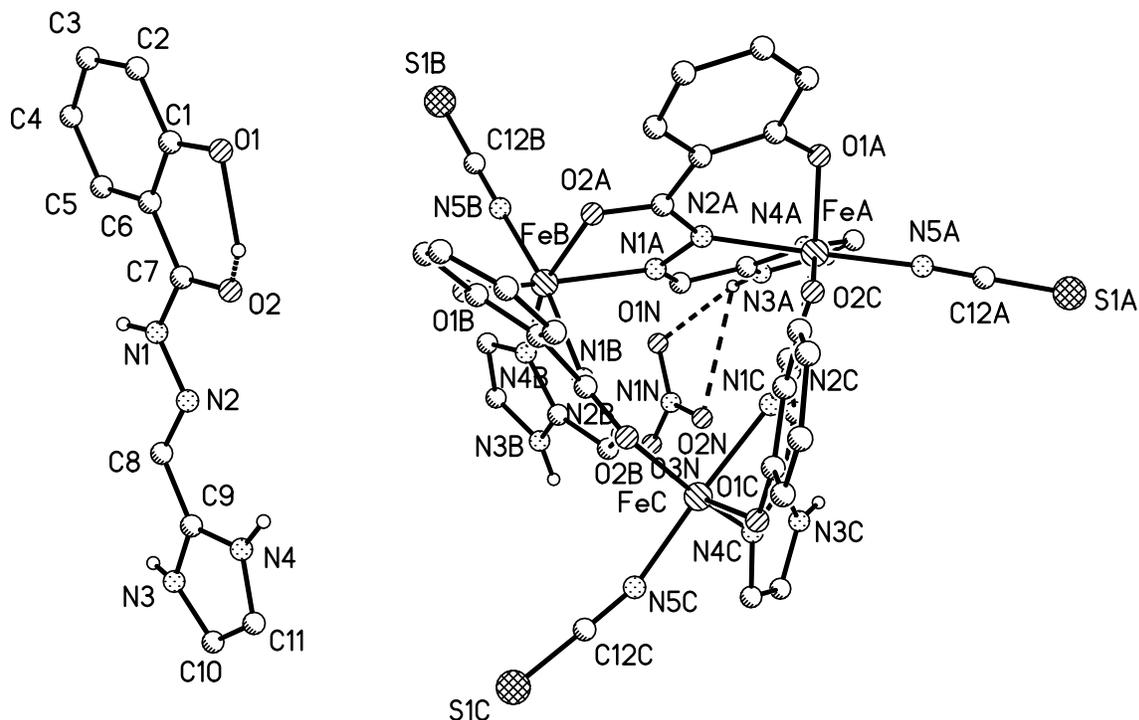


Figure 2.9: Molecular structure and selected numbering scheme of complex $[[\text{Fe}(\text{imsalhy})(\text{NCS})_3]_3 \cdot (\text{H}_3\text{imsalhy}) \cdot (\text{NO}_3) \cdot 0.5\text{H}_2\text{O} \cdot 4.25\text{CH}_3\text{OH}$ (**3**). Only selected hydrogen atoms are shown. The solvent molecules have been omitted for clarity. Broken lines represent hydrogen bonding interactions.

complex **3** are listed in Table 2.3. By comparison with previous two described trinuclear iron complexes, complex **3** crystallizes with a free ligand molecule, whereas a nitrate molecule is hosted by the 9-membered aza ring (Figure 2.9).

The architecture of the **3** metallocrown structural motif presupposes the concept of molecular recognition of anions. Similar situation has been reported for a trinuclear Cu(II) complex based on 3-(benzylimino)butanone 2-oxime, where a perchlorate anion has been hosted by the trinuclear copper core.⁸⁶ More recently, trinuclear metallocrown compounds have been reported as hosts for iron acetate⁸⁰ and/or vanadate moiety.¹⁰⁹ The negative charge of the nitrate molecule hosted by complex **3** is compensated by the ligand molecule which contains a protonated imidazole ring. The nitrate anion is in hydrogen bonding distance with an imidazole moiety of the supporting ligand (N3A(imidazole)–O1NO₂ = 276.8 and N3A(imidazole)–O2NO₂ = 312.4 pm). Intramolecular hydrogen bonding interactions have been observed in the free ligand between the phenolate oxygen

Table 2.3: Selected bond lengths (pm) and angles ($^{\circ}$) for complex **3**

FeA–O1A	190.1(5)	FeB–O1B	193.3(5)	FeC–O1C	189.1(5)
FeA–O2C	200.0(5)	FeB–O2A	199.2(5)	FeC–O2B	201.1(5)
FeA–N4A	210.4(7)	FeB–N1B	211.5(6)	FeC–N1C	211.4(6)
FeA–N2C	221.6(6)	FeB–N1A	219.8(6)	FeC–N2B	221.9(5)
FeA–N2A	209.8(6)	FeB–N4B	209.3(6)	FeC–N4C	207.9(6)
FeA–N5A	199.4(7)	FeB–N5B	199.7(6)	FeC–N5C	198.2(7)
N2A–C7A	135.2(9)	N1B–C7B	133.5(8)	N1C–C7C	134.5(9)
N2A–N1A	138.9(8)	N1B–N2B	138.7(8)	N1C–N2C	139.7(8)
O2A–C7A	127.5(8)	O2B–C7B	127.7(8)	O2C–C7C	128.6(9)
O1A–FeA–O2C	87.0(2)	O1B–FeB–O2A	86.9(2)	O1C–FeC–O2B	87.6(2)
O1A–FeA–N2A	85.2(2)	O1B–FeB–N1B	83.6(2)	O1C–FeC–N1C	85.1(2)
O1A–FeA–N2C	157.3(2)	O1B–FeB–N1A	155.7(2)	O1C–FeC–N2B	157.5(2)
O1A–FeA–N4A	109.9(2)	O1B–FeB–N4B	108.6(2)	O1C–FeC–N4C	109.9(2)
O1A–FeA–N5A	97.0(3)	O1B–FeB–N5B	96.2(2)	O1C–FeC–N5C	98.0(3)
O2C–FeA–N2A	93.7(2)	O2A–FeB–N1B	94.3(2)	O2B–FeC–N1C	91.8(2)
O2C–FeA–N2C	72.5(2)	O2A–FeB–N1A	72.5(2)	O2B–FeC–N2B	72.11(19)
O2C–FeA–N4A	162.2(2)	O2A–FeB–N5B	95.9(2)	O2B–FeC–N4C	161.0(2)
N2A–FeA–N2C	86.5(2)	N1B–FeB–N1A	85.3(2)	N1C–FeC–N2B	86.1(2)
N2A–FeA–N4A	82.7(2)	O2A–FeB–N4B	163.7(2)	N4C–FeC–N1C	82.9(2)
N4A–FeA–N2C	89.9(2)	N5B–FeB–N4B	87.5(3)	N4C–FeC–N2B	89.3(2)
N5A–FeA–O2C	94.8(3)	N4B–FeB–N1B	82.9(2)	N5C–FeC–O2B	94.0(2)
N5A–FeA–N2A	171.3(3)	N5B–FeB–N1B	169.8(2)	N5C–FeC–N1C	173.5(2)
N5A–FeA–N2C	94.4(3)	N4B–FeB–N1A	91.2(2)	N5C–FeC–N2B	93.1(3)
N5A–FeA–N4A	88.7(3)	N5B–FeB–N1A	98.6(2)	N5C–FeC–N4C	90.7(3)
N1B–N2B–FeC	113.9(4)	N1C–N2C–FeA	113.5(4)	N2C–N1C–FeC	128.1(4)
N1A–N2A–FeA	127.1(4)	N2A–N1A–FeB	113.9(4)	N2B–N1B–FeB	128.3(4)

atom (O1) and the carbonyl oxygen atom (O2) of around 253.9 pm. In addition, in the crystal lattice of **3**, the methanol molecules and the cocrystallized H₃imsalhy ligand form a hydrogen bonding channel with the shorter hydrogen contact of 294.3 pm (N3–O3M) and the longest hydrogen bond distance of 278.0 pm for N4–O3M (Figure 2.10). The observed hydrogen bonding channel is based mainly on hydrogen bonding network established among the methanol molecules with the shortest OM–OM contact of 277.9 pm and the longest OM–OM distance of around 297.3 pm. The arrangement through crystal packing shows also strong hydrogen bonding interaction between the methanol molecules and two different azametallacrown molecules by OM–N3 hydrogen bonding contacts that range between 266.2 and 278.0 pm.

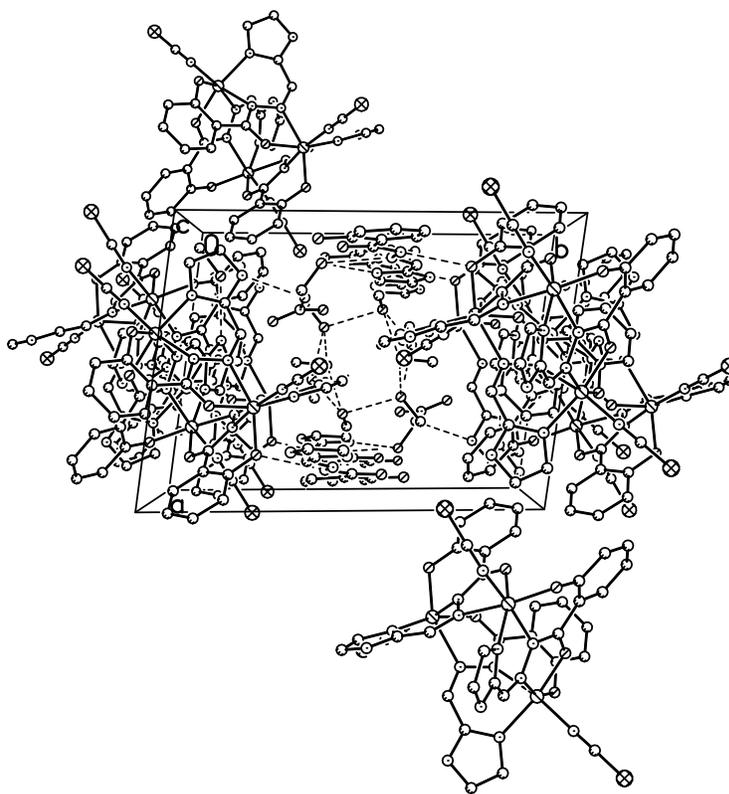


Figure 2.10: Crystal packing in complex $[[\text{Fe}(\text{imsalhy})(\text{NCS})]_3 \cdot (\text{H}_3\text{imsalhy}) \cdot (\text{NO}_3) \cdot 0.5\text{H}_2\text{O} \cdot 4.25\text{CH}_3\text{OH}$ (**3**) showing the hydrogen bonding channel formed between the cocrystallized free ligand molecules, lattice methanol molecules and trinuclear iron cluster. View along the *c* axis.

As can be observed, these azametallacrown compounds possess a labile coordination site at the iron centers which may be used as strategic points to design new dendritic

materials. A peculiar role can be played in this direction by the chloride-containing trinuclear iron(III) azacrown complex owing to known "leaving capacity" of the chloride ligand. Hence, *in situ* reaction between H₂imsalhy and Fe(NO₃)₃ salt followed by addition of [Mn(bipy)₂Cl₂] in MeOH/DMF mixture has been performed in order to isolate a dissimilar polynuclear complex. Instead, only the [Fe(imsalhy)(Cl)]₃·CH₃OH·3DMF (**1a**) has been formed which seems to be thermodynamically the most stable specie. Molecular structure determination of complex **1a** is depicted in Figure 2.11 with selected bond lengths and angles listed in Table 2.4. Conversely to initial described complex **1**, the new **1a** complex does not present the centrosymmetry observed previously. The Fe···Fe interatomic separation, although very similar differs among the three constituting iron ions, i.e 510.7 pm for FeA···FeB, 509.8 pm for FeB···Fe and 508.1 pm for Fe···FeB, respectively. The diazine-bridging torsion angles are also different within the azacrown Fe₃-triad and have values of 152.5° (FeA–N2B–N1B–FeB), 152.8° (FeA–N1A–N2A–Fe) and 150.7° (Fe–N1–N2–FeB). All the other bond lengths and angles show very close values to corresponding bond distances found in complex **1**.

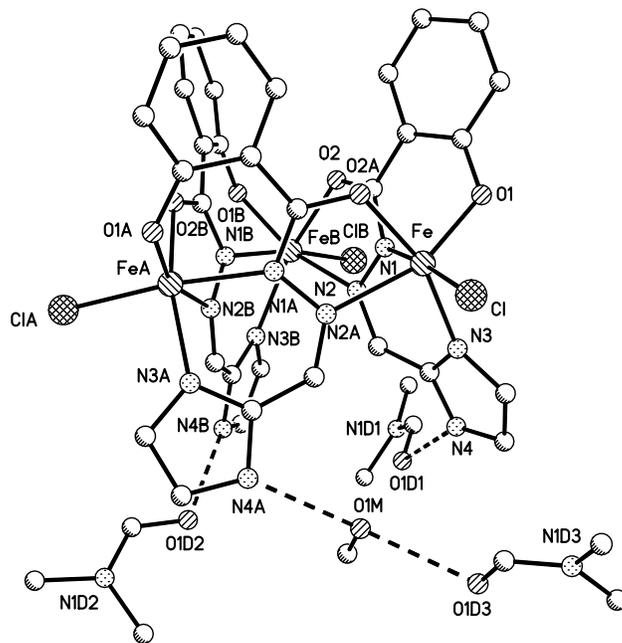


Figure 2.11: Molecular structure and selected numbering scheme of complex [Fe(imsalhy)(Cl)]₃·CH₃OH·3DMF (**1a**). Hydrogen atoms have been omitted for clarity. Dashed lines represent hydrogen bonding interactions.

Lattice solvent molecules, i.e DMF and MeOH form hydrogen bonding interactions with the protonated nitrogen atoms of the imidazole moieties, as a common crystal packing pattern observed for all 9-Fe(III)azacrown-3 complexes. In this case $O_{DMF} \cdots N_{imidazole}$ hydrogen bonding contacts fall in the 276.1-271.7 pm range, whereas the hydrogen bonding interaction $O_{MeOH} \cdots N_{imidazole}$ is 268.9 pm. Additionally, lattice solvent molecules are also in hydrogen bonding interaction distance of 264.4 pm for $O_{DMF} \cdots O_{MeOH}$ hydrogen bonding contacts.

[Fe(imsalhy)(NCS)]₄·4CH₃OH (4). The molecular structure determination exhibits a tetranuclear core of iron atoms linked by four hydrazide N–N groups, resulting in a 12-membered ring motif (Figure 2.12). Similarly to previous trinuclear iron complexes based on H₂imsalhy ligand, the diprotonated Schiff base system acts as pentadentate ligand. The first iron atom is coordinated in the tridentate pocket of the ligand through phenolate oxygen atom (O1) and two nitrogen atoms, one from the imidazole ring (N3) and the other from the hydrazide nitrogen atom (N1), respectively (Figure 2.13) with the bite angles of around 84.5° (O1–Fe–N1) and 73.8° (N3–Fe–N1).

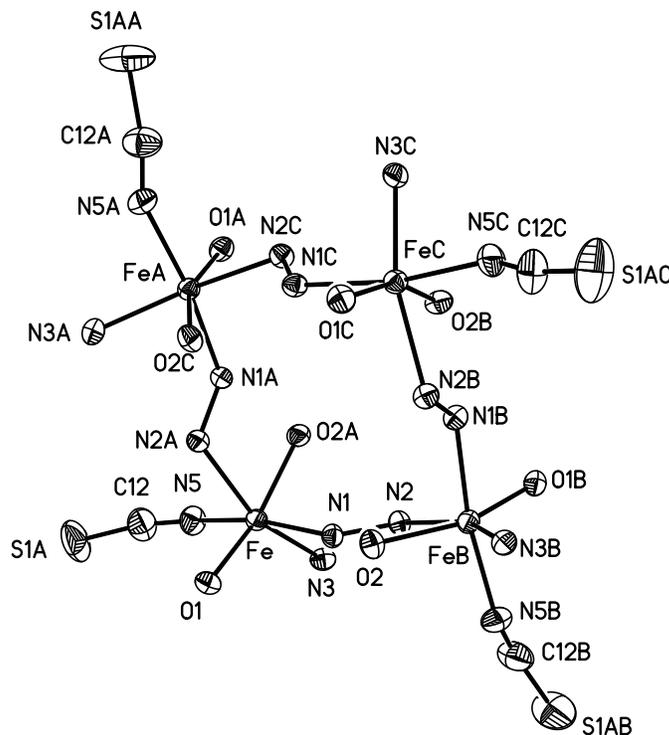


Figure 2.12: Representation of the structural core motif in complex **[Fe(imsalhy)(NCS)]₄·4CH₃OH (4)** showing the 12-membered 4-iron(III) aza ring.

Table 2.4: Selected bond lengths (pm) and angles ($^{\circ}$) for complex **1a**.

FeA–O1A	189.24(17)	FeA–O2B	200.91(17)
FeA–N1A	213.95(18)	FeA–N3A	208.8(2)
FeA–N2B	223.1(2)	FeA–ClA	231.13(7)
FeB–O2	203.13(18)	FeB–O1B	188.84(18)
FeB–N1B	213.2(2)	FeB–N3B	211.6(2)
FeB–N2	220.9(2)	FeB–ClB	230.60(8)
Fe–O1	189.14(17)	Fe–O2A	202.04(18)
Fe–N1	213.2(2)	Fe–N2A	221.8(2)
Fe–N3	210.6(2)	Fe–Cl	229.81(8)
O1A–FeA–O2B	90.64(7)	O1A–FeA–N1A	84.21(7)
O1A–FeA–N2B	158.89(7)	O1A–FeA–N3A	107.16(8)
O2B–FeA–N1A	89.98(7)	O2B–FeA–N2B	72.14(7)
O2B–FeA–N3A	159.64(8)	N3A–FeA–N1A	82.26(7)
N3A–FeA–N2B	88.25(8)	N1A–FeA–N2B	83.69(7)
N2B–FeA–ClA	93.76(5)	O1B–FeB–O2	86.95(8)
O1B–FeB–N1B	84.21(8)	O1B–FeB–N3B	108.50(8)
O1B–FeB–N2	155.58(8)	O2–FeB–N2	72.03(7)
O2–FeB–N1B	92.47(8)	O2–FeB–N3B	162.82(8)
N1B–FeB–N2	84.43(7)	N3B–FeB–N1B	81.98(8)
N3B–FeB–N2	91.19(8)	N1B–FeB–ClB	171.04(6)
O1–Fe–N1	83.77(8)	O1–Fe–N3	106.99(8)
O1–Fe–O2A	89.26(7)	O1–Fe–N2A	158.14(8)
O2A–Fe–N1	91.18(8)	O2A–Fe–N3	161.48(7)
O2A–Fe–N2A	72.63(7)	N1–Fe–N2A	84.46(7)
N3–Fe–N1	82.05(8)	N1–Fe–Cl	173.28(6)

The carbonyl oxygen atom (O2) plus the imine nitrogen atom (N2) of the same ligand molecule coordinates an adjacent iron atom with the bite angle of around 72.5° (O2–Fe–N2). The sixth coordination site at the metal center is occupied by the isothiocyanate ligand (Figure 2.14) with a bond distance Fe–NCS of 203.7 pm and Fe–N–C angle of 149.4° . Complex **4** presents a propeller configuration with an alternating Λ and Δ stereochemistry. Two thiocyanate ligands are in Λ configuration on one face of the azametallacrown compounds and the remaining two monodentate thiocyanate ligands in Δ configuration on the other face of the tetranuclear ring. The two faces of the tetranuclear azametallacrown have opposite chirality.

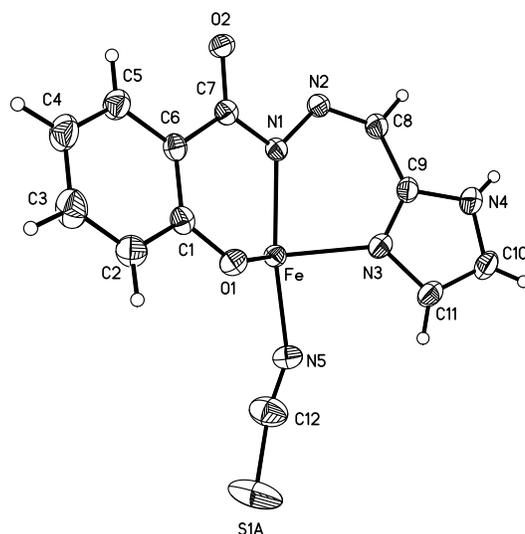


Figure 2.13: Asymmetric unit cell of the tetranuclear iron complex $[\text{Fe}(\text{imsalhy})(\text{NCS})_4] \cdot 4\text{CH}_3\text{OH}$ (**4**). Thermal ellipsoids of non-hydrogen atoms are drawn at 50% probability. Sulfur atom of the isothiocyanate functionality is distorted in a ratio of 50% A and 50% B.

The complex crystallizes in the tetragonal $P4_2/n$ space group with four crystallographically identical Fe(III) atoms. The Fe···Fe separation of around 512.3 pm is a little bit longer than in the case of trinuclear iron complexes, but significantly larger than that reported for hexanuclear iron complexes based on N-R-oylsalicylhydrazide ligands^{100,110} or the Fe···Fe separation reported for a decanuclear iron azametallacrown complex.⁸⁹ Therefore, the planar tetranuclear structure in complex **4** is different than other even-membered iron azametallacrown iron complexes, with the Fe···Fe···Fe interatomic angles

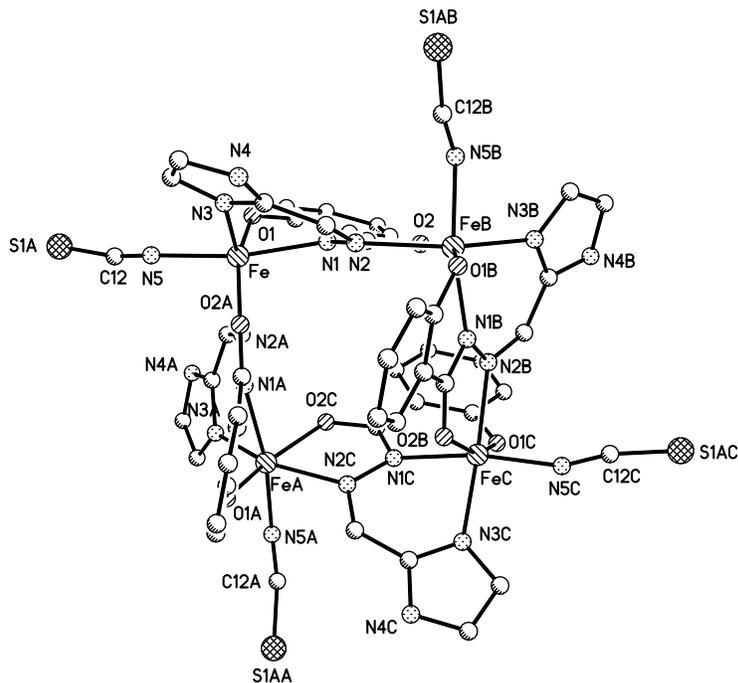


Figure 2.14: Molecular structure and selected numbering scheme of complex $[\text{Fe}(\text{imsalhy})(\text{NCS})]_4 \cdot 4\text{CH}_3\text{OH}$ (**4**). Hydrogen atoms and solvent molecules have been omitted for clarity.

of around 89.95° , value close to the interior angle in a square. The Fe–N–N–Fe torsion angle of 165° and the N–Fe–N–N torsion angle of 114° are larger than similar angles found in the centrosymmetric trinuclear iron complex **1**. The coordination mode of the ligand is similar to one found in the corresponding trinuclear iron complexes (Figure 2.2). The C7–O2 and C7–N1 bond lengths in the ligand fragments are around 127.6 and 134.9 pm, respectively, proving the tautomerization and ulterior deprotonation of the amide functionality upon iron coordination. All other Fe–O/N bond distances are within expected limits and very close to the corresponding bond lengths found in complexes **1**, **2** and **3**, respectively. Selected bond lengths and angles for complex **4** are listed in Table 2.5.

The tetranuclear iron complex **4** crystallizes with four methanol molecules as solvent of crystallization. These solvent molecules interact through hydrogen bonding with the isothiocyanate ligand of the iron centers (S–OM 309.7 pm) as well as with the protonated nitrogen atom of the imidazole ring (N4–OM 273.2 pm), resulting in a two-dimensional polymer build up by hydrogen bonding interactions (Figure 2.15).

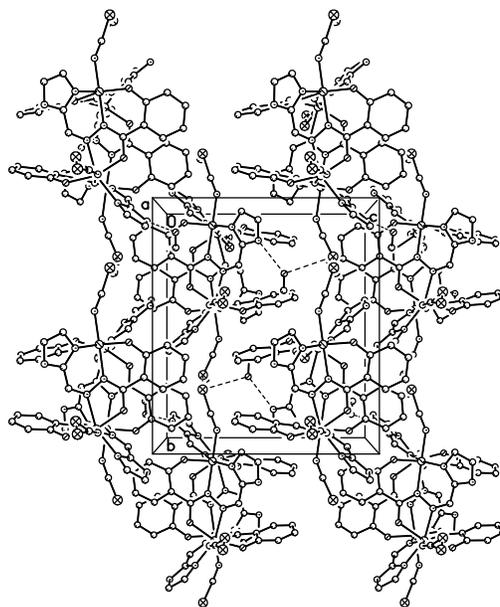


Figure 2.15: Crystal packing in complex **4** showing the hydrogen bonding network formed by the methanol molecules and tetranuclear iron cluster. View along the *a* axis.

Table 2.5: Selected bond lengths (pm) and angles (°) for complex **4**

Fe–O1	188.58(18)	Fe–N2	219.5(2)
Fe–O2	201.06(18)	Fe–N5	203.7(2)
Fe–N3	209.4(2)	N1–C7	134.9(3)
Fe–N1	212.0(2)	N1–N2	138.8(3)
O1–Fe–O2	158.36(8)	N1–Fe–N2	101.60(8)
O1–Fe–N3	114.38(8)	N3–Fe–N1	83.86(8)
O1–Fe–N1	84.47(8)	N3–Fe–N2	156.68(8)
O1–Fe–N2	88.81(8)	N5–Fe–N1	169.88(9)
O1–Fe–N5	92.82(9)	N5–Fe–N2	88.06(9)
O2–Fe–N1	88.67(8)	N5–Fe–N3	88.41(9)
O2–Fe–N2	72.47(7)	N1–N2–Fe	115.74(15)
O2–Fe–N3	85.13(8)	N2–N1–Fe	125.07(16)
O2–Fe–N5	97.20(9)		

2.3 Magnetic properties

The temperature dependence of the magnetization data of the trinuclear compounds **1** to **3** was studied on polycrystalline samples in the 2-300 K range. These data are shown in Figure 2.16 to 2.18 in the form of χT and χ vs. T plots, where χ is the molar paramagnetic susceptibility with the diamagnetism correction.

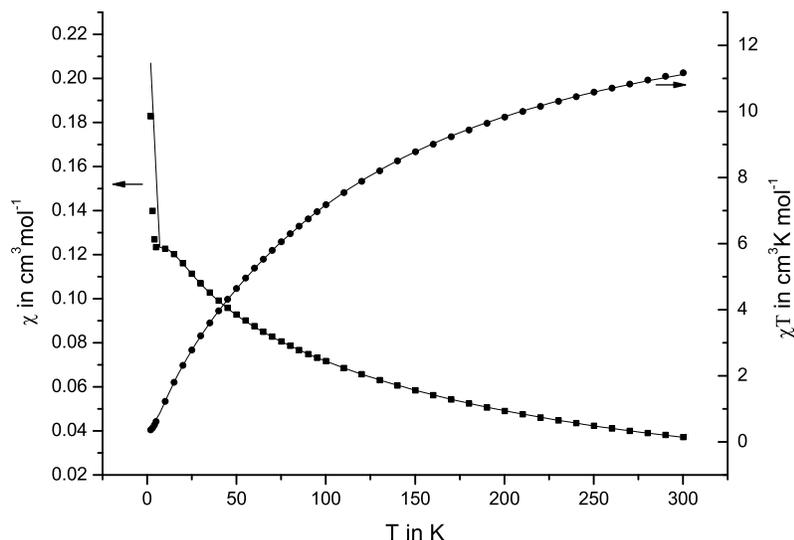


Figure 2.16: Temperature-dependent susceptibility measurements for complex **1** as χ vs. T and χT vs. T plots. The solid lines represent the theoretical curves calculated with Van Vleck equation described in the text. Squares represent the measured values.

The three iron complexes exhibit a similar behavior with the χT product decreasing monotonously on lowering the temperature. The highest χT value is 11.17 for complex **1**, 11.34 for complex **2** and 9.82 cm³ K mol⁻¹ for complex **3**. These values are significantly smaller than calculated value ($\chi T=13.15$ cm³ K mol⁻¹) for three noninteracting $S = 5/2$ spins assuming $g = 2$. This suggests an antiferromagnetic pairwise interactions that give rise to an uncompensated magnetic moment. Upon cooling, the χT product decreases monotonously and reaches at 2 K a value of around 0.42 cm³ K mol⁻¹ in complex **1**, 0.41 cm³ K mol⁻¹ in complex **2** and 0.29 cm³ K mol⁻¹ in complex **3**. In the case of complex **3** a sharp drop occurs below 7 K which might be originated either by intercluster antiferromagnetic interactions and/or zero field splitting. Since this drop could not be described properly, fitting of the magnetic parameters has been performed in the temperature range

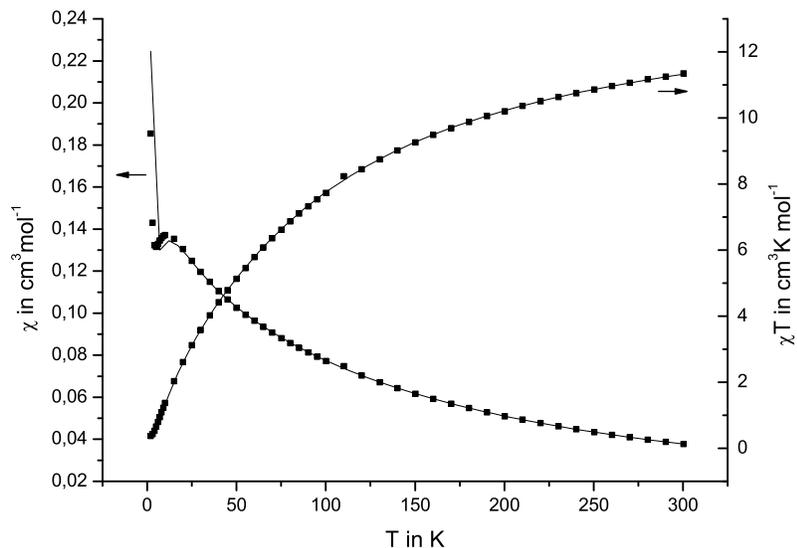


Figure 2.17: Temperature-dependent susceptibility measurements for complex **2** as χ vs. T and χT vs. T plots. The solid lines represent the theoretical curves calculated with Van Vleck equation described in the text. Squares represent the measured values.

8-300 K. A quantitative analysis of the experimental magnetic data sets χT -values has been performed using the Hamiltonian expression for an equilateral triangle:

$$\hat{H} = -J (\hat{S}_1 \hat{S}_2 + \hat{S}_2 \hat{S}_3 + \hat{S}_1 \hat{S}_3) \quad (1)$$

with $S_1 = S_2 = S_3 = 5/2$. Based on structural features, such an exchange pathway interaction is adequate for trinuclear Fe(III)-azacomplex **1**. For trinuclear iron(III) complexes **2** and **3** the magnetic properties can be interpreted considering the isosceles triangle case described by Kahn¹⁰ with an additional coupling constant J' . For the last magnetic model the appropriate Hamiltonian expression contains two coupling constants and has the following form:

$$\hat{H} = -J (\hat{S}_1 \hat{S}_2 + \hat{S}_1 \hat{S}_3) - J' (\hat{S}_2 \hat{S}_3) \quad (2)$$

with the energy eigenvalue expressed as following:

$$E(S, S') = -\frac{J}{2} S(S+1) - \frac{J' - J}{2} S'(S'+1)$$

with $\hat{S}' = \hat{S}_1 + \hat{S}_2$ and $\hat{S} = \hat{S}' + \hat{S}_3$.

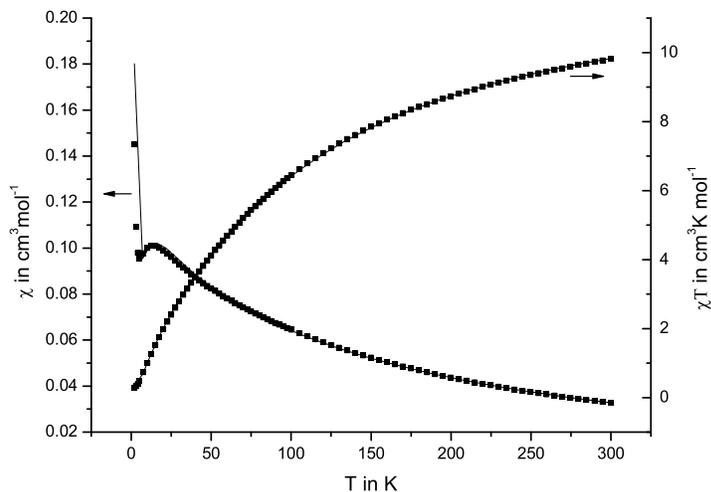


Figure 2.18: Temperature-dependent susceptibility measurements for complex **3** as χ vs. T and χT vs. T plots. The solid lines represent the theoretical curves calculated with Van Vleck equation described in the text. Squares represent the measured values.

Although the crystallographic characterization of trinuclear iron(III) azacusters **2** and **3** compounds showed no equivalence of the constituting Fe(III) centers, their magnetic properties are very close to the magnetic behavior of complex **1** that contain three equivalents metal centers and for which an isosceles triangle can be used to interpret the experimental data set. Therefore such a model may be used to interpret the magnetic behavior of all three Fe(III) azacompounds. In this case $J = J'$ in the Hamiltonian expression **2** which leads to the energy expression:

$$E(S) = -\frac{J}{2}S(S+1)$$

By inserting this energies into the Van Vleck formula and taking into account intermolecular interaction (θ) and paramagnetic impurities (ρ) the dependence of the χT product can be described by the following final equation:

$$\chi T = \frac{N_A \beta^2 g^2}{3k(T-\theta)} \left((1-\rho) \frac{\sum_{S'=0}^{2S_1} \sum_{S=|S'-S_2|}^{S'+S_2} S(S+1)(2S+1)e^{-\frac{E(S)}{kT}}}{\sum_{S'=0}^{2S_1} \sum_{S=|S'-S_2|}^{S'+S_2} (2S+1)e^{-\frac{E(S)}{kT}}} \cdot T + \rho \cdot S(S+1) \right) \quad (3)$$

For complex **1**, the best fit of the magnetic data set through the above equation was obtained for $g = 2.09 \pm 0.003$, $J = -9.28 \pm 0.06$ for fixed $\rho = 0$ in order to avoid overparametrization. The resulting reliability factor is $R^2 = 0.99987$ for $\theta = 0.29 \pm 0.10$ with the calculated curve (solid line in Figure 2.16) that matches well to experimental magnetic data set. Similar results have been obtained for complex **2**, where a good agreement between experimental data set and the calculated one was obtained for $g = 2.06 \pm 0.0015$, resulting in a coupling exchange constant $J = -7.68 \pm 0.034$ with $\theta = 0.21 \pm 0.062$ and reliability factor $R^2 = 0.99995$ (Figure 2.17, solid lines). In the case of complex **3**, the best fit of the experimental data set was obtained for ρ and θ fixed as zero values, resulting in a coupling exchange constant $J = -8.95 \pm 0.03$ for $g = 1.96 \pm 0.001$ and a reliability factor $R^2 = 0.99991$ (Figure 2.18).

Hence, it can be concluded that the three iron azacrown compounds comprising three six-coordinated Fe(III) ions facilitate an antiferromagnetic exchange coupling between 5/2 spin centers which represents a common feature for the metallocrown compounds class. The magnitude of the antiferromagnetic interaction within the triad Fe₃^{III}-core is similar with reported antiferromagnetic coupling of the Fe(III) centers in iron-containing azacrown complexes,^{90,100} but stronger than reported value of -4.92 cm^{-1} for trinuclear Fe(III) compounds with $-\text{[M-N-O]}-n$ repeating units.⁸⁰

For the tetranuclear [2+2] grid-compound **4**, the value χT at 300 K is $12.00 \text{ cm}^3 \text{ K mol}^{-1}$ which is substantially smaller than the calculated spin-only value of $17.50 \text{ cm}^3 \text{ K mol}^{-1}$ for four noninteracting Fe(III) centers, assuming $g = 2.0$. Again, the magnetic interaction suggests overall antiferromagnetic exchange coupling with χT product decreasing steadily to a value of $0.22 \text{ cm}^3 \text{ K mol}^{-1}$ at 3 K. Correspondingly, χ increases gradually reaching a maximum at 17.5 K and decreases gradually as the temperature is decreased to 3.5 K (Figure 2.19).

Based on structural topology, the magnetic interaction can be explained considering one coupling exchange constant (J) for four equivalents high spin Fe(III) centers. The Hamiltonian used in this case has the following expression:

$$\hat{H} = -J(\hat{S}_1\hat{S}_2 + \hat{S}_2\hat{S}_4 + \hat{S}_3\hat{S}_4 + \hat{S}_1\hat{S}_3)$$

with $S_1 = S_2 = S_3 = S_4 = 5/2$.

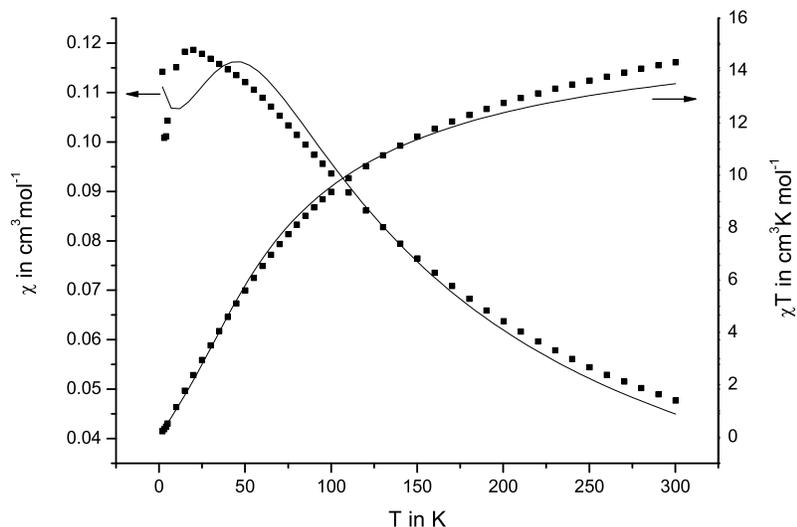


Figure 2.19: Plots of thermal dependence of χ_M (empty squares) and $\chi_M T$ product (black filled circles) for complex **4**, measured with an applied magnetic field of 2000 Oe; the solid lines represent the theoretical curves.

The best fit of the experimental values was obtained for $\chi_M T$ vs T plot based on the above mentioned Hamiltonian expression and led to $J = -6.14 \pm 0.142 \text{ cm}^{-1}$ and $g = 1.91 \pm 0.017$ for a paramagnetic impurity $\rho = 0.01 \pm 4.4 \cdot 10^{-4}$. The simulation of the experimental data set has been achieved with a reliability factor $R^2 = 0.97377$ which shows a good agreement between calculated and experimental data sets. This coupling constant value is smaller than reported magnitude of the antiferromagnetic interaction between aza-bridged Fe(III) centers estimated to be $J/k = -5.61 \text{ K}$ ($J = -8.13 \text{ cm}^{-1}$) for neighboring Fe(III) centers in octanuclear iron(III) complex⁹⁰ and very close to antiferromagnetic coupling interaction existent in Fe₆-azacrown compounds for which $J/k = -4.87 \text{ K}$ ($J = -7.00 \text{ cm}^{-1}$) has been reported between neighboring Fe(III) centers.¹⁰⁰ Compared to magnitude of the antiferromagnetic coupling interaction which occurs in the trinuclear Fe(III) aza-crown complexes described previously, in the tetranuclear iron complex **4**, the iron(III) centers are weaker antiferromagnetic coupled. This may be a consequence of larger Fe...Fe interatomic separation in the last case and also larger Fe-N-N-Fe torsion angles (165° in complex **4** compared to 150° in the symmetric complex **1**).

2.4 Ni(II)-complexes with N-imidazol-2-yl-salicyloyl hydrazide ligand

Stoichiometric reaction of N-imidazol-2-yl-salicyloyl hydrazide ($H_2\text{imsalhy}$) ligand with $Ni(NO_3)_2$ in $CH_3CN/MeOH$ solvents mixture in presence of NaOH base yield a clear yellow-solution from which $[Ni(\text{imsalhy})_2] \cdot 4CH_3CN$ complex (**5**) has been isolated. Conversely to stoichiometric reaction of the Schiff base - $H_2\text{imsalhy}$ ligand with $FeX_3 \cdot nH_2O$ salts where a self-assembly process occurred to yield tri- and tetranuclear compounds, the similar reaction pathway with nickel(II) salts affords only mononuclear Ni(II) complex **5**. The coordination mode of the supporting ligand is also different compared to its chelating fashion described for iron(III) complexes. The Schiff base ligand acts as tridentate chelate system embedding nickel ion by two pairs of five-membered rings with a uncoordinated phenolate group (Figure 2.20). The molecular structure determination shows the Ni(II) ion in distorted octahedral geometry formed by pair of N_2O donor atoms of two equivalent ligand molecules. The Ni–N bond distances are around 200.3 pm (Ni–N2) and 211.1 pm (Ni–N4), similar with corresponding bond lengths in iron(III) complexes. The Schiff base ligand is present in its iminolate form, hence a Ni–O2 bond distance of 211.2 pm and single bond character for C7–O2 bond of 127.0 pm.

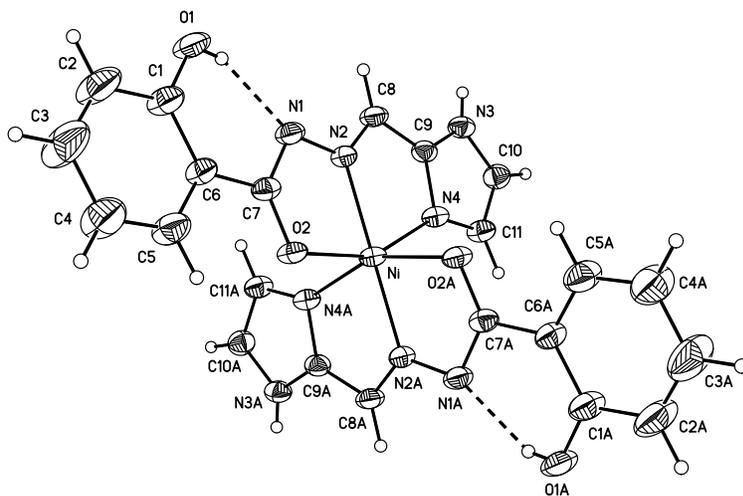


Figure 2.20: Molecular structure and numbering scheme of complex $[Ni(\text{imsalhy})_2] \cdot 4CH_3CN$ (**5**). Intramolecular hydrogen bonding interactions are also shown as dashed lines.

Table 2.6: Selected bond lengths (pm) and angles ($^{\circ}$) for complex **1a**.

Ni–O2	211.17(18)	Ni–N2	200.3(2)
Ni–N4	211.1(2)	O2–C7	127.0(3)
O2–Ni–O2A	91.74(10)	N2–Ni–N4	78.99(8)
N2–Ni–O2	76.40(7)	N2–Ni–O2A	101.49(7)
N2–Ni–N2A	177.04(11)	N2–Ni–N4A	103.09(8)
N4–Ni–N4A	93.15(11)	N4–Ni–O2A	92.76(7)
N4–Ni–O2	155.38(7)	-	-

Complex **5** crystallizes in the monoclinic C_{2c} space group as a centrosymmetric compound. The uncoordinated phenolate functionalities are involved in bifurcated intra- and intermolecular hydrogen bonding interactions. Intramolecular hydrogen bonding contacts are established with the hydrazide nitrogen atoms ($O1 \cdots N1$ and $O1A \cdots N1A$) of 253.6 pm and intermolecular hydrogen bonding contacts with the protonated nitrogen atoms of the imidazole moieties ($O1 \cdots N3$ 280.3 pm) of neighboring nickel(II) molecules (Figure 2.21). This has as result a 2-D rhombohedrons "brick-walls"-like architectures which can be imaged as infinite-columnae architectural motif similarly to Brancusi sculptural masterpiece (Figure 2.22).

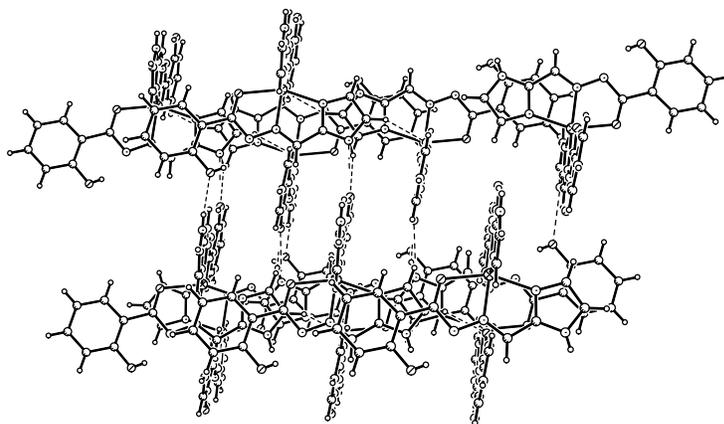


Figure 2.21: Packing diagram of complex **5** as viewed along the a axis showing the hydrogen bonding interaction between sheets of Ni(II) units. Lattice molecules have been omitted for the sake of clarity of the picture.

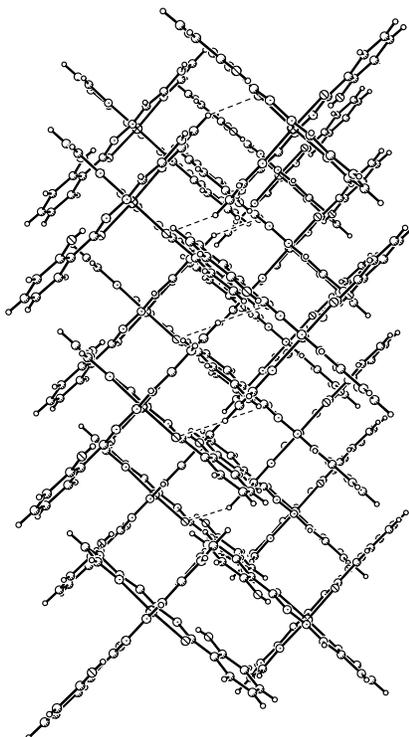


Figure 2.22: Packing diagram of complex **5** as viewed along the a axis . Lattice molecules have been omitted for a better clarity of the picture.

2.5 Conclusions and future perspectives

In summary a series of three neutral trinuclear iron complexes with mixed ligand composition have been isolated and fully characterized. Each iron atom is six-coordinated with the dianionic pentadentate ligand fulfilling five of the coordination sites of the metal center, whereas monodentate chelate coligands such as chloride, azide and isothiocyanate occupy the remained vacant position of the metal center. The structural core is based on $[\text{Fe-N-N}]_3$ linkage which led to a 9-membered aza ring motif. These complexes represent rare example of azametallacrown compounds based on Fe(III) ion metal and in addition the first examples of trinuclear iron(III) complexes in which the presence of μ_3 -bridged mode of oxygen atom is not present. The structural topology of these complexes is also retained in solution as could be proved by spectroscopic characterization methods. The magnetic behavior can be described as overall antiferromagnetically mediated by diazine bridges between neighboring Fe(III) centers with coupling constant values that fall in

the -7.68 cm^{-1} to -9.28 cm^{-1} . The very close coupling interaction J values within the series of trinuclear complexes originate from the fact that a similar Fe···Fe separation has been observed. Interesting structural features have been found for the isothiocyanate derivative of type $[\text{Fe}(\text{L})(\text{NCS})]_3$ which presuppose the *host-guest* concept, encapsulating nitrate anion in the cavity of the Fe_3 ring. Moreover, this compound supports a ring expansion leading to a tetranuclear Fe(III) complex with the structural core based on 12-membered aza-ring motif which can be regarded as **[2+2]** grid compound.³² The complex showed an alternating chirality at the iron centers with the isothiocyanate ligand in Δ and Λ configurations in relation with the two faces of the tetranuclear ring. The $[\text{Fe}-\text{N}-\text{N}]_4$ linkage is also responsible for the antiferromagnetic exchange interaction between the iron centers ($J = -6.14 \text{ cm}^{-1}$).

A common synthesis pathway for designing high-spin molecules involves reaction between cationic assemblies and anionic molecules. The triad Fe_3 -core of the series of trinuclear iron(III) complexes described herein may be considered as cationic triad-core with labile coordination position on each metal center. Hence, such a coordination unit can be successfully used as molecular brick to construct high-nuclearity metal clusters. Organic radical molecule with p -carrier electron favors strong magnetic interaction and therefore desirable to build up high-spin magnetic materials. The proposed organic radical (Figure 2.23, first structure) presents a free $-\text{COOH}$ functionality which may be used to replace the halide and pseudohalide monodentate ligands of above described trinuclear Fe(III) complexes. Cyanide-bridged polynuclear complexes of Prussian Blue type are highly desirable due to their rich chemical properties, i.e. single-molecule magnets, photomagnetism and/or building blocks to design coordination polymers with different dimensionality.¹¹¹⁻¹¹³ Cyanide-bridge mediates strong magnetic interaction between metal centers and bimetallic Prussian Blue type solids were reported to exhibit spontaneous magnetization at temperature as high as 376 K.¹¹⁴ According with the proposed strategy to isolate cyanide-bridged polynuclear complexes, halide and/or pseudohalides are the best "leaving groups", easily replaceable by cyanide ligand. Therefore, cyanide derivatives depicted in Figure 2.23 may also be used to construct extended magnetic dendrimers.

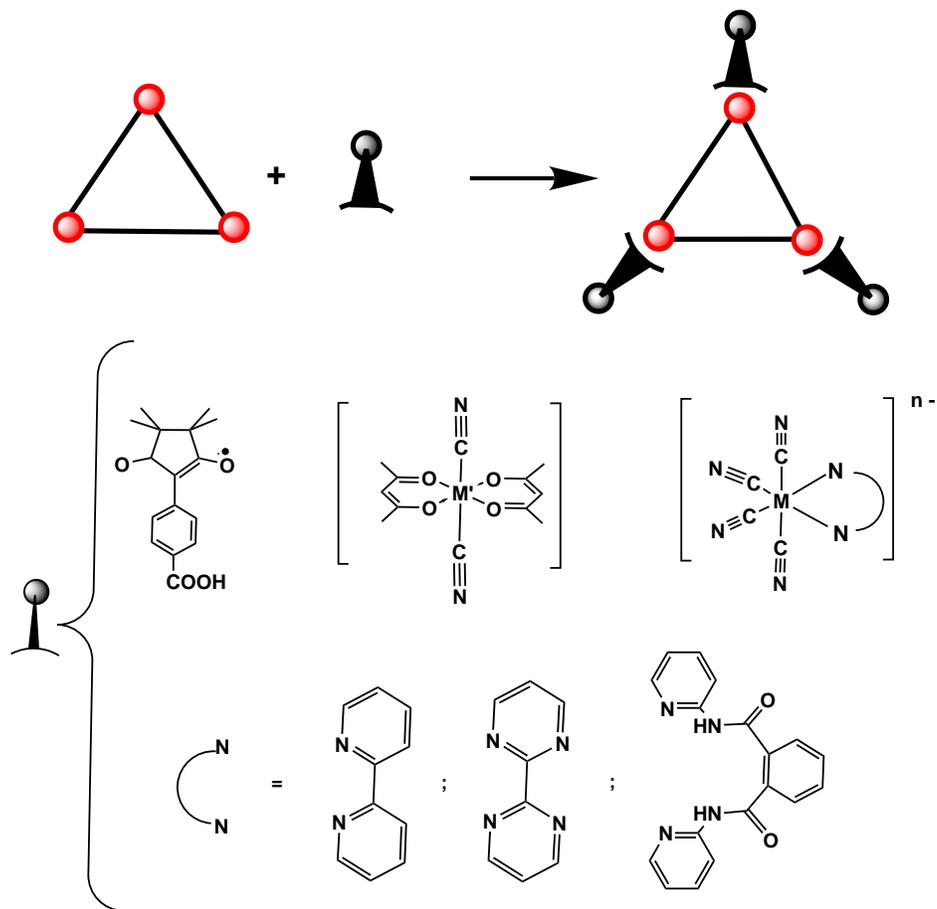


Figure 2.23: Schematic representation of the possible reactivity of trinuclear Fe(III)-core (up) and proposed "building" units (down) for design of new high-nuclearity magnetic dendrimers.

On the other hand, regarding the isolated mononuclear Ni(II)-complex **5**, an interesting future perspective is represented by modification of the supporting organic ligand, namely a hydrazide derivative of dicarboxylic acid (Figure 2.24). The new organic framework can accommodate at least two Ni(II) ions and/or following a self-assembly strategy to yield grid-type compounds with high-nuclearity topology.

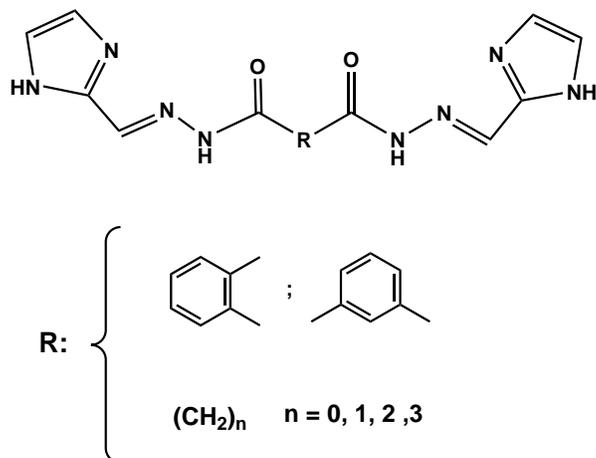


Figure 2.24: Schematic representation of the proposed organic framework capable to form polynuclear d-metal complexes.

2.6 Experimental Part

Schiff base ligand - H₂imsalhy

2-Imidazole-carboxaldehyde (2.40 g, 2.50 mmol) was added stepwise to a solution of salicyloylhydrazide (3.80 g, 2.50 mmol) dissolved in methanol (50 mL). The resulting mixture was stirred under reflux when a clear solution formed. The reflux has been continued until a precipitate starts to be formed and the reaction was continued overnight at room temperature. The precipitate was filtered off and washed with cold methanol and diethylether and used without further purification. Yield: 4.68 g (2.03 mmol, 81.2%). *Anal.* Calc. for C₁₁H₁₀N₄O₂ (230.25): C 57.39, H 4.38, N 24.34. Found: C 56.84, H 4.40, N 23.85. ¹H NMR (400 MHz, DMSO-d₆): δ = 6.93-7.00 (m, 3H, arom. CH), 7.17 (br, 2H, imidazole NH), 7.35-7.53 (m, 2H, imidazole CH), 7.80-7.86 (m, 1H, arom. CH), 8.37 (s, 1H, CH=N), 11.83 and 12.88 (br. NH and OH) ppm. ¹³C NMR (100 MHz, DMSO-d₆): δ = 116.0 116.7 (arom. C), 117.2, 117.4, 118.9, 119.3, 128.5, 130.3 (arom. CH), 133.8, 134.0 (imidazole CH), 140.4, 141.0 (CH=N) ppm), 142.2 (imidazole C), 158.9 (arom. C-OH), 167.7 (C=O) ppm. Selected IR data (cm⁻¹): 3435 (br, NH), 3213 (br, OH intermolecular hydrogen bonded), 3125 (s, NH imidazole), 1665 (s, CO), 1600 (w, -CH=N-N=C-), 1539 (s, -CH=N). UV/Vis (CH₃OH solution, λ_{max} in nm (ε in 10³ M⁻¹ cm⁻¹)): 240 (11032), 326 (4150).

Iron complexes

[Fe(imsalhy)(Cl)]₃·3CH₃OH (1). To the H₂imsalhy ligand (115 mg, 0.5 mmol) suspended in MeOH (15 mL) was added one equivalent of NaOH (0.5 mL of 1 N aqueous solution) which cause a dissolution of the ligand. To this resulting solution, FeCl₃·6H₂O (135 mg, 0.5 mmol) dissolved in MeOH (5 mL) was added stepwise under continuous stirring and the reaction mixture stirred at room temperature for 15 minutes. The black solution was filtered and left at room temperature for slow evaporation of the solvent. Black prismatic crystals suitable for X-ray measurement were obtained within two days. Yield: 88 mg (0.1 mmol, 54%). *Anal. Calc.* for C₃₃H₂₄Cl₃N₁₂O₆Fe₃·H₂O (976.521): C 40.85, H 2.55, N 17.48. Found: C 40.59, H 2.67, N 17.51. Selected IR data (cm⁻¹): 3430 (br, H₂O), 3125 (s, NH imidazole), 1595 (s, -CH=N-N=C-), 668, 639 (s, Fe-O), 560, 506 (s, Fe-N). UV/Vis (CH₃OH solution, λ_{max} in nm (ε in 10³ M⁻¹ cm⁻¹)): 257 (3913), 319 (3750), 519 (1060). FAB-MS (nba): m/e = 375 [Fe₂(imsalhy)]Cl, 851.0 [Fe₃(imsalhy)]⁻, 886.0 [Fe₃(imsalhy)Cl]⁻, 921.0 [Fe₃(imsalhy)Cl₂]⁻, 958.0 [Fe(imsalhy)Cl]₃.

[Fe(imsalhy)(Cl)]₃·3CH₃CH₂OH (1·3EtOH) has been isolated following the above procedure by replacement of MeOH with EtOH. Yield: 94 mg (0.08 mmol, 51%). *Anal. Calc.* for C₃₃H₂₄Cl₃N₁₂O₆Fe₃·3EtOH (1096.71): C 42.71, H 3.86, N 15.33. Found: C 42.43, H 4.33, N 14.62.

[Fe(imsalhy)(N₃)]₃·3.5DMF (2). To the H₂imsalhy ligand (115 mg, 0.5 mmol) suspended in MeOH (20 mL) was added one equivalent of NaOH (0.5 mL of 1 N aqueous solution) which cause a dissolution of the ligand. To this resulting solution, Fe(NO₃)₃·9H₂O (202 mg, 0.5 mmol) dissolved in MeOH (5 mL) was added stepwise under continuous stirring followed by addition of solid NaN₃ (65 mg, 1.0 mmol) and the reaction mixture stirred at room temperature for 60 minutes. The black solution was filtered and additional DMF (5 mL) was added. The solution was left undisturbed at room temperature for slow evaporation of the solvent. Black prismatic crystals suitable for X-ray measurement were obtained within one month. Yield: 42 mg (0.10 mmol, 20%). *Anal. Calc.* for C_{43.5}H_{48.5}N_{24.5}O_{9.5}Fe₃ (1234.14): C 42.33, H 3.96, N 27.80. Found: C 42.31, H 3.80,

N 18.24. Selected IR data (cm^{-1}): 3435 (br, solvent), 3132 (m, NH imidazole), 2059 (s, azide), 1597 (s, $-\text{CH}=\text{N}-\text{N}=\text{C}-$), 673, 635 (s, Fe–O), 583, 560 (s, Fe–N). UV/Vis (CH_3OH solution, λ_{max} in nm (ε in $10^3 \text{ M}^{-1} \text{ cm}^{-1}$): 256 (4841), 319 (4792), 512 (1307).

[Fe(imsalhy)(NCS)]₃·(H₃imsalhy)·(NO₃)·0.5H₂O·4.25CH₃OH (3). This complex was prepared following the procedure previously described for **2** by replacement of sodium azide with KSCN (2 equiv, 97 mg, 1.0 mmol) dissolved in methanol (5 mL). The resulting methanolic solution was filtered and left to stand at room temperature. Black needle-shape crystals start to appear within three-four hours. Yield: 109 mg (0.23 mmol, 47.5%). *Anal. Calc.* for $\text{C}_{47}\text{H}_{35}\text{N}_{19}\text{O}_9\text{S}_3\text{Fe}_3\cdot 4\text{H}_2\text{O}$ (1377.67): C 40.98, H 3.15, N 19.32, S 6.92. Found: C 40.56, H 3.12, N 19.48, S 6.96. Selected IR data (cm^{-1}): 3430 (br, H₂O), 3132 (m, NH imidazole), 2040 (s, SCN), 1646 (m, C=O), 1595 (s, $-\text{CH}=\text{N}-\text{N}=\text{C}-$), 1558 (s, $-\text{CH}=\text{N}$), 669, 640 (m, Fe–O), 560, 506 (m, Fe–O). UV/Vis (CH_3OH solution, λ_{max} in nm (ε in $10^3 \text{ M}^{-1} \text{ cm}^{-1}$): 246 (3951), 324 (5593), 511 (1054). UV/Vis (BaSO_4 mixture, λ_{max} in nm): 213, 254, 323, 538. FAB-MS (nba): $m/e = 231$ [$\text{H}_2\text{imsalhy}-\text{H}^+$], 851.0 [$\text{Fe}_3(\text{imsalhy})^-$], 886.0 [$\text{Fe}_3(\text{imsalhy})(\text{NCS})^-$], 967.0 [$\text{Fe}_3(\text{imsalhy})(\text{NCS})_2^-$], 1025.0 [$\text{Fe}(\text{imsalhy})(\text{NCS})_3^-$].

[Fe(imsalhy)(NCS)]₄·4CH₃OH (4). This tetranuclear complex was prepared following two procedures: i) similarly to previously described synthesis of **3** using two equivalents of NaOH (1.0 mL of 1 N aqueous solution) for dissolution and deprotonation of the H₂imsalhy ligand and the same amount of the KSCN (97 mg, 1.0 mmol) as coligand and ii) following the procedure described for preparation of complex **1** using additionally KSCN (2 equiv., 97 mg, 1.0 mmol) dissolved in MeOH (5 mL). In both cases the resulting black methanolic solutions were filtered and left to stand at room temperature. Black needle-shape crystals were formed within two days in both cases. Yield: 35 mg (0.1 mmol, 18%) for i) method and 90 mg (0.26 mmol, 52%) for ii) method. *Anal. Calc.* for $\text{C}_{48}\text{H}_{36}\text{N}_{20}\text{O}_8\text{S}_4\text{Fe}_4$ (1373.28): C 41.62, H 3.49, N 18.67, S 8.55. Found: C 41.28, H 3.09, N 18.94, S 8.38. Selected IR data (cm^{-1}): 3400 (br, MeOH), 3153 (m, NH imidazole), 2049 (s, SCN), 1600 (s, $-\text{CH}=\text{N}-\text{N}=\text{C}-$), 1600 (m, NO₃), 672, 638 (m, Fe–O), 560 (m, Fe–O). UV/Vis (CH_3OH solution, λ_{max} in nm (ε in $10^3 \text{ M}^{-1} \text{ cm}^{-1}$): 244 (3950), 324

(3653), 508 (1072). UV/Vis (BaSO₄ mixture, λ_{max} in nm): 241, 273, 322, 540. FAB-MS (nba): m/e = 231 [H₂imsalhy)-H⁺], 345 [Fe(imsalhy)(NCS)+3H⁺], 851.0 [Fe₃(imsalhy)]⁻, 909.0 [Fe₄(imsalhy)₃]⁻, 967.0 [Fe₄(imsalhy)(NCS)]⁻, 1080.0 [Fe₄(imsalhy)₃(NCS)₂], 1139 [Fe₄(imsalhy)₃(NCS)₃] or [Fe(imsalhy)]₄⁴⁻.

Synthesis of [Ni(imsalhy)₂].4CH₃CN (5)

To a suspension of H₂imsalhy ligand (115 mg g, 0.5 mmol) suspended in MeOH/CH₃CN 1:2 (15 mL) was added one equivalent of NaOH (0.5 mL of 1 N aqueous solution) which cause a dissolution of the ligand. To this resulting solution, Ni(NO₃)₆H₂O (135 mg, 0.5 mmol) dissolved in MeOH (5 mL) was added stepwise under continuous stirring and the reaction mixture stirred at room temperature for 15 minutes. The pale-yellow solution was filtered and left at room temperature for slow evaporation of the solvent. Brown prismatic crystals suitable for X-ray measurement were obtained within a week. Yield: 156 mg (0.28 mmol, 32%). *Anal.* Calc. for C₂₂H₁₈N₈O₄Ni·CH₃CN (558.186): C 51.64, H 3.79, N 22.58. Found: C 51.41, H 3.77, N 22.55. Selected IR data (cm⁻¹): 3400 (br, OH phenolate), 3125 (s, NH imidazole), 1610 (s, -CH=N-N=C-), 670 (s, Ni-O), 550 (s, Ni-N).

Chapter 3

Triaminoguanidine derivatives as supports to construct magnetic assemblies

The development of new strategies to design polynuclear metal complexes has led to a tremendous research activity. This has been fueled by their relevance in understanding the biological functions of metalloenzyme^{115,116} as well as due to their potential applications as catalysts and magnetic^{117,118} materials. A large variety of metallo-clusters have been reported with structural assemblies such as honeycomb, grids, diamondoid and helical motifs.⁴⁴⁻⁵¹ These have paved the field of crystal engineering^{119,120} that is close linked to supramolecular chemistry. Supramolecular chemistry defined by Lehn⁴³ as "*chemistry beyond molecule*" is regarded as self-organization in solid state of predefined molecules through non-covalent interactions, i.e hydrogen bonding, Van der Waals and π - π -stacking interactions. The non-covalent interactions lead not only to supramolecular arrangement of the molecules, but are also responsible for interesting properties. The resulting architectural edifices have been reported to function as molecular recognition agents and/or to possess ion-exchange and transport capacity.¹²¹⁻¹²⁶ Stacking interaction were found able to mediate both ferro- and antiferromagnetic coupling between the metal centers.^{127,128} In addition, cooperative effect of discrete molecules and non-covalent interactions observed in solid state have been reported as corroborative phenomena that may

induce thermal hysteresis which confers memory effect to a magnetic material.^{129,130} Inorganic supramolecular networks and coordination polymers have been isolated through self-assembly reactions between multifunctional organic ligands and metal ions. The process relies upon the preference of metal ion for a particular geometry and the number, type and arrangement of the ligand binding sites.^{119,131,132} The careful selection of the appropriate ligand plays the key role in self-assembly process and it determines the variety of molecular architecture.^{32,44,126} A rational design of supramolecular assemblies has also been developed in 1990 by Robson et al.¹³³ This is based on so called "node" and "spacer" strategy in which both, the supporting organic framework and the linker are judiciously selected. The most used bridging entity in this last synthetic pathway is represented by 4,4'-bipyridine/ or derivatives of this,^{134,135} capable of generating from one- to three-dimensional networks depending on the used metal ions. This alternative made possible the step-by-step design of extended structures. The supramolecular architectures have been isolated predominantly from C_2 symmetric organic ligands, whereas the use of C_3 symmetric organic framework has been less employed in isolation of coordination compounds.^{136,137} A multitude of inorganic-organic hybrids with C_3 -symmetry contain 1,3,5-tricarboxylic,¹³⁸⁻¹⁴² which presents the disadvantage of chelating capacity. This last organic ligand occupies limited positions of the coordination sphere of d-transition metals and hence the uncontrolled coordination polymer formation. Given the obvious importance of the supporting organic ligand, the role of tris-(N-salicylidene)-amino guanidine hydrazide is evident. The organic framework has a planar structure, with three symmetric cavities capable of stronger chelation of d-transition metals, independently on their preferred geometry.⁴⁰ Robson and Müller *et al.*¹⁴³⁻¹⁴⁸ reported the synthesis of interesting discrete cage molecules with various topologies using Pd^{II} , Cd^{II} , Cu^{II} and Mo^{VI} metal ions and triaminoguanidine-based ligand. From the magnetochemistry point of view, this polydentate system with C_3 symmetry is versatile because it may yield trinuclear metal-complexes with a resulting non-zero spin ground state when capping ligand are employed to complete the coordination sphere of the metal ions.³³⁻⁴⁰ In absence of capping ligands, inorganic coordination polymers are to be obtained through μ -phenoxy bridges formed between metal centers.¹⁴⁹ The judicious selection of capping ligand systems may give the opportunity to obtain interesting supramolecular assemblies by self-organization of trin-

uclear complex unit in solid state and in addition, the possibility to construct dendritic materials following a "step-by-step" strategy. Therefore, 2,2'-bipyridine (bipy) and 2,4,6-tris(2-pyridyl)-1,3,5-triazine (tptz) have been employed as co-ligands in order to avoid the uncontrolled polymerization of polynuclear complexes. The bipy is a middle-strong field ligand, used extensively to induce spin crossover behavior in Fe(II)-complexes,^{150,151} whereas tptz ligand shows different coordination modes. The predominant chelating capacity of tptz ligand is tri-dentate terpyridine-like (I), but may also coordinate through a combination of terpyridine and pyridine-like chelation accommodating two or three metal ions (II and III forms in Figure 3.1).¹⁵² Both ligand systems have been reported to form supramolecular assemblies through π - π -stacking interactions in solid state.^{153,154} The π - π -stacking interaction is a non-covalent interacting force, weaker than hydrogen-bond with a energy calculations around 10 KJ mol⁻¹ for typical aromatic-aromatic interactions, compared to ~ 40 KJ mol⁻¹ for hydrogen bonding interaction.^{155,156} In addition, it is worth mentioning here that, the tptz ligand can be hydrolyzed by metal ions, especially Cu^{II} to bis(2-pyridylcarbonyl) amine (bcpa) and its complexes.¹⁵⁷⁻¹⁶²

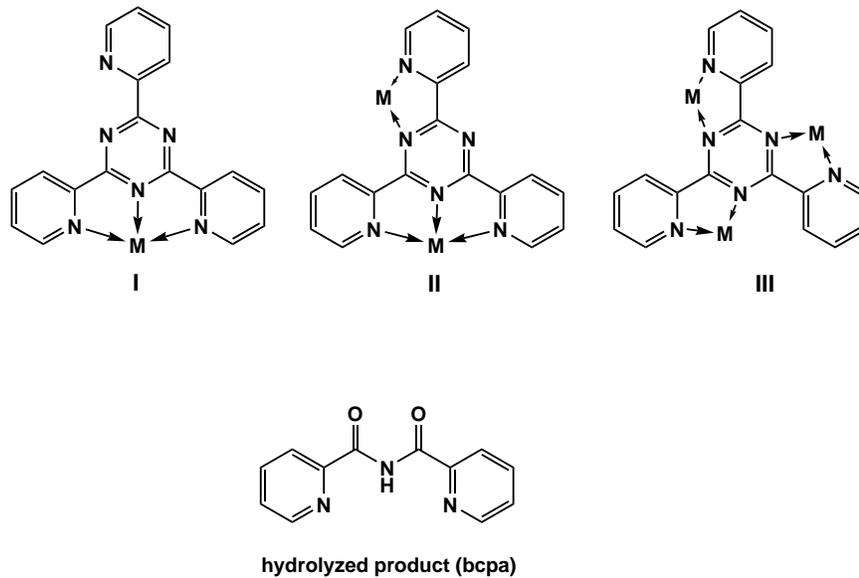


Figure 3.1: Schematic representation of the coordination modes of 2,4,6-tris(2-pyridyl)-1,3,5-triazine (tptz) ligand.

Another important aspect in coordination chemistry is represented by the influence of counter-ions in the resulting network structures, primarily by acting as either coor-

dinating or non-coordinating building blocks.^{44,163–165} In both cases, their implication in hydrogen binding interactions has lead to extended assemblies. Therefore, substituted triaminoguanidine-based Schiff base ligands have been reacted with Ni^{II} and Co^{II} salts and the magnetic properties of the resulting complexes have been analyzed. The importance of Ni^{II}-containing complexes in inorganic chemistry is well established and their relevance to biological system is obvious through large number of reports containing model complexes for nickel-containing enzymes.¹⁶⁶ In addition, single molecular magnets based on Ni^{II}-pyridone ligands and Ni₄^{II}-cubane complexes have also been reported.^{167–173} Thus, discrete trinuclear and pentanuclear Ni^{II}-containing complexes has been isolated using 2,2'-bipyridine and 2,4,6-tris(2-pyridyl)-1,3,5-triazine as co-ligands (Figure 3.2). On going from nickel to cobalt ions, a trinuclear Co^{III} complex has been isolated through hydrolysis of the tptz coligand (Figure 3.1).

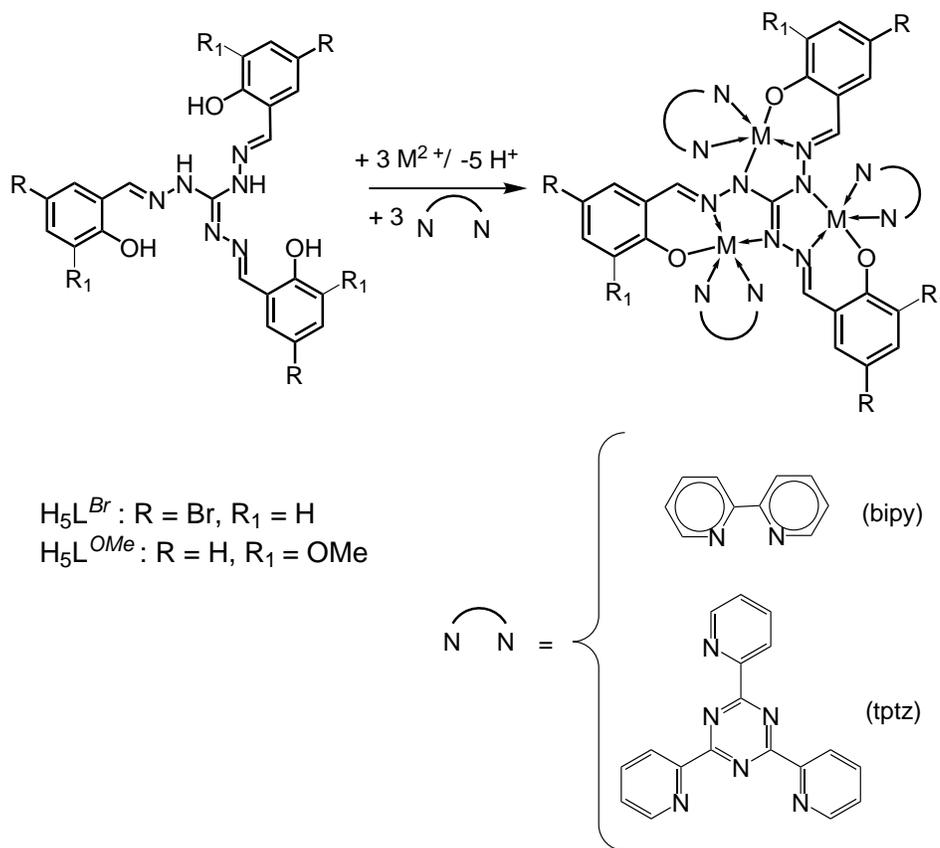


Figure 3.2: Schematic representation of the coordination mode of triaminoguanidine-based ligands and co-ligands used to isolate trinuclear Ni^{II}-complexes.

3.1 Trinuclear Ni(II)-complexes based on "triaminoguanidine"-ligand and 2,2'-bipyridine coligand

Reactions of triaminoguanidine-based ligand - H_5L^{Br} with various $NiX_{2 \cdot n}H_2O$ salts yield discrete trinuclear Ni(II)-complexes when three equivalents of 2,2'-bipyridine⁴⁰ have been used. The starting tris-nucleating ligand has been used as chlorhydrate salt, therefore excess of Bu_4NOH (six fold) has been used for both deprotection of guanidine moiety and deprotonation of the phenolic oxygen atoms in order to favor the coordination of d-transition metals.¹⁴⁷ Using $Ni(NO_3)_2 \cdot 6H_2O$ as metal salt, cationic trinuclear $[Ni_3L^{Br}(bipy)_3(OH_2)_3]NO_3 \cdot 8H_2O \cdot 1.5DMF \cdot 2.25MeOH$ complex could be isolated. Suitable crystals for X-ray diffraction with the same composition have been obtained by reaction of $Ni(ClO_4)_2 \cdot 6H_2O$ with H_5L^{Br} and 2,2'-bipyridine, using the same excess of base in presence of $Gd(NO_3)_3 \cdot 6H_2O$. The use of gadolinium salt was based on existing reports that describe the possible coordination of the lanthanide ion through μ -bridged phenolate moiety of two d-metal coordination entities (See Chapter 6). In this case, the gadolinium ion does not interfere in the previous observed coordination scheme of d-metals with triaminoguanidine-based ligand when 2,2'-bipyridine is used as coligand and it played the anion exchange role. Molecular structure and labeling scheme for complex **6** is depicted in Figure 3.3. This complex crystalizes within a month from MeOH/DMF solvents mixture as brown prismatic shaped crystals. Molecular structure determination shows a Ni_3 triad formed by Ni-N-Ni bridges with Ni...Ni interatomic separation of 499.01 pm and torsion angles of 168.73° for Ni-N-Ni and 175.76° for N-N-Ni-N respectively. Complex **6** crystallizes in the hexagonal $P6_3/m$ space group with C_3 symmetry axis that passes through the nitrate anion and the central C1 carbon atom of guanidine moiety. The nickel ions coordinated in the three symmetric tridentate pockets of the tris(5-bromo-2-hydroxybenzylidene)triaminoguanidine ligand are crystallographically identical in octahedral environment. Three coordination sites of each Ni(II) ion are occupied by the ON_2 donor atoms of the supporting ligand with the bite angles of 90.4° for O1-Ni-N2 and 77.5° for N2-Ni-N1A, respectively. Selected bond lengths and angles in complex **6** are listed in Table 3.1. The octahedral geometry of each nickel center is completed by water molecules which binds around 208.5 pm and bidentate bipy coligands

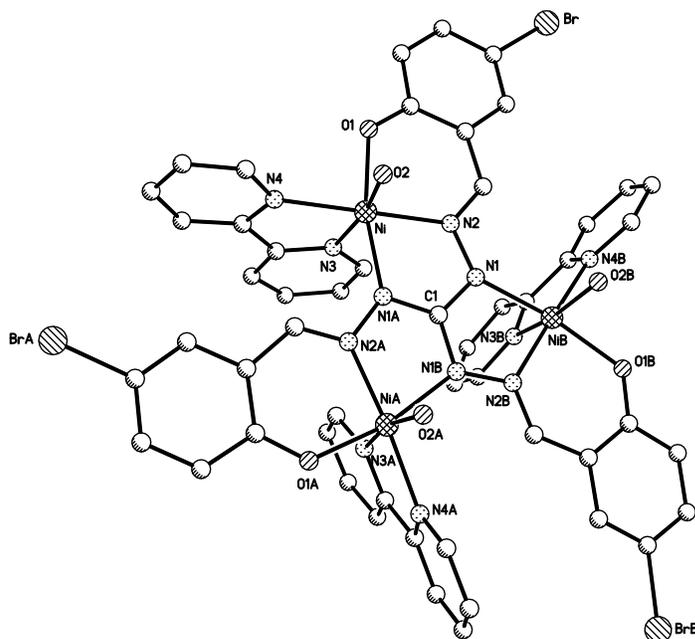


Figure 3.3: Molecular structure and selected numbering scheme of complex $[\text{Ni}_3\text{L}^{\text{Br}}(\text{bipy})_3(\text{OH}_2)_3]\text{NO}_3 \cdot 8\text{H}_2\text{O} \cdot 1.5\text{DMF} \cdot 2.25\text{MeOH}$ (**6**). Only the cationic core is shown; hydrogen atoms have been omitted for clarity.

with the bite angle N3-Ni-N4 of 78.06° and Ni-N bond distances of 209.06 (Ni-N3) and 208.99 (Ni-N4) pm. A tetragonal plane can be defined for the three donor atoms of the chelating ligand (O1-N1-N1A) and N4 nitrogen atom of the bipyridine ligand with the nickel ion displaced out from this plane by 16 pm, whereas the other nitrogen atom N3 of bidentate ligand and the water molecule occupies the apical positions of the distorted octahedron. The *trans* angles are 168.7° for N3-Ni-O1W , 173.7° and 167.01° for O1-Ni-N1A showing slight distortions compared to an ideal octahedral geometry. The dihedral angles between the defined tetragonal planes are two of 11.9° and one of 10.8° which shows a good planarity of the resulting trinuclear Ni(II) complex.

Cation complex **6** crystallizes with water, DMF and MeOH molecules as solvents of crystallization with the resulting formula $[\text{Ni}_3\text{L}^{\text{Br}}(\text{bipy})_3(\text{OH}_2)_3]\text{NO}_3 \cdot 8\text{H}_2\text{O} \cdot 1.5\text{DMF} \cdot 2.25\text{MeOH}$, whereas the nitrate anion is distorted. These lattice solvents form a strong hydrogen bonding interactions, with $\text{Ow} \cdots \text{OM}$ of 312.3 pm and $\text{Ow} \cdots \text{O}_{\text{DMF}}$ 274.5 pm (Figure 3.5). An interesting feature of the crystal packing diagram is represented by the presence of eight water molecules which form a water cluster^{174,175} through hydrogen bonding

interactions along the *a* axis (Figure 3.4) with $\text{Ow} \cdots \text{Ow}$ contacts that fall in the 256.0–287.0 pm. The un-bonded nitrate anion, placed in close vicinity of the trinuclear core is involved in hydrogen bonding interactions with the coordinated water molecules of two neighboring cation trinuclear Ni(II) units with $\text{O}_N \cdots \text{Ow}$ hydrogen bond distances of 264.7 pm.

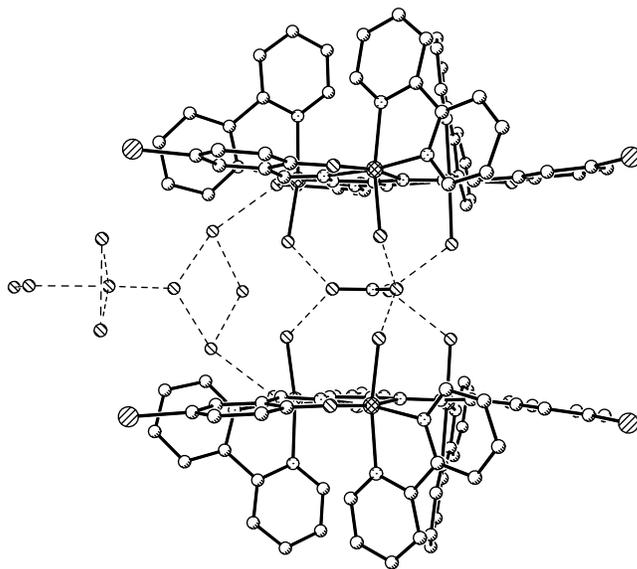


Figure 3.4: Sheets of $[\text{Ni}_3\text{L}^{\text{Br}}(\text{bipy})_3(\text{OH}_2)_3]\text{NO}_3 \cdot 8\text{H}_2\text{O}$ (**6**) complex linked by hydrogen bonding interactions formed by water lattice molecules and the nitrate anion as viewed along the *a* axis. Hydrogen atoms have been omitted for clarity.

An interesting arrangement has been noticed for the 2,2'-bipyridine co-ligands placed on the same site of the triaminoguanidine-based ligand forming an hydrophobic site, whereas the coordinated water molecules occupies the opposite site compared to the same plane (Figure 3.4) forming the hydrophilic part of the organized aggregates. The hydrophilic site of the assemblies are connected through hydrogen bonding interactions intermediated by water molecule (phenolate oxygen atom $\text{O1} \cdots \text{Ow}$ 273.6 pm) and nitrate anion, resulting in hydrogen bonding channels formed along the crystallographic *a* axis (Figure 3.5). On the other hand, the hydrophobic part with bipy constituents are additionally assembled through π - π -stacking interactions between off-slipped pyridine rings placed within interplanar distance of around 378.2 pm (Figure 3.6).

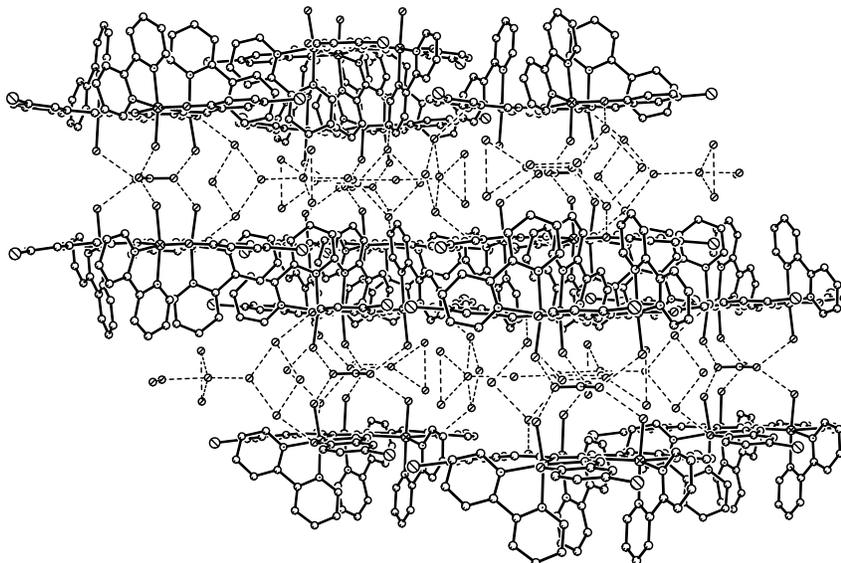


Figure 3.5: Packing diagram showing the formation of hydrogen bonding channels in $[\text{Ni}_3\text{L}^{\text{Br}}(\text{bipy})_3(\text{OH}_2)_3]\text{NO}_3 \cdot 8\text{H}_2\text{O} \cdot 1.5\text{DMF} \cdot 2.25\text{MeOH}$ (**6**) as is viewed along the crystallographic *a* axis. No hydrogen atoms have been included.

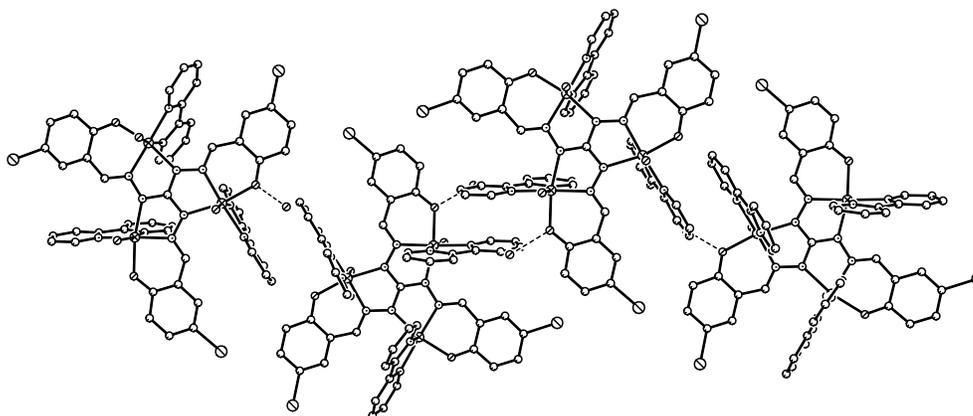


Figure 3.6: Packing diagram showing the π - π -stacking interactions as viewed along the crystallographic *c* axis in complex cation $[\text{Ni}_3\text{L}^{\text{Br}}(\text{bipy})_3(\text{OH}_2)_3]\text{NO}_3 \cdot 8\text{H}_2\text{O} \cdot 1.5\text{DMF} \cdot 2.25\text{MeOH}$ (**6**). Hydrogen atoms have been omitted for clarity.

Reaction of $\text{NiCl}_2 \cdot 6\text{H}_2\text{O}$ with $\text{H}_5\text{L}^{\text{Br}}$ and 2,2'-bipyridine in a ratio of 3:1:3 in MeOH-DMF- CH_3CN mixture and six folds base (Bu_4NOH), yields complex of type $[\text{Ni}_3\text{L}^{\text{Br}}(\text{bipy})_3(\text{DMF})_2\text{Cl}] \cdot \text{DMF} \cdot 2\text{CH}_3\text{CN} \cdot \text{MeOH} \cdot \text{H}_2\text{O}$ (**7**). Conversely to previous described cationic trinuclear Ni(II)-complex, the three nickel ions are now crystallographically distinct.

Table 3.1: Selected bond lengths (pm) and angles ($^{\circ}$) for complex **6**.

Ni–O1	203.9(3)	Ni–N1	208.2(3)
Ni–N2	202.1(4)	Ni–O2	208.4(3)
Ni–N3	209.2(4)	Ni–N4	209.3(4)
O1–Ni–N1	167.17(13)	O1–Ni–N2	90.52(13)
N2–Ni–N1	77.62(14)	N2–Ni–O2	94.78(13)
O1–Ni–O2	87.16(12)	N1–Ni–O2	88.96(13)
O1–Ni–N4	87.25(13)	O1–Ni–N3	95.16(14)
N1–Ni–N3	91.03(14)	N1–Ni–N4	105.05(14)
O2–Ni–N3	168.68(14)	O2–Ni–N4	91.05(13)
N2–Ni–N3	96.27(14)	N2–Ni–N4	173.65(14)
N3–Ni–N4	78.02(14)		

Complex **7** crystallizes in the P3 monoclinic space group. The tris(5-bromo-2-hydroxybenzylidene)triaminoguanidine ligand in classical mode and coordinates through phenolate and hydrazide nitrogen atoms accommodating one nickel ion per tridentate chelate pocket. The Ni–O and Ni–N bond distances are similar to previous described Ni(II)-complexes and fall in the 201.3-203.6 pm range for nickel-to-phenolate oxygen atom bond lengths and 200.4-210.4 pm range for nickel-to-hydrazide nitrogen bond distances. Each Ni(II) ion is sixth-coordinate, with N₄O₂ environment for Ni2 and Ni3 centers and N₄OCl coordination environment for Ni1 ion. Molecular structure and numbering scheme for complex **7** is shown in Figure 3.7. By comparison to previous described trinuclear nickel complex **6**, in complex **7** the coordinated water molecules have been replaced by DMF molecules that coordinate at Ni2 and Ni3 metal ions with bond lengths of 209.2 pm for Ni2–O4 and 215.2 pm for Ni3–O5, whereas Ni1 ion has a weak bonded chloride ligand anion (Ni1–Cl 246.2 pm) which also compensates the negative charge of the trinuclear Ni(II) complex.

Selected bond lengths and angles in complex **7** are listed in Table 3.2. The dihedral angles between the tetragonal planes defined by N₃O atoms (ONN from the chelate triaminoguanidine-based ligand and one nitrogen atom of bipy coligand) are 4.0, 8.6 and

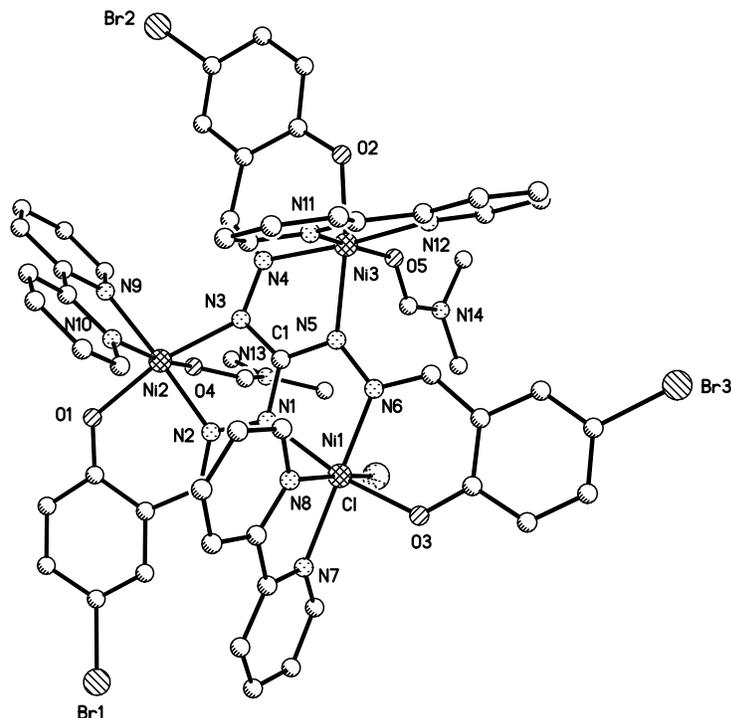


Figure 3.7: Molecular structure and selected numbering scheme of complex $[\text{Ni}_3\text{L}^{\text{Br}}(\text{bipy})_3(\text{DMF})_2\text{Cl}]\cdot\text{DMF}\cdot 2\text{CH}_3\text{CN}\cdot\text{MeOH}\cdot\text{H}_2\text{O}$ (**7**); thermal ellipsoids are drawn at 50 % probability; only the trinuclear core is shown.

11.7°, with the maximum value observed between the equatorial planes containing the coordinated DMF molecules at nickel ions. The three nickel atoms are connected through diazine N–N bridges with interatomic Ni···Ni separations of 501.0 (Ni1···Ni2), 501.3 (Ni2···Ni3) and 497.7 (Ni1···Ni3) pm and torsion angles of around 179.6–179.9° (Ni1–N6–N5–Ni3 and Ni1–N1–N2–Ni2) and 173.6° (Ni2–N3–N4–Ni3). The molecular structure of complex **7** contains also solvent of crystallization. Hydrogen bonding interactions involve only the lattice water that is within 286.7 pm hydrogen bonding away from the phenolate oxygen atom (O1) and further in hydrogen bonding contact with lattice DMF (Ow···O 292.4 pm). The crystal packing diagram is formed by trinuclear Ni(II)-entities arranged in stacking chains, with the coordinated DMF molecules oriented on the same side of the triminoguanidine-based ligand plane with the molecules of solvent of crystallization occupying the gaps between the metal-containing assemblies (Figure 3.8). Weak π - π stacking interactions are formed by 2,2'-bipyridine moieties which are not ideally face-to-face oriented (Figure 3.8) and within the interplanar distance of 368.7 pm.

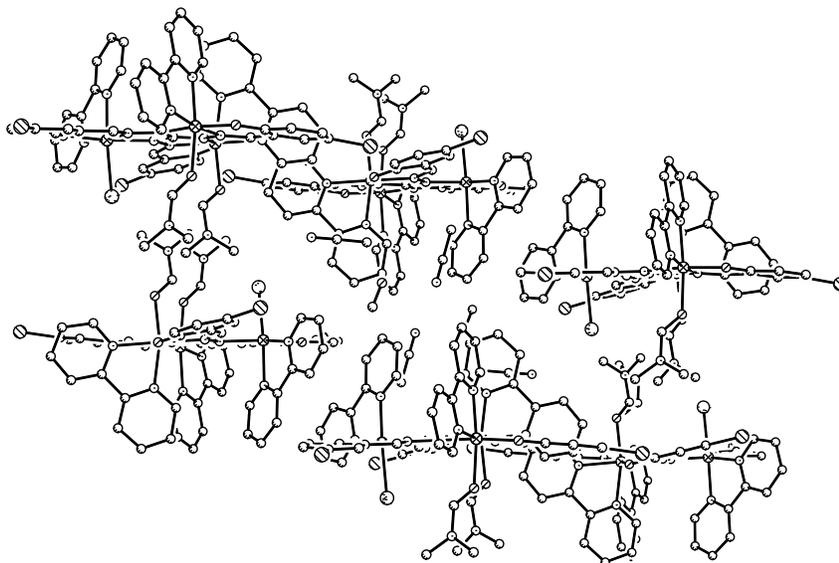


Figure 3.8: Packing diagram viewed along the *c* axis for complex $[\text{Ni}_3\text{L}^{\text{Br}}(\text{bipy})_3(\text{DMF})_2\text{Cl}] \cdot \text{DMF} \cdot 2\text{CH}_3\text{CN} \cdot \text{MeOH} \cdot \text{H}_2\text{O}$ (**7**).

IR Spectroscopy

The formation of both trinuclear Ni(II) complexes has also been confirmed spectroscopically. The IR spectra in both cases contain a broad band observed at $\sim 3400 \text{ cm}^{-1}$ due to the stretching vibrations of solvent molecules present in both crystal structures. In addition, characteristic stretching vibrations for tris(5-bromo-2-hydroxybenzylidene)triaminoguanidine ligand have been detected in IR spectra of both **6** and **7** complexes. The Schiff base stretching vibration ($-\text{CH}=\text{N}-$) has been shifted upon Ni(II)-coordination from $1696\text{--}1648 \text{ cm}^{-1}$ in the free ligand to around 1653 cm^{-1} in the trinuclear Ni(II)-complexes. The presence of 2,2'-bipyridine ligand is not easy to be identified by IR spectroscopy, but in the case of cationic complex **6**, the stretching vibration for the free nitrate ion¹⁰⁴ has been observed at 1384 cm^{-1} .

Table 3.2: Selected bond lengths (pm) and angles ($^{\circ}$) for complex **7**.

Ni1–O3	203.4(3)	Ni1–N1	208.8(4)
Ni1–N6	200.4(4)	Ni1–N7	209.9(4)
Ni1–N8	210.6(5)	Ni1–Cl	246.27(16)
Ni2–O1	203.6(4)	Ni2–O4	209.2(4)
Ni2–N2	202.1(4)	Ni2–N3	210.4(4)
Ni2–N9	208.9(4)	Ni2–N10	207.7(4)
Ni3–O2	201.3(4)	Ni3–O5	215.2(4)
Ni3–N4	201.7(4)	Ni3–N5	206.4(4)
Ni3–N11	210.2(5)	Ni3–N12	210.2(4)
O3–Ni1–N1	168.85(16)	N6–Ni1–O3	91.94(15)
N6–Ni1–N1	77.43(16)	N7–Ni1–N8	77.89(18)
O3–Ni1–Cl	95.99(11)	N6–Ni1–Cl	89.59(13)
N1–Ni1–Cl	87.38(13)	N2–Ni2–O1	90.15(15)
N2–Ni2–O4	92.63(16)	O1–Ni2–O4	90.05(15)
N2–Ni2–N3	76.70(16)	O1–Ni2–N3	166.79(15)
N10–Ni2–N9	78.64(17)	O2–Ni3–N4	91.48(16)
O2–Ni3–N5	168.51(16)	O2–Ni3–O5	87.19(17)
N5–Ni3–O5	89.97(17)	N4–Ni3–N5	77.62(16)

Magnetic properties of trinuclear Ni(II)-complexes based on "tri-aminoguanidine"-ligand and bipyridine coligands

Octahedral Ni(II) ions with d^8 electronic configuration are characterized by high-state $S = 1$ configuration.¹⁰ Variable temperature (2 - 300 K) magnetic susceptibility data were collected on microcrystalline samples for both complexes and are shown in Figure 3.10 and Figure 3.12 as $\chi_M = f(T)$ and $\chi_M T = f(T)$ plots. The room temperature values of $\chi_M T$ values are 3.39 and $\text{cm}^3\text{mol}^{-1}\text{K}$ for complex **6** and 4.88 $\text{cm}^3\text{mol}^{-1}\text{K}$ for complex **7**, respectively and decrease constantly reaching a minimum of 0.06 $\text{cm}^3\text{mol}^{-1}\text{K}$ for **6** and 1.65 $\text{cm}^3\text{mol}^{-1}\text{K}$ for complex **7** at 2 K. The room temperature measured value for complex **6** roughly corresponds to calculated value of 3.00 $\text{cm}^3\text{mol}^{-1}\text{K}$ for three uncoupled

Ni(II) ions with $S = 1$, assuming $g = 2$, but is much higher in the case of complex **7** compared to expected value. The gradual decrease of the $\chi_M T$ values observed in both cases describes an antiferromagnetic exchange coupling between the Ni(II) ions mediated by diazine N–N bridges, but the low temperature values differs from complex **6** to complex **7** and namely, it goes close to zero for complex **6** and reaches a value larger than one for complex **7**. On the basis of crystallographic data, two models in terms of exchange interaction were employed and therefore, the simulation of the magnetic data sets will be discussed separately. The Ni₃ triangular unit within the $[\text{Ni}_3\text{L}^{Br}(\text{bipy})_3(\text{OH}_2)_3]^+$ cation contains equal Ni–N–N–Ni bridges and Ni–N–N–Ni torsion angles. Thus, it can be approximated as equilateral triangle with three equal pairwise magnetic interactions.^{176–185} The magnetic exchange pathway in complex **6** is shown in Figure 3.9. The Heissenberg spin Hamiltonian involves a single exchange parameter coupling (J) and has the following expression:

$$\hat{H} = -J (\hat{S}_1\hat{S}_2 + \hat{S}_2\hat{S}_3 + \hat{S}_1\hat{S}_3)$$

for $S_1 = S_2 = S_3 = 1$

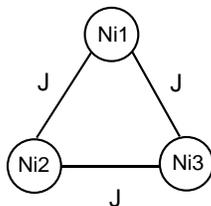


Figure 3.9: Schematic representation of the coupling exchange pathway in $[\text{Ni}_3\text{L}^{Br}(\text{bipy})_3(\text{OH}_2)_3]\text{NO}_3 \cdot 8\text{H}_2\text{O} \cdot 1.5\text{DMF} \cdot 2.25\text{MeOH}$ (**6**) complex.

The energies $E(S_T)$ of the resultant spin states S_T for the trinuclear Ni(II) unit is calculated according to the equation:

$$E(S_T) = -J[S_T(S_T + 1) - 3S(S + 1)]$$

with $S_T = S_1 + S_2 + S_3$

For antiferromagnetically coupled system, this model predicts a $S_T = 0$ ground state. The $\chi_M T$ value for complex **6** at 2 K is very close to a zero value ($0.06 \text{ cm}^3\text{mol}^{-1}\text{K}$)

and thus the appropriate applicability of the chosen model. Introducing the above S_T , $E(S_T)$ expressions in the Van Vleck equation, the theoretical χ_M vs T expression for a Ni_3^{II} equilateral triangle has the form:

$$\chi_M = \frac{2N\beta^2g^2}{kT} \frac{18\exp^A + 60\exp^B + 84\exp^C}{1 + 9\exp^A + 10\exp^B + 7\exp^C} (1 - \rho) + \frac{2N\beta^2g^2}{kT} \rho + \chi_{TIP} \quad (4)$$

with $A = J/kT$, $B = 3J/kT$ and $C = 6J/kT$: ρ defines the magnetic influence of paramagnetic impurities and χ_{TIP} represents the temperature independent paramagnetic factor.

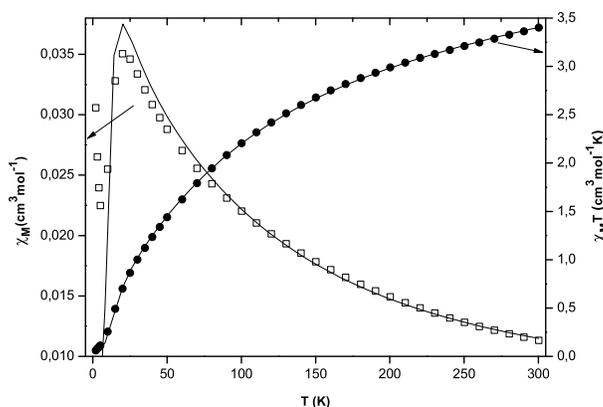


Figure 3.10: Plot of thermal dependence of χ_M (empty squares) and $\chi_M T$ product (black filled circles) for $[\text{Ni}_3\text{L}^{\text{Br}}(\text{bipy})_3(\text{OH}_2)_3]\text{NO}_3 \cdot 8\text{H}_2\text{O} \cdot 1.5\text{DMF} \cdot 2.25\text{MeOH}$ (**6**) complex measured with an applied magnetic field of 2000 Oe; the solid lines represent the theoretical curves (see text).

The best fit of the $\chi_M T$ experimental data set led to $J = -30.99 \pm 0.580 \text{ cm}^{-1}$ for $g = 2.17 \pm 0.0015$ and a paramagnetic impurity $\rho = 0.027 \pm 0.0023$. The reliability factor $R^2 = 0.99986$ for a temperature independent paramagnetic factor $\chi_{TIP} = 1.44 \cdot 10^{-3} \pm 1.3 \cdot 10^{-4} \text{ cm}^3\text{mol}^{-1}$ shows a good agreement between calculated and experimental data sets.

For complex **7** three different Ni–N–N–Ni bridges were crystallographically observed, with two nickel ions having similar coordination environment, whereas the third contains a different donor atom surrounding. Therefore, the exchange coupling scheme

involves two exchange parameters and it is based on isosceles triangle topology as is depicted in Figure 3.11. The appropriate Hamiltonian expression contains two coupling constants and has the following form:

$$\hat{H} = -J (\hat{S}_1 \hat{S}_2 + \hat{S}_1 \hat{S}_3) - J' (\hat{S}_2 \hat{S}_3)$$

$$\text{for } S_1 = S_2 = S_3 = 1$$

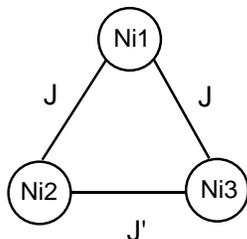


Figure 3.11: Schematic representation of the coupling exchange pathway in $[\text{Ni}_3\text{L}^{\text{Br}}(\text{bipy})_3(\text{DMF})_2\text{Cl}]\cdot\text{DMF}\cdot 2\text{CH}_3\text{CN}\cdot\text{MeOH}\cdot\text{H}_2\text{O}$ (7) complex.

Use of Kambe vector coupling method⁴² for the development of the exchange Hamiltonian and the corresponding eigenvalue of energy levels, the Van Vleck equation for a triad Ni_3^{II} isosceles triangle is:

$$\chi_M = \frac{N\beta^2 g^2}{3kT} \frac{6\exp^B + 6\exp^C + 6\exp^D + 30\exp^E + 30\exp^F + 84\exp^G}{\exp^A + 3\exp^B + 3\exp^C + 3\exp^D + 5\exp^E + 5\exp^F + 7\exp^G} (1 - \rho) + \frac{2N\beta^2 g^2}{kT} \rho + \chi_{TIP} \quad (5)$$

with $A = J - J'/kT$, $B = 3J - 2J'/kT$, $C = J/kT$, $D = J'/kT$, $E = 3J/kT$, $F = 2J' + J/kT$, $G = 3J' + 3J/kT$.

The best fit of the experimental data has been obtained on $\chi_M T$ vs T plot and led to $J = -19.88 \pm 1.297 \text{ cm}^{-1}$, $J' = -12.84 \pm 1.145$ with a paramagnetic impurity $\rho = 0.58 \pm 0.021$ for $g = 2$ fixed value. The reliability factor $R^2 = 0.99742$ resulting for a temperature independent paramagnetic factor $\chi_{TIP} = 1.27 \cdot 10^{-3} \pm 2.0 \cdot 10^{-4} \text{ cm}^3 \text{mol}^{-1}$ shows a good agreement between calculated and experimental data sets. A

variable g value did not give satisfactory results and led to a higher Weiss constant without a reliable values for the g parameter. Based on observed coupling constants that describe an antiferromagnetic intramolecular interaction, a positive θ value is not consistent. Nevertheless, the two coupling constants are similar, suggesting close magnitude of the magnetic interaction between nickel ions, but smaller than the magnitude of the antiferromagnetic interaction found in complex **6**. This may be a consequence of higher torsion Ni–N–N–Ni torsion angle close to 180° in **7**, around 11° more obtuse than corresponding one in complex **6**. Conversely to magnetic properties observed in the case of cation complex **6**, the antiferromagnetically coupled Ni_3 -core in complex **7** led to a net ground spin state ($S = 1$).¹⁰ The $\chi_M T$ value at 2 K is around $1.65 \text{ cm}^3\text{mol}^{-1}\text{K}$, value even higher than expected one for one uncoupled spin $S = 1$. The presence of the non-diamagnetic spin ground state in the trinuclear complex **7** was further confirmed by field dependence magnetization measurements performed at 2 K. The magnetization saturates above 40000 Oe to reach a value of $2 N\beta$ close to expected saturation for one ground state $S_T = 1$. Moreover, the experimental values fit the Brillouin function assuming $g = 2$, resulting in a spin state $S = 1.19 \pm 0.013$ with reliability factor $R^2 = 0.98296$ (Figure 3.13).

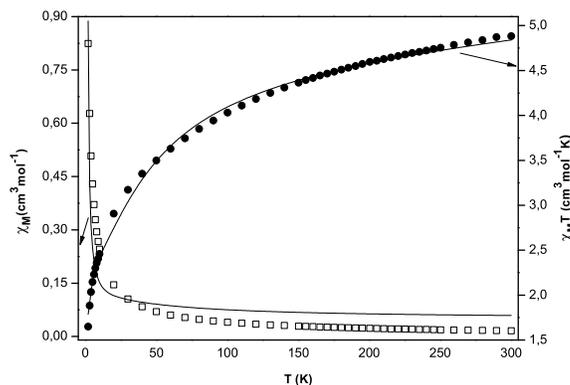


Figure 3.12: Plot of thermal dependence of χ_M (empty squares) and $\chi_M T$ product (black filled circles) for $[\text{Ni}_3\text{L}^{\text{Br}}(\text{bipy})_3(\text{DMF})_2\text{Cl}]\cdot\text{DMF}\cdot 2\text{CH}_3\text{CN}\cdot\text{MeOH}\cdot\text{H}_2\text{O}$ (**7**) complex measured with an applied magnetic field of 5000 Oe; the solid lines represent the theoretical curves (see text).

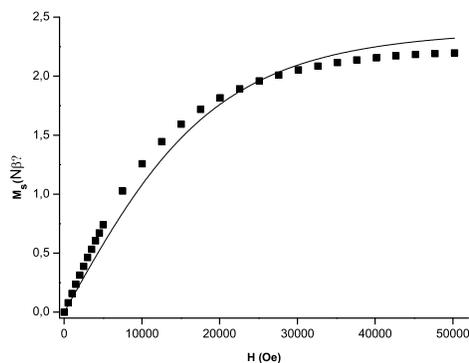


Figure 3.13: Plot of the field dependence of the magnetization for complex **7** measured at 2 K (black filled squares represent the experimental value; the solid line shows the theoretical curve generated using the Brillouin equation).

For both complexes **6** and **7**, negative coupling constant values have been obtained which reveal antiferromagnetic interaction between Ni(II) high-spin. Complex **6** is an antiferromagnetic Ni₃ cation with a $S_T = 0$, whereas the magnetic behavior of complex **7** shows a particular case of spin-frustrated antiferromagnetically coupled Ni(II) triangle with a ground state $S_T = 1$. The intensity of the antiferromagnetic coupling of the nickel ions is quite close to previous studied diazine-bridged trinuclear Ni(II)⁴⁰ complexes in agreement with Ni···Ni intramolecular separation of ~ 500 pm. A second parameter determinant of the magnitude of the antiferromagnetic interaction is represented by the Ni–N–N–Ni torsion angle. On going from complex **6** to complex **7**, small variation of this torsion angle was observed, varying from 168° in **6** to 173° and 179° in **7**, thus a bit stronger antiferromagnetic coupling of the Ni(II) ions in the triangular cation complex **6**. These values compare well with reported magnetic behavior of antiferromagnetic diazine-bridged Ni(II)-containing complexes with Ni–N–N–Ni torsion angles larger than 90° .¹⁸⁶ Conversely, smaller torsion angles have been described in linear diazine-bridged trinuclear Ni(II) complexes where ferromagnetic interaction occurs between neighboring nickel ions and weak antiferromagnetic coupling has found between terminal Ni(II) ions.¹⁸⁷ Complex **7** is a rare case of Ni^{II}-system with a net magnetic spin ground state and therefore confirms that the tris(2-hydroxybenzylidene)triaminoguanidine derivatives ligands are

versatile organic frameworks to generate trinuclear d-complexes with a non-diamagnetic ground state. Similar situation with non-diamagnetic ground state has been observed previously in trinuclear Cu(II)-complexes based on triaminoguanidine ligands, but there for antiferromagnetically paramagnetic coupled centers, a spin-frustrated mechanism is occurring.⁴⁰

3.2 Pentanuclear Ni(II)-complex based on "triaminoguanidine"-ligand and 2,2'-bipyridine coligands

Trinuclear Ni(II) complexes based on tris(5-bromo-2-hydroxybenzylidene)triaminoguanidine ligand system consist of diazine-bridged nickel ions with the metal center in distorted octahedral geometry. Each Ni(II) ion has a labile coordination site filled by solvent molecules or weak coordinating anion ligands. Such a coordination environment is believed to be adequate to synthesize high-nuclearity metal-cyanide magnetic dendrimers. Cyanide-bridged polynuclear complexes of Prussian Blue type are highly desirable due to their rich chemical properties, i.e single-molecule magnets, photomagnetism and/or building blocks to design coordination polymers with different dimensionality.¹¹¹⁻¹¹³ Cyanide-bridge mediates strong magnetic interaction between metal centers and bimetallic Prussian Blue type solids were reported to exhibit spontaneous magnetization at temperature as high as 376 K.¹¹⁴ According with the proposed strategy to isolate cyano-bridged polynuclear complexes, halide is a "leaving group", easy replaceable by cyanide ligand. Therefore, complex of type **7** has been reacted with aqueous solution of $[M(CN)_x]^{m-}$ ($M = Cr^{3+}, Fe^{3+/2+}$), but unfortunately no crystalline product could be isolated. Instead, slow diffused layers of DMF solution of complex **7** and aqueous solution of photomagnetically active¹⁸⁸ cyanide- $K_4[Mo(CN)_8]$ in 1:4 ratio lead to a pentanuclear Ni(II)-complex with no molybdenum cyanide moiety. A self-arrangement of the initial trinuclear $[Ni_3L^{Br}(bipy)_3(DMF)_2Cl] \cdot DMF \cdot 2CH_3CN \cdot MeOH \cdot H_2O$ (**7**) complex took place, most likely induced by molybdenum-cyanide salt to form a high-nuclearity Ni(II) complex of type $[Ni_5(L^{Br})_2(bipy)_4(OH_2)_4(DMF)] \cdot 1.5MeOH \cdot 6DMF \cdot 4.75H_2O$ (**8**). The molecular structure for complex **8** is shown in Figure 3.14 and selected bond lengths and angles are listed in

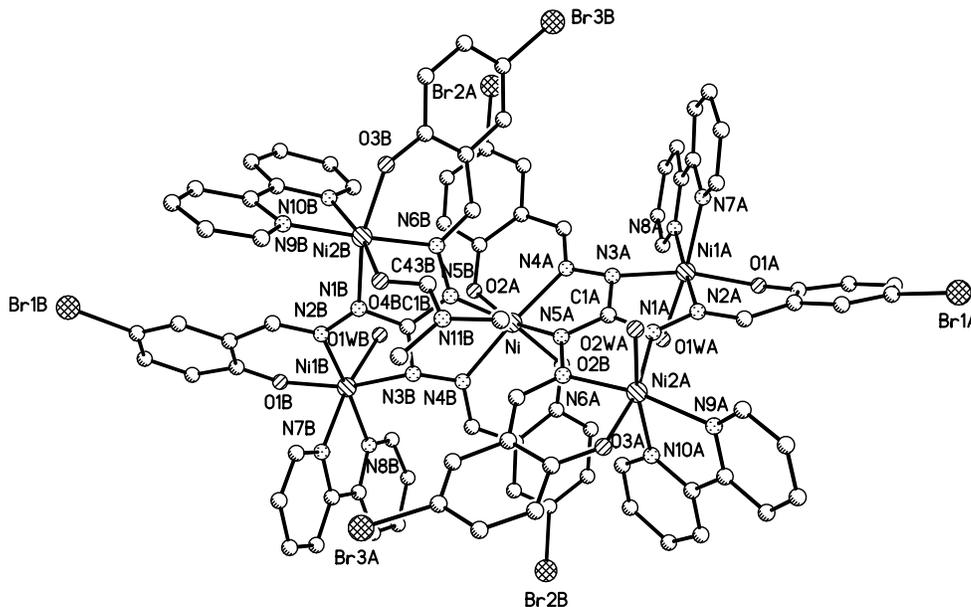


Figure 3.14: Molecular structure and selected numbering scheme of complex $[\text{Ni}_5(\text{L}^{\text{Br}})_2(\text{bipy})_4(\text{OH}_2)_4(\text{DMF})] \cdot 1.5\text{MeOH} \cdot 6\text{DMF} \cdot 4.75\text{H}_2\text{O}$ (**8**).

Table 3.3 and 3.4.

The asymmetric unit contains five Ni(II) ions in distorted octahedral environment. Two trinuclear $[\text{Ni}_3\text{L}^{\text{Br}}\text{L}']$ are interconnected by a common Ni(II) ion accommodated in two tridentate pockets of two triaminoguanidine-based ligand moieties in O_2N_4 environment. The bite angles of the two tridentate pockets are 90° (O2A–Ni–N4A) and 76° (N4A–Ni–N5A) for molecule A and 89° (O2B–Ni–N4B) and 77° (N4B–Ni–N5B) for molecule B. Similar strength binding of the two tridentate pockets around Ni ion was observed with nickel to phenolate oxygen atom bond distances of 208.0 and 210.5 pm for Ni–O2A and Ni–O2B bond lengths. The guanidine-hydrazide nitrogen atoms bond distances are around 201 pm for Ni–N4A and Ni–N4B and 211.8 and 209.9 pm nickel-to-imino nitrogen atom bond lengths (Ni–N5A and Ni–N5B). The dihedral angle between the idealized planes formed by two Ni(II)-containing triaminoguanidine-based moieties is around 85° , very close to a perpendicular orientation of the two interlocked trinuclear Ni(II)-subunits. The four peripheral Ni(II) ions have similar coordination environment to previous described trinuclear Ni(II)-complex **6**. Three of them are in octahedral $\text{ON}_3(\text{OH}_2)$ environment with Ni–O bond lengths in the 201.1–213.2 pm range, with shorter bond distances for phenolate oxygen atoms and longer for Ni–O water oxygen

Table 3.3: Selected bond lengths (pm) and angles ($^{\circ}$) for complex **8**.

Ni–O2A	208.0(4)	Ni–O2B	210.5(4)
Ni–N4A	201.0(5)	Ni–N4B	201.1(5)
Ni–N5A	211.8(5)	Ni–N5B	209.9(5)
Ni1A–O1A	202.3(4)	Ni1A–O1WA	211.8(5)
Ni1A–N2A	201.8(5)	Ni1A–N3A	204.8(5)
Ni1A–N7A	210.8(6)	Ni1A–N8A	208.6(6)
Ni2A–O3A	201.1(5)	Ni2A–O2WA	211.5(5)
Ni2A–N1A	206.6(5)	Ni2A–N6A	201.9(5)
Ni2A–N9A	213.9(5)	Ni2A–N10A	208.9(6)
Ni1B–O1WB	213.2(4)	Ni1B–O1B	204.4(4)
Ni2B–O3B	206.9(4)	Ni2B–O4B	209.6(4)
Ni1B–N2B	201.7(5)	Ni1B–N3B	209.8(5)
Ni2B–N6B	200.9(5)	Ni1B–N7B	208.9(6)
Ni1B–N8B	208.3(6)	Ni2B–N9B	208.0(5)
Ni2B–N10B	206.9(6)	-	-

atom bond distances. The remained Ni2B ion contains a coordinated DMF molecule with a Ni–O4B bond distance of 209.6 pm. The dihedral angles between the equatorial planes of each Ni(II) ion within the same tris(5-bromo-2-hydroxybenzylidene)triaminoguanidine ligand are 36.2, 11.8 and 47.5 $^{\circ}$ for molecule A and 19.1, 48.9 and 30.9 $^{\circ}$ for molecule B. The interatomic Ni \cdots Ni separation is similar within the two trinuclear Ni(II) entities as well as the Ni–N–Ni torsion angles as are listed in Table 3.5. While the interatomic Ni \cdots Ni distances are similar to interatomic nickel-nickel separation observed in previous described trinuclear complexes, the torsion angles of the diazine-bridged Ni(II) ions are smaller in complex **8** compared to complex **6** and **7**, but still in *trans* orientation compared to diazine N–N bridge.

Complex **8** crystallizes with large amounts of solvent of crystallization, i.e DMF, MeOH and H₂O which form a strong hydrogen bonding network with hydrogen bonding contacts that fall in the 264.2 - 284.8 pm. In addition, the methanol molecules estab-

Table 3.4: Selected bond lengths (pm) and angles ($^{\circ}$) for complex **8**.

N4A–Ni–N4B	173.0(2)	N4A–Ni–O2A	90.04(18)
N4B–Ni–O2A	88.87(18)	O2A–Ni–N5B	86.34(19)
N4A–Ni–N5B	109.58(19)	N4B–Ni–N5B	77.2(2)
N4A–Ni–O2B	84.04(17)	N4B–Ni–O2B	89.21(18)
O2A–Ni–O2B	95.12(17)	N5B–Ni–O2B	166.33(18)
N4A–Ni–N5A	76.32(19)	N4B–Ni–N5A	105.5(2)
O2A–Ni–N5A	164.87(18)	N5B–Ni–N5A	92.0(2)
O2B–Ni–N5A	90.00(19)	N2A–Ni1A–O1A	90.38(19)
N2A–Ni1A–N3A	77.48(19)	O1A–Ni1A–N3A	165.35(19)
O1A–Ni1A–O1WA	89.80(17)	N2A–Ni1A–O1WA	90.3(2)
N3A–Ni1A–O1WA	82.19(19)	N8A–Ni1A–N7A	78.5(2)
O3A–Ni2A–N1A	167.53(17)	O3A–Ni2A–N6A	90.94(18)
O3A–Ni2A–O2WA	89.0(2)	N1A–Ni2A–O2WA	87.6(2)
N6A–Ni2A–N1A	77.47(19)	N6A–Ni2A–O2WA	95.76(19)
N9A–Ni2A–N10A	77.7(2)	N2B–Ni1B–O1B	89.30(18)
O1B–Ni1B–N3B	165.49(18)	N2B–Ni1B–N3B	77.72(19)
N2B–Ni1B–O1WB	95.41(19)	O1B–Ni1B–O1WB	90.80(17)
N8B–Ni1B–N7B	78.5(2)	O3B–Ni2B–N1B	165.63(17)
N6B–Ni2B–O3B	88.33(19)	N6B–Ni2B–N1B	77.5(2)
O3B–Ni2B–O4B	90.40(18)	N6B–Ni2B–O4B	91.72(19)
N9B–Ni2B–N10B	79.3(2)	N9B–Ni2B–O4B	89.1(2)

Table 3.5: Interatomic separation (pm) and torsion angles ($^{\circ}$) for pentanuclear Ni(II) complex **8**.

Ni \cdots Ni1A	471.8	Ni \cdots Ni1B	471.3
Ni \cdots N2A	497.2	Ni \cdots Ni2B	498.4
Ni1A \cdots Ni2A	494.1	Ni1B \cdots Ni2B	494.3
Ni–N4A–N3A–Ni1A	130.1	Ni–N4B–N3B–Ni1B	127.1
Ni–N5A–N6A–Ni2A	153.4	Ni–N5B–N6B–Ni2B	168.1
Ni1A–N2A–N1A–Ni2A	1620.8	Ni1B–N2B–N1B–Ni2B	161.2

lishes hydrogen bonding contacts between the pentanuclear Ni(II) entities of 264.2 pm through phenolate oxygen atom (O3B) and the coordinated water molecules are in hydrogen bonding interactions with DMF molecules of 268.3 (O2WA \cdots O/DMF)) and 276.6 (O1WB \cdots O(DMF)) pm, respectively. Weak π - π stacking interactions, larger than 336 pm are formed between constituting 2,2'-bipyridine coligands of neighboring trinuclear Ni(II)-entities (Figure 3.15).

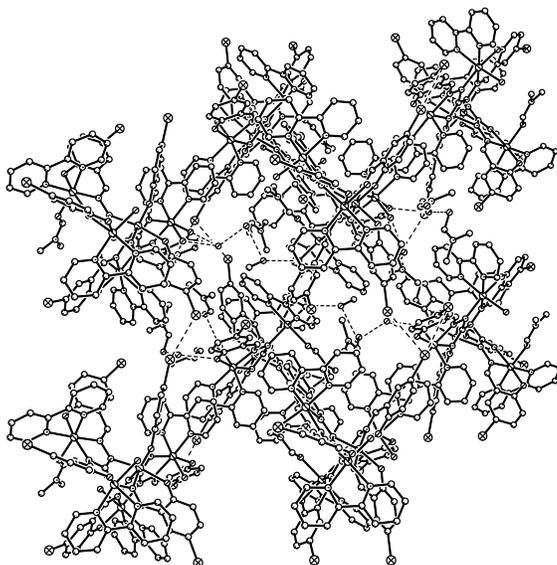


Figure 3.15: Packing diagram viewed along the c axis for complex $[\text{Ni}_5(\text{L}^{Br})_2(\text{bipy})_4(\text{OH}_2)_4(\text{DMF})] \cdot 1.5\text{MeOH} \cdot 6\text{DMF} \cdot 4.75\text{H}_2\text{O}$ (**8**). Dashed lines represent hydrogen bonding interactions.

Magnetic properties of the pentanuclear Ni(II)-containing complex

Variable temperature (300 - 2 K) magnetic susceptibility measurement was obtained on crystalline sample of complex $[\text{Ni}_5(\text{L}^{Br})_2(\text{bipy})_4(\text{OH}_2)_4(\text{DMF})] \cdot 1.5\text{MeOH} \cdot 6\text{DMF} \cdot 4.75\text{H}_2\text{O}$ (**8**) with an applied magnetic field of 2000 Oe. Plots of thermal variation of χ_M and $\chi_M T$ are shown in Figure 3.16. The measured $\chi_M T$ value at room temperature is $4.86 \text{ cm}^3\text{mol}^{-1}\text{K}$ which roughly corresponds to a calculated value of $5.00 \text{ cm}^3\text{mol}^{-1}\text{K}$ for five uncoupled $S = 1$ ions, assuming $g = 2$. On lowering the temperature, the $\chi_M T$ value decrease constantly to reach a value of $0.04 \text{ cm}^3\text{mol}^{-1}\text{K}$ at 2 K. This behavior suggest the presence of antiferromagnetic interaction within the pentanuclear cluster. The low temperature $\chi_M T$ value is close to $S_T = 0$ ground state. The antiferromagnetic interactions occur, most likely within the trinuclear subunits. The peripheral Ni ··· Ni separation is larger than 785 pm and, therefore no antiferromagnetic coupling between these ions is expected. Unfortunately, no quantitative analysis of the magnetic data have been performed.

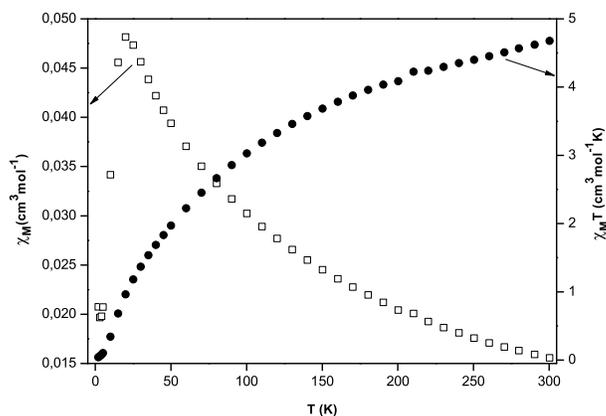


Figure 3.16: Plot of thermal dependence of χ_M (empty squares) and $\chi_M T$ product (black filled circles) for $[\text{Ni}_5(\text{L}^{Br})_2(\text{bipy})_4(\text{OH}_2)_4(\text{DMF})] \cdot 1.5\text{MeOH} \cdot 6\text{DMF} \cdot 4.75\text{H}_2\text{O}$ (**8**) complex measured with an applied magnetic field of 2000 Oe.

A possible hypothesis for the formation of the pentanuclear complex (**8**) is represented by self-rearrangement of the trinuclear Ni(II)-entities. Such architectural assemblies have been proposed to be formed by Müller *et al*¹⁴⁸ but in presence of a bridging ligand, i.e barbituric acid when the self-assembly process between two trinuclear entities with a C3 symmetric organic framework led to a trigonal bipyramid cage. Complex **8** of type M₅L₂ comprises a different architecture, with four Ni(II) ions arranged almost in one plane, whereas the remained Ni(II) ion is perpendicular on this plane, but do not form a square-pyramidal cage owing to an almost linear arrangement of three Ni(II) centers.

3.3 Trinuclear Ni(II)-complex based on "triaminoguanidine"-ligands and 2,4,6-tris(2-pyridyl)-1,3,5-triazine coligands

Non-covalent interaction forces are able of aggregating the metallo-units into larger nanoscale arrays. Hydrogen bonding interactions are known as generators of extended-dimensionality networks when appropriate building blocks which contain multiple hydrogen bonding donor and acceptor are used.¹⁸⁹⁻¹⁹¹ On the other hand, π - π -stacking interactions have also been reported as capable to assemble oligomeric units into supramolecular architectures. For example, mononuclear cation [Cu^I(aminopyrene)₃] complex has been led to 2-D layers through π - π stacking of the three pyrene moieties,¹⁹² whereas pairs of infinite chains have been aggregated through π - π stacking interactions of the aromatic components in [Ag^I(*trans*-4,4'-azopyridine)(NO₃)] complex.¹⁹³ Both types of non-covalent interactions have been reported to influence the observed interesting electrical, optical and magnetic properties of the resulting assemblies.^{129,130} Therefore, 5-bromo- and 3-methoxy-substituted triaminoguanidine-based ligands have been reacted with NiX₂·nH₂O salts using 2,4,6-tris(2-pyridyl)-1,3,5-triazine as coligand. The aromatic co-system is expected to generate extended supramolecular networks through π - π -stacking interactions as it was previously reported, whereas the presence of different anions may induce hydrogen bonding organization of the molecules. In addition, the triazine system used herein is a possible candidate for inducing spin-polarization mechanism in coordination

compounds (Figure 3.17). This last organic framework has a C₃-symmetry, similarly to triaminoguanidine-based ligands and, therefore the association of both organic ligands and metal ions may lead to extended structures with interesting net topology.¹²⁰ On the other hand, trinuclear d-metal complexes that contain both, triaminoguanidine-based ligand and 2,4,6-tris(2-pyridyl)-1,3,5-triazine coligand may be used as molecular bricks to form polynuclear clusters with alternating antiferro- and ferromagnetic coupling interactions.^{137, 152, 194–202}

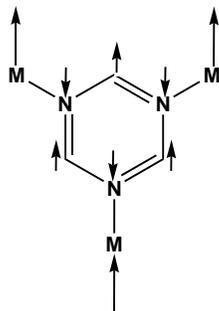


Figure 3.17: Schematic representation of the possible spin-polarization mechanism induced by the pyrimidine moiety of 2,4,6-tris(2-pyridyl)-1,3,5-triazine (tptz) ligand in transition metal complexes.

3.3.1 Trinuclear Ni(II)-complexes formed with tptz coligand and tris(5-bromo-2-hydroxy-salicylidene)triaminoguanidine ligand

Tris(5-bromo-2-hydroxy-salicylidene)triaminoguanidine (H_5L^{Br}) ligand has been reacted with $Ni(NO_3)_2 \cdot 6H_2O$ salt and 2,4,6-tris(2-pyridyl)-1,3,5-triazine (tptz) coligand in 1:3:3 ratio in DMF-MeOH solvent mixture and excess (6 equivalents) of base (NEt_3). The molecular structure determination shows a cation trinuclear Ni(II)-complex of type $[Ni_3L^{Br}(tptz)_3]NO_3 \cdot 6.75MeOH \cdot 4H_2O$ (**9**) as is depicted in Figure 3.18. The structural arrangement of complex **9** contains the nitrate anion in distorted positions, two water lattice solvent and four methanol molecules. These lattice solvents showed also partly distortions. The trinuclear cation is formed by Ni(II) ions in octahedral environment

accommodated by the threefold nucleating triaminoguanidine based ligand which coordinates in the classical tris-tridentate fashion as previously described. Complex **9** crystallizes in the rhombohedral R_3 space group with a nickel ion per asymmetric unit and therefore has C_3 symmetry axis that pass through C1 guanidine atom and the nitrate anion. Each tridentate pocket fills three coordination sites of each nickel ion with the bite angles of 92° for O1–Ni–N2 and 78° for N2–Ni–N1. Selected bond lengths and angles for complex **9** are listed in Table 3.6. The nickel-to-phenolate oxygen atoms bond distances are around 194.2 pm and the Ni–N bond distances are around 196.0 pm (Ni–N2 imino nitrogen atom) and 201.0 pm for nickel-to aminoguanidine nitrogen atom (N1). These bond lengths do not differ very much from corresponding bond distances found in cationic trinuclear Ni(II) complex **6**. Conversely to previous described complexes, no coordinated solvent molecules are to be found due to the nature of the tptz coligand that coordinated in terpyridine-like fashion (Figure 3.1 form I) acting as tridentate capping ligand. The bite angles of the coligand are 72° (N4–Ni–N3) and 73° (N4–Ni–N7) with nickel-to-nitrogen atoms bond lengths that fall in the 210–238 pm range, similar with reported bonding parameters of terpyridine-like chelation of 2,4,6-tris(2-pyridyl)-1,3,5-triazine ligand.

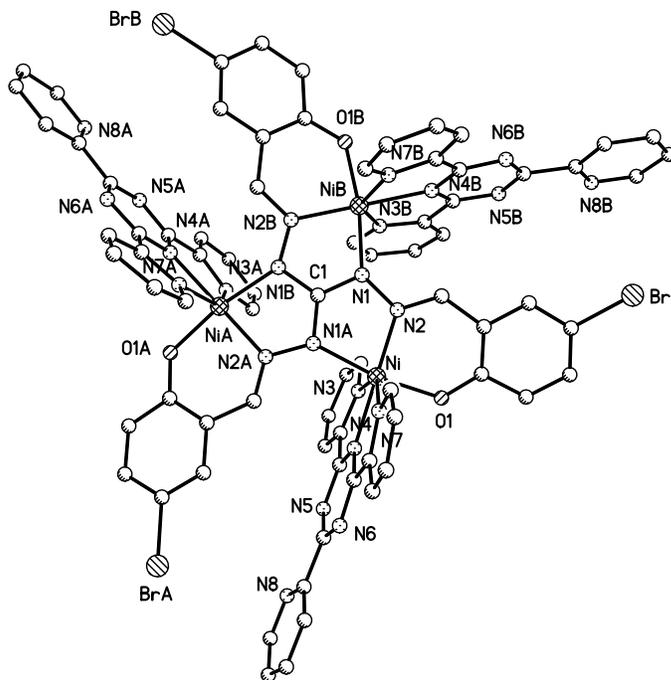


Figure 3.18: Molecular structure and selected numbering scheme of cation complex $[\text{Ni}_3\text{L}^{\text{Br}}(\text{tptz})_3]\text{NO}_3 \cdot 6.75\text{MeOH} \cdot 4\text{H}_2\text{O}$ (**9**).

Table 3.6: Selected bond lengths (pm) and angles ($^{\circ}$) for complex **8**.

Ni–O1	194.2(6)	Ni–N1	201.0(7)
Ni–N2	196.0(7)	Ni–N3	238.1(11)
Ni–N4	210.1(7)	Ni–N7	237.1(12)
O1–Ni–N1	170.4(3)	O1–Ni–N2	92.0(3)
O1–Ni–N3	89.5(3)	O1–Ni–N4	88.4(3)
O1–Ni–N7	90.8(3)	N1–Ni–N3	92.1(3)
N1–Ni–N4	101.0(3)	N1–Ni–N7	93.3(3)
N2–Ni–N1	78.6(3)	N2–Ni–N3	109.8(4)
N2–Ni–N4	177.8(5)	N2–Ni–N7	104.8(4)
N4–Ni–N3	72.3(4)	N4–Ni–N7	73.1(4)
N7–Ni–N3	145.4(3)		

The Ni \cdots Ni intermolecular separation through diazine bridge is 482 pm with Ni–N–N–Ni torsion angles of 154° . These values are slightly smaller than corresponding values found in complex **6**, therefore different magnitude of the magnetic coupling is to be expected. Nevertheless, as it was expected, interesting structural features are formed through self-organization of the molecules. The lattice solvents are in hydrogen bonding interactions of 274.5 pm (Ow \cdots OM) and in addition in hydrogen bonding interactions with donor atoms of the hydrogen acceptor groups of the organic frameworks (O1W \cdots O1 273.9 pm and O1W \cdots N8 284.6 pm). The coligand moieties are face-to-faced π - π stacked with 354 pm distance between the aromatic planes (Figure 3.19) with the nitrate anions placed in the gaps between assembled molecules in a spatial distance of 463 pm reported to the central carbon atom C1 of the guanidine moiety.

Similar trinuclear Ni(II)-containing complexes have been isolated through reaction of tris(5-bromo-2-hydroxy-salicylidene)triaminoguanidine (H_5L^{Br}) ligand with $NiCl_2 \cdot 6H_2O$ and $Ni(ClO_4)_2 \cdot 6H_2O$ salts and tptz coligand in the same conditions as described for complex **9**. The cationic complexes $[Ni_3L^{Br}(tptz)_3]Cl \cdot 10H_2O$ (**10**) and $[Ni_3L^{Br}(tptz)_3]ClO_4 \cdot 7H_2O \cdot DMF$ (**11**) have been spectroscopically characterized. The IR spectroscopy shows similar features regarding the characteristic stretching vibrations of the two organic

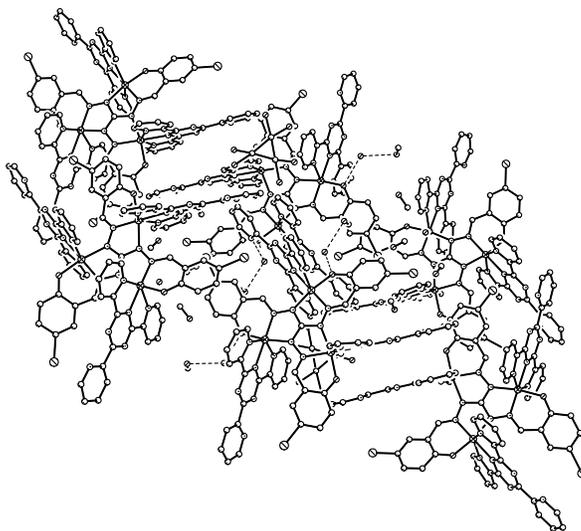


Figure 3.19: Packing diagram for complex $[\text{Ni}_3\text{L}^{\text{Br}}(\text{tptz})_3]\text{NO}_3 \cdot 6.75\text{MeOH} \cdot 4\text{H}_2\text{O}$ (**9**) as viewed along the c axis.

frameworks. The stretching vibration of the $-\text{CH}=\text{N}$ group has been observed in the IR spectra of all three cation complexes at around 1653 cm^{-1} range, a little bit shifted compared to the free ligand. Stretching vibrations owing to the terpyridine-like coordinated capping ligands have been detected at $1441\text{--}1468\text{ cm}^{-1}$ assigned to pyrimidine ring system. In addition, strong absorption band characteristic for the NO_3^- anion has been detected at 1384 cm^{-1} , similarly to its vibration detected in the IR spectrum of complex **6**. Stretching vibration characteristic for the perchlorate anion has been detected at 1177 cm^{-1} in complex **11**. The elemental analyzes of the cationic structure of all these three complexes agree well with the proposed compositions.

Magnetic properties

The magnetic measurements of all three complexes have been performed in the temperature range 300–2 K and the plots of thermal variation of the magnetic susceptibility in form of χ_M vs T and $\chi_M T$ vs T are shown in Figure 3.20 to Figure 3.22 for complex **9**, **10** and **11**, respectively. The experimental magnetic data sets show similar features with the $\chi_M T$ values at 300 K of $2.76\text{ cm}^3\text{mol}^{-1}\text{K}$ for complex **9**, $2.56\text{ cm}^3\text{mol}^{-1}\text{K}$ for complex **10** and $2.79\text{ cm}^3\text{mol}^{-1}\text{K}$ for complex **11**. These values are a little bit lower than expected value ($3.00\text{ cm}^3\text{mol}^{-1}\text{K}$) for three uncoupled Ni(II) ions, assuming $g = 2$. On lowering the

temperature, in all three cases a constant decrease of the $\chi_M T$ product values have been observed until 5 K. Below this temperature a slow decline of the $\chi_M T$ values has been registered, with minimum values of $0.03 \text{ cm}^3 \text{ mol}^{-1} \text{ K}$ for complex **9**, $0.009 \text{ cm}^3 \text{ mol}^{-1} \text{ K}$ for complex **10** and $0.01 \text{ cm}^3 \text{ mol}^{-1} \text{ K}$ for complex **11**, respectively at 2 K. These lowest values are very close to a ground state $S_T = 0$, similarly to the previous magnetic behavior of complex **6**.

The best fit of the magnetic data sets has been obtained considering the isotropic exchange Hamiltonian developed for complex **6** based on the exchange scheme shown in Figure 3.9 for three equivalents Ni(II) ions. Simulation of the experimental $\chi_M T$ values according with equation 4 obtained with Heissenberg-Van Vleck-Dirac formalism yielded the data sets listed in Table 3.7. Except for $[\text{Ni}_3\text{L}^{\text{Br}}(\text{tptz})_3]\text{ClO}_4 \cdot 7\text{H}_2\text{O} \cdot \text{DMF}$ (**11**) complex, the quantitative analyze of the experimental magnetic data sets has been performed with a fixed $g = 2$ parameter. A variable Landé factor for simulation of the magnetic behavior of complex $[\text{Ni}_3\text{L}^{\text{Br}}(\text{tptz})_3]\text{NO}_3 \cdot 6.75\text{MeOH} \cdot 4\text{H}_2\text{O}$ (**9**) and $[\text{Ni}_3\text{L}^{\text{Br}}(\text{tptz})_3]\text{Cl} \cdot 10\text{H}_2\text{O}$ (**10**) yield no significant difference in J values, but the resulting g values of around 1.88 (for **10**) and 1.93 (for **9**) are inconsistent with EPR spectra of Ni(II)-containing complexes, i.e 2.001 measured value for complex **10**.

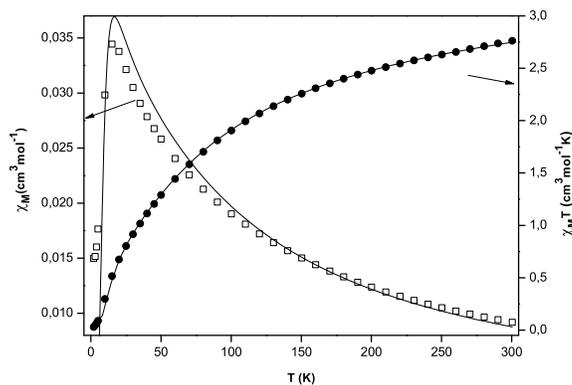


Figure 3.20: Plot of thermal dependence of χ_M (empty squares) and $\chi_M T$ product (black filled circles) for $[\text{Ni}_3\text{L}^{\text{Br}}(\text{tptz})_3]\text{NO}_3 \cdot 6.75\text{MeOH} \cdot 4\text{H}_2\text{O}$ (**9**) complex measured with an applied magnetic field of 2000 Oe; the solid lines represent the theoretical curves (see text).

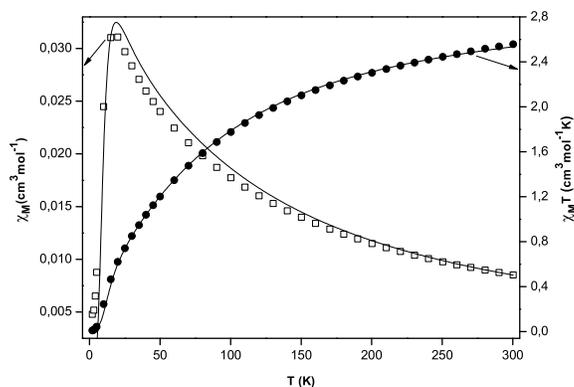


Figure 3.21: Plot of thermal dependence of χ_M (empty squares) and $\chi_M T$ product (black filled circles) for $[\text{Ni}_3\text{L}^{\text{Br}}(\text{tptz})_3]\text{Cl}\cdot 10\text{H}_2\text{O}$ (**10**) complex measured with an applied magnetic field of 2000 Oe; the solid lines represent the theoretical curves (see text).

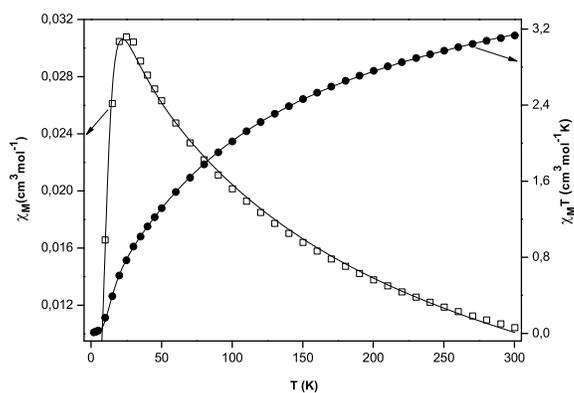


Figure 3.22: Plot of thermal dependence of χ_M (empty squares) and $\chi_M T$ product (black filled circles) for $[\text{Ni}_3\text{L}^{\text{Br}}(\text{tptz})_3]\text{ClO}_4\cdot 7\text{H}_2\text{O}\cdot \text{DMF}$ (**11**) complex measured with an applied magnetic field of 2000 Oe; the solid lines represent the theoretical curves (see text).

In all three cases antiferromagnetic interactions mediated by diazine bridges occur between the triad Ni(II) core. The coupling constant parameter is very similar within the cationic trinuclear Ni(II) complexes owing to superexchange mechanism operating via Ni–N–N–Ni linkage when the corresponding torsion angle is close to 180° .³²

Table 3.7: Simulated magnetic data set for complex **9**, **10** and **11**.

	9	10	11
g	2.00	2.00	2.11±0.007
J	-27.06±0.31	-28.56±0.40	-30.88±0.30
ρ	0.021±2.66·10 ⁻³	0.013±3.15·10 ⁻³	0.006±1.1·10 ⁻³
χ_{TIP}	5.6·10 ⁻⁴ ±3.0·10 ⁻⁵	9.4·10 ⁻⁶	1.27·10 ⁻³ ±6.0·10 ⁻⁵
R ²	0.99968	0.99847	0.99974

The interesting feature of these isolated cationic trinuclear Ni(II) complexes of general type $[\text{Ni}_3\text{L}^{Br}(\text{tptz})_3]^+$ is represented by the presence of free coordination sites at 2,4,6-tris(2-pyridyl)-1,3,5-triazine coligands, and therefore they can be used as building blocks to design dissimilar polynuclear complexes. While an antiferromagnetic interaction is mediated by the triaminoguanidine-based ligand, the 2,4,6-tris(2-pyridyl)-1,3,5-triazine coligand may mediate ferromagnetic interaction through spin-polarization mechanism (Figure 3.17) and hence an alternating ferro- antiferro-magnetic coupling may be present.

3.4 Pentanuclear Ni(II)-complexes formed with tptz coligand and tris(5-brom-2-hydroxy-salicylidene)-triaminoguanidine ligand

In situ reaction of $\text{Ni}(\text{NO}_3)_2 \cdot 6\text{H}_2\text{O}$ with H_5L^{Br} and tptz organic ligands in MeOH/DMF/ H_2O in a ratio of 3:1:3, followed by addition of three equivalents of $\text{Gd}(\text{NO}_3)_3 \cdot 6\text{H}_2\text{O}$ produces a dark-brown solution from which the pentanuclear $[\text{Ni}_5(\text{L}^{Br})_2(\text{tptz})_4] \cdot 7.5\text{H}_2\text{O} \cdot 6\text{MeOH}$ (**12**) complex crystallizes upon slow evaporation of the solvents mixture at room temperature. The reaction has been performed in basic media by use of excess of Bu_4NOH 40 % aqueous solution. Conversely to beforehand mentioned synthesis for complex **6** where the $\text{Gd}(\text{NO}_3)_3 \cdot 6\text{H}_2\text{O}$ salt functioned as anion exchange for the isolation of the final cation trinuclear Ni(II) complex **6**, in this case a self-assembly process took place with

an rearrangement of the constituent trinuclear Ni(II) units to form a final pentanuclear nickel(II)-containing complex. Complex **12** (Figure 3.23) crystallizes in the triclinic space group P1 with two trinuclear Ni(II) units, interlocked by a common Ni3 ion. The peripheral nickel ions are surrounded by ON₅ donor atom sets arranged in distorted octahedral geometry with *trans* angles in the 150-169° range.

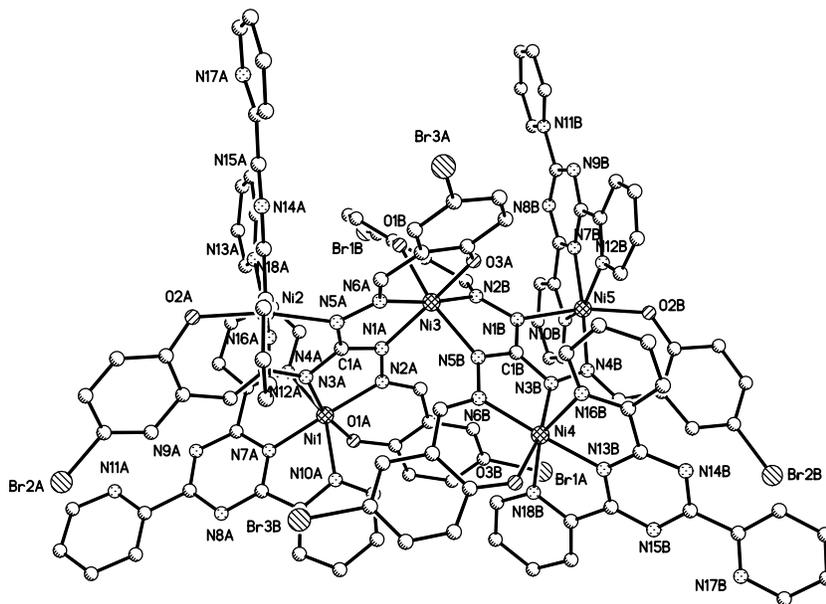


Figure 3.23: Molecular structure and selected numbering scheme of complex $[\text{Ni}_5(\text{L}^{\text{Br}})_2(\text{tptz})_4] \cdot 7.5\text{H}_2\text{O} \cdot 6\text{MeOH}$ (**12**); Hydrogen atoms have been omitted for clarity.

The triaminoguanidine-based ligand acts as threefold tridentate chelate system, whereas the 2,4,6-tris(2-pyridyl)-1,3,5-triazine coligand wraps around each peripheral Ni(II) ion in the terpyridine chelating fashion (Figure 3.1, form I). The bite angles of tris(5-brom-2-hydroxy-salicylidene)triaminoguanidine ligand are a bit smaller compared to corresponding angles found in complex **8** with nickel to phenolate bond distances that fall in 201.8-203.7 pm range and the Ni–N bond distances within the 199.4-207.3 pm limits. The four tridentate tptz coligands form two five-membered chelate rings with Ni–N bond lengths within the 198.9-221.9 pm range and bite angles falling in the 74.3-77.5° range. Two tris(5-brom-2-hydroxy-salicylidene)triaminoguanidine ligand units are hold together by the Ni3 ion, accommodated in two tridentate pockets of A and B such molecules with a O₂N₄ environment. The nickel-to-phenolate oxygen atoms bond distances are very close within the two supporting organic ligands with Ni3–O3A and Ni3–O1B of around

204 pm. The same binding strength within A and B moieties has been observed for Ni3-to-imine nitrogen atoms (Ni3–N6A and Ni3–N2B) of around 203 pm. Longer bond distances were observed for the hydrazide nitrogen atoms with Ni3–N1A of 210.5 pm and Ni3–N5B of 207.6 pm. The dihedral angle between the idealized planes formed by two Ni(II)-containing triaminoguanidine-based moieties is around 87°, very close to a perpendicular orientation of the two interlocked trinuclear Ni(II)-subunits and also very similar to corresponding dihedral angle found in the pentanuclear complex **8**.

Table 3.8: Interatomic separation (pm) and torsion angles (°) for pentanuclear Ni(II) complex **12**.

Ni1···Ni12	497.6	Ni1···Ni3	500.1
Ni2···Ni3	492.1	Ni3···Ni4	495.5
Ni4···Ni5	495.1	Ni3···Ni5	491.5
Ni1–N3A–N4A–Ni2	166.3	Ni1–N2B–N1A–Ni3	178.5
Ni2–N5A–N6A–Ni3	151.6	Ni3–N5B–N6B–Ni4	170.7
Ni4–N3B–N4B–Ni5	162.1	Ni3–N2B–N1B–Ni5	144.9

In addition, the dihedral angles between the equatorial planes of each Ni(II) ion within the same tris(5-bromo-2-hydroxybenzylidene)triaminoguanidine ligand are 17.9, 18.2 and 31.1° for molecule A and 13.7, 19.4 and 33.2° for molecule B. The interatomic Ni···Ni separation is similar within the two trinuclear Ni(II) entities as well as the Ni–N–N–Ni torsion angles as are listed in Table 3.8. These values differ from the corresponding parameters found in complex **8** and namely, there are increasing from bipyridine-containing coligand to 2,4,6-tris(2-pyridyl)-1,3,5-triazine coligand. The torsion Ni–N–N–N torsion angles in complex **12** are closer to 180° and hence maybe a stronger antiferromagnetic interaction will take place. Complex **12** crystallizes with solvent molecules such as MeOH and H₂O, which are partly distorted. Nevertheless, strong hydrogen bonding interactions within the lattice solvent molecules have been observed within the 250.8-263.6 pm range for OM···OM, 273.6-285.2 pm for Ow···Ow and 255.9-294.6 pm for Ow···OM hydrogen bonding contacts. In addition, the lattice water molecules also establish hydrogen

Table 3.9: Selected bond lengths (pm) for complex **12**.

Ni1–O1A	203.7(5)	Ni1–N2A	199.4(6)
Ni1–N3A	208.9(6)	Ni1–N7A	200.1(6)
Ni1–N10A	217.0(6)	Ni1–N12A	213.5(7)
Ni2–O2A	201.8(5)	Ni2–N4A	201.1(6)
Ni2–N5A	205.7(6)	Ni2–N13A	198.9(6)
Ni2–N16A	215.6(7)	Ni2–N18A	217.8(6)
Ni3–O3A	204.0(5)	Ni3–O1B	204.6(5)
Ni3–N1A	210.5(6)	Ni3–N2B	203.3(6)
Ni3–N5B	207.6(6)	Ni3–N6A	203.9(6)
Ni4–O3B	202.3(5)	Ni4–N3B	207.2(6)
Ni4–N6B	200.7(6)	Ni4–N13B	201.1(7)
Ni4–N16B	215.0(7)	Ni4–N18B	220.2(7)
Ni5–O2B	202.8(5)	Ni5–N1B	207.3(6)
Ni5–N4B	201.8(6)	Ni5–N7B	201.4(6)
Ni5–N10B	221.9(6)	Ni5–N12B	216.0(6)

bonding interactions with the phenolate ($\text{Ow} \cdots \text{O1B}$ 270.1 pm, $\text{Ow} \cdots \text{O1A}$ 269.6 pm and $\text{Ow} \cdots \text{3A}$ 275.9 pm) and nitrogen atoms of the pyridine ring belonging to the tptz coligands (283.3–300.9 pm). This hydrogen bonding network fulfils the rectangular channel formed along the a axis by the pentanuclear Ni(II) units (Figure 3.24). On the other hand, a close look on the packing diagram along the b axis reveals a zigzag π - π -stacking interaction as a consequence of face-to-face orientation of the 2,4,6-tris(2-pyridyl)-1,3,5-triazine moieties of two parallel layers and face-to-tail arrangement of the pyridine rings of tptz coligands to the phenylene rings of the tris(5-brom-2-hydroxy-salicylidene)triamino-guanidine ligands (Figure 3.25).

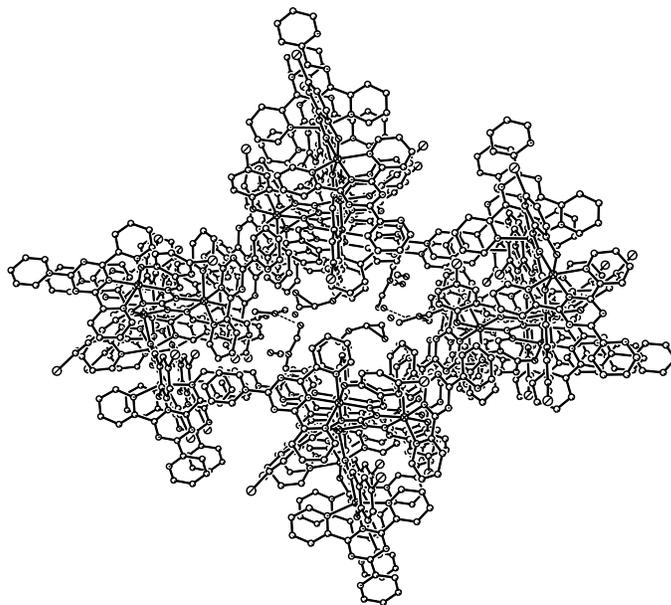


Figure 3.24: Packing diagram for complex $[\text{Ni}_5(\text{L}^{Br})_2(\text{tptz})_4] \cdot 7.5\text{H}_2\text{O} \cdot 6\text{MeOH}$ (**12**) viewed along the a axis showing the hydrogen bonding channel formed by the lattice solvent molecules; hydrogen atoms have been omitted for clarity.

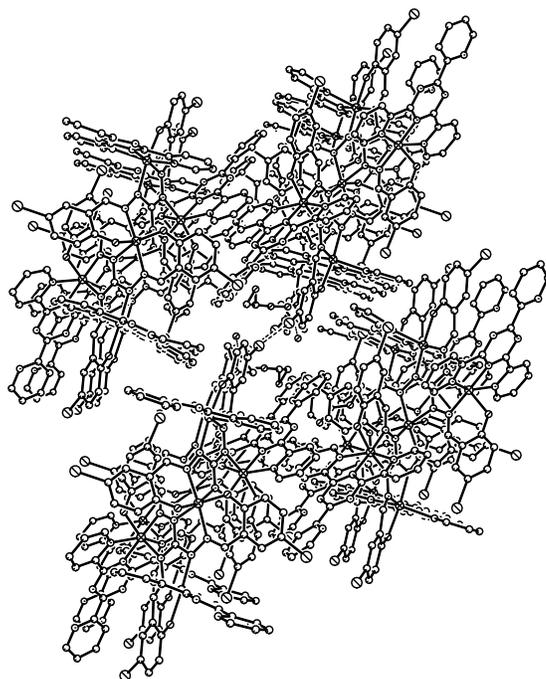


Figure 3.25: Packing diagram for complex $[\text{Ni}_5(\text{L}^{Br})_2(\text{tptz})_4] \cdot 7.5\text{H}_2\text{O} \cdot 6\text{MeOH}$ (**12**) viewed along the b axis showing the π - π -stacking interaction of the tptz coligands.

Table 3.10: Selected angles ($^{\circ}$) for complex **12**.

O1A–Ni1–N3A	167.5(2)	N2A–Ni1–O1A	90.2(2)
N2A–Ni1–N3A	78.0(2)	N7A–Ni1–N10A	75.8(3)
N7A–Ni1–N12A	77.1(2)	N10A–Ni1–N12A	152.9(2)
O2A–Ni2–N5A	168.6(2)	N4A–Ni2–O2A	91.9(2)
N4A–Ni2–N5A	77.3(2)	N13A–Ni2–N16A	76.6(2)
N13A–Ni2–N18A	76.2(2)	N16A–Ni2–N18A	152.2(2)
O3A–Ni3–N1A	165.0(2)	O3A–Ni3–N6A	89.4(2)
N6A–Ni3–N1A	77.0(2)	O3A–Ni3–O1B	90.82(17)
O3A–Ni3–N5B	88.69(17)	O1B–Ni3–N5B	162.4(2)
O1B–Ni3–N1A	94.31(17)	N2B–Ni3–O1B	86.2(2)
O1B–Ni3–N1A	94.31(17)	N6A–Ni3–O1B	86.20(16)
N6A–Ni3–N5B	111.34(17)	N2B–Ni3–N1A	103.41(17)
N2B–Ni3–N6A	172.38(17)	N2B–Ni3–O3A	90.93(16)
N2B–Ni3–N5B	76.3(2)	N5B–Ni3–N1A	90.59(17)
O3B–Ni4–N3B	168.4(2)	O3B–Ni4–N6B	91.0(2)
N3B–Ni4–N6B	77.5(2)	N13B–Ni4–N16B	76.4(3)
N13B–Ni4–N18B	75.4(3)	N16B–Ni4–N18B	151.8(3)
O2B–Ni5–N1B	166.3(2)	O2B–Ni5–N7B	94.9(2)
N1B–Ni5–N7B	98.8(2)	N7B–Ni5–N10B	74.3(2)
N7B–Ni5–N12B	76.6(3)	N10B–Ni5–N12B	150.5(2)

Magnetic properties of pentanuclear Ni(II)-complex based on tris(5-brom-2-hydroxy-salicylidene)triaminoguanidine ligand and tptz coligands

Thermal variation of magnetic susceptibility for $[\text{Ni}_5(\text{L}^{Br})_2(\text{tptz})_4] \cdot 7.5\text{H}_2\text{O} \cdot 6\text{MeOH}$ (**12**) has been measured on crystalline sample in the 300 - 2 K temperature range with an applied magnetic field of 2000 and 5000 Oe. The magnetic behavior for both magnetic fields is very similar, hence plots of thermal variation of χ_M and $\chi_M T$ are shown in Figure 3.26 for 2000 Oe. The measured $\chi_M T$ value at room temperature is $5.26 \text{ cm}^3\text{mol}^{-1}\text{K}$

which roughly corresponds to a calculated value of $5.00 \text{ cm}^3\text{mol}^{-1}\text{K}$ for five uncoupled $S = 1$ ions, assuming $g = 2$. On lowering the temperature, the $\chi_M T$ value decrease constantly until 10 K ($\chi_M T = 0.16 \text{ cm}^3\text{mol}^{-1}\text{K}$) and then decline slowly to reach a value of $0.39 \text{ cm}^3\text{mol}^{-1}\text{K}$ at 2 K. This behavior suggest the presence of antiferromagnetic interaction within the pentanuclear cluster. The low temperature $\chi_M T$ value is not zero, but close to a $S_T = 1/2$ ground state. The antiferromagnetic interactions occur, most likely within the trinuclear subunits through the common Ni3 ion. The peripheral Ni...Ni separation is within 695 pm (Ni1...Ni4) and 981 pm (Ni2...Ni5) range and, therefore no significant antiferromagnetic coupling between these ions is expected. Field dependance of magnetization measurement performed at 2 K (Figure 3.27) shows an increase of magnetization with heightening the magnetic field and shows a saturation of $0.75 N\beta$ at 50213 Oe. The resulting curve fits the Brillouin equation for $S = 0.405 \pm 0.005$. This behavior may suggest a competing magnetic interaction between the trinuclear Ni(II)-subunits which shares a common nickel ion resulting in an intermediate spin ground state. Similar situation has been reported for butterfly-type compounds where the resulting spin ground state is always an intermediate one and not completely canceled.¹⁰

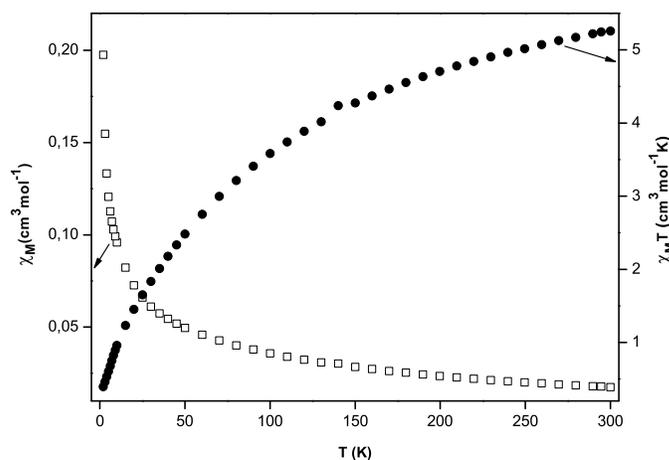


Figure 3.26: Plot of thermal dependence of χ_M (empty squares) and $\chi_M T$ product (black filled circles) for $[\text{Ni}_5(\text{L}^{Br})_2(\text{tptz})_4] \cdot 7.5\text{H}_2\text{O} \cdot 6\text{MeOH}$ (**12**) complex measured with an applied magnetic field of 2000 Oe.

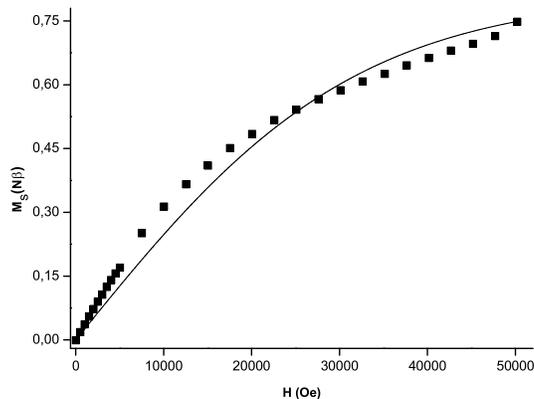


Figure 3.27: Plot of the field dependence of the magnetization for complex **12** measured at 2 K (black filled squares represent the experimental value; the solid line shows the theoretical curve generated using the Brillouin equation).

3.5 Trinuclear Ni(II)-complexes based on tris(3-methoxy-2-hydroxy-salicylidene)-triaminoguanidine ligand and tptz coligands

Changing from 5-bromo-substituted triaminoguanidine-based ligand to vanillin derivative, similar reaction pathways have been followed. In this case, only cationic trinuclear Ni(II)-complexes have been isolated with crystallographical characterization for $[\text{Ni}_3\text{L}^{\text{OMe}}(\text{tptz})_3]\text{NO}_3 \cdot 4.5\text{H}_2\text{O} \cdot 1.5\text{MeOH}$ (**13**) and $[\text{Ni}_3\text{L}^{\text{OMe}}(\text{tptz})_3]\text{Cl} \cdot 2\text{DMF}$ (**14**), whereas the corresponding $[\text{Ni}_3\text{L}^{\text{OMe}}(\text{tptz})_3]\text{ClO}_4 \cdot 5\text{H}_2\text{O}$ (**15**) has been spectroscopically characterized. The molecular structures for complexes **13** and **14** are shown in Figure 3.28 and Figure 3.29, respectively. Similarly to previous described trinuclear Ni(II) complexes, the triaminoguanidine-based ligand ($\text{H}_5\text{L}^{\text{OMe}}$) acts as threefold tridentate system with the topology of the Ni_3 core close related to trinuclear cation complex **9**. The methoxy-substitution of the aromatic ring on the tris-nucleating supporting organic framework led to small variations of the metal ion binding strength. The steric effect of the methoxy group has weakened the phenolate binding strength compared to **9** with the Ni-O phenolate bond lengths of around 201-202 in complex **13** and Ni-O bond lengths within

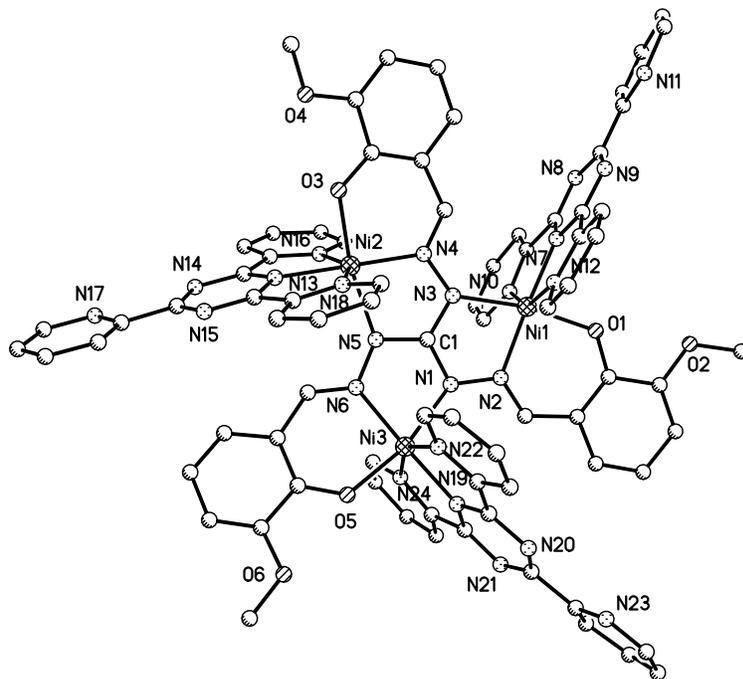


Figure 3.28: Molecular structure and selected numbering scheme of complex $[\text{Ni}_3\text{L}^{\text{OMe}}(\text{tptz})_3]\text{NO}_3 \cdot 4.5\text{H}_2\text{O} \cdot 1.5\text{MeOH}$ (**13**); Hydrogen atoms have been omitted for clarity; only the cationic structural motif is shown

200-204 pm range in complex **14**.

The nickel-to-nitrogen atoms bond lengths are also lengthened compared to previous described similar cation complex **9**. Selected bond lengths and angles for complex **13** and **14** are listed in Table 3.11 and Table 3.12, respectively. The 2,4,6-tris(2-pyridyl)-1,3,5-triazine coligands coordinate in the terpyridine-like chelate mode, with the Ni–N bond distances within the 199.0-220.9 pm range for both complex **13** and **14**, showing that the variation of the anion system does not influence the structural feature of the trinuclear Ni(II) core. The main difference between these last two complexes and the similar described complex **9** is represented by the absence of C3-symmetry axis. Complex **13** crystallizes in the hexagonal $P6_3/m$ space group, whereas complex **14** crystallizes in the triclinic space group P1 with three crystallographically distinct Ni(II) ions, all in distorted octahedral environment formed by ON_5 donor set atoms. For complex **13**, the observed interatomic Ni···Ni separations are 493.8 pm (Ni1···Ni2 and Ni2···Ni3) and 498.7 pm (Ni1···Ni3) with the torsion angles of around 177.7° (Ni1–N3–N4–Ni2), 155.9° (Ni2–N5–N6–Ni3) and 160.5° (Ni1–N2–N1–Ni3). Similar Ni···Ni interatomic separations

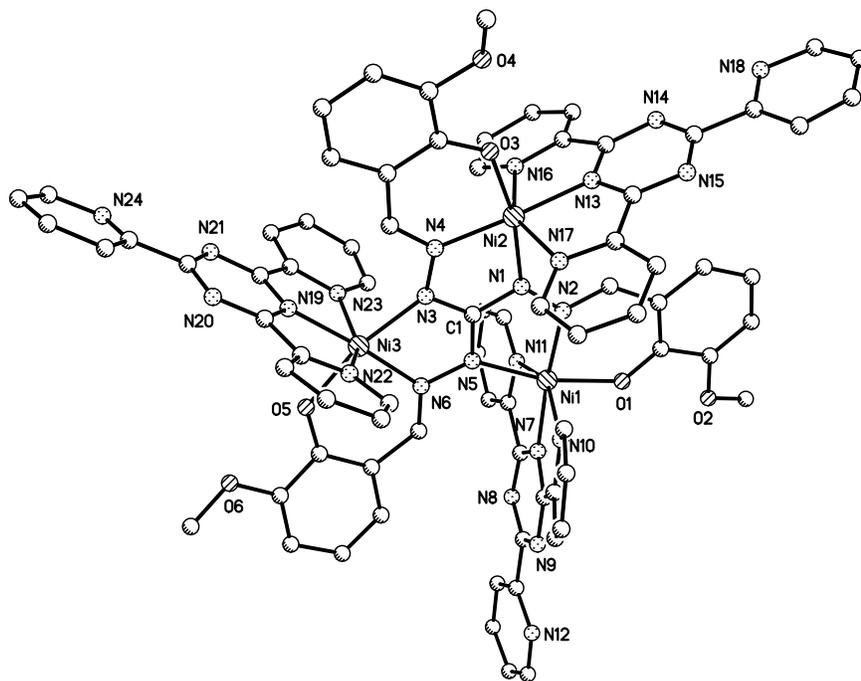


Figure 3.29: Molecular structure and selected numbering scheme of complex $[\text{Ni}_3\text{L}^{\text{OMe}}(\text{tptz})_3]\text{Cl}\cdot 2\text{DMF}$ (**14**); Hydrogen atoms have been omitted for clarity; only the cationic structural motif is shown

were observed for complex **14** which are around 497.9 (Ni1···Ni2), 497.2 (Ni2···Ni3) and 498.2 pm (Ni1···Ni3), but with larger torsion angles for diazine bridged nickel ions, i.e. 173.9° for Ni1–N2–N1–Ni2, 177.6° for Ni2–N4–N3–Ni3 and 179.4° for Ni1–N5–N6–Ni3, respectively. Again, if a tetragonal plane is defined around each Ni(II) ion, described by the ON₂ donor set of the triaminoguanidine-based ligand and one nitrogen atom of the tptz coligand, the dihedral angle between these planes are differing from complex **13** to complex **14**, for example smaller dihedral angles are to be found in complex **14** (5.5°, 8.4° and 10.1°), whereas larger are formed in complex **13** (11.8°, 13.5° and 25.4°). This can be a consequence of the resulting packing diagram that differs among these two cation complexes.

Table 3.11: Selected bond lengths (pm) and angles ($^{\circ}$) for complex **13**.

Ni1–O1	202.9(6)	Ni1–N2	201.2(6)
Ni1–N3	205.6(6)	Ni1–N7	200.7(6)
Ni1–N10	216.6(6)	Ni1–N12	217.7(6)
Ni2–O3	201.2(5)	Ni2–N4	198.7(6)
Ni2–N5	208.7(6)	Ni2–N13	199.0(6)
Ni2–N16	216.5(6)	Ni2–N18	219.3(5)
Ni3–O5	202.9(6)	Ni3–N1	212.1(7)
Ni3–N6	201.2(6)	Ni3–N19	201.3(7)
Ni3–N22	218.9(6)	Ni3–N24	220.9(6)
O1–Ni1–N2	91.9(3)	O1–Ni1–N3	169.6(3)
N2–Ni1–N3	77.8(3)	N7–Ni1–N10	75.7(3)
N7–Ni1–N12	76.4(2)	N10–Ni1–N12	151.5(3)
N4–Ni2–O3	91.9(2)	N4–Ni2–N5	78.4(2)
O3–Ni2–N5	169.8(2)	N13–Ni2–N16	76.2(2)
N13–Ni2–N18	76.1(2)	N16–Ni2–N18	152.3(2)
O5–Ni3–N6	89.9(2)	N6–Ni3–N1	76.6(3)
O5–Ni3–N1	166.4(2)	N19–Ni3–N22	75.9(2)
N19–Ni3–N24	75.7(2)	N22–Ni3–N24	151.6(3)

In both cases lattice solvents are present. Complex **13** crystallizes with water and DMF as solvent of crystallization which are involved in hydrogen bonding interactions among themselves and also with the donor atoms of the trinuclear Ni(II) core. The nitrate anion is unbounded and distorted and also hydrogen bonding interacting with the water lattice molecules. In addition, the tptz coligands are involved in π - π -stacking interactions, with the relative distance between the aromatic planes of around 320 pm. This results in a zigzag arrangement of the Ni₃ sheets along the b axis (Figure 3.30).

Table 3.12: Selected bond lengths (pm) and angles ($^{\circ}$) for complex **14**.

Ni1–O1	202.3(8)	Ni1–N2	200.1(9)
Ni1–N5	207.5(9)	Ni1–N7	202.2(9)
Ni1–N10	215.5(9)	Ni1–N11	217.3(9)
Ni2–O3	199.9(9)	Ni2–N16	206.6(9)
Ni2–N4	199.9(9)	Ni2–N16	215.7(10)
Ni2–N13	2.013(9)	Ni2–N17	220.3(11)
Ni3–O5	204.4(8)	Ni3–N3	206.2(9)
Ni3–N6	199.4(9)	Ni3–N19	199.8(9)
Ni3–N22	217.4(10)	Ni3–N23	217.0(10)
O1–Ni1–N5	166.7(3)	O1–Ni1–N2	90.1(3)
N2–Ni1–N5	77.1(3)	N7–Ni1–N10	75.6(3)
N7–Ni1–N11	76.0(3)	N10–Ni1–N11	150.2(3)
O3–Ni2–N1	168.4(4)	N4–Ni2–O3	91.4(3)
N1–Ni2–N4	77.1(4)	N13–Ni2–N16	76.1(4)
N13–Ni2–N17	76.0(4)	N16–Ni2–N17	151.1(4)
O5–Ni3–N3	167.8(3)	O5–Ni3–N6	90.7(3)
N6–Ni3–N3	77.8(4)	N19–Ni3–N22	75.8(4)
N19–Ni3–N23	75.8(4)	N22–Ni3–N23	150.7(4)

Supramolecular assemblies resulting through hydrogen bonding and π - π -stacking interactions are formed by self-organization of the trinuclear Ni(II) core and the unbounded chloride anion in complex **14** (Figure 3.31, 3.33 and 3.34). The chloride anion is in hydrogen bonding interaction with aromatic CH atoms of tptz coligands with CH \cdots Cl contact of around 340 pm (Figure 3.31, resulting in a pillared arrangement of the trinuclear Ni(II) entities along the c axis (Figure 3.32). These pillars are assembled along the a axis through π - π -stacking interactions between the offset slipped pyridine moieties of the tptz coligands which are interplanar separated by 338.1 pm distances (Figure 3.33 and 3.34). The resulting supramolecular aggregate contains a free tubular channels which is partly occupied by DMF molecules placed in the gaps between the methoxy-substituted

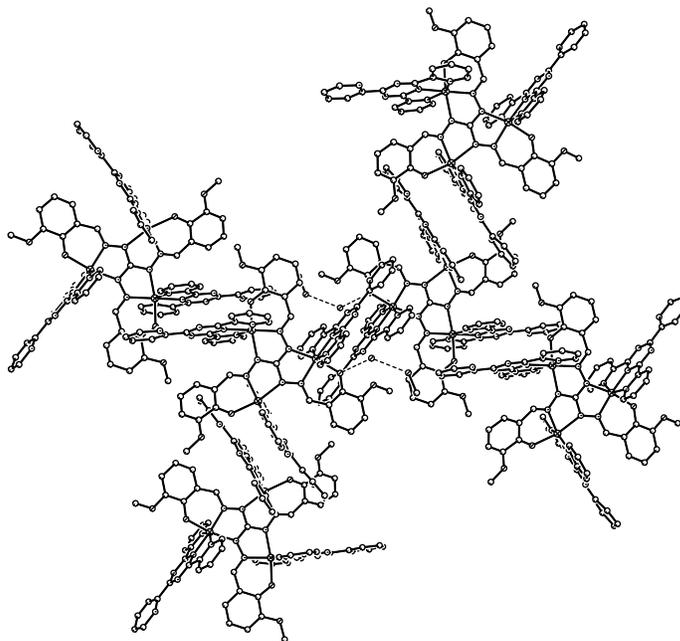


Figure 3.30: Packing diagram for complex $[\text{Ni}_3\text{L}^{\text{OMe}}(\text{tptz})_3]\text{NO}_3 \cdot 4.5\text{H}_2\text{O} \cdot 1.5\text{MeOH}$ (**13**) showing the hydrogen bonding interactions (dashed lines) and the zigzag π - π stacking interactions between tptz coligands.

rings of the triaminoguanidine-based ligand. The 3-D extension of this architectural motif leads to honeycomb channels with a central void space surrounded by other six empty void spaces (Figure 3.35). This resulting supramolecular architecture may assemble the requirements for a nanoporous material and hence its potential application for adsorption/desorption processes. Supramolecular network assembled by π - π -stacking interactions has been reported as stable at temperature up to 190° with possible replacement of guest molecules without breaking down the rigidity of the aggregates.²⁰³ Therefore, thermogravimetric analysis of complex **14** might be useful to verify the stability of the supramolecular assemblies.

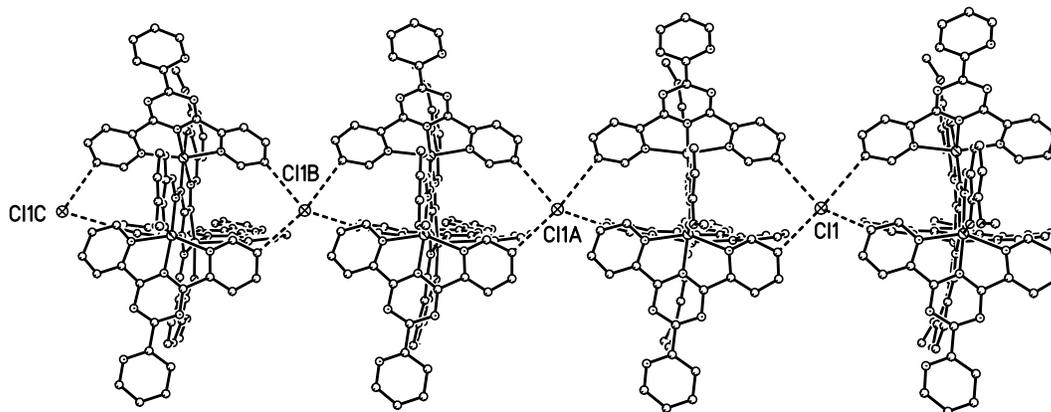


Figure 3.31: Packing diagram for complex $[\text{Ni}_3\text{L}^{\text{OMe}}(\text{tptz})_3]\text{Cl}\cdot 2\text{DMF}$ (**14**) showing the hydrogen bonding interaction formed by the chloride anion and aromatic system of the tptz coligands.

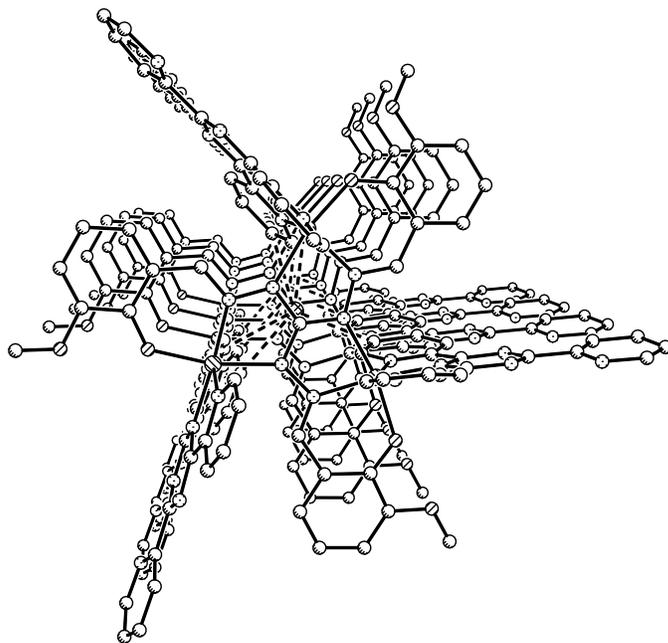


Figure 3.32: Packing diagram for complex **14** showing the pillared trinuclear Ni(II) entities formed through hydrogen bonding interactions of chloride anion with the aromatic system of the tptz coligands.

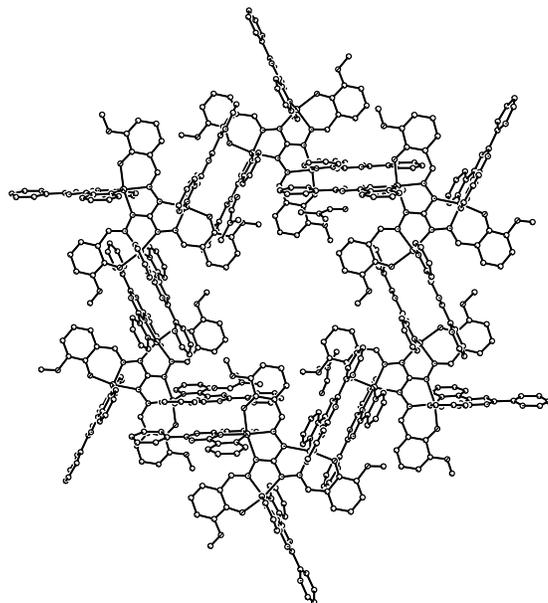


Figure 3.33: Packing diagram for complex **14** showing the formation of void space formed by π - π -stacking interaction of the offset slipped triazine-constituting moieties as viewed along the a axis. Hydrogen atoms and solvent molecules have been omitted for clarity.

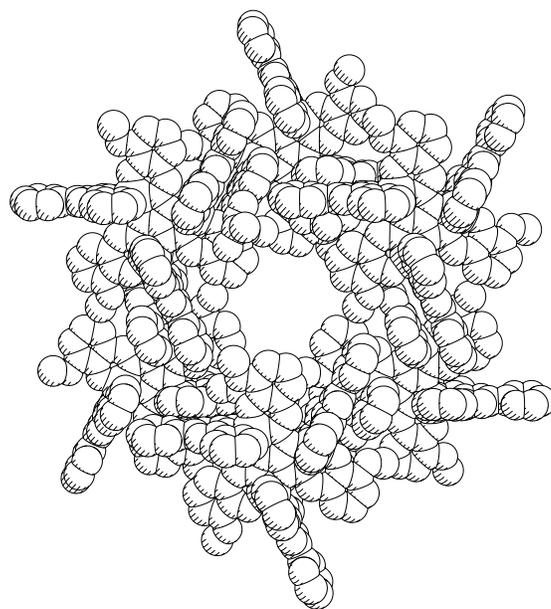


Figure 3.34: Space filling representation of the void space formed by π - π -stacked triazine-constituting moieties of complex **14**.

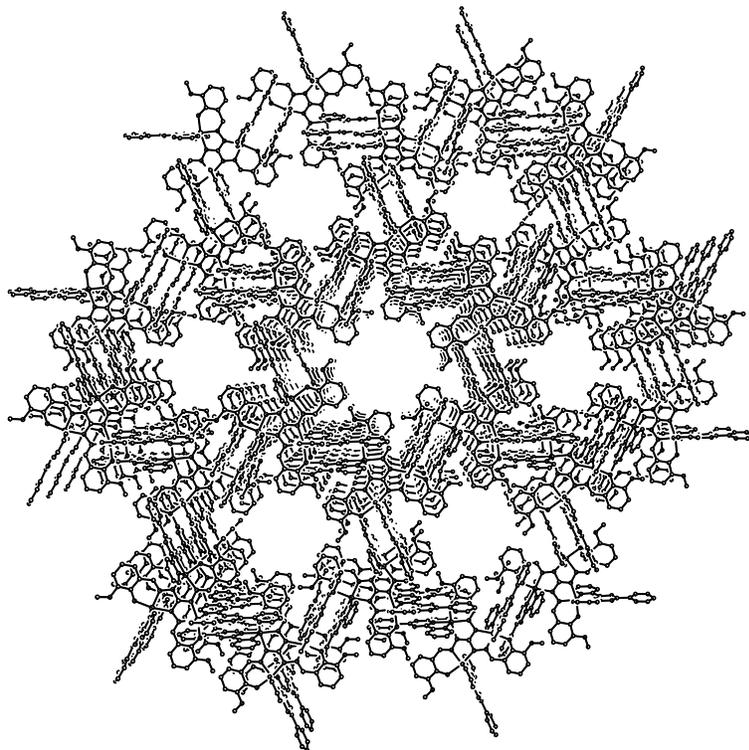


Figure 3.35: Representation of the honeycomb motif formed through packing of trinuclear entities of complex **14** as viewed along the *a* axis.

Magnetic properties

The magnetic susceptibility measurements for all three complexes have been performed in the temperature range of 300-2 K. The $\chi_M=f(T)$ and $\chi_M T=f(T)$ plots for an applied magnetic field of 2000 Oe are depicted in Figure 3.36 to 3.38 for complexes **13**, **14** and **15**, respectively. In the high limit temperature value, the χ_M values are $2.65 \text{ cm}^3\text{mol}^{-1}\text{K}$ for complex **13**, $3.24 \text{ cm}^3\text{mol}^{-1}\text{K}$ for complex **14** and $2.79 \text{ cm}^3\text{mol}^{-1}\text{K}$ for complex **15**, respectively. These values roughly correspond to an expected value of $3.00 \text{ cm}^3\text{mol}^{-1}\text{K}$ calculated for three uncoupled Ni(II) high-spin ions, assuming $g = 2$. On lowering the temperature, in all three cases a constant decrease of $\chi_M T$ product values have been registered reaching minima at 2 K of $0.06 \text{ cm}^3\text{mol}^{-1}\text{K}$ for **13**, $0.05 \text{ cm}^3\text{mol}^{-1}\text{K}$ for **14** and 0.01 for **15**, respectively. These low limit temperature values are very close to zero, therefore a resulting ground state $S_T = 0$ spin is reached by antiferromagnetic coupling in the Ni_3 core. The magnetic data sets have been simulated for all three complexes

using the Heissenberg-Van Vleck formalism developed for an equilateral Ni₃ triangle, in a similar manner as developed for cation complexes **6**, **9**, **10** and **11**, considering a single coupling parameter J . Although the structural features for complexes **13** and **14**, respectively showed crystallographically distinct Ni(II) centers, the chemical composition as well as the intermolecular separation are very similar within the Ni(II)-triad.

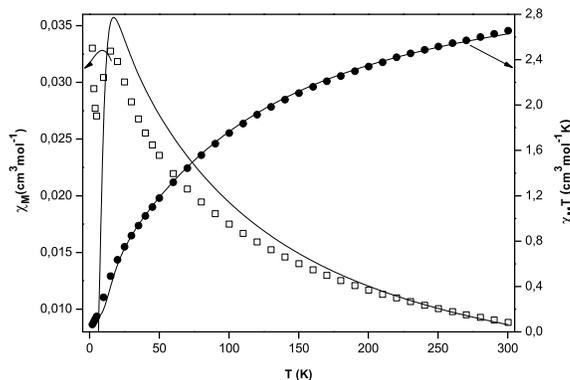


Figure 3.36: Plot of thermal dependence of χ_M (empty squares) and $\chi_M T$ product (black filled circles) for $[\text{Ni}_3\text{L}^{OMe}(\text{tptz})_3]\text{NO}_3 \cdot 4.5\text{H}_2\text{O} \cdot 1.5\text{MeOH}$ (**13**) complex measured with an applied magnetic field of 2000 Oe; the solid lines represent the theoretical curves (see text).

The best fit of the experimental data sets have been obtained fixing the $g = 2$ value, as previously described with the resulting fitting parameters listed in Table 3.13. The magnetic behavior of these three complexes is overall antiferromagnetic, with the coupling constant values very similar for cation complexes containing chloride (**14**) and perchlorate (**15**) anions and has a value around -31 cm^{-1} . For cation complex **13**, that contains a nitrate lattice anion, a relative higher coupling constant has been obtained ($J = -33 \text{ cm}^{-1}$), owing to smaller interatomic Ni···Ni separation and smaller torsion angles for diazine-bridged Ni(II) ions as compared to structurally characterized trinuclear Ni(II)-complex **14**. On the other hand, a variable g value led to inconsistent fitting parameters, similarly to previous described situation for corresponding trinuclear Ni(II) complexes based on tris(5-brom-2-hydroxy-salicylidene)triaminoguanidine ligand. It is also worth mentioning that no improvement of the quantitative simulation of the magnetic data sets

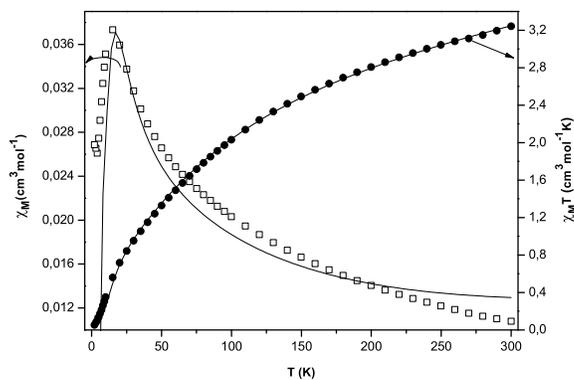


Figure 3.37: Plot of thermal dependence of χ_M (empty squares) and $\chi_M T$ product (black filled circles) for $[\text{Ni}_3\text{L}^{\text{OMe}}(\text{tptz})_3]\text{Cl}\cdot 2\text{DMF}$ (**14**) complex measured with an applied magnetic field of 2000 Oe; the solid lines represent the theoretical curves (see text).

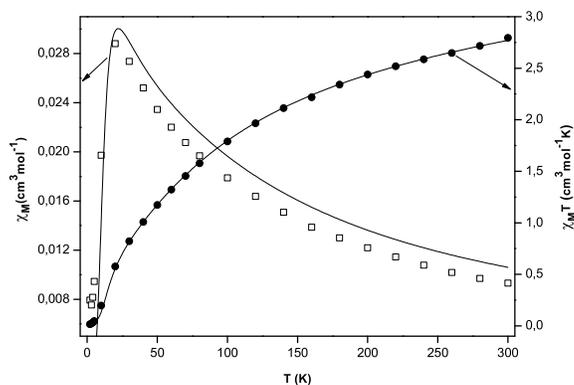


Figure 3.38: Plot of thermal dependence of χ_M (empty squares) and $\chi_M T$ product (black filled circles) for $[\text{Ni}_3\text{L}^{\text{OMe}}(\text{tptz})_3]\text{ClO}_4\cdot 5\text{H}_2\text{O}$ (**15**) complex measured with an applied magnetic field of 2000 Oe; the solid lines represent the theoretical curves (see text).

have been observed using the isosceles triangle model (Figure 3.11), by contrary the fit of the $\chi_M=f(T)$ plots became very problematic using this last exchange model pathway.

Table 3.13: Simulated magnetic data set for complex **13**, **14** and **15**.

	13	14	15
J (cm^{-1})	-33.55 ± 0.72	-31.17 ± 0.63	-31.45 ± 0.45
ρ	$0.04 \pm 4.65 \cdot 10^{-3}$	$0.05 \pm 4.28 \cdot 10^{-3}$	$0.01 \pm 2.87 \cdot 10^{-3}$
χ_{TIP} ($\text{cm}^3 \text{mol}^{-1}$)	$2.9 \cdot 10^{-4} \pm 5.0 \cdot 10^{-5}$	$1.9 \cdot 10^{-3} \pm 6.0 \cdot 10^{-5}$	$9.6 \cdot 10^{-4} \pm 4.0 \cdot 10^{-5}$
R^2	0.99879	0.998889	0.99969
Ni···Ni (pm)	493.8	497.9	-
	493.8	497.2	-
	498.7	498.2	-
torsion angles ($^\circ$) Ni–N–N–Ni	177.7	173.8	-
	155.9	177.6	-
	160.5	179.4	-

3.6 Conclusions

Threefold chelating ligands of type 5-bromo- and 3-methoxy- tris(salicylidene)triamino-guanidine ligands have been successfully use to isolated trinuclear Ni(II) complexes, using 2,2'-bipyridine and 2,4,6-tris(2-pyridyl)-1,3,5-triazine as coligands. The topology of the Ni₃^{II} triad is very similar among these series of complexes and it consists of octahedral nickel ions linked by three diazine (N–N) bridges with Ni–N–N–Ni torsion angles in the 150-178° range, responsible for the observed antiferromagnetic coupling within the Ni(II) triangles. The magnitude of the exchange coupling within the trinuclear Ni(II) complexes is determined by Ni···Ni interatomic separation which is close to 500 pm in complexes described herein. Moreover, rearrangement of the trinuclear Ni(II)-complexes took place in presence of Gd(NO₃)₃·6H₂O or K₄[Mo(CN)₈] to form pentanuclear Ni(II) complexes. The structural feature of these high-nuclearity Ni(II) complexes is better described as two triangular units hold together by a common nickel ion. In addition, interesting packing diagram have been obtained by variation of the counter ions with the highlight self-organization resulting in formation of nanochannels through hydrogen bonding and π - π -stacking interactions.

3.7 Trinuclear Co(III)-complexes with tris(3-methoxy-2-hydroxy-salicylidene)triaminoguanidine ligand

Following the previous synthetic pathway, tris(3-methoxy-2-hydroxy-salicylidene)triaminoguanidine ligand has been reacted with $\text{Co}(\text{ClO}_4)_2 \cdot 6\text{H}_2\text{O}$ and tptz coligand in MeOH/DMF solution. The solution turned immediately black when base (NEt_3) has been added and faded dark-brown in presence of acetone solution of $\text{Gd}(\text{NO}_3)_3 \cdot 6\text{H}_2\text{O}$. Co(II) ion has a peculiar role in magnetochemistry, being the d-metal with highest magnetic anisotropy, one of the important property that one should consider when magnetic materials are to be designed. Molecular structure determination shows a cation trinuclear Co(III) complex $[\text{Co}_3\text{L}^{\text{OMe}}(\text{bcpa})_3]\text{NO}_3 \cdot 6\text{DMF}$ (**16**) which contains the triaminoguanidine-based ligand and the hydrolyzed 2,4,6-tris(2-pyridyl)-1,3,5-triazine coligand (Figure 3.39). The hydrolysis of the triazine-type ligand has been previously reported to occur in presence of Cu(II) salts accompanied by *in situ* copper complex formation.^{157–162} The cobalt perchlorate salt behaved similarly with the resulting trinuclear Co(III) complex containing bis(2-pyridylcarbonyl)amine as new coligand system (see also Figure 3.1).

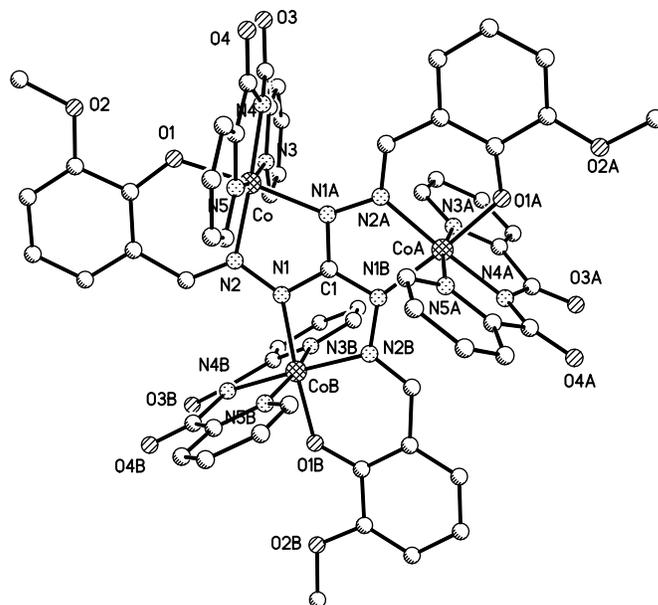


Figure 3.39: Molecular structure and selected numbering scheme of complex $[\text{Co}_3\text{L}^{\text{OMe}}(\text{bcpa})_3]\text{NO}_3 \cdot 6\text{DMF}$ (**16**); Hydrogen atoms have been omitted for clarity; only the cationic structural motif is shown

The reaction is also accompanied by aerial oxidation of the initial cobalt(II) ion to Co(III) metal ions owing to no efforts to exclude air or moisture during the reaction. The triaminoguanidine-based ligand coordinates in the classical fashion as threefold tridentate system, accommodating three Co(III) ions. The Co-to-phenolate oxygen bond lengths are smaller compared to corresponding bond distances in trinuclear Ni(II) complexes, due to the closed-shell electronic structure of the diamagnetic cobalt ions. The same effect has been observed for cobalt-to-nitrogen atoms bond lengths that fall in the 192.2-196.1 pm range. The bis(2-pyridylcarbonyl)amine (Hbcpa) wraps around each Co(III) ion in tridentate chelation fashion through a pair of pyridyl-nitrogen atoms and deprotonated amide nitrogen atom with the bite angles of 83.7° for N3–Co–N4 and 83.8° for N4–Co–N5. The Co–N bond lengths are 192.5 pm (Co–N5) and 193.7 pm (Co–N3) for cobalt-to pyridine nitrogen atoms and 189.2 pm for cobalt-to-amide nitrogen atom (N4). These bond distances are close to reported similar bond lengths in mononuclear d-complexes of type [M(bcpa)₂].

The resulting ON₅ environment describes a distorted octahedral geometry for each Co(III) ion with the *trans* angles of 175.6° (O1–Co–N1) and 177.0° (N4–Co–N2). The positive charge of the Co₃^{III} core is compensated by the unbounded nitrate anion placed

Table 3.14: Selected bond lengths (pm) and angles (°) for complex **16**.

Co–O1	188.8(3)	Co–N1	196.1(3)
Co–N2	192.2(3)	Co–N3	193.7(5)
Co–N4	189.2(3)	Co–N5	192.5(5)
O1–Co–N1	175.62(12)	O1–Co–N2	94.67(12)
O1–Co–N3	89.82(17)	O1–Co–N4	82.62(13)
O1–Co–N5	88.31(17)	N2–Co–N1	81.01(13)
N2–Co–N3	95.07(16)	N2–Co–N5	97.32(18)
N3–Co–N1	91.28(19)	N4–Co–N1	101.71(13)
N4–Co–N2	177.04(14)	N4–Co–N3	83.75(17)
N4–Co–N5	83.84(19)	N5–Co–N3	167.58(19)
N5–Co–N1	91.51(18)		

in close vicinity of the trimetallic core. Again, as previously observed for crystallization procedure adopted for complex **6**, the lanthanide ion played the role of anion exchanger and/or most likely helps the crystallization process. It is worth mentioning that neither crystals of complex **16**, nor with an intact triazine-coligand could be isolated in absence of the lanthanide salt. Complex **16** crystallizes in the monoclinic $P6_3$ space group, with a C_3 symmetry that passes through the guanidine carbon atom C1 and the nitrate anion. The $\text{Co} \cdots \text{Co}$ intermolecular separation through diazine linkers is 477.4 pm with the Co-N-N-Co torsion angle is 177.9° , value very close to a linear arrangement of the diazine-bridged cobalt ions. If a tetragonal plane is defined, as previously described, the dihedral angles between these planes are 9.2° which confirms the planarity of the structure.

The trinuclear Co(III) -complex **16** contains lattice solvents, such as DMF with the final formula $[\text{Co}_3\text{L}^{OMe}(\text{bcpa})_3]\text{NO}_3 \cdot 6\text{DMF}$. The packing diagram viewed along the crystallographic c axis shows π - π stacking interaction between the pyridine rings of the bis(2-pyridylcarbonyl)amine coligand molecules with the interplanar separation of 337.8 pm (Figure 3.40). The resulting extended two-dimensional network presents a close alternating arrangement of the π -stacked moieties as observed for complex **14**. However, conversely to organization observed for cation trinuclear Ni(II) complex **14**, the hydrolyzed tptz ligand do not assemble to form nano-channels owing to a smaller volume occupied by bcpa coligands. Complex **16** is diamagnetic also according with SQUID measurements where a specific diamagnetic answer has been registered.

Nevertheless, interesting magnetostructural features of this trinuclear Co(III) -complex are represented by electrochemical investigations that might result in corresponding reduced Co(II) complex. On the other hand, the diamagnetic Co(III) complex may also be used as molecular brick to construct interesting photomagnetic materials. Exiting reports of $[\text{M}(\text{bcpa})_2]$ complexes showed that this simple unit can be successfully used as "complex-ligand" owing to their bidentate chelating capacity *via* the carbonyl sites leading to extended structural assemblies in controlled manner.^{159, 204, 205} For example association of cobalt(III) complex with iron(II) species (known to be well accommodated by bcpa coligands) may represent a very beautiful example of intramolecular electron-transfer system. Lanthanide complexes are well documented as light-emitting diodes. Therefore, association of the diamagnetic trinuclear Co(III) complex with lanthanides

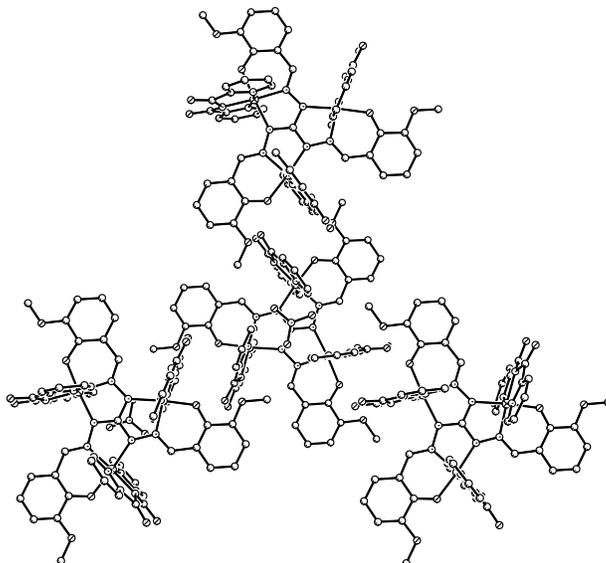


Figure 3.40: Packing diagram for complex **16** showing π - π -stacking interactions of the bcpa-coligands; the nitrate anion are also shown.

salts (i.e. hexafluoroacetylacetonate lanthanide derivatives) can result in interesting assemblies with optical properties.

3.8 Future perspectives

Triazine-type organic framework has been extensively used to generate interesting extended network architectures. The topologies of the 3-D nets have been described to vary according to used metal ions as well as the anions that influence the organization of the oligomeric constituent units. For example, Cu^I- complexes based on 2,4,6-tri(4-pyridyl)-1,3,5-triazine (tpt) ligand has been reported as octahedral-like cages,²⁰⁶ whereas the zinc-containing complexes have been assembled in 3-D nets with (10,3) topology²⁰⁷ and/or interpenetrating cubing-like networks with large sealed-off chambers,²⁰⁸ these last two supramolecular architectures been determined by the used anions. In addition, [Ni(tpt)(NO₃)₂] \cdot solvent complex polymerize to form a rare 3-D net with (12,3) topology formed by alternation of T- and trigonal nodes.²⁰⁹ Hence, the importance of the isolated trinuclear Ni(II)-complexes with triazine-type coligands as molecular bricks to construct interesting architectural assemblies trough a controlled process. Slight modification of the triazine coligand²¹⁰ (Figure 3.41) may also be used to follow the "node" and "spacer"

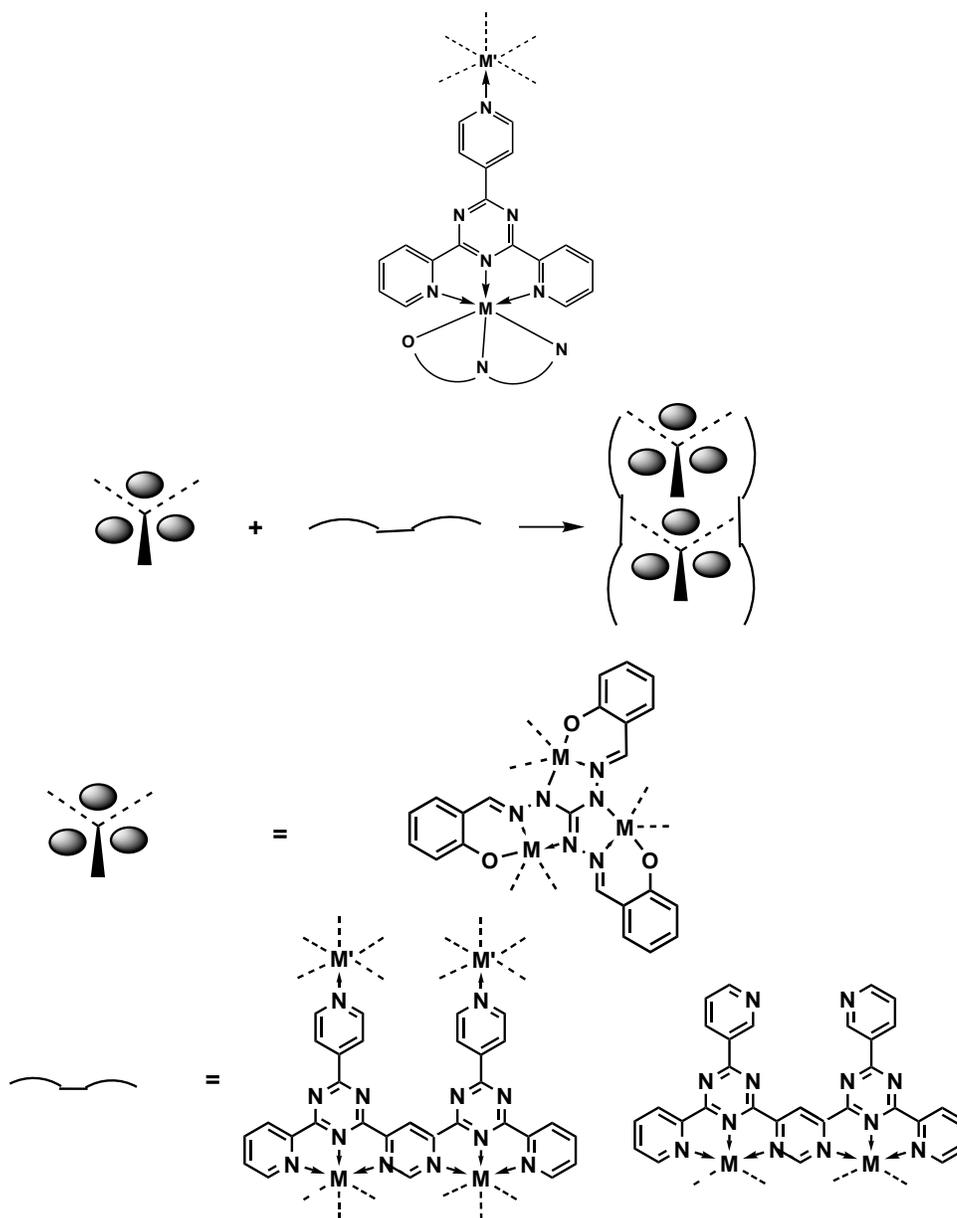


Figure 3.41: Proposed new triazine-like coligand with linking capacity similar to 4,4'-bipyridine (up) and schematic representation of possible high-nuclear clusters assembled by extended terpyridine-like coligands.

strategy developed by Robson *et al*, theory applied very well for 4,4'-bipyridine linker.

The new proposed triazine linker can coordinated in the known terpyridine-like fashion as coligand to the trinuclear d-metal complexes of triminoguanidine-based ligands, whereas the terminal pyridine nitrogen atom may be successfully used to link another metal-complex entity. The variation of the triazine-derivatives to more extended

terpyridine-like ligand may show interesting feature, giving the possibility to design high-nuclearity clusters (Figure 3.41 bottom picture).

3.9 Experimental Part

Triaminoguanidine and the corresponding Schiff base ligands have been prepared according with the existing reports.^{40,147}

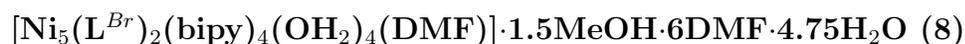
Synthesis of polynuclear Ni(II)-complexes with tris(5-bromo-2-hydroxy-salicylidene)triaminoguanidine ligand and 2,2'-bipyridine coligand



To a DMF solution (15 mL) of tris(5-bromo-2-hydroxy-salicylidene)triaminoguanidine ligand (H_5L^{Br}) (57.0 mg, 0.0893 mmol) was added a methanol (5 mL) solution of $\text{Ni}(\text{ClO}_4)_2 \cdot 6\text{H}_2\text{O}$ (92.5 mg, 0.25 mmol) and the resulting solution has been stirred for around 15 minutes at room temperature. A methanol (5 mL) solution of 2,2'-bipyridine (bipy) (40.0 mg, 0.25 mmol) was added stepwise, followed by addition of tetrabutylammoniumhydroxyde (0.33 mL, 0.5 mmol) and the resulting solution has been allowed to react for additional 10 minutes. $\text{Gd}(\text{NO}_3)_3 \cdot 6\text{H}_2\text{O}$ (110.0 mg, 0.25 mmol) dissolved in MeOH (5 mL) was added stepwise under continuing stirring. The reaction has been continued for other 10 minutes, filtered and allowed to stand at room temperature. Crystal suitable for X-ray measurement have appeared within a month. Yield: 42.0 mg (0.026 mmol, 32.6%). *Anal. Calc.* for $\text{C}_{55}\text{H}_{59}\text{N}_{14}\text{Br}_3\text{O}_{15}\text{Ni}_3$ ($[\text{Ni}_3\text{L}^{Br}(\text{bipy})_3(\text{OH}_2)_3]\text{NO}_3 \cdot 5\text{H}_2\text{O}$) (1571.04): C 42.02, H 3.78, N 12.48. Found: C 42.14, H 3.58, N 12.46. Selected IR data (cm^{-1}): 3400 (br, H_2O), 1653 (s, $-\text{CH}=\text{N}$), 1384 (s, NO_3^-). Additionally, the trinuclear Ni(II) complex **6** can be obtained following the above conditions, but without gadolinium salt. In this case a precipitate is formed by allowing the resulting solution to stand at r.t. for slow evaporation.

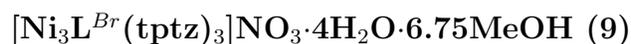


Tris(5-bromo-2-hydroxy-salicylidene)triaminoguanidine ligand (H_5L^{Br}) (57.0 mg, 0.0893 mmol) has been dissolved in a mixture DMF/ CH_3CN (1:1) (10 mL). To this resulting pale yellow solution $\text{NiCl}_6\cdot\text{H}_2\text{O}$ (60.0 mg, 0.25 mmol) dissolved in methanol (5 mL), followed by addition of a methanolic (5 mL) solution of 2,2'-bipyridine (bipy) (40.0 mg, 0.25 mmol) and tetrabutylammoniumhydroxyde (0.33 mL, 0.5 mmol). The resulting solution has been allowed to react for 15 minutes, filtered and allowed to stand at room temperature. Crystals suitable for X-ray measurement have appeared approximately within a month. Yield: 73.0 mg (0.044 mmol, 52.6%). *Anal. Calc.* for $\text{C}_{66}\text{H}_{68}\text{N}_{17}\text{Br}_3\text{ClO}_7\text{Ni}_3$ ($[\text{Ni}_3\text{L}^{Br}(\text{bipy})_3(\text{DMF})_2\text{Cl}]\cdot 2\text{DMF}\cdot\text{CH}_3\text{CN}$) (1662.64): C 47.68, H 4.12, N 14.32. Found: C 48.18, H 5.46, N 13.10. Selected IR data (cm^{-1}): 3400 (br, solvent), 1653 (s, $-\text{CH}=\text{N}$).



Complex **7** (73.0 mg, 0.44 mmol) dissolved in DMF (5 mL) was layered in a test-tube with a layer of 2 mL MeOH/ H_2O (1:1) mixture. At the end a third layer of an aqueous solution (2 mL) of $\text{K}_4[\text{Mo}(\text{CN})_8]$ (21.0 mg, 0.041 mmol). Crystals suitable for X-ray measurements are formed within two days and in general fall on the bottom of the test-tube. Yield: 25.8 mg (0.009 mmol, 39.0%). *Anal. Calc.* for $\text{C}_{105}\text{H}_{128}\text{N}_{27}\text{Br}_6\text{O}_{24}\text{Ni}_5$ ($[\text{Ni}_5\text{L}_2^{Br}(\text{bipy})_4(\text{OH}_2)_4]\cdot 1.5\text{MeOH}\cdot 6\text{DMF}\cdot 4.75\text{H}_2\text{O}$) (2916.26): C 43.86, H 4.46, N 12.97. Found: C 43.67, H 4.41, N 12.93. Selected IR data (cm^{-1}): 3400 (br, solvent), 1653 (s, $-\text{CH}=\text{N}$). EPR (r.t): $g = 2.0048$.

Synthesis of polynuclear Ni(II)-complexes with tris(5-bromo-2-hydroxy-salicylidene)triaminoguanidine ligand and 2,4,6-tris(2-pyridyl)-1,3,5-triazine coligands



To a DMF solution (15 mL) of tris(5-bromo-2-hydroxy-salicylidene)triaminoguanidine ligand (H_5L^{Br}) (57.0 mg, 0.0893 mmol) was added a methanol (5 mL) solution of $\text{Ni}(\text{NO}_3)_2\cdot 6\text{H}_2\text{O}$ (70.0 mg, 0.25 mmol), followed by addition of triethyl amine (1 mL 1N solution

in methanol) and the resulting solution has been stirred for around 15 minutes while a precipitate is formed. A methanol (5 mL) solution of 2,4,6-tris(2-pyridyl)-1,3,5-triazine (tptz) (78.0 mg, 0.25 mmol) was added stepwise. This cause a dissolution of the mixture and the reaction has been continued for 15 minutes at r.t. The resulting solution has been filtered and allowed to stand at room temperature. Crystal suitable for X-ray measurement have been obtained by slow diffusion of diethyl ether in the reaction solution. Yield: 88.0 mg (0.040 mmol, 52.2%). *Anal.* Calc. for $C_{80}H_{72}N_{25}Br_3O_{14}Ni_3$ ($[Ni_3L^{Br}(tptz)_3]NO_3 \cdot 4H_2O \cdot 6.75MeOH$) (2077.90): C 47.40, H 3.27, N 17.19. Found: C 47.41, H 3.46, N 17.53. Selected IR data (cm^{-1}): 3420 (br, solvent), 1653 (s, -CH=N), 1468, 1441 (-triazine CH=N), 1384 (s, NO_3^-). EPR (r.t): $g = 2.001$.

$[Ni_3L^{Br}(tptz)_3]Cl \cdot 10H_2O$ (10)

Complex **10** has been obtained following the same reaction pathway as above, replacing the nickel nitrate salt with $NiCl_2 \cdot 6H_2O$ (70.0, 0.25 mmol). Yield: 88.0 mg (0.040 mmol, 52.2%). *Anal.* Calc. for $C_{76}H_{63}N_{24}Br_3O_{13}ClNi_3$ ($[Ni_3L^{Br}(tptz)_3]Cl \cdot 10H_2O$) (1971.74): C 46.30, H 3.22, N 17.05. Found: C 46.10, H 4.15, N 17.19. Selected IR data (cm^{-1}): 3401 (br, solvent), 1653 (s, -CH=N), 1468, 1441 (-triazine CH=N). EPR (r.t): $g = 2.002$.

$[Ni_3L^{Br}(tptz)_3]ClO_4 \cdot 7H_2O \cdot DMF$ (11)

Complex **11** has been synthesized following the same strategy as described for 9 but with $Ni(ClO_4)_2 \cdot 6H_2O$ (92.5 mg, 0.25 mmol). Yield: 77.0 mg (0.038 mmol, 46.6%). *Anal.* Calc. for $C_{79}H_{64}N_{25}Br_3O_{14}ClNi_3$ ($[Ni_3L^{Br}(tptz)_3]ClO_4 \cdot 7H_2O \cdot DMF$) (2054.78): C 46.18, H 3.14, N 17.04. Found: C 46.10, H 3.82, N 17.04. Selected IR data (cm^{-1}): 3420 (br, solvent), 1653 (s, -CH=N), 1468, 1441 (-triazine CH=N), 1177 (s, Cl_4^-). EPR (r.t): $g = 2.001$.

$[Ni_5(L^{Br})_2(tptz)_4] \cdot 7.5H_2O \cdot 6MeOH$ (12)

To a methanol solution (15 mL) of tris(5-bromo-2-hydroxy-salicylidene)triaminoguanidine ligand (H_5L^{Br}) (57.0 mg, 0.0893 mmol) was added a mixture of aqueous solution of $Ni(NO_3)_2 \cdot 6H_2O$ (70.0 mg, 0.25 mmol) and methanol solution of 2,4,6-tris(2-pyridyl)-1,3,5-triazine (tptz) (78.0 mg, 0.25 mmol), followed by addition of tetrabutylammonium hydroxide (0.30 mL 40% aqueous solution) and the resulting solution has been stirred for

around 5 minutes while a precipitate is formed. This has been redissolved in DMF and the reaction has been continued for another 15 minutes. The resulting solution has been filtered and allowed to stand at room temperature. Crystal suitable for X-ray measurement have been obtained upon slow evaporation within two days. Yield: 58.0 mg (0.036 mmol, 55.0%). *Anal. Calc.* for $C_{116}H_{90}N_{36}Br_6O_{15}Ni_5$ ($[Ni_5L_2^{Br}(tptz)_4] \cdot 9H_2O$) (3001.14): C 46.42, H 3.02, N 16.80. Found: C 46.53, H 3.09, N 16.60. Selected IR data (cm^{-1}): 3434 (br, solvent), 1666 (s, -CH=N), 1468, 1433 (-triazine CH=N).

Synthesis of polynuclear Ni(II)-complexes with tris(3-methoxy-2-hydroxy-salicylidene)triaminoguanidine ligand and 2,4,6-tris(2-pyridyl)-1,3,5-triazine coligands

The synthesis of trinuclear Ni(II) complexes with tris(3-methoxy-2-hydroxy-salicylidene)triaminoguanidine ligand (46.0 mg, 0.0893 mmol) have been prepared as described above for analogous nickel complexes synthesized with tris(5-bromo-2-hydroxy-salicylidene)triaminoguanidine ligand.

$[Ni_3L^{OMe}(tptz)_3]NO_3 \cdot 4.5H_2O \cdot 1.5MeOH$ (13)

Crystal suitable for X-ray measurement have been obtained by slow diffusion of diethyl ether into the reaction solution. Yield: 90.0 mg (0.048 mmol, 58.4%). *Anal. Calc.* for $C_{79}H_{70}N_{25}O_{15}Ni_3$ ($[Ni_3L^{OMe}(tptz)_3]NO_3 \cdot 6H_2O$) (1785.67): C 53.14, H 3.95, N 19.61. Found: C 53.27, H 4.07, N 19.16. Selected IR data (cm^{-1}): 3420 (br, solvent), 1669 (s, -CH=N), 1472, 1447 (-triazine CH=N), 1384 (s, NO_3^-).

$[Ni_3L^{OMe}(tptz)_3]Cl \cdot 2DMF$ (14)

Crystal suitable for X-ray measurement have been obtained upon slow evaporation of the reaction solution within two days. Yield: 54.0 mg (0.027 mmol, 32.45%). *Anal. Calc.* for $C_{88}H_{93}N_{27}O_{16}Ni_3$ ($[Ni_3L^{OMe}(tptz)_3]Cl \cdot 3DMF \cdot 7H_2O$) (1996.42): C 52.94, H 4.70, N 18.94. Found: C 53.04, H 4.09, N 18.65. Selected IR data (cm^{-1}): 3422 (br, solvent), 1669 (s, -CH=N), 1472, 1447 (-triazine CH=N).

[Ni₃L^{OMe}(tptz)₃]ClO₄·4H₂O·4MeOH (15)

Yield: 105.0 mg (0.058 mmol, 69.8%). *Anal.* Calc. for C₇₉H₆₈N₂₄O₁₅Ni₃ ([Ni₃L^{OMe}(tptz)₃]ClO₄·5H₂O) (1805.11): C 52.57, H 3.80, N 18.62. Found: C 52.59, H 4.37, N 18.70. Selected IR data (cm⁻¹): 3420 (br, solvent), 1662 (s, -CH=N), 1472, 1447 (-triazine CH=N), 1208 (s, Cl₄⁻). EPR (r.t): g = 1.998. EPR (r.t in MeOH): g = 2.184. EPR (77 K): g = 2.003.

[Synthesis of trinuclear Co(III) complex

Co₃L^{OMe}(bcpa)₃]NO₃·6DMF (16)

To a DMF (5 mL) of tris(3-methoxy-2-hydroxy-salicylidene)triaminoguanidine ligand (46.0 mg, 0.0893 mmol) was added a methanolic solution of Co(ClO₄)₂ (92.0 mg, 0.25 mol), followed by addition of triethyl amine (0.5 mL 1 N solution). The reaction mixture was stirred for around five minutes and then 2,4,6-tris(2-pyridyl)-1,3,5-triazine (78.0 mg, 0.25 mmol) dissolved in MeOH (5 mL) was added to the first solution, followed by addition of Gd(NO₃)₃·6H₂O (110.0 mg, 0.25 mmol) dissolved in acetone (5 mL). The reaction was continued for 15 minutes, filtered and left at room temperature for slow evaporation. Crystal suitable for X-ray measurement have been obtained within two weeks. Yield: 72.0 mg (0.046 mmol, 55.0%). *Anal.* Calc. for C₆₇H₆₀N₁₈O₁₇Co₃ ([Co₃L^{OMe}(bcpa)₃]NO₃·2DMF) (1566.14): C 51.38, H 3.86, N 16.10. Found: C 51.26, H 3.97, N 15.47. Selected IR data (cm⁻¹): 3435 (br, solvent), 1723 (s, C=O), 1669 (s, -CH=N), 1329 (s, NO₃⁻).

Chapter 4

Polynuclear oxo-bridged d-metal complexes

Magnetic molecular clusters formed by small number of metallic centers are active research area which involves both magnetochemistry and biochemistry. A reason for this intensive research is based on possibility to use simple molecular clusters that exhibit unusual magnetic properties as academic tool to understand the properties of multinuclear assemblies. In addition such small molecules may be used as building blocks for the assembly of high-spin dendritic magnetic materials²¹¹ and/or molecular-based magnets.^{9,26,212,213} Oxo-bridged transition metal ion complexes are a class of compounds of general interest due to their molecular structure, magnetic properties and intramolecular electron transfer features.²¹⁴ Dinuclear and trinuclear $[M(\mu_2-O)_n]$ ($n = 1, 2$) containing compounds have been intensively studied especially due to their intriguing magnetic behavior²¹⁵⁻²¹⁷ that vary from anti- to ferromagnetic interaction mediated by oxygen-containing bridges. A particular attention has been paid to dinuclear iron(III) complexes bridged by carboxylate residues and/or water-derived ligands (i.e. oxo or hydroxy) designed as synthetic analogues for the active site of iron-containing enzymes such as hemerytin,^{218,219} ribonucleotide reductase,²²⁰ methane monooxygenase^{221,222} and purple acid phosphatase.²²³ The functions performed by these metalloproteins led to a broad range of biomimetic catalytic reactions with the Fe(III) metal complexes reported as catalysts for various oxidation reactions.^{224,225} Moreover, iron(III) is an interesting metal ion in magnetochemistry due to the large number (five) of unpaired electrons ($S = 5/2$), a

property which for certain topologies, offers the potential to form high-spin clusters with ground state spin reaching a value of $S = 33/2$.²¹¹ On the other hand copper-containing complexes are also relevant for both magnetochemistry and biochemistry. Polynuclear Cu(II) complexes have been reported in large numbers as models for metalloenzymes²²⁶ and in addition used as molecular bricks to generate different magnetic materials.²²⁷ In biological systems, triangular copper oxo-centered structure has been reported in a subunit of methane mono-oxygenase with ferromagnetic coupling between the paramagnetic centers.²²⁸ Even though the magnetic interaction in oxo-bridged Cu(II) complexes has mainly been found to be antiferromagnetic, spin-frustration in limited number of trinuclear copper complexes has also been observed.³⁴ The self-organization of inorganic-organic hybrid led to unpredicted ferromagnetic interaction between the paramagnetic centers induced by accidental orthogonality of the magnetic orbitals.¹⁰ Moreover, in d-transition metal ion complexes competing spin interactions that led to unpredictable ground state spins has been often observed.²²⁹ Therefore, magneto-structural characterization of simple molecular cluster is worth investigating. The feasibility of salen-type ligands to generate d-metal complexes is well established.²³⁰ Hence dinuclear oxo-bridged Fe(III) complexes based on N,N'-ethylene-bis(pyridoxylideneiminato) Schiff base ligand (H₂pyren) has been isolated. This salen-type organic frameworks present a hydroxymethylene arm which builded up a 1-D polymeric architectures through hydrogen bonding interactions. The topology of the iron(III) centers in this homodinuclear oxo-bridged complex comprises pentacoordinated iron ions that sometimes may show intriguing magnetic properties.¹⁰ Further on, magneto-structural characterization of a dinuclear Fe(III) complex based on N-salicylidene-2-bis(2-hydroxyethyl)amino)ethylamine (H₂sabhea) will be also discussed. This organic ligand has been used by our group to generate bioinspired d-metal complexes²³¹⁻²³⁴ and to establish magneto-structural relationships for V(IV)-oxo complexes.^{235,236} In addition lanthanide-containing H₂sabhea compounds have also been reported and magnetostructural properties have been discussed.²³⁷ Last, but not least a partial cubane-like structural motif in trinuclear oxo-bridged Cu(II) complex will be presented. This last complex contains phenoxy- and hydroxy-bridged Cu(II) centers and has been isolated using [2-(2-dimethylamino-ethylimino)-methyl]-phenol ligand. Instead, the methoxy-derivative of the same supporting ligand made possible the isolation of a

dinuclear Cu(II) complex with a Cu–O(Ph)–Cu unit. By comparison to the trinuclear Cu(II) complex, an antiferromagnetic interaction between the metal ions occurs.

4.1 Dinuclear oxo-bridged Fe(III)-complex with N,N'-ethylene-bis(pyridoxylideneiminato) ligand

Salen-type ligands represent a class of organic ligands extensively used to generate coordination compounds.²³⁰ These ligands are in general based on N-salicylidene- and derivatives of salicylaldehyde components, and the reports of pyridoxal Schiff base derivatives is rather scarce. Pyridoxal hydrochloride-vitamin B6, has been reacted with ethylene diamine to form a salen-like ligand of type bis(N,N'-pyridoxal-ethylene)diamine (H₂pyren).²³⁸ Although this organic ligand presents several coordination sites, only the phenol and imine nitrogen atoms have been found to be involved in iron coordination. The phenol oxygen atoms are deprotonated upon reaction with iron perchlorate in the presence of NaOH base, in methanol solution. The molecular structure of the homodinuclear [Fe(pyren)]₂O·3H₂O (**17**) complex is depicted in Figure 4.1 with selected bond lengths and angles listed in Table 4.1. The structure comprises two FeO₂N₂ coordination cores linked by an oxo-group, resulting in two pentadentate Fe(III) centers. Each organic ligand chelates in salen-type fashion acting as tetradentate coordinating system through six- and five-membered rings. The two mononuclear iron(III) constituting units are very similar with iron to phenolate bond distances of around 192 pm and iron to imine nitrogen atoms bond distances with 210.3–211.7 pm range. The two "salen"-type ligand units bind Fe(III) ion very similarly, with bite angles of around 85.6° for O–Fe–N binding angles and 76.8° for N–Fe–N binding angles, respectively. The resulting coordination environment of Fe(III) centers can be described as distorted square-pyramidal geometries with distortions from an ideal square pyramidal geometry of $\tau = 0.167$ for FeA center and $\tau = 0.08$ for FeB ion, respectively. The distortion of the coordination geometry from the square pyramid to the trigonal bipyramid have been calculated by the τ parameter as an index of the degree of trigonality. This τ value is defined as the difference between the two largest donor-metal-donor angles divided by 60 and has a $\tau = 0$ value

for an ideal square pyramid and $\tau = 1$ for the trigonal bipyramid.²³⁹ This structural data indicates that the FeB center has a more regular square-pyramidal geometry, being displaced out from the ligand plane by 57.66 pm, whereas FeA ion in a more distorted square-pyramidal environment is displaced out from the ligand plane by 56.24 pm, both towards the bridged oxygen atom O1.

The apical position of the defined geometry for both ions is occupied by μ_2 -O ligand which holds together the two Fe(III) entities, with bond distance FeA–O1 of 179.3 pm and FeB–O1 bond length of 178.8 pm forming a FeA–O1–FeB angle of 143.1°. The Fe–O–Fe angle value is similar to corresponding reported value for pentacoordinated [(Fesalen)₂O] complexes for which the oxo-bridge has been reported to mediate strong antiferromagnetic interaction when bridges close to linearity and within the 116–180° range reported for other oxo-bridged complexes.^{240–242}

Complex **17** crystallizes with three water molecules per unit cell as solvent of crystallization. These lattice water molecules are in hydrogen bonding interactions of 280.5 pm and further in hydrogen bonding interactions with the hydroxy-methylene functionalities of the salen-type supporting ligand (Ow···O2A 296.8 pm and Ow···O2B 277.7 pm).

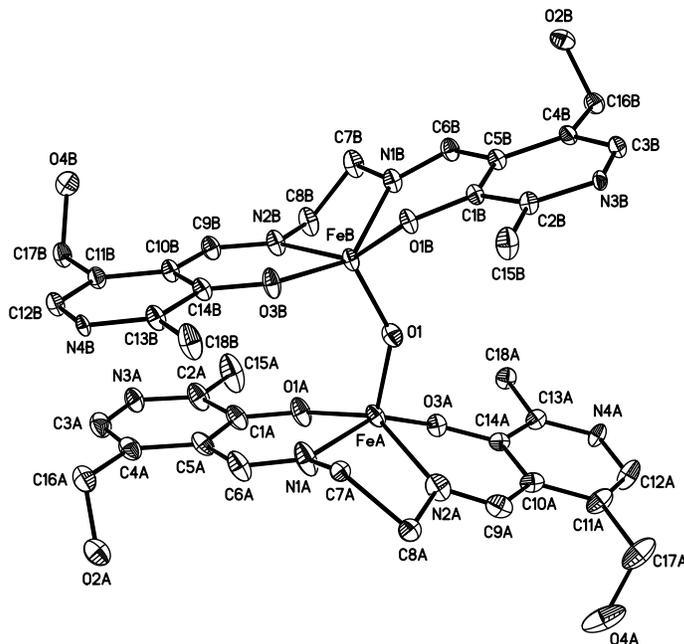


Figure 4.1: Molecular structure for $[\text{Fe}(\text{pyren})]_2\text{O}\cdot 3\text{H}_2\text{O}$ (**17**) complex. Thermal ellipsoids are drawn at 50% probability. Hydrogen atoms have omitted for clarity.

Table 4.1: Selected bond lengths (pm) and angles ($^{\circ}$) for complex **17**.

FeA–O1	179.28(17)	FeA–O1A	192.05(17)
FeA–O3A	194.65(17)	FeA–N1A	211.7(2)
FeA–N2A	210.3(2)	FeB–O1	178.86(17)
FeB–O3B	192.41(16)	FeB–O1B	194.77(15)
FeB–N1B	210.79(19)	FeB–N2B	211.50(18)
O1–FeA–O1A	112.24(8)	O1–FeA–O3A	108.19(7)
O1–FeA–N1A	98.63(9)	O1–FeA–N2A	104.48(8)
O1–FeB–O1B	108.33(7)	O1A–FeA–O3A	93.11(7)
O1A–FeA–N1A	85.83(8)	O1A–FeA–N2A	141.29(8)
O3A–FeA–N1A	151.31(9)	O3A–FeA–N2A	86.61(8)
N2A–FeA–N1A	76.80(9)	FeA–O1–FeB	143.11(10)
O1–FeB–O3B	111.79(8)	O1–FeB–N1B	103.57(8)
O1–FeB–N2B	101.69(8)	O1B–FeB–N1B	86.28(7)
O1B–FeB–N2B	148.29(8)	O3B–FeB–O1B	92.43(7)
O3B–FeB–N1B	143.04(8)	O3B–FeB–N2B	85.64(7)
N1B–FeB–N2B	76.84(7)	-	-

An interesting feature of the crystal packing diagram is represented by direct hydrogen bonding interaction between the hydroxy-methylene arms of 290.4 pm (O2A \cdots O3A) and 292.0 pm (O1B \cdots O4B) resulting in infinite zigzag chains as viewed along the crystallographic b axis (Figure 4.2).

The molecular composition of complex **17** has been also confirmed by IR spectroscopy. The IR spectra shows the characteristic features of the ligand stretching vibrations which are shifted compared to the their characteristic vibration bands in the IR spectrum of the free N,N'-ethylene-bis(pyridoxylideneiminato) ligand. Asymmetric stretching vibration of the Fe–O–Fe mode has been detected at around 821 cm^{-1} .²⁴⁰ In addition, broad band at 3420 cm^{-1} has been attributed to hydrogen bonded hydroxy-methylene groups confirming thus, the 1-D arrangement build up by hydrogen bonding interactions.

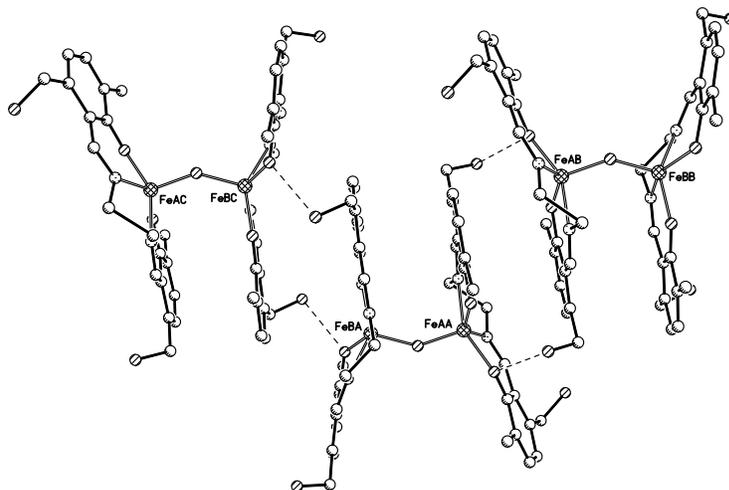


Figure 4.2: Zigzag 1-D polymer formed by hydrogen bonding interaction between units of $[\text{Fe}(\text{pyren})]_2\text{O}$; view along the b axis.

4.1.1 Magnetic properties of homodinuclear μ_2 -oxo bridged Fe(III) complex

Thermal variation of magnetic susceptibility have been performed in the temperature range of 300-2 K and is depicted in Figure 4.3 as χ_M vs T and $\chi_M T$ vs T plots for an applied magnetic field of 2000 Oe. At room temperature the experimental χ_M value is $1.03 \text{ cm}^3\text{mol}^{-1}\text{K}$, value much lower than expected for two uncoupled Fe(III) high-spin ions, assuming $g = 2$. On lowering the temperature a constant decrease of $\chi_M T$ product values have been registered until 45 K with a $0.076 \text{ cm}^3\text{mol}^{-1}\text{K}$ value. Below this temperature the decrease of the $\chi_M T$ value is very slow and reaches a minimum of $0.015 \text{ cm}^3\text{mol}^{-1}\text{K}$ at 2 K. The shape of the curve suggests an antiferromagnetic interaction between the Fe(III) centers with a resultant ground state zero owing to antiferromagnetic coupling of spins at very low temperature.

Simulation of the magnetic data set has been achieved using the isotropic spin exchange Hamiltonian:

$$\hat{H} = -J_{FeFe} S_{Fe1} S_{Fe2}$$

with $S_1=S_2=5/2$.

Considering the energies of the low-lying states and taking into account paramagnetic impurities, the magnetic susceptibility was calculated using the following formula:¹⁰

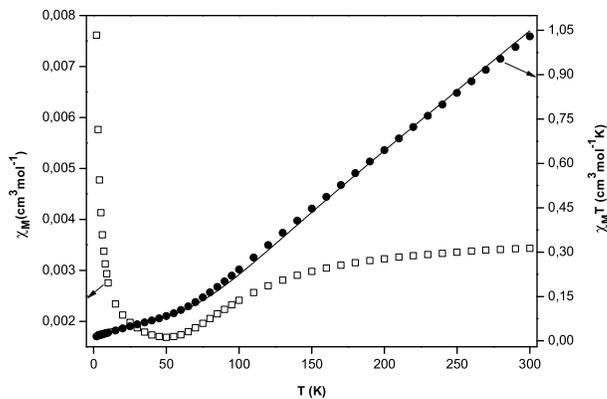


Figure 4.3: Plot of thermal dependence of χ_M (empty squares) and $\chi_M T$ product (black filled circles) for $[\text{Fe}_2(\text{pyren})_2\text{O}] \cdot 3\text{H}_2\text{O}$ (**17**) complex measured with an applied magnetic field of 2000 Oe; the solid lines represent the theoretical curves (see text).

$$\chi_M = \frac{2N\beta^2 g^2}{kT} \frac{A}{B} (1 - \rho) + 2 \frac{N\beta^2 2^2 \rho}{3kT} S(S+1) \quad (6)$$

$$A = \exp(x) + 5\exp(3x) + 14\exp(6x) + 30\exp(10x) + 55\exp(15x)$$

$$B = 1 + 3\exp(x) + 5\exp(3x) + 7\exp(6x) + 9\exp(10x) + 11\exp(15x)$$

$$\text{with } x = J/kT$$

A good fit of the magnetic data set through the above equation could be obtained only for $\chi_M T$ vs. T data points with $g = 2$ as fixed value, resulting a coupling constant $J = -232.88 \pm 9.01$ for a paramagnetic impurity $\rho = 0.003 \pm 4.0 \cdot 10^{-4}$ and a reliability factor $R^2 = 0.99892$ for temperature independent paramagnetism factor $\chi_{TIP} = 1.0 \cdot 10^{-3} \pm 1.3 \cdot 10^{-4} \text{ cm}^3 \text{ mol}^{-1}$. The calculated data curve (solid line in Figure 4.3) matches well the experimental magnetic data and the magnitude of the antiferromagnetic interaction mediated by μ_2 -O bridge is a bit higher than reported value (-178 cm^{-1}) for $[\text{Fe}(\text{salen})_2\text{O}]$ complex.²⁴³ All the μ -oxo bridged Fe(III) complexes display an antiferromagnetic interaction from -170 to -230 cm^{-1} with the Fe–O–Fe bridging angle taking

values between 135° and 175° .^{240–242} In accordance with these reports is also the magnetic behavior of complex **17** for which the magnitude of the antiferromagnetic interaction is close to the upper limit. Problematic fit of the χ_M vs. T data set for low temperature values has been observed. The fit over entire temperature range led to very small value of g parameter. Attempts to fix $g = 2$ did not improve the fitting process leading to a very bad reliability factor. Therefore the accuracy of the fitting $\chi_M T$ vs. T data set can have large errors. It has been reported that pentacoordinate Fe(III) ions in a square-pyramidal geometry may exist in intermediate spin state and/or spin-admixed states, mainly for porphyrin- and phthalocyanine-iron(III) complexes.^{244–248} No better fit of the experimental χ_M vs. T data set could be obtained considering a spin state $S = 3/2$ for Fe(III) ions.¹⁰ Although such a situation has not been previously confirmed in similar salen-type oxo-bridged dinuclear iron(III) complex,²⁴³ the problematic fitting of the χ_M vs T can not be fully explained. In this sense, Mössbauer spectra are expected to clarify the spin state of the Fe(III) ion in homodinuclear complex **17**.

4.2 Dinuclear oxygen-bridged Fe(III)-complex with N-salicylidene-2-bis(2-hydroxyethyl)amino)ethylamine ligand

The N-salicylidene-2-bis(2-hydroxyethyl)amino)ethylamine ($H_3sabhea$) ligand formed by Schiff base condensation between salicylaldehyde and 2-bis(2-hydroxyethyl)amino)ethylamine (Figure 4.4) possesses a rigid and nearly planar backbone formed by three donor atoms of the Schiff base linkage with a preferred meridional coordination mode.^{231–234} The polydentate nature of the ligand can vary according with the accommodated metal ion and was found as pentadentate chelate system in the case of vanadium(V) and copper(II) complexes,^{233,234} whereas a tetradentate chelating fashion was observed in the case of molybdenum(VI) and lanthanide(III) complexes.^{231,237}

In the homonuclear Fe(III) of type $[\{Fe(sabhea)\}_2\{Fe(Hsabhea)\}_2](ClO_4)_2$ (**18**) complex that will be described herein, this Schiff base organic framework acts as pentadentate chelating system, accommodating the iron ion through its O_3N_2 donor atom set.

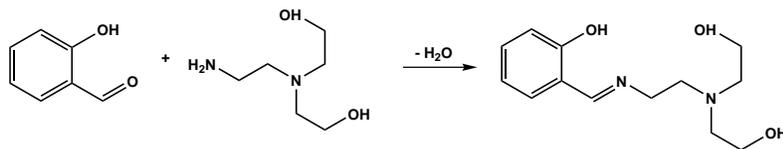


Figure 4.4: Schematic representation of the synthesis pathway for the N-salicylidene-2-bis(2-hydroxyethyl)amino)ethylamine (H₃sabhea) ligand.

The crystal structure determination shows a pair of two hexacoordinated iron(III) ions surrounded by the donor atoms of two pairs of Schiff base ligand units (Figure 4.6). Each N-salicylidene-2-bis(2-hydroxyethyl)amino)ethylamine ligand binds an iron(III) ion through phenolate, imine and tertiary amine nitrogen atoms, as well as pair of hydroxyethylene oxygen atoms resulting in one six- and two five-membered chelating rings. The asymmetric unit cell is composed by one [Fe(Hsabhea)]⁺ and [Fe(sabhea)] entities with different chemical composition and also crystallographically distinct (Figure 4.5). The cationic [Fe(Hsabhea)]⁺ asymmetric subunit B contains a doubly deprotonated N-salicylidene-2-bis(2-hydroxyethyl)amino)ethylamine ligand with a protonated hydroxyethylene side-arm resulting in FeB–O2B bond distance of 198.9 pm. The second iron(III)-subunit A of the asymmetric unit contains a fully deprotonated N-salicylidene-2-bis(2-hydroxyethyl)amino)ethylamine ligand with the corresponding FeA–O2A of 195.5 pm, approximately 3.4 pm shorter than in B subunit.

The iron ion is in the 3+ oxidation state and the positive charge is compensated by an unbounded perchlorate anion with three from four oxygen atoms in distorted positions over two sets of tetrahedral sites with a common Cl–O side. The two subunits A and B are strong hydrogen bonded with O···O distance of 241.6 pm, resulting in a 1-D chain (Figure 4.7). The other iron-to-oxygen and iron-to-nitrogen atom bond distances are similar within the two constituting molecules of the asymmetric unit cell and close to similar bond lengths of reported vanadium(V) complex. The iron-to-imine nitrogen atom bond length fall in the 215.1–216.3 pm, whereas the Fe(III)-to-tertiary amine nitrogen atom bond lengths are 7–8 pm longer, owing to their *trans* position to strongly bonded (Fe–O1 around 190 pm) phenolate oxygen atoms. Each Schiff base ligand function as bridge between the iron centers through one of its hydroxy-ethylene arm, resulting in

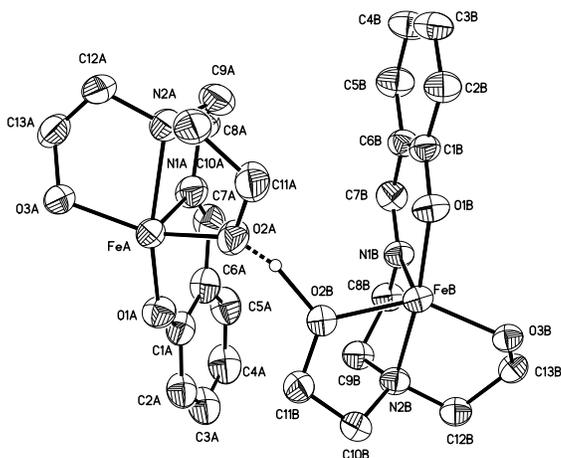


Figure 4.5: Asymmetric unit cell representation of $[\{\text{Fe}(\text{sabhea})\}_2\{\text{Fe}(\text{Hsabhea})\}_2](\text{ClO}_4)_2 \cdot 2\text{DMF}$ (**18**) complex. Thermal ellipsoids are drawn at 50% probability. Dashed line represent hydrogen bonding interaction.

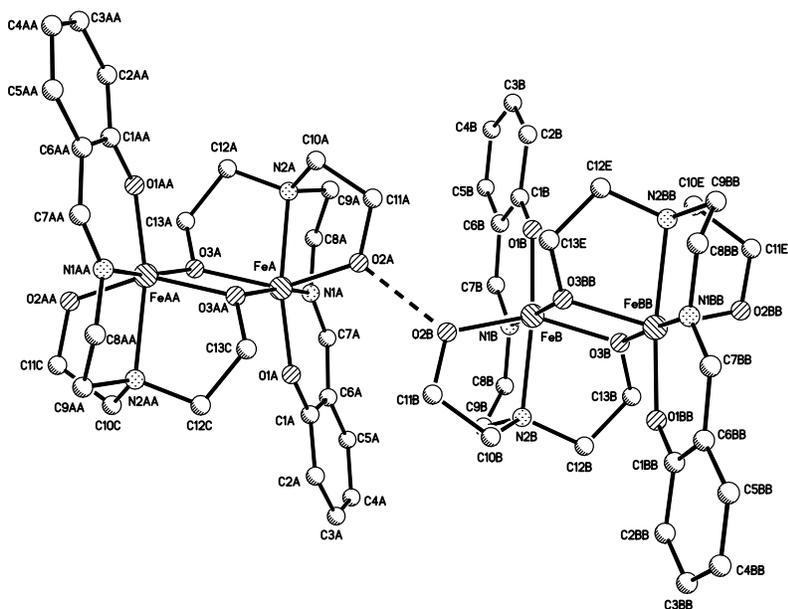


Figure 4.6: Molecular structure and labelling scheme of $[\{\text{Fe}(\text{sabhea})\}_2\{\text{Fe}(\text{Hsabhea})\}_2](\text{ClO}_4)_2 \cdot 2\text{DMF}$ (**18**) complex. Hydrogen atoms have omitted for clarity.

Fe_2O_2 core formed by two Fe–O–Fe entities. The Fe–O bond lengths within the oxygen-bridged iron ions are 196.0 in molecule A and 196.2 pm in molecule B, respectively with a Fe–O–Fe angle of 105.1° . Selected bond lengths and angles in complex **18** are listed in Table 4.2.

Table 4.2: Selected bond lengths (pm) and angles ($^{\circ}$) for complex **18**.

FeA–O1A	189.9(3)	FeA–O2A	195.5(4)
FeA–O3A	196.0(4)	FeA–O3A	206.5(4)
FeA–N1A	216.3(5)	FeA–N2A	223.3(4)
FeB–O1B	190.8(3)	FeB–O2B	198.9(4)
FeB–O3B	196.2(3)	FeB–O3B	205.9(3)
FeB–N1B	215.1(4)	FeB–N2B	223.0(4)
O1A–FeA–O2A	100.10(16)	O1A–FeA–O3A	109.43(16)
O1A–FeA–O3A	88.89(15)	O1A–FeA–N1A	84.66(17)
O1A–FeA–N2A	160.70(17)	O2A–FeA–O3A	146.70(15)
O2A–FeA–O3A	91.03(17)	O2A–FeA–N1A	99.31(19)
O2A–FeA–N2A	77.29(17)	O3A–FeA–O3A	74.89(16)
O3A–FeA–N1A	98.43(18)	O3A–FeA–N1A	168.62(18)
O3A–FeA–N2A	79.57(16)	O3A–FeA–N2A	110.17(16)
N1A–FeA–N2A	77.01(18)	FeA–O3A–FeA	105.11(16)
O1B–FeB–O2B	104.00(15)	O1B–FeB–O3B	107.12(15)
O1B–FeB–O3B	90.58(13)	O1B–FeB–N1B	85.89(14)
O1B–FeB–N2B	162.11(15)	O2B–FeB–O3B	87.18(15)
O2B–FeB–N1B	97.23(16)	O2B–FeB–N2B	76.93(15)
O3B–FeB–O2B	143.94(14)	O3B–FeB–O3B	74.83(14)
O3B–FeB–N1B	102.69(15)	O3B–FeB–N1B	174.91(15)
O3B–FeB–N2B	78.98(14)	O3B–FeB–N2B	107.30(14)
N1B–FeB–N2B	76.31(15)	FeB–O3B–FeB	105.17(14)

Complex **18** crystallizes in the triclinic space group P1 with an inversion center that passes through the center of the Fe_2O_2 plane. The resulting dimeric cation $[\{\text{Fe}(\text{sabhea})\}_2\{\text{Fe}(\text{Hsabhea})\}_2]^{2+}$ units are organized in hydrogen bonded dimers that assemble in 1-D sheets along the b crystallographic axis (Figure 4.7). The perchlorate anions separate the chains (Figure 4.8) with interchain $\text{Fe}\cdots\text{Fe}$ distance larger than 1014 pm. The interatomic $\text{Fe}\cdots\text{Fe}$ separation within the homodinuclear cation complex is 319.5 pm, and 550.9 pm within the hydrogen bonded 1-D chain.

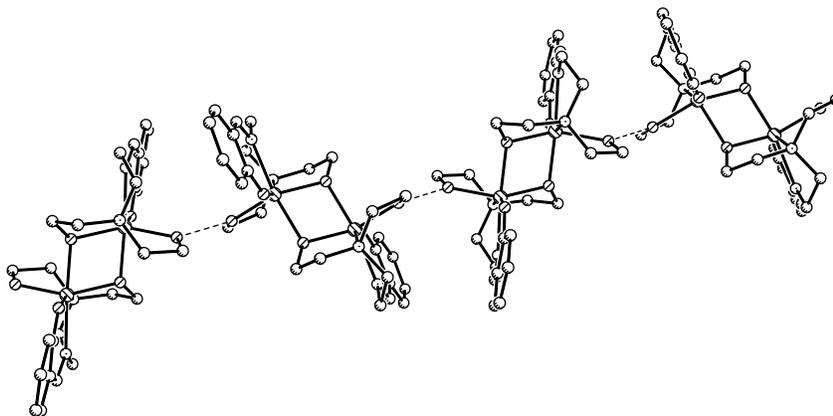


Figure 4.7: Hydrogen bonding interaction between molecules of $[\{\text{Fe}(\text{sabhea})\}_2\{\text{Fe}(\text{Hsabhea})\}_2](\text{ClO}_4)_2 \cdot 2\text{DMF}$ (**18**) as viewed along the b crystallographic axis. Hydrogen atoms have omitted for clarity.

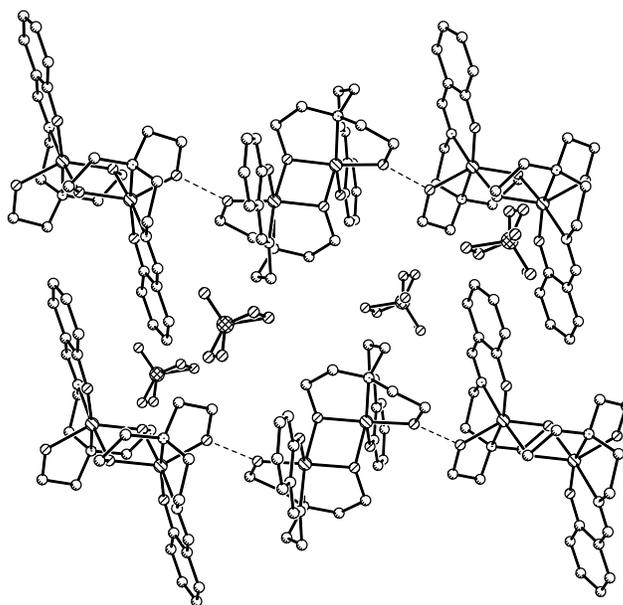


Figure 4.8: Packing diagram showing the separation of the 1-D hydrogen bonded $[\{\text{Fe}(\text{sabhea})\}_2\{\text{Fe}(\text{Hsabhea})\}_2](\text{ClO}_4)_2$ units of complex **18** by the distorted perchlorate anions. View along the b crystallographic axis. Hydrogen atoms have omitted for clarity.

The spectroscopic characterization of the $[\{\text{Fe}(\text{sabhea})\}_2\{\text{Fe}(\text{Hsabhea})\}_2](\text{ClO}_4)_2 \cdot \text{DMF}$ (**18**) complex is consistent with the proposed structures. The IR spectra contain strong stretching vibration at 3435 cm^{-1} assigned to the hydrogen bonded hydroxyl-ethylene constituents ($\nu(\text{OH})$ vibration). Similarly to reported d-metal complexes,^{231–233} stretching vibration characteristic for the Schiff base ligand coordination mode were detected

at 1631 cm^{-1} , owing to Schiff base bond vibration. This stretching mode is very similar compared to its vibrations in the free ligand, due to weak coordination of the imine nitrogen atoms. Strong bands have been observed at 905 cm^{-1} most likely owing to $\nu(\text{Fe-O-Fe})$ stretching mode.²⁴⁹ The cationic nature of the dinuclear Fe(III)-core is in agreement with the specific stretching vibrations of the ClO_4^- anion observed at 1097 cm^{-1} (ν_3 mode) and 623 cm^{-1} (ν_4 mode).¹⁰⁴

4.2.1 Magnetic properties

The magnetic behavior of homodinuclear Fe(III)-complex has been studied through magnetic susceptibility measurements on powdered crystals of $[\{\text{Fe}(\text{sabhea})\}_2\{\text{Fe}(\text{Hsabhea})\}_2](\text{ClO}_4)_2 \cdot \text{DMF}$ (**18**) in the temperature range 300 - 2 K. The thermal variation of χ_M and $\chi_M T$ are plotted in Figure 4.9 as have been measured with a fixed 2000 Oe magnetic field. The $\chi_M T$ value is 6.62 $\text{cm}^3 \text{mol}^{-1} \text{K}$ at 300 K which is much lower than calculated value for two uncoupled high spin Fe(III) ions, assuming $g = 2$. The $\chi_M T$ values are decreasing steadily on lowering the temperature reaching a value of 0.15 $\text{cm}^3 \text{mol}^{-1} \text{K}$ at 10 K. Below this temperature the decrease of the $\chi_M T$ product is very slow with a minimum of 0.03 $\text{cm}^3 \text{mol}^{-1} \text{K}$ at 2 K. The nature of the curve obtained by plotting the $\chi_M T$ against temperature indicates an antiferromagnetic coupling interaction between the iron(III) centers consistent with $S = 0$ ground state.

The data were fitting using the isotropic Hamiltonian expression previously discussed for a dinuclear Fe(III) complex with two equivalent metal centers with spin state $S_1 = S_2 = 5/2$. The best fit was obtained on $\chi_M T$ vs T data set with $g = 2.08 \pm 1.2 \cdot 10^{-3}$ and $J = -21.64 \pm 0.008 \text{ cm}^{-1}$ for a paramagnetic impurity $\rho = 0.005 \pm 4.5 \cdot 10^{-4}$. The reliability factor $R^2 = 0.99999$ shows a very good agreement between experimental and calculated values through equation **6**, with a Weiss constant $\theta = -3.02 \pm 0.310 \text{ K}$. This parameter accounts for intermolecular antiferromagnetic $\text{Fe} \cdots \text{Fe}$ interactions and the value is consistent with 550.9 pm intermetallic separation along the 1-D sheets formed by hydrogen bonding interaction between two neighboring cation $[\{\text{Fe}(\text{sabhea})\}_2\{\text{Fe}(\text{Hsabhea})\}_2]^{2+}$ entities. The fit of the $\chi_M T$ vs T data set, excluding the Weiss parameter (θ) from the χ_M equation led to $g = 2.08 \pm 2.3 \cdot 10^{-3}$ and a similar

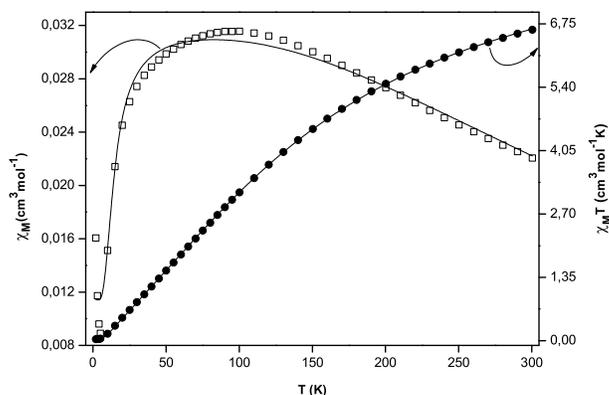


Figure 4.9: Plot of thermal dependence of χ_M (empty squares) and $\chi_M T$ product (black filled circles) for $[\{\text{Fe}(\text{sabhea})\}_2\{\text{Fe}(\text{Hsabhea})\}_2](\text{ClO}_4)_2 \cdot 2\text{DMF}$ (**18**) complex measured with an applied magnetic field of 2000 Oe; the solid lines represent the theoretical curves (see text).

magnitude of the intradimer antiferromagnetic coupling interaction $J = -22.33 \pm 0.089 \text{ cm}^{-1}$ with a reliability factor $R^2 = 0.99995$. But, nonetheless considering the small interchain $\text{Fe} \cdots \text{Fe}$ separation, the Weiss parameter that accounts for intermolecular interactions can not be simply ignored.

Gorun and Lippard have established an empirical correlation between the coupling parameter, J (cm^{-1}) and average metal-oxygen distance, P , or the metal-oxygen-metal angle, α .²⁵⁰ This empirical approach has been verified on large number of oxo-bridged iron(III) pairs and its validity has been said to exist only in the case of weak antiferromagnetic interactions.^{26,251} In dinuclear Fe(III) complexes of type **17**, described in the first part of this chapter, such an empirical equation can not be applied. The coupling constant is largely insensitive to the Fe-O-Fe angle for $\alpha > 120^\circ$, therefore this empirical approach can not be used to describe the strong antiferromagnetic interaction observed in dinuclear *salen-type*-Fe(III) complex.

Nevertheless, magnetic data recorded on a large series of oxo-bridged iron complexes suggest that the P-dependence of the exchange coupling constant, J , is well represented by the following equation:

$$-J = -1.753 \cdot 10^{12} \exp(-12.663 P) \quad (7)$$

where J is expressed in cm^{-1} and P in \AA for the exchange Hamiltonian in the form

$$\hat{H} = -JS_1S_2$$

According to this empirical approach, the magnitude of the antiferromagnetic coupling between the Fe(III) ions in cationic $[\text{Fe}_2(\text{Hsabhea})(\text{sabhea})]^+$ complex is -17.6 cm^{-1} (Fe–O distance 2.0 \AA). For metal–oxygen–metal angles (α) smaller than 120° , the magnitude of the magnetic interaction between Fe(III) centers was reported to be affected on the Fe–O–Fe bending, i.e. J becomes smaller as the angle α is reduced.²⁶ A systematic study has been performed in a series of binuclear complexes with alkoxo-bridges and similar Fe–O distances with α values within the 102 to 106° range with J varying between ca. 15 and 21 cm^{-1} . The simplest correlation was found to be of the type:

$$-J = 1.48 \alpha - 135 \quad (8)$$

Applying this final equation in order to describe the magnitude of the antiferromagnetic interaction in complex **18** as a function of Fe–O–Fe angle (105°), a coupling constant of -20.4 cm^{-1} was resulting. This J value is very close to the magnitude of the antiferromagnetic interaction resulted by fitting the $\chi_M T$ vs T data following the Van Vleck formalism.

It can be concluded that, following both theoretical pathways to describe the magnetic behavior of cation complex $[\{\text{Fe}(\text{sabhea})\}_2\{\text{Fe}(\text{Hsabhea})\}_2](\text{ClO}_4)_2 \cdot 2\text{DMF}$ (**18**) an antiferromagnetic interaction occurs between the metal centers within the dimer unit. The Weiss constant value obtained following the Van Vleck equation for two $S = 5/2$ iron ions shows that an intermolecular antiferromagnetic interaction occurs between the dimer units along the 1-D chains.

4.3 Trinuclear copper complex with partial cubane-like core

Schiff base ligands with flexible backbones are versatile organic ligands to design polynuclear complexes with interesting magnetic properties. "Serendipity" as a tool to generate high-nuclearity coordination compounds has led to interesting assemblies that sometimes exhibit unpredictable magnetic behavior.¹⁶⁴ Copper(II) ion is a peculiar paramagnetic center with a high degree of flexibility of its geometry with varied distortions owing to Jahn-Teller effect.¹⁰ The coordination number of Cu(II) ions can be easily varied from four- to five-coordination environment with easy uptake of oxygen-ligation to form Cu–O(H)–Cu linkage.²⁵² A peculiar attention from the magnetic point of view has been attributed to copper(II) cubane complexes based on Cu₄O₄-core.^{229, 253–255} Such species have been reported to possess ferromagnetic exchange interaction between the paramagnetic center and hence, their versatility as building blocks for designing high-nuclearity assemblies. The Schiff base ligand derived from salicylaldehyde and N,N-dimethylethylenediamine has been successfully used to generate trinuclear copper(II) complexes with partial cubane motif formed by Cu₃O₄ core (Figure 4.11). The trinuclear copper complex crystallizes in the P2₁/c space group, with no threefold symmetry and presents a cationic Cu₃O₄ core formed by [Cu₃L₃(μ₃-OH)]²⁺ (Figure 4.10).

The positive charge of the core is compensated by two unbounded perchlorate anions. One ClO₄⁻ anion is distorted with three of the four oxygen atoms distributed over two sets of tetrahedral sites around the chlorine atom, whereas the second perchlorate anion is ordered. In addition, the molecular structure determination shows water lattice with the final formulation of the structure as [(CuL)₃(μ₃-OH)](ClO₄)₂·H₂O. The trinuclear cationic part is formed by three Cu(II)-ligand subunits in which each copper(II) ion is coordinated to a deprotonated tridentate monoanionic [2-(2-dimethylaminoethylimino)-methyl]-phenol ligand. This tridentate chelate ligand coordinates copper(II) ions through N,N,O-donor atoms forming six- and five-membered chelating rings with bite angles around 92° (O1_N–Cu_N–N1_N) and 84° (N1_N–Cu_N–N2_N). The copper-to-phenolate bond distances within this mononuclear Cu(II)-constituting subunits are very close among themselves and fall in the 191.6–192.9 pm range, whereas the Cu–N bond

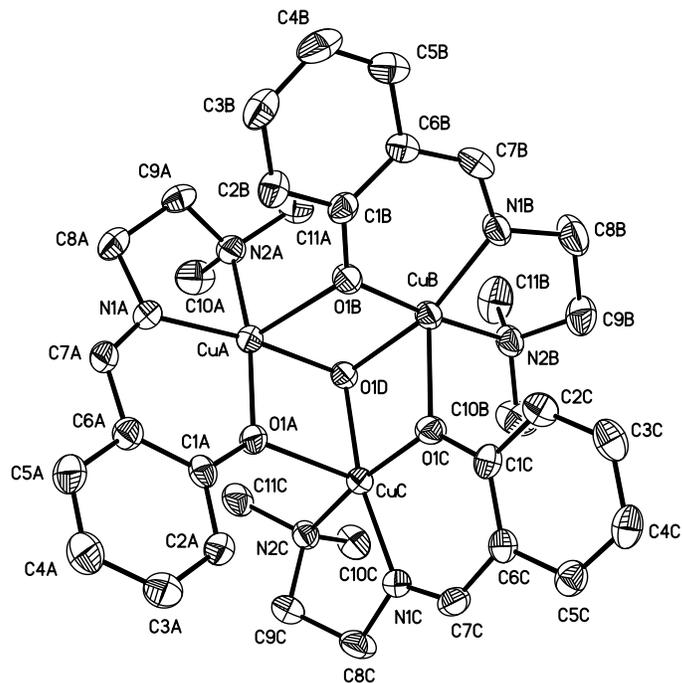


Figure 4.10: Molecular structure and labeling scheme of $[(\text{CuL})_3(\mu_3\text{-OH})](\text{ClO}_4)_2 \cdot \text{H}_2\text{O}$ (**19**) complex. Only the cationic $[\text{Cu}_3\text{L}_3(\mu_3\text{-OH})]^{2+}$ core is shown. Hydrogen atoms have omitted for clarity.

distances depend on the provenance of the nitrogen atoms and are shorter for copper-to-imine nitrogen atom bonds (around 194 pm) and longer for the coordinated tertiary nitrogen atoms (N2) which fall in the 203.5-205.0 pm range. These three subunits are held together by two distinct bridging systems: one is represented by μ_2 -phenolate oxygen atoms and secondly by the μ_3 -bridging-hydroxo group (O1D) that binds asymmetrically to the three copper centers within 201.7-207.5 pm range.

In each Cu(II)-[2-(2-dimethylamino-ethylimino)-methyl]-phenol subunit the phenolate oxygen atoms act as μ_2 -bridge between two copper centers with unequal Cu–O distances owing to steric effects induced in the molecular structure by dimethyl-amino constituents of the organic framework. Selected bond lengths and angles in complex **19** are listed in Table 4.3. The O–Cu–O connecting angles are within 91.1-97.2° range and Cu–O–Cu bond angles within 96.4 -100.3° limits for phenolate-bridged copper atoms and 100.7-102.5° for hydroxy-bridged copper ions. The copper atoms are five-coordinated in a distorted trigonal bipyramidal geometry with the donor atoms of the supporting tridentate ligand forming the basal isosceles triangular plane, whereas the common hydroxy-

Table 4.3: Selected bond lengths (pm) and angles ($^{\circ}$) for complex **19**.

CuA–O1A	192.9(2)	CuA–N1A	193.4(3)
CuA–O1D	201.7(2)	CuA–N2A	205.0(3)
CuA–O1B	230.4(2)	O1A–CuC	2239.(2)
CuB–O1B	191.9(2)	CuB–N1B	194.0(3)
CuB–N2B	204.8(3)	CuB–O1D	207.5(2)
CuB–O1C	219.1(2)	CuC–O1C	191.6(2)
CuC–N1C	194.7(3)	CuC–O1D	203.2(2)
CuC–N2C	203.5(3)		
O1A–CuA–O1D	83.47(9)	O1A–CuA–O1B	97.20(10)
O1A–CuA–N1A	92.85(11)	O1A–CuA–N2A	167.77(11)
O1D–CuA–O1B	77.10(9)	O1D–CuA–N2A	97.93(11)
N1A–CuA–O1B	110.59(11)	N1A–CuA–O1D	171.91(11)
N1A–CuA–N2A	84.15(12)	N2A–CuA–O1B	94.95(10)
O1B–CuB–O1C	91.13(10)	O1B–CuB–O1D	85.06(10)
O1D–CuB–O1C	75.28(9)	O1B–CuB–N1B	92.94(11)
O1B–CuB–N2B	174.22(11)	N1B–CuB–N2B	83.48(12)
N1B–CuB–O1D	159.81(12)	N1B–CuB–O1C	124.89(11)
N2B–CuB–O1D	96.74(11)	N2B–CuB–O1C	94.64(11)
O1C–CuC–O1A	93.37(10)	O1C–CuC–O1D	82.62(10)
O1C–CuC–N1C	92.60(11)	O1C–CuC–N2C	169.95(11)
N1C–CuC–O1A	115.49(11)	N1C–CuC–O1D	168.13(11)
N1C–CuC–N2C	84.19(12)	N2C–CuC–O1A	96.61(10)
O1D–CuC–O1A	75.77(9)	O1D–CuC–N2C	98.66(11)

and the bridging phenolate oxygen atoms are placed on the apex positions of the pyramid. The phenolate oxygen atom is in turn part of the equatorial plane of a second copper center, resulting in three bipyramid geometries with common apex represented by the central hydroxy ligand (O1DH). The Cu_3O_4 -core is arranged in partial cub motif with angles around 90° (Figure 4.11). Complex **19** crystallizes with a water molecule as solvent of crystallization which is involved in bifurcated hydrogen bonding interactions

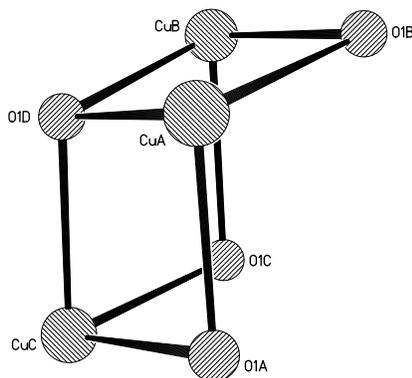


Figure 4.11: Partial-cubane core motif of $[(\text{CuL})_3(\mu_3\text{-OH})](\text{ClO}_4)_2 \cdot \text{H}_2\text{O}$ complex.

with the phenolate oxygen atoms of two neighboring trimeric units within bond distances of 292.2 pm ($\text{O1w} \cdots \text{O14}$) and 275.4 pm ($\text{O1w} \cdots \text{O21}$).

The molecular structure determined by X-ray crystallography is also confirmed by spectroscopic characterizations of complex **19**. The noncoordinating water molecule has been detected in IR spectrum of the complex as broad band at 3523 cm^{-1} , attributable to hydrogen interacting water lattice,¹⁰⁴ while the μ_3 -hydroxyl group show strong band at 3055 cm^{-1} . The Schiff base bond stretching vibration has been observed at around 1632 cm^{-1} , just a bit shifted compared to its stretching vibrations in the free ligand owing to a weak coordination of the imine nitrogen atom to copper(II) ion. Concerning the ClO_4^- anions, the ν_3 mode at 1098 cm^{-1} is broadening but the ν_4 mode at 623 cm^{-1} is consistent with the IR-active mode of tetrahedral symmetry of perchlorate anions, suggesting that these anions are not coordinated to the copper ions as it has been seen in the crystal structure determination.¹⁰⁴

4.3.1 Magnetic properties

Magnetic susceptibility measurements for complex **19** have been performed over the 300-2 K temperature range. Plots of χ_M vs T and $\chi_M T$ vs T are shown in Figure 4.12 as have been measured with an applied field of 5000 Oe. The room temperature measured $\chi_M T$ value is $1.43 \text{ cm}^3 \text{ mol}^{-1} \text{ K}$ which is a little bit higher than the calculated spin-only value for three non-interacting $S = 1/2$ spins with $g = 2$. As the temperature is decrease, the $\chi_M T$ values increase to reach a maximum value of $1.79 \text{ cm}^3 \text{ mol}^{-1} \text{ K}$ at 4 K. Below

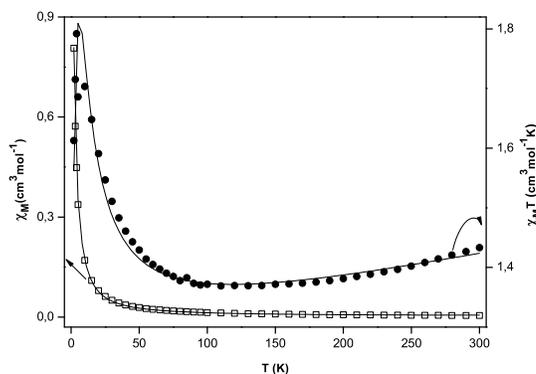


Figure 4.12: Plot of thermal dependence of χ_M (empty squares) and $\chi_M T$ product (black filled circles) for $[(\text{CuL})_3(\mu_3\text{-OH})](\text{ClO}_4)_2 \cdot \text{H}_2\text{O}$ (**19**) complex measured with an applied magnetic field of 5000 Oe; the solid lines represent the theoretical curves (see text).

this temperature, the $\chi_M T$ value is decreasing again to $1.61 \text{ cm}^3 \text{mol}^{-1} \text{K}$ at 2 K. This suggests overall a ferromagnetic interaction in the Cu_3O_4 -core, with a weak intercluster antiferromagnetic coupling described by the observed decrease of the $\chi_M T$ product below 4 K.

The magnetic-exchange interaction in a triangular $S = 1/2$ system results in three electronic states: a quartet state ($S = 3/2$, ${}^4\text{A}_2$) and two doublets states ($S = 1/2$, ${}^2\text{E}$). Within the simple model of the isotropic Heissenberg-Dirac-van Vleck (HDVV) Hamiltonian formalism

$$\hat{H} = -J_{12}S_1S_2 - J_{13}S_1S_3 - J_{23}S_2S_3$$

with $J_{12} = J_{13} = J_{23} = J$ and $S_1 = S_2 = S_3 = 1/2$.

The magnetic susceptibility for a triangular $\text{Cu}(\text{II})$ complex in which all the metal ions are equivalent has the following expression:

$$\chi_M = \frac{N\beta^2 g^2}{k(T - \theta)} \frac{[1 + 5\exp(3J/2kT)]}{[1 + \exp(3J/2kT)]} (1 - \rho) + 3 \frac{N\beta^2 2^2 \rho}{3kT} S(S + 1) + \chi_{TIP} T \quad (9)$$

The best fit set has been obtained for $\chi_M T$ vs T experimental data set for $g = 2.11 \pm 0.01$ and $J = 8.50 \pm 0.64 \text{ cm}^{-1}$ for a Weiss constant $\theta = -0.68 \pm 0.05 \text{ K}$. The reliability factor $R^2 = 0.95516$ shows a very good agreement between experimental and calculated

values for a temperature independent paramagnetism parameter $\chi_{TIP} = 4.8 \cdot 10^{-4} \pm 7 \cdot 10^{-5}$ $\text{cm}^3 \text{mol}^{-1}$. The Weiss constant counts for antiferromagnetic interaction which may take place between $[\text{Cu}_3\text{L}_3(\mu_3\text{-OH})]^{2+}$ units at low temperature and it is described by the observed decrease of $\chi_M T$ value below 4 K. A very similar trinuclear Cu(II)-complex with similar structural motif has been reported²⁵³ while complex **19** has been isolated. The magnitude of the ferromagnetic interaction is very close to one described herein, owing to structural similarities. The ferromagnetic interaction in the trimeric $[\text{Cu}_3\text{L}_3(\mu_3\text{-OH})]^{2+}$ cation is due to accidental orthogonality arrangement of the magnetic orbitals of copper(II) centers, for which the Cu–O–Cu angles are in the 96.4 - 100.7° range.

4.4 Dinuclear phenoxo-bridged copper complex

On going from salicylaldehyde to its 3-methoxy derivative, the new 2-((2-dimethylamino-ethylimino)-methyl]-6-methoxy-phenol ligand has been reacted with copper perchlorate salt in presence of gadolinium salt in methanol solution. A different organization of the ligand and metal ions occurred yielding a cationic dinuclear Cu(II) complex **20** with only one phenoxo-bridge. The molecular structure determination of $[(\text{CuL}^{OMe})_2](\text{ClO}_4)_2 \cdot 0.5\text{H}_2\text{O}$ (**20**) complex is shown in Figure 4.4 with selected bond lengths and angles listed in Table 4.4. Each copper(II) ion is coordinated in the tridentate pocket of 2-[(2-dimethylamino-ethylimino)-methyl]-6-methoxy-phenol as previously observed for complex **19**. The copper-to-nitrogen bond lengths are longer for the binding strength of the tertiary nitrogen atom (Cu1–N2B 206.1 pm and Cu2–N2A 203.4 pm) and shorter for the copper-to-imine nitrogen atom bond lengths of around 193.2 pm (Cu1–N1B and Cu2–N1A). These bond lengths are very similar to corresponding bond distances in complex **19** in line with a similar coordination mode of the tridentate core of the supporting organic ligand. The difference among the two homonuclear copper(II) complexes appears for the two phenolate binding strength. The phenolate oxygen atom O1A that establishes the bridge between the metal centers and binds quite similar to Cu1 (Cu1–O1A 198.9 pm) and Cu2 centers (Cu2–O1A 197.1 pm) resulting in a relative symmetric Cu–O(Ph)–Cu bridge with the bridging angle of 111.2°. Conversely in complex **19**, these phenoxo-bridges were quite unequal most likely due to the additional hydroxy-bridged unit which may also be

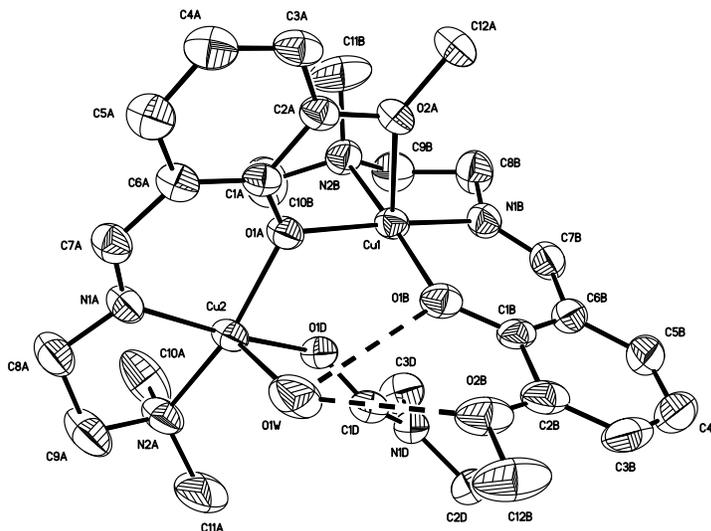


Figure 4.13: Molecular structure and labeling scheme of $[(\text{CuL}^{\text{OMe}})_2](\text{ClO}_4)_2 \cdot 0.5\text{H}_2\text{O}$ (**20**) complex. Only the cationic $[(\text{CuL}^{\text{OMe}})_2]^{2+}$ core is shown. Hydrogen atoms have omitted for clarity. Dashed line represent intramolecular hydrogen bonding interactions.

responsible for the observed cubane-like core.

The non-bridging phenolate oxygen coordinates only to Cu1 center with Cu1–O1B bond length of 192.6 pm. The coordination sphere of the copper ion centers is completed by coordinated methoxy-oxygen atom in the case of Cu1 ion (Cu1–O2A 234.2 pm) and water and DMF molecules for Cu2 ion with bond distances of 24.8 pm (Cu2–O1W) and 197.7 pm (Cu2–O1D). Both copper(II) ions are in slight distorted square-pyramidal environment with the distortion parameter²³⁹ $\tau = 0.01$ for Cu1 ion and $\tau = 0.05$ for Cu2 ion, respectively. The uncoordinated methoxy-group of the first ligand moiety is instead involved in intramolecular hydrogen bonding interaction with the coordinated water molecule (O2B···O1W 299.6 pm) which in turn is hydrogen bonded to the non-bridged phenolate oxygen atom (O1W···O1B 288.3 pm) (see Figure 4.4). Complex **20** crystallizes in the monoclinic space group C_2c with two perchlorate anions and water lattice with the final formula $[(\text{CuL}^{\text{OMe}})_2](\text{ClO}_4)_2 \cdot \text{H}_2\text{O}$. One perchlorate anion is distorted with the oxygen atoms occupying two tetrahedral sites with a common chlorine atom whereas the other ClO_4^- is ordered. Both of them are in hydrogen bonding interaction with the lattice water molecule of 290.2 pm for $\text{Ow} \cdots \text{O}_{\text{ClO}_4}$ (ordered anion) and 270.3 pm for distorted oxygen atom of perchlorate anion (Figure 4.14).

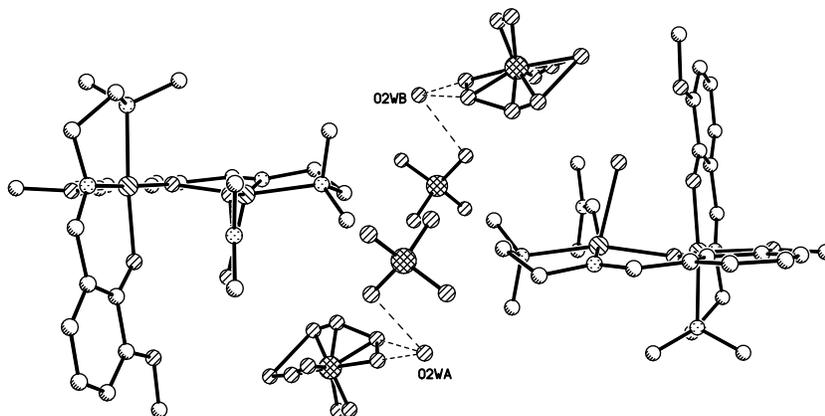


Figure 4.14: Hydrogen bonding interaction between water lattice molecules and perchlorate anions in the crystal packing of $[(\text{CuL}^{\text{OMe}})_2](\text{ClO}_4)_2 \cdot 0.5\text{H}_2\text{O}$ (**20**) complex as viewed along the *b* crystallographic axis. Hydrogen atoms have omitted for clarity.

Table 4.4: Selected bond lengths (pm) and angles ($^\circ$) for complex **20**.

Cu1–O1A	198.9(2)	Cu1–O1B	192.6(3)
Cu1–N1B	193.2(3)	Cu1–O2A	234.2(3)
Cu1–N2B	206.1(3)	Cu2–O1A	197.1(2)
Cu2–N1A	193.3(3)	Cu2–N2A	203.4(3)
Cu2–O1D	197.7(3)	Cu2–O1W	224.8(4)
O1A–Cu1–N2B	92.82(11)	O1A–Cu1–O1B	88.78(11)
O1A–Cu1–O2A	74.06(9)	O1A–Cu2–O1D	88.58(10)
O1B–Cu1–N1B	92.86(12)	O1B–Cu1–N2B	173.93(12)
O1B–Cu1–O2A	89.69(10)	N1B–Cu1–O1A	174.68(12)
N1B–Cu1–O2A	111.00(11)	N1B–Cu1–N2B	85.04(13)
N2B–Cu1–O2A	96.38(11)	O1A–Cu2–N2A	164.46(13)
O1A–Cu2–O1W	84.52(13)	N1A–Cu2–O1A	91.73(11)
N1A–Cu2–N2A	85.24(13)	N1A–Cu2–O1D	167.55(13)
N1A–Cu2–O1W	97.67(15)	O1D–Cu2–N2A	91.14(12)
O1D–Cu2–O1W	94.75(13)	N2A–Cu2–O1W	110.98(15)

4.4.1 Magnetic properties

Magnetic susceptibility measurements for complex **20** have been performed in the 300-2 K temperature range with χ_M vs T and $\chi_M T$ vs T plots depicted in Figure 4.15 for an applied magnetic field of 2000 Oe. The room temperature measured $\chi_M T$ value is $0.767 \text{ cm}^3 \text{ mol}^{-1} \text{ K}$ which corresponds to calculated spin-only value for two non-interacting $S = 1/2$ spins, assuming $g = 2$. As the temperature is decreased, the $\chi_M T$ values decrease smoothly until 25 K with a value of $\chi_M T$ product of $0.18 \text{ cm}^3 \text{ mol}^{-1} \text{ K}$. Below this temperature, the decrease is more constant with a minimum of $0.17 \text{ cm}^3 \text{ mol}^{-1} \text{ K}$ at 2 K. This suggests overall antiferromagnetic interaction within the Cu–O(Ph)–Cu unit, according with 111.2° bridging angle, which is higher than corresponding angles in complex **19**.

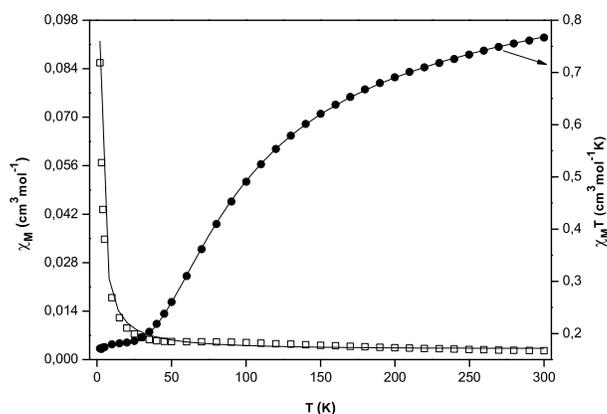


Figure 4.15: Plot of thermal dependence of χ_M (empty squares) and $\chi_M T$ product (black filled circles) for $[(\text{CuL}^{OMe})_2](\text{ClO}_4)_2 \cdot 0.5\text{H}_2\text{O}$ (**20**) complex measured with an applied magnetic field of 2000 Oe; the solid lines represent the theoretical curves (see text).

The magnetic-exchange interaction pathway in dinuclear $S = 1/2$ system has been interpreted in terms of isotropic Hamiltonian:

$$\hat{H} = -JS_1S_2$$

with $S_1 = S_2 = 1/2$.

based on Bleaney-Bowers equation (**13**) for a pair of copper ions.²⁵⁶ The best fit of the magnetic susceptibility was obtained using $\chi_M T$ vs T plot and led to: $g = 2.11 \pm 0.008$ and $J = -119.76 \pm 0.51 \text{ cm}^{-1}$ for a paramagnetic impurity $\rho = 0.23 \pm 0.001$, resulting in a reliability factor $R^2 = 0.99993$ that shows a very good agreement between experimental and calculated values for a temperature independent paramagnetism parameter $\chi_{TIP} = 1.9 \cdot 10^{-4} \pm 2 \cdot 10^{-5} \text{ cm}^3 \text{ mol}^{-1}$. Conversely to magnetism phenomenon observed in complex **19**, an obtuse phenolate-bridging unit mediates an antiferromagnetic exchange interaction. The magnitude of the antiferromagnetic coupling of the copper(II) ions in complex **20** is much lower than reported antiferromagnetic coupling reported for bis(phenoxide) Cu(II)-complexes.^{252,257} Thompson *et al.*²⁵⁷ establishes a magneto-structural correlation for bis(phenoxide)-bridged dinuclear copper(II) complexes in which the magnitude of the antiferromagnetic interaction is linear dependent of the Cu–O(Ph)–Cu bridging angle (α):

$$-J = 31.95 \alpha - 2462 \text{ cm}^{-1}$$

The J value calculated using this empirical approach is not consistent with the value obtained using Bleaney-Bowers equation in the case of magnetic behavior of complex **20**. This inconsistency of the empirical approach may be a consequence of different structural motif present in complex **20**, namely only one phenoxy-bridge by comparison to double-phenoxide bridged copper(II) complexes for which the linear correlation has been established.

4.5 Conclusions

In conclusion two homodinuclear Fe(III) complexes based on *salen-type* N,N'-ethylene-bis(pyridoxylideneiminato) ligand and N-salicylidene-2-bis(2-hydroxyethyl)amino)ethylamine ligand have been isolated. The *salen-type* ligand yield a neutral oxo-bridged homodinuclear Fe(III) complex, whereas the N-salicylidene-2-bis(2-hydroxyethyl)amino)ethylamine ligand yielded an hydroxy-bridge cationic dinuclear iron(III) complex. The magnetic coupling of the iron(III) ions has been found to be antiferromagnetic, stronger in the case of oxo-bridged dinuclear Fe(III) complex, whereas a weak antiferromagnetic

interaction has been mediated by N-salicylidene-2-bis(2-hydroxyethyl)amino)ethylamine ligand. In both cases 1-D coordination polymers have been formed through hydrogen bonding interaction between the donor atoms of the supporting ligands. In addition self-assembly reaction between [2-(2-dimethylamino-ethylimino)-methyl]-phenol and its methoxy-derivative ligands with $\text{Cu}(\text{ClO}_4)_2$ salt in presence of different outer metal salts has yielded to tri- and dinuclear $\text{Cu}(\text{II})$ complexes. The homotrinnuclear copper(II) complex present a partial cubane-like structural core formed by cationic $[\text{Cu}_3\text{L}_3(\mu_3\text{-OH})]^{2+}$ cation which can be simply formulated as Cu_3O_4 -motif. The organic framework enforced, in this case an orthogonal orientation of the magnetic orbital of the three copper(II) ions, resulting in a ferromagnetic interaction between the metal centers of $J = 8.50 \text{ cm}^{-1}$ magnitude. Instead, the homodinuclear copper(II) complex comprises only one phenoxo-bridged Cu-O(Ph)-Cu moiety with an obtuse bridging angle, most likely responsible for the antiferromagnetic exchange pathway between the copper(II) ions. All these simple molecular clusters can be used as precursors to build-up high-nuclear coordination compounds. For example, d-transition metal complexes based on N-salicylidene-2-bis(2-hydroxyethyl)amino)ethylamine (H_2sabhea) ligand (Figure 4.16, inset a) may form alkoxy-bridges between two different metal ions, most likely lanthanide ions. The most appropriate organic framework based on 2-bis(2-hydroxyethyl)amino)ethylamine side-arms will be the Schiff base derivative formed with 3-methoxy-2-hydroxy-benzaldehyde (o-vanillin). The resulting d-complex may be used as precursor to design d-f metal complexes (Figure 4.16, inset b).

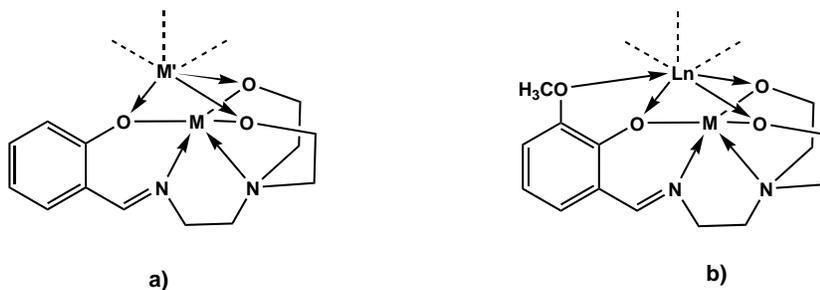


Figure 4.16: Schematic representation of potential pathway reaction for d-transition metal complexes with N-salicylidene-2-bis(2-hydroxyethyl)amino)ethylamine (H_2sabhea) ligand (inset a) and its 3-methoxyderivative (inset b).

4.6 Experimental Part

The Schiff base ligands have been prepared following reported procedures^{233, 238, 253}

Synthesis of $[\text{Fe}(\text{pyren})]_2\text{O}\cdot 3\text{H}_2\text{O}$ (17) complex

To a suspension of bis(*N,N'*-pyridoxalidene)ethylenediamine ligand (90 mg, 0.25 mmol) in MeOH (10 mL) was added stepwise a methanolic solution (5 mL) of $\text{Fe}(\text{ClO}_4)_3\cdot n\text{H}_2\text{O}$ (88.5 mg, 0.25 mmol) followed by addition of NaOH (0.5 mL 1 N aqueous solution). The resulting clear solution was stirred at room temperature for 20 minutes, then filtered and the black filtrate was allowed to stand at room temperature for slow evaporation of the solvent. Yield: 65.0 mg (0.07 mmol, 59.0%). *Anal. Calc.* for $\text{C}_{36}\text{H}_{44}\text{N}_8\text{O}_{11}\text{Fe}_2$ (876.46) ($[\text{Fe}(\text{pyren})]_2\text{O}\cdot 2\text{H}_2\text{O}$): C 49.33, H 5.06, N 12.78. Found: C 48.89, H 4.84, N 12.66. Selected IR data (cm^{-1}): 3420 (br s, H_2O and OH intermolecular hydrogen bonded), 1627 (s, $-\text{CH}=\text{N}$), 1390 (s, $-\text{CH}=\text{N}_{\text{pyridine}}$), 821 (s, Fe–O–Fe).

Synthesis of $[\{\text{Fe}(\text{sabhea})\}_2\{\text{Fe}(\text{Hsabhea})\}_2](\text{ClO}_4)_2\cdot 2\text{DMF}$ (18) complex

To a solution of *N*-salicylidene-2-bis(2-hydroxyethyl)amino)ethylamine ligand (63 mg, 0.25 mmol) in acetone (10 mL) was added stepwise a methanolic solution (5 mL) of $\text{Fe}(\text{ClO}_4)_3\cdot n\text{H}_2\text{O}$ (177 mg, 0.50 mmol) followed by addition of NEt_3 (1.5 mL 1 N methanol solution). The resulting clear solution was stirred at room temperature for 10 minutes, while a precipitate is forming. This was redissolved by addition of DMF (5 mL) and the reaction was continued for other 10 minutes. Then was filtered and the reddish filtrate was allowed to stand at room temperature for slow evaporation of the solvent mixture. Yield: 72.0 mg (0.09 mmol, 36.7%). *Anal. Calc.* for $\text{C}_{29}\text{H}_{42}\text{N}_5\text{ClO}_{11}\text{Fe}_2$ (783.80) ($[\text{Fe}_2(\text{Hsabhea})(\text{sabhea})]\text{ClO}_4\cdot \text{DMF}$): C 44.44, H 5.40, N 8.94. Found: C 44.31, H 5.20, N 8.92. Selected IR data (cm^{-1}): 3435 (br, OH intermolecular hydrogen bonded), 1695 (s, DMF), 1631 (s, $-\text{CH}=\text{N}$), 1097 (s, ClO_4), 905 (s, Fe–O–Fe) and 623 (s, ClO_4).

Synthesis of $[(\text{CuL})_3(\mu_3\text{-OH})](\text{ClO}_4)_2\cdot \text{H}_2\text{O}$ (19) complex

To a solution of [2-(2-dimethylamino-ethylimino)-methyl]-phenol ligand (192 mg, 1.0 mmol) in methanol (10 mL) was added stepwise a methanol solution (5 mL) of $\text{Cu}(\text{ClO}_4)_2$

$\cdot 6\text{H}_2\text{O}$ (365 mg, 1.0 mmol) followed by addition of aqueous solution (10 mL) of $\text{Na}_4[\text{Cu}_2(\text{m-phenyleneoxamide})_2]^{258}$ (200 mg, 0.25 mmol). A precipitate is formed in the first few minutes of reaction and the reaction was continued for 10 minutes in the suspension form. This was filtered and the filtrate was allowed to stand at room temperature for slow evaporation of the solvent mixture. Yield: 100.0 mg (0.10 mmol, 10.0%). *Anal.* Calc. for $\text{C}_{33}\text{H}_{47}\text{N}_6\text{Cl}_2\text{O}_{13}\text{Cu}_2$ (997.28) ($[(\text{CuL})_3(\mu_3\text{-OH})](\text{ClO}_4)_2\cdot\text{H}_2\text{O}$): C 39.74, H 4.75, N 8.43. Found: C 39.73, H 4.66, N 8.30. Selected IR data (cm^{-1}): 3523 (br, OH), 3055 (br, H_2O), 1632 (s, -CH=N), 1098 (s, ClO_4) and 623 (s, ClO_4).

Synthesis of $[(\text{CuL}^{OMe})_2](\text{ClO}_4)_2\cdot 0.5\text{H}_2\text{O}$ (20) complex

To a solution of 2-((2-dimethylamino-ethylimino)-methyl]-6-methoxy-phenol ligand (222 mg, 1.0 mmol) in methanol (10 mL) was added stepwise a methanol solution (10 mL) of $\text{Cu}(\text{ClO}_4)_2\cdot 6\text{H}_2\text{O}$ (365 mg, 1.0 mmol) followed by addition of NaOH (1 mL aqueous 1 N solution) and then a methanol solution (5 mL) of $\text{Gd}(\text{NO}_3)_3\cdot 6\text{H}_2\text{O}$ (220 mg, 0.50 mmol). A precipitate is formed in the first few minutes of reaction which was redissolved by addition of DMF (5 mL). The reaction was continued for 10 minutes at room temperature and allowed to stand at room temperature for slow evaporation of the solvent mixture. Yield: 243.0 mg (0.30 mmol, 30.0%). *Anal.* Calc. for $\text{C}_{27}\text{H}_{44}\text{N}_5\text{Cl}_2\text{O}_{14.5}\text{Cu}_2$ (868.67) ($[(\text{CuL}^{OMe})_2](\text{ClO}_4)_2\cdot 0.5\text{H}_2\text{O}$): C 37.33, H 5.11, N 8.06. Found: C 30.41, H 4.36, N 9.26. Selected IR data (cm^{-1}): 3502 and 3428 (br, H_2O), 1652 (s, -CH=N), 1085 (s, ClO_4) and 624 (s, ClO_4).

Chapter 5

Polynuclear oxamato-bridged d-metal complexes

Polynuclear metal-complexes with homo- and hetero-constituency are of general interest in the field of molecular magnetism. This is fueled by their challenging magnetic behavior and in addition the efforts to design molecular ferromagnets with possible applications in material science. The self-assembly process led to a great variety of interesting molecular assemblies,¹⁶⁴ but a rational pathway to approach high-nuclearity compounds is more desirable.¹¹ One of the most powerful synthetic pathway used to isolate predefined inorganic-organic hybrids is based on "complex-as-ligand" strategy.^{11,259,260} In this case the chosen organic framework plays the key-role and has to possess two or more coordination sites that will permit accommodation of more than one metal ion. One of such polynucleating organic systems is based upon oxalic-acid derivatives, e.g. oxamate²⁶¹⁻²⁶⁵ and *bis*-oxamide²⁶⁶⁻²⁷⁰ class organic ligands (Figure 5.1) that yielded a great variety of polynuclear complexes with interesting structural topologies.^{265,266,271,272} Besides the beauty of these structural assemblies, an important aspect is played by their magnetic behavior that vary from antiferromagnetic coupling of the constituting metal ions to rare examples of one-dimensional ferrimagnetic compounds.^{10,273-281}

A plethora of oxalate- and oxamate-bridged transition-metal complexes has been reported and magnetically investigated.^{10,282-284} This tremendous research activity has been fueled by initial reports concerning an oxalato-bridged dinuclear copper(II) complex in which the relatively well-separated metal ions (514 pm) have been found to

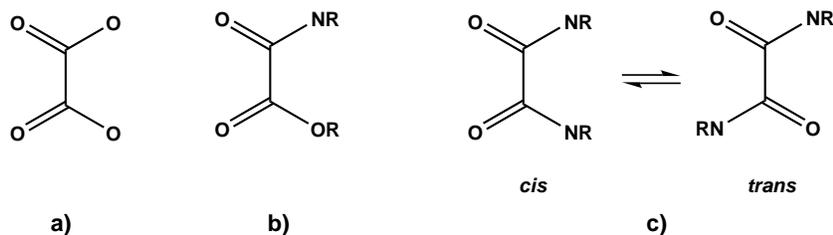


Figure 5.1: Schematic representation of the oxalic acid (a) and its derivatives: oxamate (b) and oxamide (c).

be strongly antiferromagnetically coupled (-384.5 cm^{-1}).¹⁰ While the oxalate dianion can yield uncontrolled polymerization of the d-transition metal complexes, the oxamate- and *bis*-oxamide derivatives yield more stable metal-complexes.^{275–281,285} The last mentioned organic ligand systems can accommodate metal ions in both *cis* and *trans* isomeric forms yielding mono- and dinuclear d-metal complexes.^{265,266,286,287} The oxamate related bridging ligand framework has been successfully used to isolated hetero-trinuclear metal-complexes, generally abbreviated as ABA systems.^{10,261,283,288} These last d-transition metal complexes are rare examples of ferromagnetic-like behavior with large spin ground state, even though the interaction between near-neighboring metal ions is antiferromagnetic. Such a magnetic behavior has been explained by Kahn *et al.* as a consequence of polarization by the small central spin of the two terminal spins in ferromagnetic-like fashion and the mechanism is known as *irregular spin state structure* and was found mainly in trinuclear Mn–Cu–Mn and Ni–Cu–Ni oxamate-bridged complexes.^{10,289,290} It has to be emphasized that ferromagnetic coupling of the metal ions appears in strictly orthogonal oriented magnetic orbitals ($\text{V}^{\text{IV}}\text{-Cu}^{\text{II}}$, $\text{Ni}^{\text{II}}\text{-Cr}^{\text{III}}$ and $\text{Fe}^{\text{III}}\text{-Cu}^{\text{II}}$ combination) and/or d-transition metals with accidental orthogonal orientation of their magnetic orbitals.^{10,291,292} The oxamato-bridged metal-complexes are a particular case of molecular ferromagnets which comprise both irregular spin state and/or ferrimagnetic chains. Based on these consideration, a novel mononuclear Cu(II) anion complex has been isolated. The anionic copper(II)-core is assembled in one-dimensional polymer *via* coordination surroundings of potassium cations. Moreover, this Cu(II)-precursor posses additional coordination sites, namely two carbonyl-like oxygen atoms that allowed coordination of cobalt(II) ion to yield a hetero-trinuclear $[\text{Cu}_2\text{Co}]$ -complex. This last polynuclear complex

is also self-assembled through hydrogen bonding interaction into layered sheets of trinuclear entities. In addition, a possible combination between cyanide-bridged and oxamate-ligands will be briefly presented. The cyanide-bridges represent another important class of appropriate linkers to generate polynuclear complexes. Such bridges are mediating very well the magnetic interaction between the paramagnetic centers and polynuclear complexes of Prussian Blue type have been reported as single-molecule magnets with spontaneous magnetization at temperature as high as 376 K.¹¹⁴

5.1 Mononuclear Cu(II)-complex based on oxamate-derivative ligand

Oxamide ligands behave as most amide functional groups which are neutral throughout the pH range and relatively instable towards hydrolysis reaction. The N-(2-dimethylamino-ethyl)-oxalamide ligand is easily accessible by reaction of commercially available ethyl oxamate with N,N-dimethylethane-1,2-diamine compound. The resulting dissymmetric N-(2-dimethylamino-ethyl)-oxalamide ligand has been reacted with copper nitrate salt in presence of potassium thiocyanate yielding an anionic mononuclear Cu(II) complex **21**. The starting oxamide-based ligand is hydrolyzed to N-(2-dimethylamino-ethyl)-oxalamic acid upon copper(II) coordination due to strong alkaline reaction conditions (Figure 5.2).

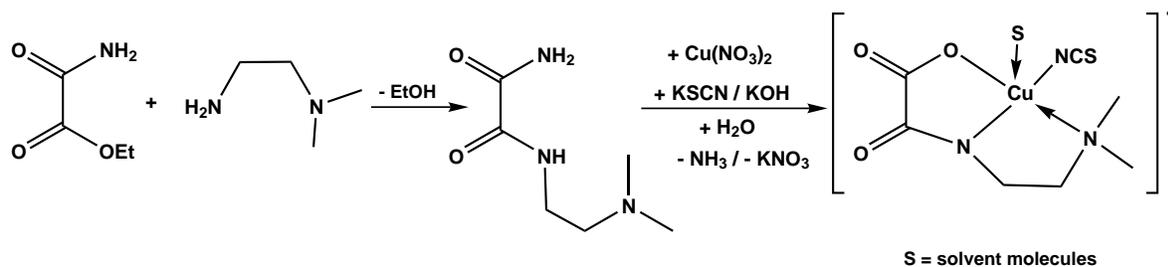


Figure 5.2: Schematic representation of the reaction pathways involved in synthesis of $[\text{Cu}(\text{dmae-oximate})(\text{OH}_2)(\text{NCS})]^-$ complex.

The copper(II) ion is five-coordinated, accommodated by the N-(2-dimethylamino-ethyl)-oxalamic acid ligand through NNO-donor set through a pair of five-membered

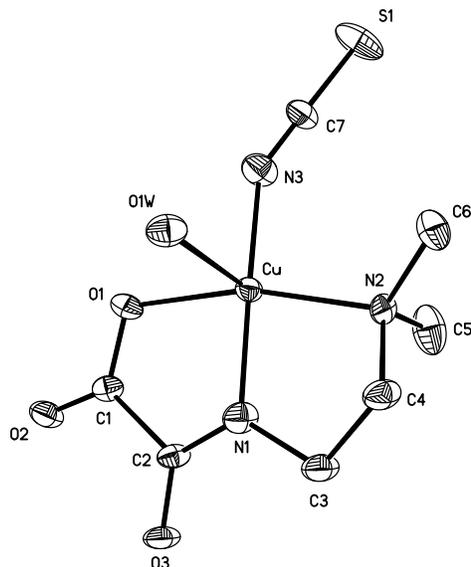


Figure 5.3: Molecular structure and numbering scheme of $([\text{Cu}(\text{dmae-oximate})(\text{OH}_2)(\text{NCS})]\text{K}\cdot\text{H}_2\text{O})_n$ (**21**) complex. Thermal ellipsoids are drawn at 50% probability. Only the $[\text{Cu}(\text{dmae-oximate})(\text{OH}_2)(\text{NCS})]^-$ anion core is shown. Hydrogen atoms have omitted for clarity.

chelate rings. The coordination sphere of the metal ion is completed by coordinated water molecule and monodentate iso-thiocyanate ligand. The molecular structure determination of compound **21** is shown in Figure 5.3, whereas selected bond lengths and angles for $([\text{Cu}(\text{dmae-oximate})(\text{OH}_2)(\text{NCS})]\text{K}\cdot\text{H}_2\text{O})_n$ complex are listed in Table 5.1. The resulting geometry around the Cu(II) ion can be described as distorted square-pyramid with $\tau = 0.05$ as a characteristic parameter for the trigonality distortions.²³⁹ The coordinating donor atoms of the tridentate organic ligand defines the equatorial plane with the copper ion displaced out from this plane by 16.8 pm, towards the coordinated water molecule placed on the apex of the defined geometry. The equatorial plane of the coordination geometry of the Cu(II) ions is completed by isothiocyanate monodentate anion, that coordinates in bent fashion with a torsion angle Cu–N–C–S of 67.7 °, bonded at around 194.4 pm on the metal ion. The amine-nitrogen-to copper bond length of 204.8 pm is significantly longer than that involving the deprotonated amide nitrogen atom (190.7 pm) consistent with a stronger coordination mode of the last functionality. These bond lengths are very close to corresponding bond distances reported for similar copper

oxamato-bridged complexes.^{293,294} The ligand acts as tridentate system with bite angles of the two five-membered chelate rings of 82.6 ° (O1–Cu–N1) and 83.3° (N1–Cu–N2).

The negative charge of the copper(II)-core is compensated by potassium cation, which is [5+1] coordinated, first weakly by the isothiocyanate nitrogen atom N3 (267 pm) and more tightly by the oxamate carbonyl-like oxygen atoms in η_2 -fashion, and additionally by carboxylate-oxygen atoms and coordinated water molecules with potassium-to-oxygen bond distances that fall in the 236.0-244.9 pm range (Figure 5.4). These potassium cations are placed between layers of anionic copper units resulting in μ_2 -oxygen bridges between K⁺ ions *via* carboxylate oxygen (O1) and oxamate oxygen (O2) atoms, resulting in alternating rhombic and octahedron geometric arrangement along the b crystallographic axis (Figure 5.5). Complex **21** crystallizes in P2/c space group with a water molecule as solvent of crystallization. These lattice water molecules are placed in the octahedron cavities of the one-dimensional polymer and are involved in bifurcated hydrogen bonding interaction with the coordinated water molecules of the copper(II) ions (OW...O1OH 281.0 pm) (Figure 5.4).

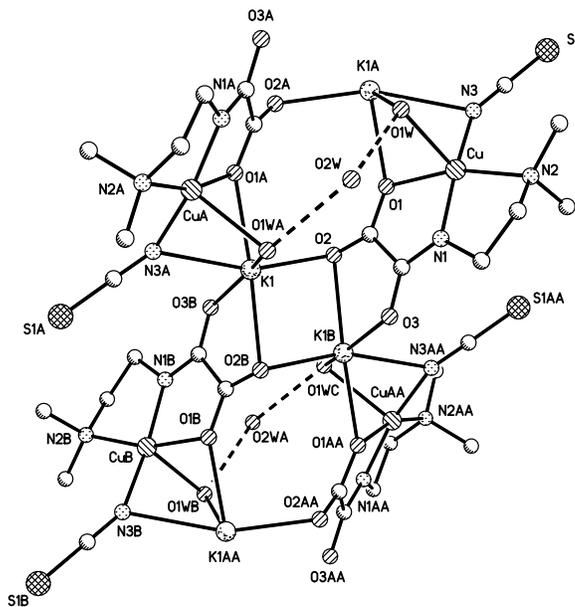


Figure 5.4: Molecular structure and selected numbering scheme for $([\text{Cu}(\text{dmae-oximate})(\text{OH}_2)(\text{NCS})]\text{K}\cdot\text{H}_2\text{O})_n$ (**21**) complex showing the formation of the coordination sphere of potassium cation. Hydrogen atoms have omitted for clarity. Dashed lines represent hydrogen bonding interactions.

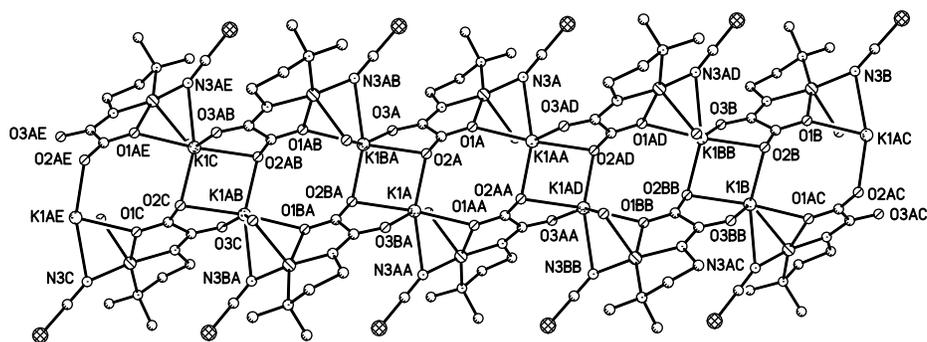


Figure 5.5: Representation of crystal packing in $([\text{Cu}(\text{dmaeoximate})(\text{OH}_2)(\text{NCS})]\text{K}\cdot\text{H}_2\text{O})_n$ (**21**) complex showing the formation of polymeric structure. Hydrogen atoms have omitted for clarity. Only the heteroatoms which are relevant for the coordination mode of potassium cation are labeled. Water lattice molecules have been also omitted.

The IR spectrum of the complex is also in agreement with molecular structure determination. Strong band corresponding to stretching vibration of the isothiocyanate-coordination mode of the SCN^- anion has been observed at 2061 cm^{-1} , around 10 pm shifted compared to its vibration band in iron-azametallacrown complexes described in Chapter 2, but very close to established vibration band for N-coordinating mode.¹⁰⁴ The oxamate-based ligand showed strong band at 1636 and 1617 cm^{-1} , owing to ν_{CO} vibrations in acid and amide functionalities, respectively. These are shifted to lower frequencies

Table 5.1: Selected bond lengths (pm) and angles ($^\circ$) for complex **21**.

Cu–O1	203.5(9)	Cu–N1	190.7(11)
Cu–N2	204.8(10)	Cu–N3	194.4(11)
Cu–O1W	235.1(9)		
O1–Cu–N1	82.6(4)	O1–Cu–N2	163.7(4)
O1–Cu–N3	93.9(4)	O1–Cu–O1W	84.6(4)
N1–Cu–N2	83.3(4)	N1–Cu–N3	168.8(5)
N1–Cu–O1W	100.8(4)	N2–Cu–N3	98.3(5)
N2–Cu–O1W	106.2(4)	N3–Cu–O1W	89.4(4)

compared to their stretching vibrations in N-(2-dimethylamino-ethyl)-oxalamide acid ligand (1696 and 1660 cm^{-1}) in accordance with "in situ" hydrolysis of the oxamide-like ligand upon copper(II) ion coordination. Medium-to-strong intense bands centered at 1335-1317 and 802 cm^{-1} have been also detected owing to $\nu_{sym}(NCO)$ stretching and $\delta(CO)$ deformation modes of the amide group. In addition, broad band of medium intensity has been detected at 3392 cm^{-1} which was attributed to water stretching vibration modes.

5.2 Oxamate-bridged trinuclear $[\text{Cu}_2\text{Co}]$ -complex

The anionic Cu(II) precursor **21** reacts with divalent transition metal ions, e.g. Co(II) perchlorate under reflux in methanol solution to afford a trinuclear $[(\text{Cu}(\text{dmae-oximate})-\text{MeOH})(\text{NCS})]_2\text{Co}(\text{MeOH})_2$ (**22**) complex (Figure 5.6). Cobalt(II) ion plays a very important role in molecular magnetism due to its highest magnetic anisotropy as compared to other d-transition metals. Taking into consideration the strong magnetic interaction mediated by oxalate-derivatives compounds, the association of Cu(II) metal ions with Co(II) might lead to interesting magnetic behavior of the resulting polynuclear complex. Molecular structure determination shows a centrosymmetric $[\text{Cu}_2\text{Co}]$ -complex which crystallizes in the $C2/c$ space group with an inversion center that passes through the cobalt ion.

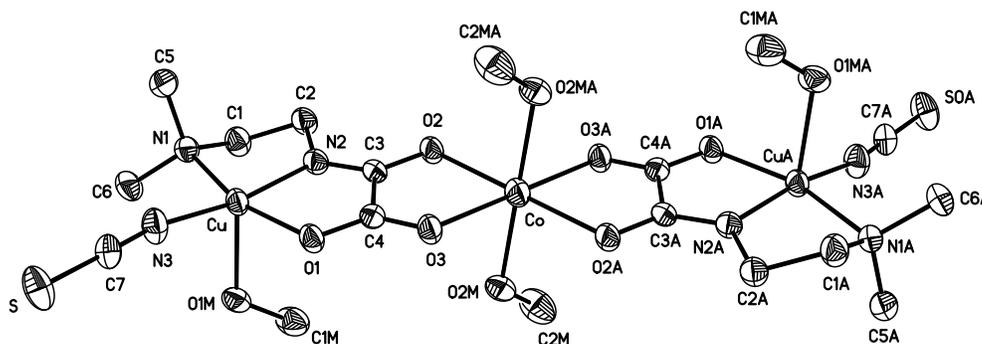


Figure 5.6: Molecular structure and numbering scheme of $[(\text{Cu}(\text{dmae-oximate})(\text{MeOH})(\text{NCS}))_2\text{Co}(\text{MeOH})_2]$ (**22**) complex. Thermal ellipsoids are drawn at 50% probability. Hydrogen atoms have omitted for clarity.

The copper(II) ions maintain their classical position in the tridentate pocket of the N-(2-dimethylamino-ethyl)-oxalamic acid ligand with Cu–N and Cu–O bond lengths very close to corresponding bond distances in the mononuclear precursor **21** complex. A net difference in the coordination sphere of the copper(II) ion has been observed for the isothiocyanate-monodentate ligand which binds in linear fashion (Cu–N–C–S torsion angle is equal 177.9 °) with a Cu–N3 bond length of 192.6 pm. The cobalt(II) ion is surrounded by two copper oxamate-like anionic units, and completes its slightly distorted octahedral geometry with two methanol molecules. The Co–O_M bond distances are 221.6 pm, only 5 pm longer than cobalt-to-oxygen atoms bond lengths formed with the bridging oxamate-ligand. Selected bond lengths and angles in complex **22** are listed in Table 5.2.

The cobalt-to-oxamate bridging oxygen atoms are very similar and within the error of measurement (Co–O2 216.2 pm and Co–O3 216.9 pm), resulting in a planar structural arrangement with the dihedral angle between the bridging entities of 3.9°. This implies that Cu–O–C–O–Co and Cu–N–C–O–Co fragments are delocalized units as a result of

Table 5.2: Selected bond lengths (pm) and angles (°) for complex **22**.

Cu–O1	204.8(2)	Cu–N1	207.6(3)
Cu–N2	191.6(2)	Cu–N3	192.6(3)
Cu–O1M	226.6(2)	Co–O2	216.2(2)
Co–O3	216.9(2)	Co–O2M	221.6(3)
O1–Cu–N1	164.52(10)	O1–Cu–N2	81.92(9)
O1–Cu–N3	95.53(10)	O1–Cu–O1M	92.49(9)
N1–Cu–N2	83.28(10)	N1–Cu–N3	97.82(11)
N1–Cu–O1M	94.29(10)	N2–Cu–N3	166.57(12)
N2–Cu–O1M	99.04(10)	N3–Cu–O1M	94.23(11)
O2–Co–O2A	180.00(10)	O2–Co–O3A	101.87(8)
O2–Co–O3	78.13(8)	O3–Co–O3A	180.00
O2–Co–O2M	89.28(9)	O3–Co–O2M	83.39(9)
O3–Co–O2MA	96.61(9)	O2A–Co–O2M	90.72(9)
O3A–Co–O2M	96.61(9)	O2M–Co–O2MA	180.00(12)

conjugation of electrons from from the oxygen atoms and lone pairs on the nitrogen atoms. This is further supported by the average C–O (C4–O3 124.8 pm, C4–O1 126.7 pm and C3–O2 127.4 pm) and C–N (C3–N2 128.6 pm) bond distances, which are shorter than expected single C–O and C–N bonds of 148.1 and 146.2 pm, respectively. The intramolecular Cu···Co separation is around 543.7 pm, similarly to intrametallic separation in reported similar oxamate-bridged polynuclear complexes.^{270, 285, 295} The trinuclear units are pillared *via* hydrogen bonding interactions forming polymeric structures along the ab planes (Figure 5.8) with OM···O contacts of 273.1 pm (O2···O1M) and 276.2 pm (O1···O2M) (Figure 5.7). Within these hydrogen bonded one-dimensional polymers, the Cu···Co interchain separation is even smaller than the intramolecular Cu···Co separation, namely 522.7 pm. In addition equal intrachains Cu···Cu and Co···Co separations have been observed of around 689.4 pm, much shorter than Cu···Cu intra-trimer separation of 1087.4 pm.

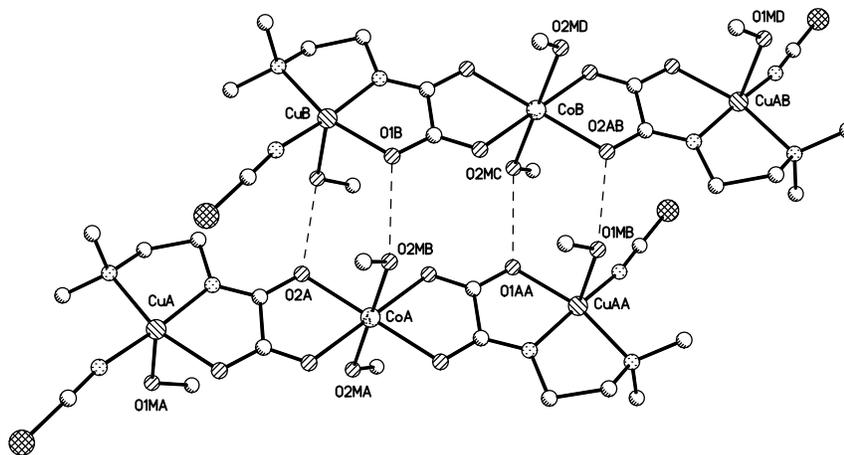


Figure 5.7: Hydrogen bonding interaction in $[(\text{Cu}(\text{dmae-oximate})(\text{MeOH})(\text{NCS}))_2\text{Co}(\text{MeOH})_2]$ (**22**) complex as viewed along the *c* crystallographic axis.

The IR spectrum of complex **22** is also in line with the molecular structure determination. Characteristic IR features of the Cu(II)-precursor have been detected, e.g. the medium-to-strong intense bands centered at 1336-1316 and 810 cm^{-1} have been also detected owing to $\nu_{\text{sym}}(\text{NCO})$ stretching and $\delta(\text{CO})$ deformation modes of the amide group. The ν_{CO} vibrations mode have been observed at 1653 and 1610 cm^{-1} , slightly

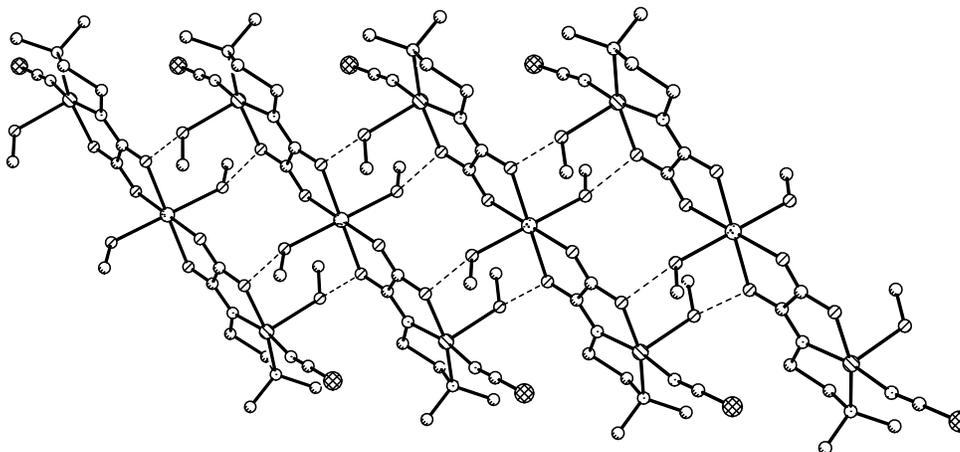


Figure 5.8: Packing diagram in $[(\text{Cu}(\text{dmae-oximate})(\text{MeOH})(\text{NCS}))_2\text{Co}(\text{MeOH})_2]$ (**22**) complex showing the formation of polymeric structure formed by hydrogen bonding interactions as is viewed along the *c* crystallographic axis.

shifted compared to their IR features in complex **21**, owing to an extended bridging mode of the N-(2-dimethylamino-ethyl)-oxalamic acid supporting-ligand. Very broad bands of medium intensity have been detected at 3420 and 3254 cm^{-1} which were attributed to ν_{OH} stretching vibration of the coordinated methanol molecules. By comparison to mononuclear Cu(II)-precursor, the isothiocyanate stretching vibration has been observed at 2094 cm^{-1} , owing to a linear coordination mode of the isothiocyanate monodentate anion in trinuclear complex **22**.

5.2.1 Magnetic properties

Variable temperature (300 - 2 K) magnetic susceptibility measurements were performed on powdered crystals of complex $[(\text{Cu}(\text{dmae-oximate})(\text{MeOH})(\text{NCS}))_2\text{Co}(\text{MeOH})_2]$ (**22**) complex. The χ_M vs T and $\chi_M T$ vs T plots are depicted in Figure 5.9 as have been measured with a fixed 2000 Oe magnetic field. The $\chi_M T$ value is $5.05\text{ cm}^3\text{mol}^{-1}\text{K}$ at 300 K which is much higher than expected value for uncoupled spin carriers. The $\chi_M T$ value at 300 K for Co(II) ion in octahedral environment is about $2.5\text{ cm}^3\text{mol}^{-1}\text{K}$, value which takes into account the orbital contribution in addition to the $S_{Co} = 3/2$ local spin.¹⁰ The experimental $\chi_M T$ values are decreasing steadily on lowering the temperature reaching a rounded minimum of $2.10\text{ cm}^3\text{mol}^{-1}\text{K}$ at 15 K and then increase again to reach a

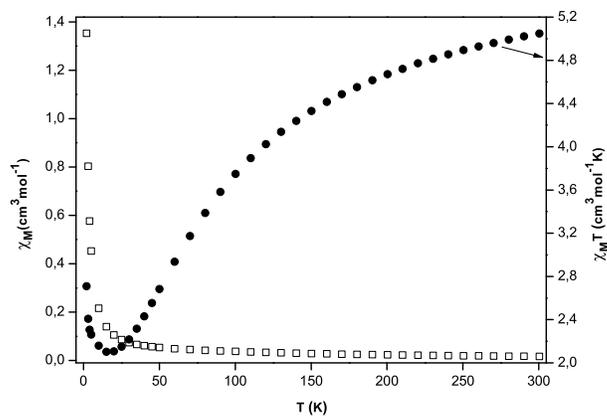


Figure 5.9: Plot of thermal dependence of χ_M (empty squares) and $\chi_M T$ product (black filled circles) for $[(\text{Cu}(\text{dmae-oximate})(\text{MeOH})(\text{NCS}))_2\text{Co}(\text{MeOH})_2]$ (**22**) complex measured with an applied magnetic field of 2000 Oe.

maximum of $2.71 \text{ cm}^3 \text{ mol}^{-1} \text{ K}$ at 2 K. The $\chi_M T$ vs T profile curve reveals a ferrimagnetic behavior and has been mainly found in [CuCo]-chain and ABA systems described by Kahn.¹⁰

The decrease of the $\chi_M T$ values in the 300-15 K temperature regime may be a consequence of antiparallel alignment of the local Co(II) and Cu(II) spins. On lowering the temperature an increase of the $\chi_M T$ values may be correlated to possible ferrimagnetic interaction that occurs in the bulk material. The magnetic behavior of Co(II) ion in octahedral environment is governed by strong magnetic anisotropy and orbital contribution, with last feature arising from $^4T_{1g}$ ground state, therefore a detailed interpretation of the magnetic data has to take into account the orbital contribution of the cobalt(II) ion. Nevertheless, owing to the planarity of the bridging organic ligand, known as one of the best mediators of magnetic interaction between the paramagnetic centers, a strong magnitude of the magnetic interaction is to be expected. This is based on well established system for which the extended conjugated π -system of the oxalate-derivatives bridges assure a good overlap of the d-magnetic orbitals.²⁹⁶

An important feature of this polynuclear [Cu₂Co]-complex **22** consists of its possible function as "magnetic molecular sponges". This will be to be found if the coordinated

methanol molecules are totally or partly removed and therefore, a new arrangement of the structural motif to form coordination polymers is to be expected. This hypothesis is sustained by short interchain Cu···Co separation of 522.7 pm, in which two possible coordination modes are plausible: I) the carboxylate oxygen atom of the oxamate-based ligand may function as μ_2 bridges or II) the isothiocyanate ligand change the coordination mode from end-off to end-to-end bridges between the metal centers.²⁶⁸ This will be a similar situation with one reported by Kahn for hydrated [CuMn] and [CuCo]-containing complexes for which the dehydration process has led to ferrimagnetic ordering due to the polymerization of the bimetallic units.^{28,29}

5.3 Conclusions and future perspectives

The "complex-as-ligand" approach allows synthesis of polynuclear metal complexes with predefined structural motif. A novel mononuclear Cu(II) complex with oxamate-based ligand (N-(2-dimethylamino-ethyl)-oxalamic acid) has been isolated and successfully used to synthesize trinuclear [Cu₂Co]-complex. Co²⁺ ion is an appropriate paramagnetic center for designing magnetic materials due to its very anisotropic spin carrier property. Besides the additional coordination sites of the supporting oxamate-ligand in Cu(II)-precursor complex **21** that allows the coordination of the outer metal ions, an interesting feature of this molecular "brick" is represented by labile coordination positions existent at the copper center. The isothiocyanate monodentate end-off ligand may be replaced with other pseudohalides like, i.e. azide which can better bridge end-to-end metal ions. Another interesting bridging entity, known to mediate very well the magnetic interaction between the paramagnetic centers is the cyanide ligand. On this basis, the "in situ" formed Cu^{II}-complex precursor has been reacted with KCN, under reflux in presence of FeCl₃·6H₂O in basic aqueous solution. A tetranuclear mixed-valence copper complex [(Cu^{II}(dmae-oximate)(μ_2 -CN)₃)Cu^I(Cl)_{0.5}]K₃(NO₃)_{0.5}·xH₂O (**23**) has been obtained for which the molecular structural motif is shown in Figure 5.10.

The quality of the isolated crystals was not good enough for an accurate determination of the molecular structure. It is most likely that no iron(III) ion is present in the structural motif, but instead the "copper-oxamate" entities are cyanide bridged through a

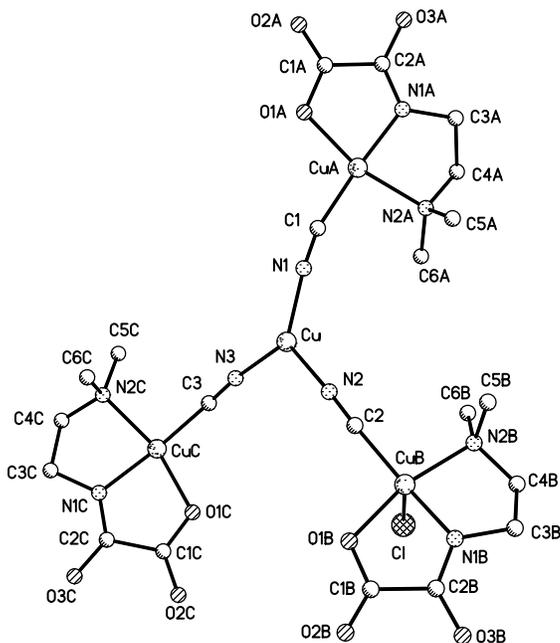


Figure 5.10: Representation of molecular structure fragment and the corresponding numbering scheme for $[(\text{Cu}^{\text{II}}(\text{dmae-oximate})(\mu_2\text{-CN})_3)\text{Cu}^{\text{I}}(\text{Cl})_{0.5}]\text{K}_3(\text{NO}_3)_{0.5}\cdot x\text{H}_2\text{O}$ (**23**) complex.

diamagnetic Cu^{I} center. The overall synthetic scheme to generate mixed-valence homonuclear copper-cyanide bridged complexes may be explained as partial reduction of $\text{Cu}(\text{II})$ ions in the used reaction conditions: reflux and excess of KCN reagent. It has been reported that copper(II) cyanide complexes are not stable but are reduced by cyanide to a copper(I) ion under release of cyanogen.²⁹⁷ The $\text{Cu}(\text{I})$ cyanide complexes have been reported to be very stable towards oxygen, i.e. $[\text{Cu}(\text{CN})_3]^{2-}$ is known to be very stable towards oxygen streams. Any attempt to isolate crystals of complex **23** in absence of FeCl_3 salt was unsuccessful, therefore the iron(III) ion might be interfering in the crystallization process. The structural motif consists of three copper-N-(2-dimethylamino-ethyl)-oxalamic acid ligand moieties linked presumably by a Cu^{I} center and three μ_2 -cyanide bridging anions with $\text{Cu}^{\text{I}}\text{-N}(\equiv\text{C})$ bond lengths of 194.5-195.9 pm, a little bit shorter compared to corresponding bond distances of 200.3 pm found in discrete $\text{K}_3[\text{Cu}^{\text{I}}(\text{CN})_4]$.²⁹⁸ Selected bond lengths and angles of complex **23** are listed in Table 5.3. The CuA , CuB , CuC centers presumably Cu^{II} ions have square-planar (CuA and CuC centers) and square pyramidal geometries ($\tau = 0.03$)²³⁹ with the cyanide and the donor set atoms of the tri-

Table 5.3: Selected bond lengths (pm) and angles ($^{\circ}$) for complex **22**.

Cu–N1	194.8(17)	Cu–N2	195.9(17)
Cu–N3	194.5(19)	O1A–CuA	202.3(11)
N1A–CuA	191.9(13)	N2A–CuA	207.9(15)
CuA–C1	195.9(13)	O1B–CuB	200.6(14)
N1B–CuB	188.3(15)	N2B–CuB	205.7(17)
CuB–C1	245.2(2)	CuB–C2	193.0(17)
O1C–CuC	198.9(12)	N1C–CuC	193.8(13)
N2C–CuC	207.2(14)	CuC–C3	195.7(14)
N1–Cu–N2	121.5(7)	N1–Cu–N3	127.6(7)
N3–Cu–N2	110.5(8)	O1A–CuA–N1A	82.6(5)
O1A–CuA–N2A	164.0(5)	N1A–CuA–N2A	82.8(6)
O1B–CuB–N1B	81.7(6)	O1B–CuB–N2B	165.8(6)
N1B–CuB–N2B	84.1(7)	O1C–CuC–N1C	81.9(5)
O1C–CuC–N2C	162.2(6)	N1C–CuC–N2C	82.2(6)

dentate supporting-ligand forming the equatorial planes. The distance between Cu^{I} and Cu^{II} cyanide-bridged centers range from 493.8 to 499.2 pm, distances that compare well with 454.4–467.2 pm reported for Cu^{I} - Cu^{II} separation found in mixed-valence homonuclear copper complexes.²⁹⁹ The Cu^{I} -center is three-coordinated with bridging cyanide angles in the 110.6–127.6 $^{\circ}$ range.

A possible overcome of the reduction-process that occurred in the synthetic pathway used to isolate complex **23**, may be the replacement of KCN reagent with hexacyanide metal complexes, e.g. $\text{K}_3[\text{M}(\text{CN})_6]$ ($\text{M} = \text{Fe}, \text{Cr}$) and octacyanide complexes of 4 d-block metals. Moreover, the existing reports showed that d-metal precursor complexes based on oxalate-derivative ligands are suitable "bricks" to "construct" ferromagnetic d-f mixed polynuclear complexes. Hence, a proposed reaction pathway shown in Figure 5.11 may be followed.

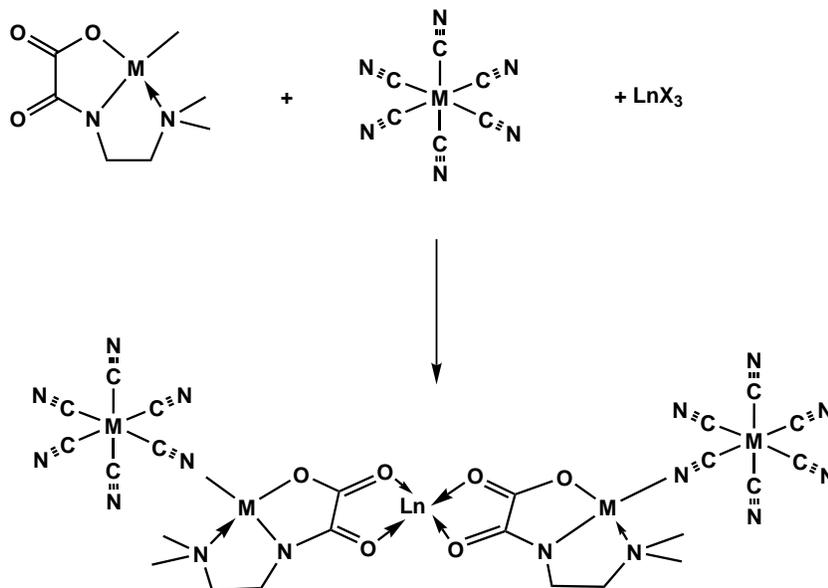


Figure 5.11: Proposed reaction pathway involving the Cu-oxamide precursor as building brick to approach polynuclear metal-complexes with d-f topology and high-spin ground state due to a rational chosen ferromagnetic interaction between the paramagnetic centers.

5.4 Experimental Part

Synthesis of N-(2-dimethylamino-ethyl)-oxalamide acid ligand

To a suspension of ethyl oxamate (1.17 g, 0.01 mol) in iso-propanol (50 mL) was stepwise a isopropanol solution (30 mL) of N,N-dimethylethane-1,2-diamine (0.88 g, 0.01 mol). The resulting solution was refluxed for one hour and than cooled down on ice-bath when a colorless precipitate is formed. The precipitate was filtered, washed with a minimum amount of isopropanol and dried in air. Yield: 1.44 g (9.00 mmol, 90.0%). *Anal.* Calc. for C₆H₁₃N₃O₂ (159.18): C 45.27, H 8.23, N 26.40. Found: C 45.33, H 7.99, N 26.06. ¹H NMR (400 MHz, DMSO-d₆): δ = 2.14 (s, 6H, CH₃), 2.33 (t, 2H, CH₂N, J = 6.6 Hz), 3.17-3.22 (q, 2H, CH₂NH, J = 6.36 Hz), 7.74, 8.01 (br, total 2H, NH₂, ν_{1/2} = 6.91 Hz), 8.42 (t. NH, J = 6.28 Hz) ppm. ¹³C NMR (100 MHz, DMSO-d₆): δ = 36.7 (CH₂NH), 45.0 (CH₃), 57.5 (CH₂N), 160.1 (C=O-NH), 162.2 (C=O-NH₂) ppm. Selected IR data (cm⁻¹): 3376, 3319 (s, NH, NH₂), 1696, 1661 (s, CO), 1322, 1311 (m, sym NCO), 858 (m, δ_{CO}).

Synthesis of $[(\text{Cu}(\text{dmae-oximate})(\text{OH}_2)(\text{NCS})]\text{K}\cdot\text{H}_2\text{O})_n$ (**21**) complex

To a solution of N-(2-dimethylamino-ethyl)-oxalamide acid ligand (1.56 g, 0.01 mol) in MeOH-H₂O mixture (1/3) (60 mL) was added stepwise an aqueous solution (15 mL) of Cu(NO₃)₂·3H₂O (2.61 g, 0.01 mol) followed by addition of KOH (0.03 mol) aqueous solution (1.68 g in 30 mL H₂O). To the resulting solution, KSCN (1.125 g, 0.011 mol) was added as aqueous solution (10 mL) and the final solution mixture refluxed for around one hour with continuous stirring. By cooling at room temperature a black precipitate was formed which was removed by filtration. The water solvent of the clear filtrate was removed to dryness. The solid material was extracted twice with MeOH and redissolved at the end in minimum amount of the same solvent. Yield: 1.64 g (4.60 mmol, 46.0%). *Anal. Calc.* for C₇H₁₆N₃O₆SCuK (372.92) ([Cu(dmae-oximate)(OH₂)(iso-NCS)]K·2H₂O): C 22.55, H 4.32, N 11.27. Found: C 22.39, H 4.39, N 10.01. Selected IR data (cm⁻¹): 3392 (br m, H₂O), 2061 (s, NCS), 1636, 1617 (s, CO), 1335, 1317 (m, sym NCO), 802 (m, δ_{CO}).

Synthesis of $[(\text{Cu}(\text{dmae-oximate})(\text{MeOH})(\text{NCS}))_2\text{Co}(\text{MeOH})_2]$ (**22**) complex

To a solution of precursor complex **21** (88.5 mg, 0.25 mmol) in methanol/water mixture (5/1) (12 mL) was added stepwise a methanol solution (5 mL) of Co(ClO₄)₂·6H₂O (45.5 mg, 0.125 mmol). The resulting clear solution was refluxed for one hour. The solution was cooled down when a precipitate is forming. This was filtered off and the resulting solution is allowed to stand at room temperature in a closed vessel. Yield: 20.0 mg (0.03 mmol, 21.5%). *Anal. Calc.* for C₁₈H₄₂N₆O₁₃S₂Cu₂Co (800.72) ([Cu(dmae-oximate)(MeOH)(NCS))₂Co(MeOH)₂·3H₂O): C 27.00, H 5.29, N 10.50. Found: C 27.14, H 3.80, N 10.87. Selected IR data (cm⁻¹): 3420, 3254 (br m, OH, MeOH), 2094 (s, NCS), 1653, 1610 (s, CO), 1336, 1316 (m, sym NCO), 810 (m, δ_{CO}).

Synthesis of $[(\text{Cu}^{\text{II}}(\text{dmae-oximate})(\mu_2\text{-CN})_3)\text{Cu}^{\text{I}}(\text{Cl})_{0.5}]\text{K}_3(\text{NO}_3)_{0.5}\cdot x\text{H}_2\text{O}$ (23) complex

To a suspension of N-(2-dimethylamino-ethyl)-oxalamide acid ligand (78.0 mg, 0.5 mmol) in water (5 mL) was added stepwise an aqueous solution (5 mL) of $\text{Cu}(\text{NO}_3)_2\cdot 3\text{H}_2\text{O}$ (120.0 mg, 0.5 mmol) followed by addition of NaOH (1 mL of 1 N aqueous solution). The resulting clear solution was stirred at room temperature for five minutes, followed by addition of KCN (65.0 mg, 1.0 mmol) dissolved in H_2O (2 mL). The resulting solution was stirred at room temperature for around two hours leading to a blue precipitate. This precipitate was redissolved using additional NaOH (1 mL 1N aqueous solution), followed by addition of a methanol solution of $\text{FeCl}_3\cdot 6\text{H}_2\text{O}$ (33.75 mg, 0.17 mmol). The clear formed solution was refluxed for one hour, filtered hot and left at room temperature for slow evaporation of the solvents mixture. Blue crystals, accompanied by a colorless material were collected from the solution within one months. Selected IR data (cm^{-1}): 3397 (br, OH_2), 2136 (s, CN), 1653, 1610 (s, CO), 1335, 1311 (m, sym NCO), 800 (m, δ_{CO}).

Chapter 6

Novel heterometallic 3d-4f complexes

The synthesis of heteronuclear metal complexes has started at the end of the 1960s when interesting physicochemical properties have been reported for dissimilar d-metals ions placed in the close proximity.³⁰⁰ According to the chosen metal ions and their geometry the exchange interaction pathway can vary from ferromagnetic to antiferromagnetic coupling.¹⁰ The design of heteronuclear complexes has also been extended to d-f composition in 1985 when Gatteschi *et al.* reported unique magnetic properties for a trinuclear $\text{Cu}^{\text{II}}\text{-Gd}^{\text{III}}$ complex.³⁰¹ A very important role in the strategy of synthesis of such dissimilar metal complexes is played by the starting tectonic compound that is used in fact as "complex-ligand". *Salen*-type ligands are versatile organic supports for synthesizing a broad range of metal complexes.³⁰² These tetradentate Schiff base ligands are extensively used to isolate d-metal complexes (manganese, iron, vanadium, molybdenum, titanium, etc.) which are one of the best catalysts for various organic reaction.³⁰³ In addition, these complexes are also reported as versatile building blocks for interesting magnetic materials.^{302,304} A peculiar role is attributed to copper-salen and analogous polydentate Schiff base complexes that provide di- $(\mu\text{-phenoxo})\text{-Cu}^{\text{II}}\text{-Ln}^{\text{III}}$ complexes.³⁰⁵⁻³⁰⁹ Dinuclear $[\text{Cu}(\text{salen})\text{Ln}(\text{NO}_3)]$ and trinuclear $[(\text{Cu}(\text{salen}))_2\text{Ln}(\text{NO}_3)_3]$ were prepared by reaction of the $[\text{Cu}(\text{salen})]$ -complex with $\text{Ln}(\text{NO}_3)_3 \cdot 6\text{H}_2\text{O}$ salts.³¹⁰⁻³¹⁴ Similarly $\text{Ni}^{\text{II}}\text{-Ln}^{\text{III}}$ complexes have been isolated and according to the existing reports it seems that heavier lanthanide ions with smaller ionic radius (Eu–Lu) prefers the formation of heterodinuclear com-

plexes, whereas the other lanthanide metals yield trinuclear d-f complexes.³¹⁴⁻³¹⁶ In all these complexes the nitrate groups function as chelating end-cap ligand to the lanthanide ion. Discrete dinuclear d-f complexes have also been isolated by replacing the nitrate capping ligand with hexafluoroacetylacetonate,³¹⁷ tetramethylheptadione³¹⁸ and/or trifluoroacetic acid.^{319,320}

The initial work in this area showed that Cu^{II} and Gd^{III} brought in close vicinity are coupling ferromagnetically.³⁰¹ This was surprising since the Gd^{III} ion possesses all seven unpaired electrons in 4f-orbitals and it might be expected that at least one of these orbitals would overlap with the semi-occupied orbital of Cu^{II} ion and hence such an interaction would be anti-ferromagnetic. Instead, it has been demonstrated that the real countable interaction takes place between the semi-occupied $d_{x^2-y^2}$ orbital of Cu^{II} center and an empty orbital of the Gd^{III} ion, most likely the d-orbital.³²¹ In this case there are two possible orientations for the electron transferred from Cu^{II} to Gd^{III} . If an anti-parallel alignment is present this would lead to an $S = 3$ spin state and counts for an antiferromagnetic exchange. If the alignment of the d-electron is parallel to the 4f-electrons, the resulting state $S = 4$ is equivalent to a ferromagnetic exchange. According to Hund's rule the later is lower in energy and, therefore the excited state of the system favors the ferromagnetic exchange^{306,321,322} (Figure 6.1).

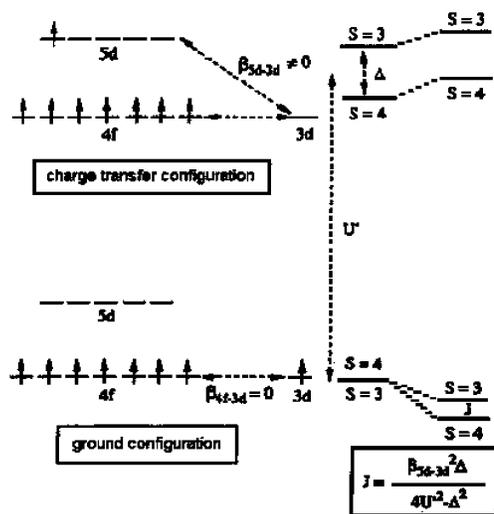


Figure 6.1: Scheme of the ground and charge transfer configuration relevant to the exchange mechanism in Cu-Gd species taken from reference.³²¹

The ferromagnetic interaction reported initially in 1985 by *Gatteschi et al* in the trinuclear $\text{Cu}^{\text{II}}\text{-Gd}^{\text{III}}$ complex³⁰¹ was weak with a coupling constant $J \simeq 5 \text{ cm}^{-1}$. This rises two important questions: i) can the interaction $\text{Cu}^{\text{II}}\text{-Gd}^{\text{III}}$ be conducted to a stronger coupling and therefore the design of new heterodinuclear d-f complexes will be more than an academic interest? and ii) if a larger nuclearity or polymeric complexes will bring high-spin molecules or even molecular ferromagnets with immediate application. Taking into account these two considerations compartmental salen-type Schiff bases have used extensively to synthesize the starting "d-metalloligand". Such ligands are based on dissymmetric 3-carboxy-2-hydroxy benzaldehyde^{323,324} and more recently 3-alkoxy substituted salicylaldehydes developed by Costes *et al*³²⁵⁻³²⁷ With these two organic frameworks a large number of discrete d-f heterodinuclear complexes have been isolated.^{313,314,318,319,325-334} The majority of the heterodinuclear complexes are based on $\text{Cu}^{\text{II}}\text{-Gd}^{\text{III}}$ composition and the magnitude of the magnetic interaction is larger or even smaller than the initial report. Moreover, according with the starting organic framework antiferromagnetic interaction between $\text{Cu}^{\text{II}}\text{-Gd}^{\text{III}}$ has also been reported.^{312,335} This led to an tremendous research activity focused on understanding and tuning the d-f magnetic interaction.

Following Costes's strategy and keeping in mind the two concerns regarding the design of new heteronuclear d-f complexes, a known Cu-salen-type complex has been isolated according to literature data.^{326,335} In instance, 1,3-propane diamine and/or 2,2-dimethyl-1,3-propane diamine have been reacted with 3-methoxy-2-hydroxy benzaldehyde (trivially known as ortho-vanillin) in a 1:2 ratio to yield the compartmental N,N'-bis(3-methoxy salicylidene)-R-1,3-diamino propane ligands. These Schiff base ligands reacts stoichiometrically with copper(II) acetate in methanol solution to form the mononuclear $[\text{Cu}(\text{OMesalen})\text{H}_2\text{O}]$ (**24**) precursor. The molecular structure determination is depicted in Figure 6.2. The copper ion is five coordinated in an almost ideal square-pyramidal geometry formed by N_2O_2 donor atoms in the equatorial plane and a coordinated water molecule in the apical position (Cu-O1w 237.8 pm). This tectonic complex crystalize in Pnma orthorhombic space group with the copper atom displaced out from the equatorial plane only by 15.08 pm, towards the apical oxygen atom with O1-Cu-O1A angle of 83.7°. Selected bond lengths and angles in complex $[\text{Cu}(\text{OMesalen})\text{H}_2\text{O}]$ are given in Table 6.1.

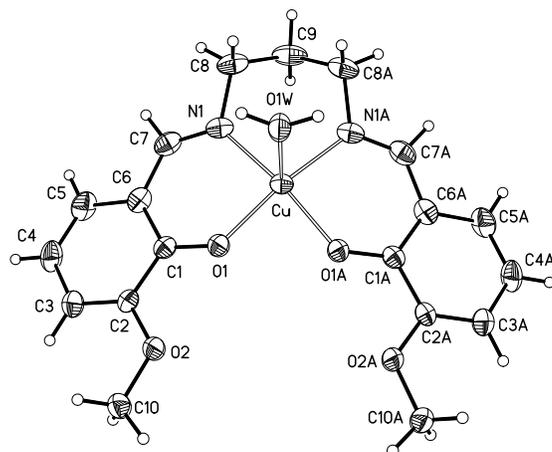


Figure 6.2: Molecular structure and numbering scheme atoms in complex $[\text{Cu}(\text{OMesalen})\text{H}_2\text{O}]$ (**24**) complex. Thermal ellipsoids are drawn at 50 % probability.

The coordinated water molecule is in hydrogen bonding interactions with the methoxy groups of neighboring molecules forming a 1D-chain through O–O hydrogen contacts (Ow–OCH₃ 272.1 pm) (Figure 6.3).

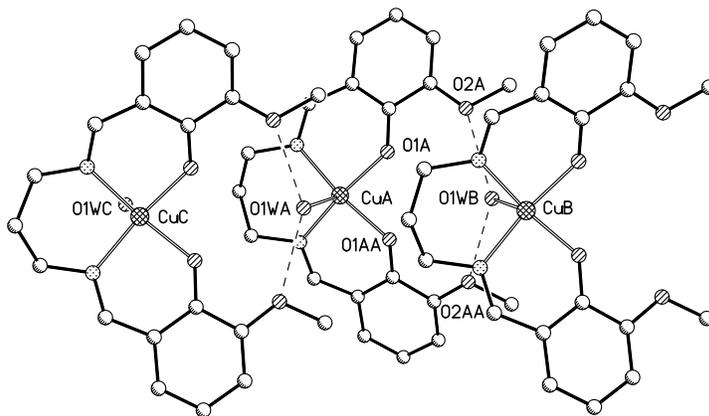


Figure 6.3: Hydrogen bonding interaction in complex $[\text{Cu}(\text{OMesalen})\text{H}_2\text{O}]$ (**24**) showing the formation of the 1-D polymer. Dashed lines represent hydrogen bonding interactions. Hydrogen atoms have been omitted for clarity.

Such a *salen-type* copper complex is an appropriate framework for accommodation of lanthanide ions. As can be seen, the copper ion is accommodated in the inner O₂N₂ pocket of the supporting organic ligand, whereas the outer site formed by phenoxy and methoxy oxygen atoms of the *salen-type* ligand form the appropriate pocket for oxophilic lanthanide ions.³³⁶

Table 6.1: Selected bond lengths (pm) and angles ($^{\circ}$) for complex **24**.

Cu–O1	195.4(2)	Cu–O1	1.954(2)
Cu–N1	201.1(3)	Cu–N1	201.1(3)
Cu–O1W	237.8(3)	-	-
O1–Cu–O1A	83.74(12)	O1–Cu–N1A	90.36(10)
O1–Cu–N1	90.36(10)	N1–Cu–N1A	94.22(16)
O1–Cu–O1W	99.70(9)	N1–Cu–O1W	89.45(9)

By changing the diamine "spacer" to 2,2-dimethyl-1,3-propane diamine similar reaction pathway can be followed. This last N,N'-bis(3-methoxysalicyliden)-2,2-dimethyl 1,3-diamino propane ligand was reacted with copper(II) acetate to form a similar copper-salen complex. In presence of NaNO₃, an cationic [Cu(OMesalen)Na(H₂O)]NO₃ (**25**) complex was isolated³³⁷ (Figure 6.4).

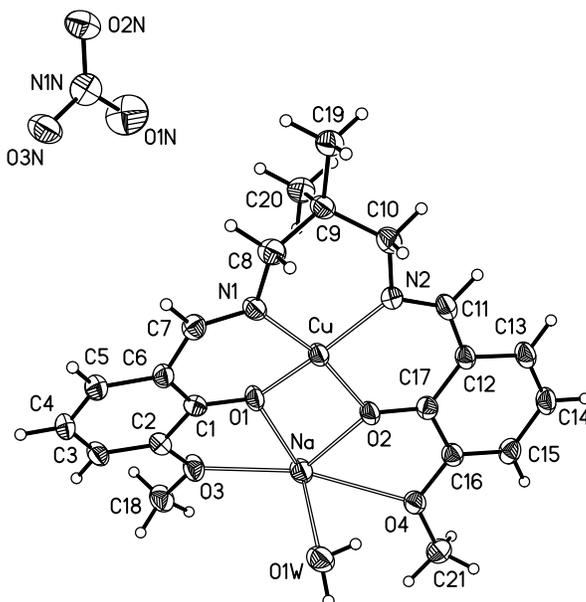


Figure 6.4: Molecular structure and numbering scheme atoms in complex [Cu(OMesalen)Na(H₂O)]NO₃ (**25**). Thermal ellipsoids are drawn at 50% probability. The unbounded nitrate anion is also shown.

The copper atom is placed in the classical dianionic N₂O₂ inner coordination site in a square-planar environment. The Cu–O (191.6 and 192.8 pm) and Cu–N (197.5 and

198.0 pm) are slightly shorter than in [Cu(OMesalen)OH₂] complex due to different coordination number of the copper ion. The sodium ion has been inserted in the outer O₂(OCH₃)₂ coordination site of the compartmental hexadendate Schiff base ligand in a pentacoordinated environment with a H₂O occupying the apical position of the s-metal in a bond distance of 244.1 pm. The Na–O bond lengths depend on the provenance of the oxygen atoms and are shorter as expected for μ -phenoxy bridged oxygen atom (Na–O1 232.8 and Na–O1 238.0 pm) and longer for the methoxy oxygen atoms that fall in the 242.5 (Na–O3) and 262.8 (Na–O4) pm range. Selected bond lengths and angles in complex [Cu(OMesalen)Na(H₂O)]NO₃ (**25**) are given in Table 6.2. The compensation of the positive charge of the alkaline ion is accomplished by the nitrate anion (Figure 6.4).

Table 6.2: Selected bond lengths (pm) and angles (°) for complex **25**.

Cu–O1	191.6(2)	Cu–O2	192.8(2)
Cu–N1	197.5(33)	Cu–N2	198.0(2)
Na–O1	232.8(2)	Na–O2	237.9(2)
Na–O3	242.5(2)	Na–O4	262.8(2)
Na–O1W	244.1(3)		
O1–Cu–O2	81.66(9)	O1–Cu–N1	91.90(10)
O1–Cu–N2	161.92(10)	O2–Cu–N1	167.63(10)
O2–Cu–N2	92.48(10)	N1–Cu–N2	96.71(10)
O1–Na–O2	64.54(8)	O1–Na–O3	66.66(8)
O1–Na–O4	127.06(9)	O1–Na–O1W	103.34(9)
O2–Na–O3	131.20(9)	O2–Na–O4	62.87(8)
O2–Na–O1W	86.96(9)	O3–Na–O4	164.99(9)
O3–Na–O1W	104.22(9)	O1W–Na–O4	68.51(8)

The formation of the d-s complex proves once again the versatility of the organic framework to accommodate dissimilar metal ions. The sodium ion can be replaced by lanthanide metals by reacting the copper(II)-salen complex with lanthanide nitrate salts. In instance, equimolecular reaction of the Cu-precursor **23** with Gd(NO₃)₃·6H₂O in methanol solution yields the dinuclear Cu-Gd complex of type [Cu(MeOH)(OMesalen)

Gd(NO₃)₃] (**26**). The molecular structure is depicted in Figure 6.5, whereas selected bond lengths and angles in complex (**26**) are listed in Table 6.3. As it was expected, the gadolinium ion coordinates in the outer site of the compartmental salen ligand similarly to sodium ion in complex [Cu(OMesalen)Na(H₂O)]NO₃. These O₂O₂ pocket fills partly the coordination environment of the gadolinium ion, whereas three nitrate ions complete the ten-coordination sphere of the lanthanide ion and also compensate its 3+ charge. Each nitrate ligand coordinates in η^2 -bidentate fashion with the bond distances in the 245.3-256.6 pm range. The copper ion, accommodated in the inner pocket is five-coordinated in a square pyramidal geometry with a methanol molecule coordinated on apical position in a bond distance of 235.4 pm. A similar Cu-Gd complex has been reported in literature,³²⁵ with a small difference in the coordination environment of the d-metal, namely a coordinated acetone molecule instead of methanol that has been found in molecular structure of [Cu(MeOH)(OMesalen)Gd(NO₃)₃] complex described herein.

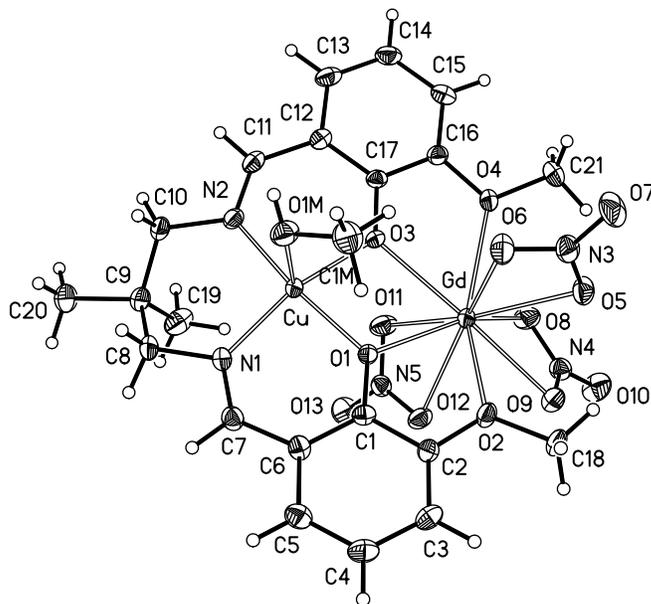


Figure 6.5: Molecular structure and numbering scheme of complex [Cu(MeOH)(OMesalen)Gd(NO₃)₃] (**26**) with thermal ellipsoids drawn at 50% probability.

The Cu–O and Cu–N bond lengths are closed to corresponding bond distances in the similar reported complex, as well as the Cu–Gd intermolecular separation of around 353.6 pm. The longest Gd–O bond lengths involves the methoxy-oxygen atoms of the side arm of the vanillin-based ligand (250.6 pm for Gd–O2 and 254.7 pm for Gd–O4,

Table 6.3: Selected bond lengths (pm) and angles ($^{\circ}$) for complex **26**.

Gd–O1	236.3(2)	Gd–O2	250.6(2)
Gd–O3	240.5(2)	Gd–O4	254.7(2)
Gd–O5	245.3(2)	Gd–O6	249.5(2)
Gd–O8	246.4(2)	Gd–O9	253.8(2)
Gd–O11	254.1(2)	Gd–O12	256.6(2)
Cu–O1	196.0(2)	Cu–O3	196.4(2)
Cu–N1	199.9(3)	Cu–N2	197.2(3)
Cu–O1M	235.4(3)	Cu–Gd	353.5(6)
O1–Gd–O2	64.22(7)	O1–Gd–O3	62.39(7)
O1–Gd–O4	124.90(7)	O1–Gd–O5	130.22(8)
O1–Gd–O6	87.50(8)	O1–Gd–O8	148.67(8)
O1–Gd–O9	121.85(7)	O1–Gd–O11	78.94(8)
O1–Gd–O12	72.92(8)	O2–Gd–O4	148.91(7)
O2–Gd–O9	68.35(7)	O2–Gd–O11	122.76(8)
O2–Gd–O12	77.24(7)	O3–Gd–O2	121.74(7)
O3–Gd–O4	63.28(7)	O3–Gd–O5	121.17(8)
O3–Gd–O6	77.24(8)	O3–Gd–O8	118.06(8)
O3–Gd–O9	166.90(7)	O3–Gd–O11	66.62(8)
O3–Gd–O12	107.05(7)	O4–Gd–O12	132.92(7)
O5–Gd–O2	79.13(8)	O5–Gd–O4	73.86(8)
O6–Gd–O2	78.89(8)	O6–Gd–O4	72.42(8)
O8–Gd–O2	119.48(7)	O8–Gd–O4	69.83(8)
O9–Gd–O4	113.15(7)	O11–Gd–O4	88.02(8)
O1–Cu–O3	78.03(9)	O1–Cu–N1	90.90(10)
O1–Cu–N2	168.61(10)	O1–Cu–O1M	98.35(9)
O3–Cu–N1	165.48(10)	O3–Cu–N2	92.74(10)
O3–Cu–O1M	96.71(9)	N1–Cu–O1M	94.16(10)
N2–Cu–N1	97.01(11)	N2–Cu–O1M	89.27(10)

respectively), while the Gd–O bond distances formed with the bridging phenoxy oxygen atoms are shorter and fall in the 236.3–240.5 pm range. The O1–Cu–O3 is around 78.0° and the O1–Gd–O3 angle of around 62.4° with the dihedral angle (c) between these two halves of around 14.5°. This dihedral angle is around 2° smaller than in similar reported complex,³²⁵ therefore a very small difference in the ferromagnetic coupling between Cu^{II}–Gd^{III} is to be expected. This is due to an established and well verified rule according with, a decrease of the above mentioned dihedral angle leads to an increase of the magnetic interaction between the Cu^{II} and Ln^{III} metal centers.^{334,338}

$$|J| = 11.5 \exp(-0.054 c) \quad (10)$$

The magnetic properties of rare-earth metals are dominated by the internal nature of the f-orbitals that rise a strong orbital angular momentum and spin-orbit coupling. In addition lanthanide ions present high magnetic anisotropy and therefore the interpretation of the magnetic behavior is more complicated compared to d-block metals.^{10,321,338,339} The ground state of Gd^{III} is ⁸S_{7/2} and the lowest excited energy level is very high. Thus, the contribution of the orbital angular momentum and the anisotropic effect do not need to be taken into consideration when the properties of its complexes are discussed on the basis of electronic configuration. This is the reason why gadolinium complexes are better studied compared to other lanthanide-containing compounds. From the magnetic point of view the magnetic data of gadolinium-containing complexes can be interpreted using the isotropic Heissenberg Hamiltonian. The magnetic behavior of Cu^{II}–Gd^{III} complex (26) described here is depicted in Figure 6.6 in form of thermal variation of χ_M and $\chi_M T$ product, where χ_M represents the molar susceptibility corrected for diamagnetism. At 300 K, the $\chi_M T$ product is 8.98 cm³mol⁻¹K which is very close to a calculated value of 8.25 cm³mol⁻¹K for uncoupled Cu^{II} and Gd^{III} ions. On lowering the temperature the $\chi_M T$ values increase, reaching a maximum of 10.67 cm³mol⁻¹K at 7 K. This last value roughly corresponds to a calculated one (10.00 cm³mol⁻¹K) for S = 4 spin ground state which results from ferromagnetic coupling of Cu^{II} (S = 1/2) and Gd^{III} (S = 7/2), assuming $g_{Gd} = g_{Cu} = 2$.

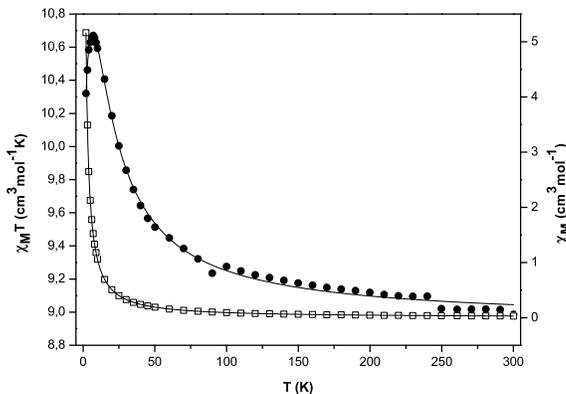


Figure 6.6: Plot of thermal dependence of χ_M (empty squares) and $\chi_M T$ product (black filled circles) for $[\text{Cu}(\text{MeOH})(\text{OMesalen})\text{Gd}(\text{NO}_3)_3]$ (**26**) measured with an applied magnetic field of 2000 Oe; the solid lines represent the theoretical curves (see text).

A quantitative analysis of the experimental data has been performed on the basis of spin-only Hamiltonian:^{10,321}

$$\hat{H} = -J_{\text{CuGd}} S_{\text{Cu}} S_{\text{Gd}}$$

Taking into consideration the g values associated to the low lying levels³⁰¹ $E(4) = 0$

$$g_4 = \frac{7g_{\text{Gd}} + g_{\text{Cu}}}{8}$$

and $E(3) = 4J$

$$g_3 = \frac{9g_{\text{Gd}} - g_{\text{Cu}}}{8}$$

the following expression was obtained:

$$\chi_M T = \frac{N\beta^2 T}{3k(T - \theta)} \frac{180g_4^2 + 84g_3^2 \exp(-4J/kT)}{9 + 7\exp(-4J/kT)} \quad (11)$$

The best fit of the magnetic data lead to $J_{\text{CuGd}} = 5.27 \pm 0.12 \text{ cm}^{-1}$ for $g_4 = 2.08 \pm 0.002$ and $g_3 = 2.06 \pm 0.0005$ which correspond to a $g_{\text{Gd}} \simeq 2.07$ and $g_{\text{Cu}} \simeq 2.12$. The reliability factor $R^2 = 0.9983$ for $\theta = -0.11 \pm 0.008 \text{ K}$ shows a good agreement between calculated and experimental data sets. The negative Weiss constant θ counts for weak antiferromagnetic exchange interaction that occurs between neighboring molecules at very low

temperature and it is illustrated by the decrease of $\chi_M T$ values below 7 K. The coupling constant between Cu^{II}-Gd^{III} centers of around 5.27 cm⁻¹ is only a little bit higher than reported 4.8 cm⁻¹ found in the similar reported heterodinuclear Cu^{II}-Gd^{III} complex.³²⁵ This is in agreement with observed small difference for the dihedral angle formed between O1-Cu-O3 and O1-Gd-O3 planes which led according to empirical equation beforehand mentioned to $J_{CuGd} = 5.25$ cm⁻¹. It is worth mentioning that the steric effect induced by the two methyl groups of the used diamine-spacer led to a larger dihedral angle between the two halves (namely O1-Cu-O3 and O1-Gd-O3 angles) which plays a very important role in transmitting the magnetic interaction between the metal centers. In agreement with this argument are the reported higher coupling constant values determined in non-substituted diamine spacers of compartmental Schiff base ligands. In instance, the heterodinuclear Cu-Gd complex formed with Schiff base ligands derived from o-vanillin and 1,3-diamino propane display a coupling constant of around 8.63 cm⁻¹.³³² Therefore, the following results described in this chapter will be focused on non-methyl derivatives of the diamine spacer involved in formation of the compartmental Schiff base ligands. The ferromagnetic interaction between Cu^{II}-Gd^{III} centers in complex **26** was also confirmed by field dependence magnetization measurements performed at 2 K. The experimental data set is fitting well the Brillouin equation for and ground state $S = 4.07 \pm 0.007$ with a reliability factor $R^2 = 0.99935$ assuming $g_{av} = 2.00$ (Figure 6.7).

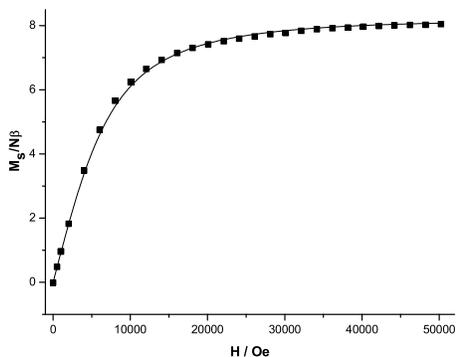


Figure 6.7: Plot of the field dependence of the magnetization for complex (**26**) measured at 2 K (black filled squares represent the experimental value; the solid line shows the theoretical curve generated using the Brillouin equation).

6.1 1-D chains based on copper-lanthanide topology

The last decade of chemistry research has witnessed a great interest of the scientific community towards design of coordination polymers that contain transition metals in the main chain.^{153,340,341} This is due to the observed application of such architectures in organic synthesis where these polymers possess high catalytic activity due to possible recycling of the catalysts and in addition easy separation of the reaction components.^{121,342,343} Moreover, coordination polymers have been reported to possess chemical sensor functions,^{121,344} fluorescence^{345,346} and/or to function as magnetic materials.^{16,347,348} Among the variety of bridging units, cyanate,^{112,349–359} thiocyanate,³⁶⁰ dicyanamide,^{332,361} oximate,^{348,362} amidato³²⁸ oxamato^{227,363} and diverse carboxylic acids^{174,346,364–385} have been received particular attention. From the magnetic properties point of view, these materials are expected to function as good transmitters of the magnetic interaction between the constituent oligomers of the polymeric structure. More recently, particular attention has been devoted to heterometallic polymeric structures that contain d-f topologies which are expected to possess interesting magnetic properties and therefore their possible use as nanometer scale magnets. New class of single molecular SMM^{318,386–390,390–394} or SMC¹⁶ magnets have been prepared using lanthanide ions alone and as d-f association. The lanthanide chemistry based on dysprosium and terbium complexes provided d-f clusters which have fairly large ground state values as well as slow relaxation of magnetization in relation with significant magnetic anisotropy. These are two compulsory properties of single molecular magnets which are associated with ferromagnetic coupling exchange of the paramagnetic centers. In instance, discrete Cu^{II}-Tb^{III} complex based on compartmental-Schiff base ligand has been recently reported as single molecular magnet behavior with the blocking temperature of the slow time relaxation of the magnetization in the very low temperature range.³¹⁸ It is worth mentioning here that single molecular magnets (SMM) discovered firstly in 1993²⁴ and well magnetically documented later by Sessoli *et al.*^{395,396} showed a slow relaxation time of magnetization and hysteresis effect. This compound formed by acetate- and oxo-bridged Mn₁₂ core possesses a ground state $S = 10$ and high anisotropy barrier between the degenerate $\pm M_s$ energy levels. The topic has an academic fundament that will permit to fully understand the mag-

netic interaction between paramagnetic centers and, in addition immediate application as storage of magnetic information at molecular scale. Oligodinuclear 3d-4f complexes are particularly attractive as building blocks^{332,336,349,360} in constructing extended architectures, especially when gadolinium to dysprosium ions are part of the assemblies. These heterometallic units exhibit ferromagnetic intermetallic coupling and therefore the resulting polymeric architectures are expecting to show interesting magnetic properties. The selection of bridging functionalities able to mediate the magnetic interaction between the constituent entities is an opened and challenging topic. A judicious choice of the bridging linkers allows in principle the synthesis of predetermined coordination compounds through recognition of donor atoms by metal ions. For example, both copper and lanthanide centers in complexes of type $[\text{Cu}(\text{MeOH})(\text{OMesalen})\text{Gd}(\text{NO}_3)_3]$ (**26**) (see Figure 6.5) present labile coordination sites. Firstly, the copper ion has a square pyramidal geometry with an apical coordinated solvent molecule that can be easily replaced by an appropriate linker. Such linker, i.e. 4,4'-dipyridine will allow building of extended structures without alteration of the lanthanide coordination environment.³⁴⁹ Secondly, the bidentate nitrate ligands of the lanthanide ion (Figure 6.5) can also be substituted by oxygen and/or nitrogen bearing organic linkers and a limited number of 1-D structures have been reported.^{332,333,336,349,350,360} The purpose of these polymeric architectures is to scrutinize the effectivity of ligand systems for the extend of interchain communication between the oligomeric units and possibly to enhance the magnetic exchange interaction between the constituent paramagnetic ions along the chain architecture. The recognition of donor atoms by metal ions represent a potential approach to synthesize coordination polymers with dissimilar ions. It is well known that lanthanide ions bind preferentially to hard oxygen-donor atoms, whereas the copper ion prefers more soft donor atoms. To combine lanthanide and copper atoms in polymeric architectures, polydentate 2,3-pyrazine dicarboxylic acid has been used as bridging linker of the oligomeric $\text{Cu}^{\text{II}}\text{-Ln}^{\text{III}}$ units. This type of linker posses a mixed N- O- constituency that allows various modes of coordination through the pyrazine-ring and also through the two carboxylate functionalities.^{373,381,397} The -COOH functional group can accommodate metal ions in η^1 -, η^2 -fashion and therefore can connect metal centers in different directions, whereas the pyrazine nitrogen atoms will impose a rigidity of the resulting coordination

architecture. Using the "in situ" approach synthesis, one-dimensional Cu^{II}-Ln^{III} chains have been isolated. The Cu-salen precursor - [Cu(OMesalen)H₂O] (**24**) (Figure 6.2) reacts stoichiometrically with Ln(NO₃)₃·6H₂O salts, followed by addition of equimolecular amount of 2,3-pyrazine dicarboxylic acid to form 1-D polymers in which the dinuclear Cu^{II}-Ln^{III} units are linked by the pyrazine 2,3-dicarboxylic polydentate bridge. Following this strategy 1-D chains containing lanthanides from La to Tb has been isolated, with the exception of Ce- and Nd-containing ions. The molecular structures of this series of compounds are shown in Figure 6.9 to Figure 6.14. From crystallographical point of view the molecular structure determination show isostructural constituency with very small differences in bond length distances (Table 6.4 to Table 6.9) according to small variation in the ion radius in the lanthanide series and namely, it decrease from La to Ho with around 1 % for each lanthanide atom. Although structurally there is no difference between the 1-D [LCuLn] chains which will be described herein, the magnetic behavior differs very much within lanthanide-containing compounds. Kahn *et al.*^{323,339} and Costes *et al.*³³⁸ reported that for f¹ to f⁶ electronic configurations, an antiferromagnetic interaction is to be expected, whereas from f⁷ to f¹⁰ electronic configuration a ferromagnetic exchange interaction takes place between 3d-4f paramagnetic centers. Nevertheless, the type of magnetic exchange coupling is very much influenced by the environment of the d and f ions and therefore magnetic measurements will be discussed for the whole series of [Cu(OMesalen)Ln(NO₃)(Pyr(COO)₂)]_n·(DMF)_n compounds.

The molecular structure determination will be discussed for copper-gadolinium compound (**27**). The first 1-D chain of this type is depicted in Figure 6.9 and consist of Cu^{II}-Gd^{III} bridged entities (Figure 6.8). The asymmetric entity is formed by Cu(II)-Gd(III) dinuclear entity with the copper(II) ion preserving the O₂N₂ inner coordination compartment of the compartmental N,N'-bis(3-methoxysalicylidene)-1,3-diamino propane ligand and gadolinium ion coordinated in the O₂O₂ outer cavity of the *salen-type* ligand (two oxygen atoms from phenol groups and two other oxygen atoms from the methoxy groups). The copper-ion preserves the square-pyramidal geometry with a deviation from the N₂O₂ ligand plane of around 14.2 pm, below the plane. The CuO₂Gd segment is not planar and the dihedral angle between O1-Cu-O3 and O1-Gd-O3 is around 20° with the Gd ion out of O₄-ligand plane by around 61.0 pm on the same side with the Cu(II) ion.

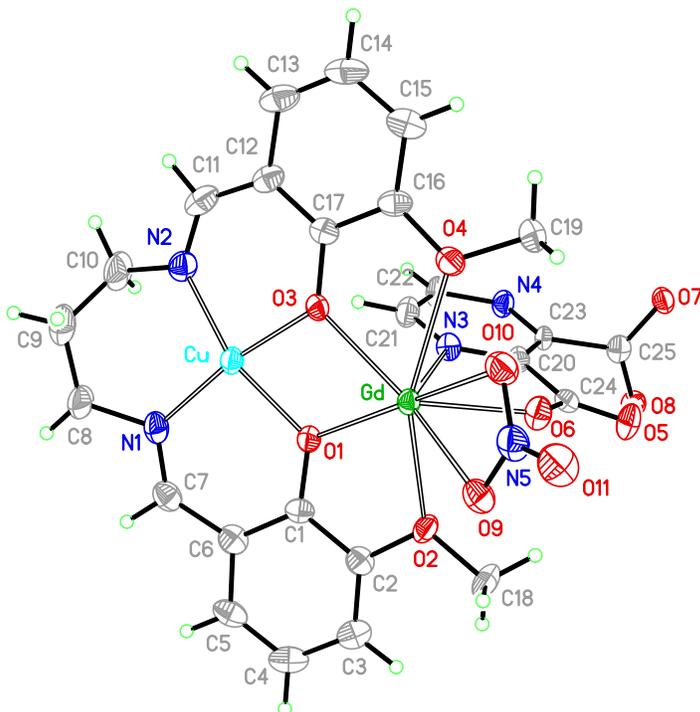


Figure 6.8: Asymmetric structural unit and numbering scheme atoms for $[\text{Cu}(\text{OMesalen})\text{Gd}(\text{NO}_3)(\text{Pyr}(\text{COO})_2)]_n$ 1-D complex **27**.

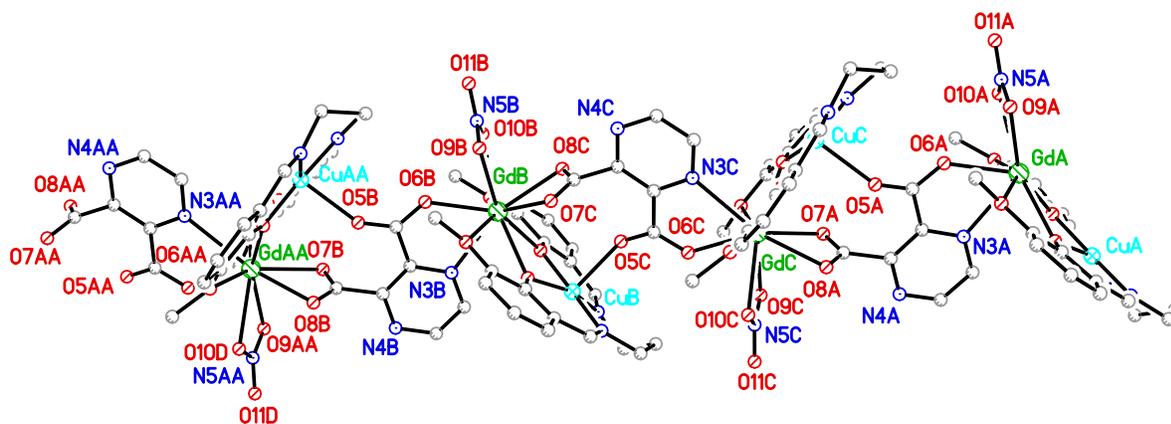


Figure 6.9: One-dimensional polymer structure of complex **27** with the pyrazine 2,3-dicarboxylic acid as bridging ligand between two heterobimetallic entities.

The 2,3-pyrazine dicarboxylic acid bridges two different $[\text{Cu}(\text{OMesalen})\text{Gd}(\text{NO}_3)]$ entities coordinating through one nitrogen atom and a η^2 -carboxylate to one Gd atom, whereas the other carboxylic moieties bridges in a μ_2 -fashion the copper and gadolinium atoms of two different $[\text{Cu}(\text{OMesalen})\text{Gd}(\text{NO}_3)]$ units. This coordination mode lead to a five coordinated copper center with an apical carboxylate oxygen atom and a 10-

coordinated gadolinium ion with the η^2 -nitrate ligand completing the above mentioned coordination environment of the lanthanide ion. The μ_2 -bridged carboxylate functionality of the linker coordinates the lanthanide ion with a Gd–O6 bond distance of around 234 pm of one dinuclear entity and it also occupies the apical position of the square pyramidal geometry of the Cu atom from a neighboring unit with a Cu–O5 bond distance of 229 pm. Selected bond lengths and angles in compound **26** are listed in Table 6.4. The two carboxylate and the nitrate ligand compensate also the 3+ charge of the gadolinium ion yielding a neutral 1-D chain. The Cu–Gd separation within the constructing units of the chain is around 353.2 pm. The bis-chelating linker binds gadolinium atom within 234-246 pm range for Gd–O bond lengths and around 273 pm for Gd–N3 bond distance with a Gd–Gd interchain separation of around 830.7 pm. So, each dicarboxylate functionality of the bridging ligand functions as bidentate anion and coordinates simultaneously to three metal centers: one copper and two gadolinium ions leading to a zigzag alternation along the chain of the [Cu(OMesalen)Gd(NO₃)] units. The interchain distances between the copper atom and two Gd ions bridged by the dianionic linker are slightly different and alternates between 637.3 pm for μ_1 -carboxy-bridged Cu–Gd segment and around 1043.27 for non-bridged Cu–Gd fragments along the polymeric chain. This 1-D chain results from alternating pairs of Cu–Gd and Gd–Gd interactions through the pyrazine 2,3-dicarboxylic acid, yielding an infinite zigzag chain. The compound crystallize with DMF molecules as solvent of crystallization and the resulting polymer can be formulated as [Cu(OMesalen)Gd(NO₃)₃(Pyr(COO)₂)]_n·(DMF)_n.

Similar structural 1-D zigzag chain have been observed in [Cu(OMesalen)Dy(NO₃)(Pyr(COO)₂)]_n·(DMF)_n (**28**) (Figure 6.10) and [Cu(OMesalen)Tb(NO₃)(Pyr(COO)₂)]_n·(DMF)_n (**29**) (Figure 6.11) for $f^{>7}$ and [Cu(OMesalen)Eu(NO₃)(Pyr(COO)₂)]_n·(DMF)_n (**30**), [Cu(OMesalen)Sm(NO₃)(Pyr(COO)₂)]_n·(DMF)_n (**31**) and [Cu(OMesalen)Pr(NO₃)(Pyr(COO)₂)]_n·(DMF)_n (**32**) (Figure 6.12 to Figure 6.14) for $f^{<7}$ lanthanide electronic configurations. It has to be emphasize that only small changes occur in the ionic radius of Ln(III) on going from La(III) to Lu(III). This fact means that the lanthanide-to-donor atoms bond distances are regulated by the [Cu(OMesalen)] core. In accordance with this the Cu–Ln and Ln–Ln interchain separation show no distinct change within lanthanide ions. Selected bond lengths and angles in these complexes [Cu(OMesalen)Ln(NO₃)

Table 6.4: Selected bond lengths (pm) and angles ($^{\circ}$) for complex **27**.

Gd–O1	243.7(4)	Gd–O2	255.2(4)
Gd–O3	238.2(4)	Gd–O4	251.0(4)
Gd–O6	234.1(4)	Gd–O7	249.9(4)
Gd–O8	246.9(4)	Gd–O9	253.1(4)
Gd–O10	263.1(4)	Gd–N3	273.3(5)
Cu–O1	195.6(4)	Cu–O3	196.1(4)
Cu–N1	199.1(5)	Cu–N2	196.1(5)
Cu–O5	229.3(4)	Gd–Cu	353.15(8)
O1–Gd–O2	63.28(13)	O1–Gd–O3	61.79(13)
O1–Gd–O4	121.94(13)	O1–Gd–O7	67.37(13)
O1–Gd–O9	125.00(13)	O1–Gd–O10	166.66(14)
O1–Gd–N3	74.28(14)	O2–Gd–O10	119.14(13)
O2–Gd–N3	82.65(14)	O3–Gd–O2	123.51(13)
O3–Gd–O4	63.76(13)	O3–Gd–O7	98.54(13)
O3–Gd–O8	78.29(13)	O3–Gd–O9	154.82(14)
O3–Gd–O10	117.35(13)	O3–Gd–N3	71.14(14)
O4–Gd–O9	112.80(13)	O4–Gd–N3	70.62(14)
O6–Gd–O1	120.41(14)	O6–Gd–O2	72.04(14)
O6–Gd–O3	128.57(14)	O6–Gd–O4	80.54(14)
O6–Gd–O9	71.80(14)	O6–Gd–O10	71.30(14)
O6–Gd–N3	62.40(14)	O8–Gd–O7	52.85(13)
O9–Gd–O2	73.54(13)	O9–Gd–O10	49.60(13)
O9–Gd–N3	132.99(14)	O10–Gd–N3	118.66(14)
O1–Cu–O3	78.38(16)	O1–Cu–O5	100.25(16)
O1–Cu–N1	92.98(19)	O3–Cu–O5	89.87(16)
O3–Cu–N1	170.78(19)	N1–Cu–O5	88.49(18)
N2–Cu–O1	159.0(2)	N2–Cu–O3	92.0(2)
N2–Cu–O5	98.4(2)	N2–Cu–N1	97.3(2)

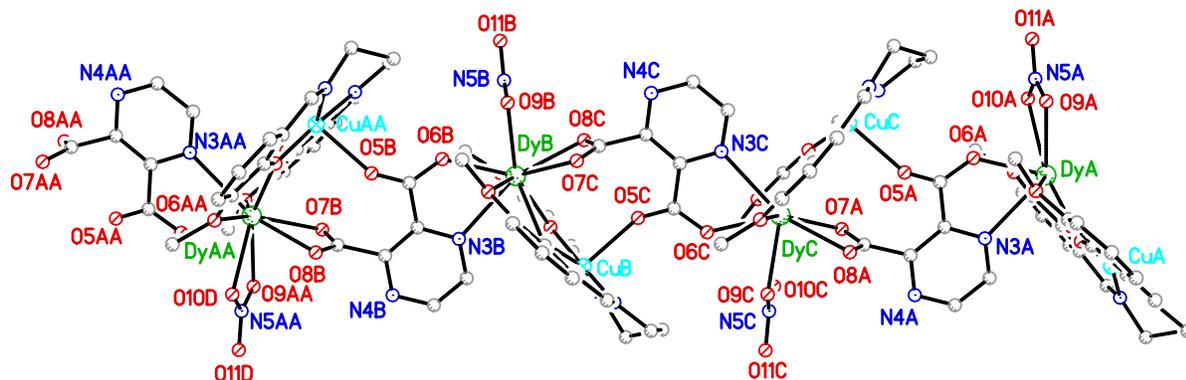


Figure 6.10: One-dimensional polymer structure of complex $[\text{Cu}(\text{OMesalen})\text{Dy}(\text{NO}_3)(\text{Pyr}(\text{COO})_2)]_n \cdot (\text{DMF})_n$ (**28**) with the pyrazin 2,3-dicarboxylic acid as bridging ligand between two heterobimetallic entities.

$(\text{Pyr}(\text{COO})_2)]_n \cdot (\text{DMF})_n$ (Ln is the lanthanide ion in general) are given in Table 6.5 to Table 6.9.

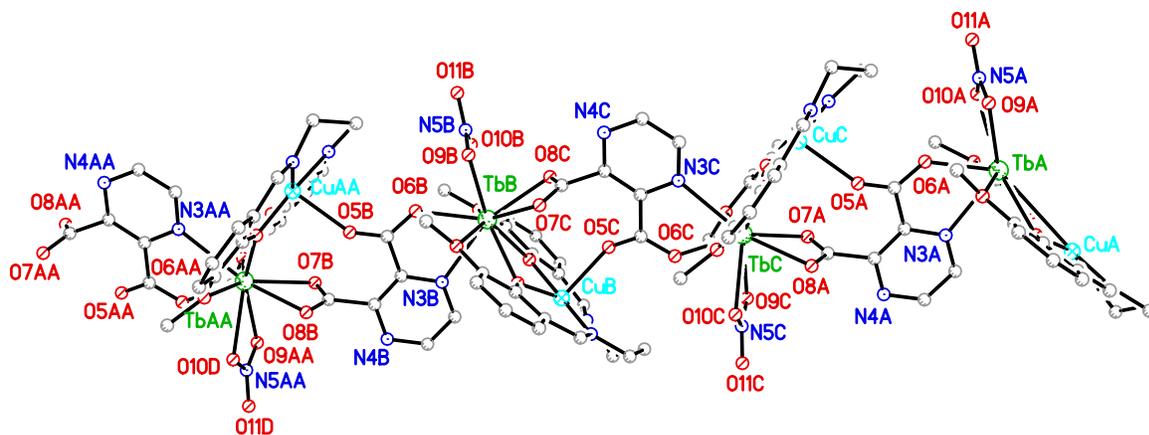


Figure 6.11: One-dimensional polymer structure of $[\text{Cu}(\text{OMesalen})\text{Tb}(\text{NO}_3)(\text{Pyr}(\text{COO})_2)]_n \cdot (\text{DMF})_n$ complex (**29**) with the pyrazin 2,3-dicarboxylic acid as bridging ligand between two heterobimetallic entities.

Table 6.5: Selected bond lengths (pm) and angles ($^{\circ}$) for complex **28**.

Dy–O1	241.3(3)	Dy–O2	253.2(3)
Dy–O3	236.5(3)	Dy–O4	249.6(3)
Dy–O6	231.3(4)	Dy–O7	247.2(3)
Dy–O8	244.9(3)	Dy–O9	250.3(3)
Dy–O10	262.6(3)	Dy–N3	269.8(4)
Cu–O1	196.0(3)	Cu–O3	195.3(6)
Cu–N1	197.7(4)	Cu–N2	196.1(4)
Cu–O5	229.8(3)	Dy–Cu	351.35(6)
O1–Dy–O2	63.35(10)	O1–Dy–O3	62.05(10)
O1–Dy–O4	122.41(10)	O1–Dy–O7	67.35(10)
O1–Dy–O9	125.05(11)	O1–Dy–O10	166.78(11)
O1–Dy–N3	73.87(10)	O2–Dy–O10	119.10(10)
O2–Dy–N3	82.58(11)	O3–Dy–O2	123.92(10)
O3–Dy–O4	64.23(10)	O3–Dy–O7	98.31(10)
O3–Dy–O8	77.72(10)	O3–Dy–O9	154.20(11)
O3–Dy–O10	116.97(11)	O3–Dy–N3	71.28(11)
O4–Dy–O2	147.99(11)	O4–Dy–N3	70.82(11)
O6–Dy–O1	120.54(11)	O6–Dy–O2	72.05(11)
O6–Dy–O3	128.92(11)	O6–Dy–O4	79.98(11)
O6–Dy–O9	71.83(11)	O6–Dy–O10	71.08(11)
O6–Dy–N3	62.89(11)	O8–Dy–O7	53.29(10)
O9–Dy–O2	73.63(11)	O9–Dy–O10	49.59(11)
O9–Dy–N3	133.46(11)	O10–Dy–N3	118.93(11)
O1–Cu–O3	78.02(12)	O1–Cu–O5	101.05(13)
O1–Cu–N1	93.47(15)	O3–Cu–O5	90.13(13)
O3–Cu–N1	170.67(15)	N1–Cu–O5	87.75(15)
N2–Cu–O1	158.69(15)	N2–Cu–O3	92.03(15)
N2–Cu–O5	97.74(15)	N2–Cu–N1	97.25(17)

Table 6.6: Selected bond lengths (pm) and angles ($^{\circ}$) for complex **29**.

Tb-O1	241.7(4)	Tb-O2	254.1(4)
Tb-O3	237.0(3)	Tb-O4	250.4(4)
Tb-O6	232.1(3)	Tb-O7	248.4(4)
Tb-O8	245.4(4)	Tb-O9	251.4(4)
Tb-O10	261.7(4)	Tb-N3	271.3(4)
Cu-O1	195.7(3)	Cu-O3	195.3(4)
Cu-N1	197.8(5)	Cu-N2	196.0(4)
Cu-O5	230.1(4)	Gd-Cu	353.15(8)
O1-Tb-O2	63.31(11)	O1-Tb-O3	61.83(12)
O1-Tb-O4	121.98(11)	O1-Tb-O7	67.21(12)
O1-Tb-O9	125.05(12)	O1-Tb-O10	166.74(12)
O1-Tb-N3	74.10(12)	O2-Tb-O10	119.14(12)
O2-Tb-N3	82.78(12)	O3-Tb-O2	123.65(12)
O3-Tb-O4	63.94(12)	O3-Tb-O7	98.19(11)
O3-Tb-O8	77.79(12)	O3-Tb-O9	154.50(12)
O3-Tb-O10	117.20(12)	O3-Tb-N3	71.14(12)
O4-Tb-O9	112.72(13)	O4-Tb-N3	70.46(13)
O6-Tb-O1	120.64(13)	O6-Tb-O2	72.39(13)
O6-Tb-O3	128.59(12)	O6-Tb-O4	79.97(13)
O6-Tb-O9	71.96(12)	O6-Tb-O10	71.05(12)
O6-Tb-N3	62.62(12)	O8-Tb-O7	52.96(12)
O9-Tb-O2	73.58(12)	O9-Tb-O10	49.62(12)
O9-Tb-N3	133.32(12)	O10-Tb-N3	118.74(12)
O1-Cu-O3	77.94(14)	O1-Cu-O5	100.81(14)
O1-Cu-N1	93.45(17)	O3-Cu-O5	90.18(14)
O3-Cu-N1	170.63(16)	N1-Cu-O5	87.81(17)
N2-Cu-O1	158.72(17)	N2-Cu-O3	91.93(18)
N2-Cu-O5	97.86(17)	N2-Cu-N1	97.4(2)

Table 6.7: Selected bond lengths (pm) and angles ($^{\circ}$) for complex **30**.

Eu–O1	244.9(4)	Eu–O2	257.0(4)
Eu–O3	240.0(4)	Eu–O4	252.2(4)
Eu–O6	236.0(4)	Eu–O7	250.6(4)
Eu–O8	249.2(4)	Eu–O9	254.1(4)
Eu–O10	263.3(4)	Eu–N3	273.4(4)
Cu–O1	196.7(4)	Cu–O3	196.5(4)
Cu–N1	199.0(5)	Cu–N2	196.2(5)
Cu–O5	229.7(4)	Eu–Cu	354.43(0)
O1–Eu–O2	62.71(12)	O1–Eu–O3	61.91(12)
O1–Eu–O4	121.88(12)	O1–Eu–O7	67.33(12)
O1–Eu–O9	124.89(12)	O1–Eu–O10	166.63(12)
O1–Eu–N3	74.42(13)	O2–Eu–O10	119.44(12)
O2–Eu–N3	82.61(13)	O3–Eu–O2	123.05(12)
O3–Eu–O4	63.56(12)	O3–Eu–O7	98.59(12)
O3–Eu–O8	78.47(13)	O3–Eu–O9	155.16(13)
O3–Eu–O10	117.52(13)	O3–Eu–N3	71.05(13)
O4–Eu–O9	112.99(13)	O4–Eu–N3	70.46(13)
O6–Eu–O1	120.35(13)	O6–Eu–O2	72.39(14)
O6–Eu–O3	128.46(13)	O6–Eu–O4	80.64(14)
O6–Eu–O9	71.59(13)	O6–Eu–O10	71.27(13)
O6–Eu–N3	62.33(13)	O8–Eu–O7	52.66(12)
O9–Eu–O2	73.77(12)	O9–Eu–O10	49.52(13)
O9–Eu–N3	132.72(13)	O10–Eu–N3	118.62(13)
O1–Cu–O3	78.77(15)	O1–Cu–O5	100.18(15)
O1–Cu–N1	93.01(17)	O3–Cu–O5	89.68(15)
O3–Cu–N1	170.99(17)	N1–Cu–O5	88.15(18)
N2–Cu–O1	158.76(19)	N2–Cu–O3	91.72(19)
N2–Cu–O5	98.70(19)	N2–Cu–N1	97.3(2)

Table 6.8: Selected bond lengths (pm) and angles ($^{\circ}$) for complex **31**.

Sm–O1	249.1(3)	Sm–O2	259.5(4)
Sm–O3	244.8(3)	Sm–O4	255.8(3)
Sm–O6	241.4(3)	Sm–O7	254.5(3)
Sm–O8	253.7(3)	Sm–O9	259.6(4)
Sm–O10	265.6(4)	Sm–N3	280.2(4)
Cu–O1	197.2(3)	Cu–O3	196.9(3)
Cu–N1	198.7(5)	Cu–N2	196.9(4)
Cu–O5	230.1(4)	Eu–Cu	354.43(0)
O1–Sm–O2	61.81(11)	O1–Sm–O3	61.11(11)
O1–Sm–O4	120.75(11)	O1–Sm–O7	67.85(11)
O1–Sm–O9	125.51(11)	O1–Sm–O10	166.83(11)
O1–Sm–N3	74.65(11)	O2–Sm–O10	119.91(11)
O2–Sm–N3	82.29(11)	O3–Sm–O2	121.24(11)
O3–Sm–O4	62.76(11)	O3–Sm–O7	98.95(11)
O3–Sm–O8	79.75(11)	O3–Sm–O9	156.03(12)
O3–Sm–O10	118.85(11)	O3–Sm–N3	70.66(11)
O4–Sm–O9	113.43(12)	O4–Sm–N3	70.51(12)
O6–Sm–O1	119.48(12)	O6–Sm–O2	72.90(12)
O6–Sm–O3	127.20(12)	O6–Sm–O4	81.70(13)
O6–Sm–O9	72.33(12)	O6–Sm–O10	71.85(12)
O6–Sm–N3	60.88(11)	O8–Sm–O7	51.70(11)
O9–Sm–O2	74.95(12)	O9–Sm–O10	48.66(12)
O9–Sm–N3	132.19(12)	O10–Sm–N3	118.28(11)
O1–Cu–O3	79.18(13)	O1–Cu–O5	98.74(14)
O1–Cu–N1	93.06(16)	O3–Cu–O5	89.29(14)
O3–Cu–N1	171.59(16)	N1–Cu–O5	88.70(16)
N2–Cu–O1	159.15(17)	N2–Cu–O3	91.76(17)
N2–Cu–O5	99.90(17)	N2–Cu–N1	96.63(19)

Table 6.9: Selected bond lengths (pm) and angles ($^{\circ}$) for complex **32**.

Pr–O1	249.5(2)	Pr–O2	259.9(2)
Pr–O3	244.8(3)	Pr–O4	257.7(2)
Pr–O6	241.1(2)	Pr–O7	254.9(2)
Pr–O8	253.3(2)	Pr–O9	259.3(2)
Pr–O10	265.7(2)	Pr–N3	280.1(3)
Cu–O1	196.7(2)	Cu–O3	196.9(2)
Cu–N1	199.1(3)	Cu–N2	196.3(3)
Cu–O5	229.4(2)	Pr–Cu	358.62(4)
O1–Pr–O2	61.93(7)	O1–Pr–O3	61.02(7)
O1–Pr–O4	120.71(7)	O1–Pr–O7	67.93(7)
O1–Pr–O9	125.56(7)	O1–Pr–O10	166.53(8)
O1–Pr–N3	74.77(7)	O2–Pr–O10	120.01(7)
O2–Pr–N3	82.32(8)	O3–Pr–O2	121.22(7)
O3–Pr–O4	62.75(7)	O3–Pr–O7	99.20(7)
O3–Pr–O8	79.84(7)	O3–Pr–O9	156.15(8)
O3–Pr–O10	118.76(8)	O3–Pr–N3	70.55(7)
O4–Pr–O9	113.42(8)	O4–Pr–N3	70.42(8)
O6–Pr–O1	119.67(8)	O6–Pr–O2	72.89(8)
O6–Pr–O3	127.19(8)	O6–Pr–O4	81.68(8)
O6–Pr–O9	72.20(8)	O6–Pr–O10	72.00(8)
O6–Pr–N3	60.96(8)	O8–Pr–O7	51.82(7)
O9–Pr–O2	74.94(7)	O9–Pr–O10	48.67(8)
O9–Pr–N3	132.15(8)	O10–Pr–N3	118.41(8)
O1–Cu–O3	79.27(9)	O1–Cu–O5	98.55(9)
O1–Cu–N1	92.82(11)	O3–Cu–O5	89.46(9)
O3–Cu–N1	171.53(10)	N1–Cu–O5	88.74(11)
N2–Cu–O1	159.24(11)	N2–Cu–O3	91.46(11)
N2–Cu–O5	99.91(11)	N2–Cu–N1	97.00(12)

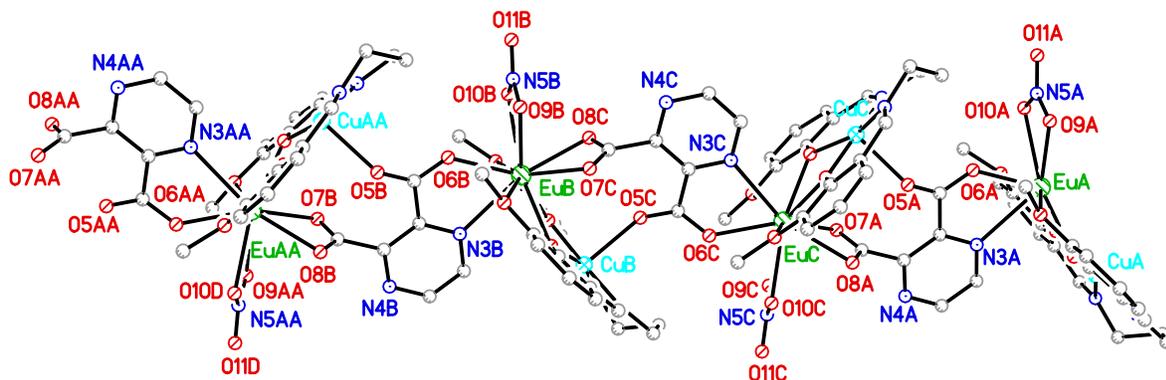


Figure 6.12: One-dimensional polymer structure of complex $[\text{Cu}(\text{OMesalen})\text{Eu}(\text{NO}_3)(\text{Pyr}(\text{COO})_2)]_n \cdot (\text{DMF})_n$ (**30**) with the pyrazine 2,3-dicarboxylic acid as bridging ligand between two heterobimetallic entities.

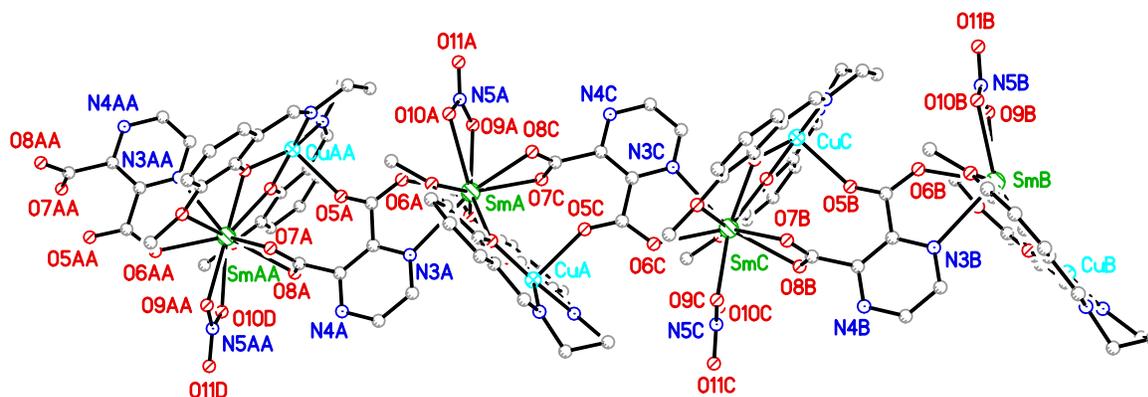


Figure 6.13: One-dimensional polymer structure of complex $[\text{Cu}(\text{OMesalen})\text{Sm}(\text{NO}_3)(\text{Pyr}(\text{COO})_2)]_n \cdot (\text{DMF})_n$ (**31**) with the pyrazine 2,3-dicarboxylic acid as bridging ligand between two heterobimetallic entities.

The similar lanthanum-containing 1-D chain has been spectroscopically characterized and by analogy with the crystallographically characterized lanthanide-containing complexes its formulation is $[\text{Cu}(\text{OMesalen})\text{La}(\text{NO}_3)(\text{Pyr}(\text{COO})_2)]_n \cdot (\text{DMF})_n$ (**33**). The coordination modes of the supporting compartmental *salen-type* ligand and of pyrazine 2,3-dicarboxylic acid-bridging ligand as has been described by molecular structure determinations for these $[\text{Cu}(\text{OMesalen})\text{Ln}(\text{NO}_3)(\text{Pyr}(\text{COO})_2)]_n \cdot (\text{DMF})_n$ polymeric chains have been also confirmed by IR spectroscopy. Stretching vibrations characteristic for nitrate bidentate ion has been detected at 1384 cm^{-1} in all series of complexes. In addition pyrazine 2,3-dicarboxylic acid shows strong stretching vibrations at 1750 and 1734 cm^{-1}

$$E(^{2S+1}L_J) = \frac{\lambda}{2}[J(J+1) - L(l+1) - S(S+1)]$$

where λ is the spin-orbit coupling parameter, L is the orbital quantum number and J is the angular momentum calculated as:

$$J = L + S \quad \text{for } n > 7$$

$$J = L - S \quad \text{for } n < 7$$

The free-ion states of the same J arising from different ^{2S+1}L terms may mix through the spin-orbit coupling. The resulting states are split further and mixed by the ligand field such that the spectrum of lying states and the magnetic properties are rather complicated. The energy separation between low lying states and excited states are well separated except for Eu(III) and Sm(III). The excited state 7F_1 is at 350 cm^{-1} from the ground state 2F_0 for Eu(III), whereas for Sm(III) the ground state is $^6H_{5/2}$ with the excited state $^6H_{7/2}$ at around 700 cm^{-1} . For weak energy separation, the first excited state may be thermally populated and when the energy separation is large only the ground state is thermally populated. Taking into account the Zeeman Hamiltonian with:

$$g_J = \frac{3}{2} + \frac{S(S+1) - L(L+1)}{2J(J+1)}$$

the magnetic susceptibility obeys Curie law according to the following equation:

$$\chi_M = \frac{N\beta^2 g_J^2}{3kT} J(J+1) \quad (12)$$

When the excited state is close in energy to the ground state (i.e. Eu(III) and Sm(III) ions) there is a significant temperature-independent contribution (χ') to the magnetic susceptibility found to be:

$$\chi' = \frac{2N\beta^2(g_J - 1)(g_J - 2)}{3\lambda}$$

where λ is the spin-orbit coupling parameter.

Due to this impediment the magnetic behavior will be discussed in detail for $[\text{Cu}(\text{OMesalen})\text{Gd}(\text{NO}_3)(\text{Pyr}(\text{COO})_2)]_n \cdot (\text{DMF})_n$ 1-D chain compound (27) for which the

plot of thermal variation of the χ_M and $\chi_M T$ are depicted in Figure 6.15, where the χ_M is the molar magnetic susceptibility corrected for diamagnetism.

At 300 K, $\chi_M T$ is equal to $8.59 \text{ cm}^3 \text{ mol}^{-1} \text{ K}$, which roughly corresponds with the expected value for the two uncoupled metal ions. Lowering the temperature causes an increase of the $\chi_M T$ value reaching a maximum of $9.82 \text{ cm}^3 \text{ mol}^{-1} \text{ K}$ at 6 K. This last value is very close to $10.00 \text{ cm}^3 \text{ mol}^{-1} \text{ K}$ value, calculated for $S = 4$ spin ground state resulting from ferromagnetic coupling within the same unit of copper(II) ($S = 1/2$) and gadolinium(III) ($S = 7/2$) assuming $g_{Cu} = g_{Gd} = 2$. A quantitative analysis has been performed using the spin-only Hamiltonian:

$$\hat{H} = -J_{CuGd} S_{Cu} S_{Gd}$$

according with equation 11 including an additional term that describes the temperature independent paramagnetism (χ_{TIP}). The best fit of the experimental data leads to a coupling constant $J_{CuGd} = 4.72 \pm 0.04 \text{ cm}^{-1}$ for $g_4 = 1.99 \pm 8.0 \cdot 10^{-4}$ and

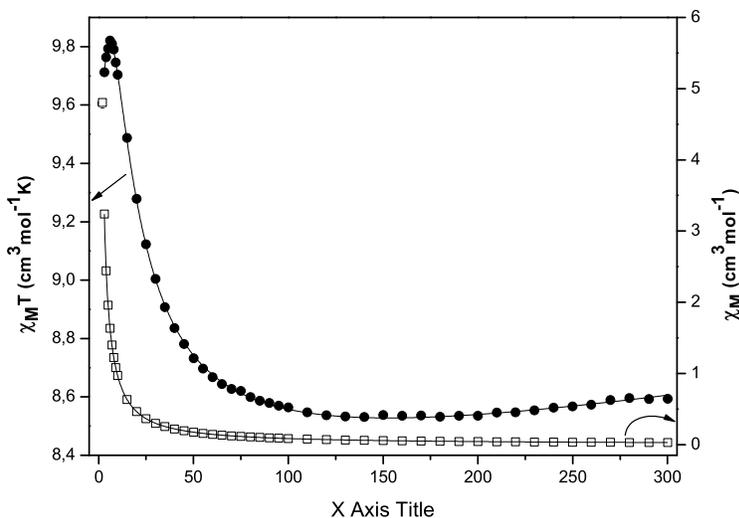


Figure 6.15: Plot of thermal dependence of χ_M (empty squares) and $\chi_M T$ product (black filled circles) for $[\text{Cu}(\text{OMesalen})\text{Gd}(\text{NO}_3)(\text{Pyr}(\text{COO})_2)]_n \cdot (\text{DMF})_n$ (**27**) 1-D chain complex measured with an applied magnetic field of 2000 Oe; solid lines represent the theoretical curve (see text).

$g_3 = 1.97 \pm 0.002$ which correspond to a $g_{Gd} \simeq 1.98$ and $g_{Cu} \simeq 2.03$. The reliability factor $R^2 = 0.9998$ for $\theta = -0.08 \pm 0.003$ K show a good agreement between calculated and experimental data sets. The small negative value for the Weiss constant (θ) describes a very weak antiferromagnetic exchange interaction that occurs between neighboring molecules at very low temperature and it is illustrated by the decrease of $\chi_M T$ value from $9.82 \text{ cm}^3 \text{ mol}^{-1} \text{ K}$ at 6 K to around $9.60 \text{ cm}^3 \text{ mol}^{-1} \text{ K}$ at 2 K. This weak antiferromagnetic interaction occurs most likely between two gadolinium(III) ions of two neighboring $[\text{Cu}(\text{OMesalen})\text{Gd}(\text{NO}_3)]$ entities of the infinite 1-D chain. The Gd–Gd interchain separation of around 830.7 pm is slightly smaller than Cu–Cu interchain separation (938.8 pm). Therefore, the Weiss constant is most likely a consequence of $\text{Gd} \cdots \text{Gd}$ interchain magnetic coupling. This is also in agreement with the magnetic behavior of the corresponding $[\text{Cu}(\text{OMesalen})\text{La}(\text{NO}_3)_3(\text{Pyr}(\text{COO})_2)]_n \cdot (\text{DMF})_n$ (**33**), which has been spectroscopically characterized.

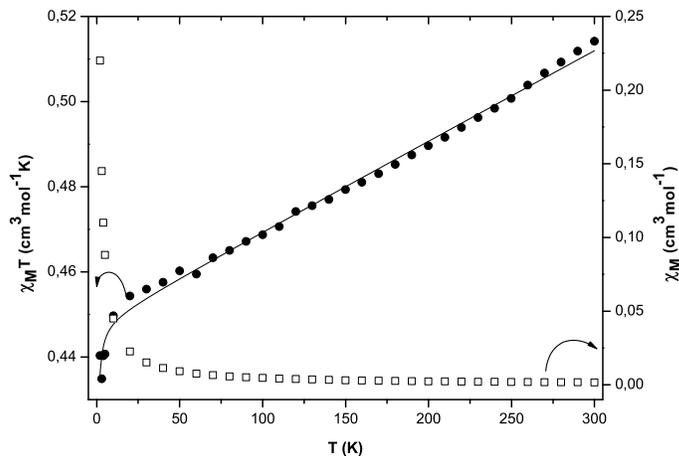


Figure 6.16: Plot of thermal dependence of χ_M (empty squares) and $\chi_M T$ product (black filled circles) for $[\text{Cu}(\text{OMesalen})\text{La}(\text{NO}_3)(\text{Pyr}(\text{COO})_2)]_n \cdot (\text{DMF})_n$ (**33**) 1-D chain complex measured with an applied magnetic field of 5000 Oe; solid lines represent the theoretical curve derived from Bleaney-Bowers equation (see text).

The thermal variation of magnetic susceptibility as χ_M and $\chi_M T$ vs. T plots are shown in Figure 6.16. Using the Bleaney-Bowers equation (**13**) for a pair of copper

ions,²⁵⁶ the interchain coupling constant between two constituting [CuLa]-units led to $J_{CuCu} < -0.0001 \text{ cm}^{-1}$ for $g_{Cu} = 2.18 \pm 0.003$ and $\chi_{TIP} = 1.6 \cdot 10^{-6} \pm 2 \cdot 10^{-4} \text{ cm}^3 \text{ mol}^{-1}$.

$$\chi_M = \frac{2N\beta^2 g^2}{k(T - \theta)} \frac{1}{[3 + \exp(-J/kT)]} (1 - \rho) + \frac{N\beta^2 2^2 \rho}{2kT} S(S + 1) + \chi_{TIP} T \quad (13)$$

On the other hand the gadolinium-gadolinium coupling interaction has been reported as being antiferromagnetic^{237,399} with small exceptions reported for polymeric gadolinium compounds with malonic and salicylic acid as supporting organic ligands.^{377,378,380,400} The simulation of the magnetic data set shows that the countable ferromagnetic interaction takes place between Cu(II)-Gd(III) metal ions of the same [Cu(OMesalen)Gd(NO₃)] unit and it is not transmitted through the pyrazine 2,3-dicarboxylic acid linker. Use of a magnetic model^{332,349} that takes into account the [Cu-Gd] 1-D chain indicates that the intradimer interaction ($zJ' \ll -0.01 \text{ cm}^{-1}$, where z represents the number of neighboring molecules and J' is the interdimer coupling interaction) is almost nonexistent. The [Cu(OMesalen)Gd(NO₃)] units are connected through the pyrazine 2,3-dicarboxylic acid with a μ_2 -carboxylate coordinating simultaneously the Cu(II) and Gd(III) metal ions. Since one carboxylate oxygen atom occupies the axial position of the square-pyramidal Cu(II) atom, its $d_{x^2-y^2}$ magnetic orbital is localized in the basal plane leading to a very weak spin density in the axial position, thus the intradimer Cu(II)-Gd(III) ferromagnetic interaction is negligible. This is also caused by a large μ_2 -carboxylate bridged Cu-Gd intradimer separation of around 637.3 pm. The ferromagnetic interaction between the copper and gadolinium ions has been also confirmed by field dependence of the magnetization performed at 2 K. The experimental values fit the Brillouin function assuming $g_{av} = 2$, resulting in a spin ground state $S = 3.91 \pm 0.009$ with reliability factor $R^2 = 0.9986$ (Figure 6.17). The magnetization reach a saturation level of 7.8 N β at around 4830 Oe, maximum very close to expected one for a [CuGd]-couple.

The magnetic properties of this 1-D chain are comparable with similar reported Cu-Gd 1-D chain compounds where dicyanamide and/or thiocyanate have been used to link the heterodinuclear entities.^{332,360} The magnetic properties of these complexes have shown that in all cases the limited number of existing 1-D chain compounds behave as isolated heterodinuclear compounds. Additional ladder-chain [CuGd]-complexes have been reported more recently³⁴⁹ and the magnetic behavior is consistent with pre-

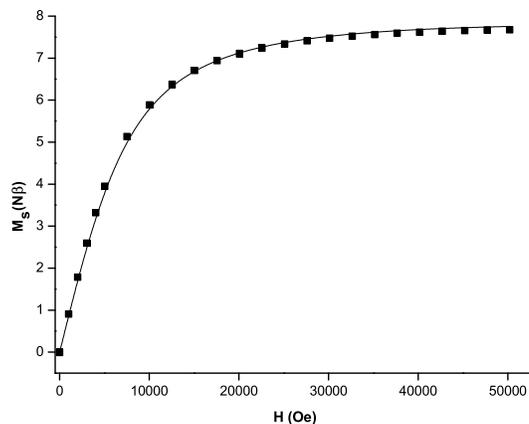


Figure 6.17: Plot of the field dependence of the magnetization for complex **27** measured at 2 K (black filled squares represent the experimental value; the solid line shows the theoretical curve generated using the Brillouin equation).

vious observations. The range of the coupling constant within the constituent [CuGd]-entities of the polymeric chain compounds range from 3.53 cm^{-1} to a maximum of 9.20 cm^{-1} and it is close correlated with the dihedral angle formed between CuO_2 and GdO_2 planes.^{349,360} The dihedral angle formed between O1–Cu–O3 and O1–Gd–O3 planes in compound $[\text{Cu}(\text{OMesalen})\text{Gd}(\text{NO}_3)(\text{Pyr}(\text{COO})_2)]_n \cdot (\text{DMF})_n$ (**27**) is around 20.2° and it is relatively larger than 17.1° value reported for the corresponding dihedral angle when thiocyanate is the linker of the [CuGd]-units of the 1-D chain.³⁶⁰ Nevertheless, the W-band EPR measurements performed at different temperatures show interesting features for the $[\text{Cu}(\text{OMesalen})\text{Gd}(\text{NO}_3)(\text{Pyr}(\text{COO})_2)]_n$ compound. As is depicted in Figure 6.18, no big difference has been observed when the EPR spectrum is recorded at 55 and 95 K. Instead, the low temperature W-band EPR spectrum exhibit many features with apparent fine structure progressions at high fields due to the zero field splitting of the $S = 4$ state. This will lead to a large number of permitted transitions between m_S levels ($\Delta m_S = \pm 1$) and therefore a complicated EPR spectrum that contains overlapping of bands.^{357,401} In addition, magnetic dipolar interaction between unpaired electrons combined with zero field splitting contribute to further complicate interpretation of the spectra and for the moment, no final simulation has been performed.

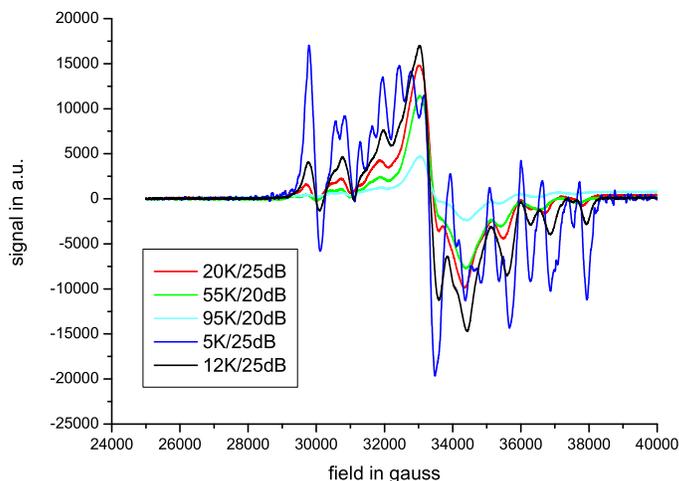


Figure 6.18: W-band EPR spectrum for $[\text{Cu}(\text{OMesalen})\text{Gd}(\text{NO}_3)(\text{Pyr}(\text{COO})_2)]_n$ (**27**) 1-D chain complex measured at different temperature values.

All other paramagnetic 4f-ion are anisotropic and this will introduce anisotropy into the magnetic ground state. The magnetic data sets measured in the 2-300 K temperature range are depicted in Figure 6.19 to Figure 6.21 for $[\text{Cu}(\text{OMesalen})\text{Eu}(\text{NO}_3)(\text{Pyr}(\text{COO})_2)]_n \cdot (\text{DMF})_n$ (**30**), $[\text{Cu}(\text{OMesalen})\text{Sm}(\text{NO}_3)(\text{Pyr}(\text{COO})_2)]_n \cdot (\text{DMF})_n$ (**31**) and $[\text{Cu}(\text{OMesalen})\text{Pr}(\text{NO}_3)(\text{Pyr}(\text{COO})_2)]_n \cdot (\text{DMF})_n$ (**32**), respectively as χ_m vs T and $\chi_m T$ vs T plots. The room temperature $\chi_m T$ value of around $0.83 \text{ cm}^3 \text{ mol}^{-1} \text{ K}$ measured for $[\text{Cu}(\text{OMesalen})\text{Sm}(\text{NO}_3)(\text{Pyr}(\text{COO})_2)]_n \cdot (\text{DMF})_n$ (**31**) is much higher than theoretical value $0.65 \text{ cm}^3 \text{ mol}^{-1} \text{ K}$ expected for noninteracting Cu(II) - Sm(III) ions (Figure 6.20). This is because the first excited state ${}^6\text{H}_{7/2}$ of Sm(III) ion can be populated at room temperature. The same situation has been observed in the case of europium containing 1-D chain - $[\text{Cu}(\text{OMesalen})\text{Eu}(\text{NO}_3)(\text{Pyr}(\text{COO})_2)]_n \cdot (\text{DMF})_n$ (**30**) compound (Figure 6.19) where the energetic separation between the ground state and first excited state is much smaller than in Sm(III) ion case. The measured $\chi_M T$ value is around $2.04 \text{ cm}^3 \text{ mol}^{-1} \text{ K}$ 300 K. For $[\text{Cu}(\text{OMesalen})\text{Pr}(\text{NO}_3)(\text{Pyr}(\text{COO})_2)]_n \cdot (\text{DMF})_n$ (**32**) (Figure 6.21), the room temperature measured $\chi_m T$ value of $2.02 \text{ cm}^3 \text{ mol}^{-1} \text{ K}$ is a little bit higher than calculated value of $1.78 \text{ cm}^3 \text{ mol}^{-1} \text{ K}$ for Cu(II)-Pr(III) noninteracting ions calculated according with the following equation:

$$\chi_M T = \frac{N\beta^2 g_{\text{Cu}}^2}{3k} S_{\text{Cu}}(S_{\text{Cu}} + 1) + \frac{N\beta^2 g_{\text{J}}^2}{3k} J_{\text{Ln}}(J_{\text{Ln}} + 1) \quad (14)$$

In this case the ground state is well separated in energy from the first excited state. For all these three complexes the $\chi_m T$ product decrease on lowering the temperature from 300 K to 15 K, except for $[\text{Cu}(\text{OMesalen})\text{Eu}(\text{NO}_3)(\text{Pyr}(\text{COO})_2)]_n \cdot (\text{DMF})_n$ (**30**) for which the $\chi_M T$ product decrease constantly on lowering the temperature, reaching a value of $0.51 \text{ cm}^3 \text{ mol}^{-1} \text{ K}$ at 2 K (Figure 6.19). For Sm(III)-containing 1-D chain, the decrease is constant in the 300-25 K with a value of $0.46 \text{ cm}^3 \text{ mol}^{-1} \text{ K}$ which corresponds actually to the calculated value for uncoupled Cu(II)-Sm(III) ions (Figure 6.20). Below 25 K, the decrease of $\chi_M T$ value is more abrupt being around $0.14 \text{ cm}^3 \text{ mol}^{-1} \text{ K}$ at 2 K. These profiles indicate an antiferromagnetic coupling operates in the $\text{Cu}^{\text{II}}\text{Sm}^{\text{III}}$ and $\text{Cu}^{\text{II}}\text{Pr}^{\text{III}}$ complexes. For Eu(III) and Sm(III) ion the energy separation between the ground state and excited state is very small, whereas for Pr(III) ion the ground state $^3\text{H}_4$ is separated by 2100 cm^{-1} to the first excited state $^5\text{H}_5$. In this case the two phenomena are possible, the thermal depopulation of Stark levels and the d-f exchange interaction, therefore a quantitative analyze using the isotropic Hamiltonian is not accurate for Eu(III) (**29**) and Sm(III) (**31**) complexes.

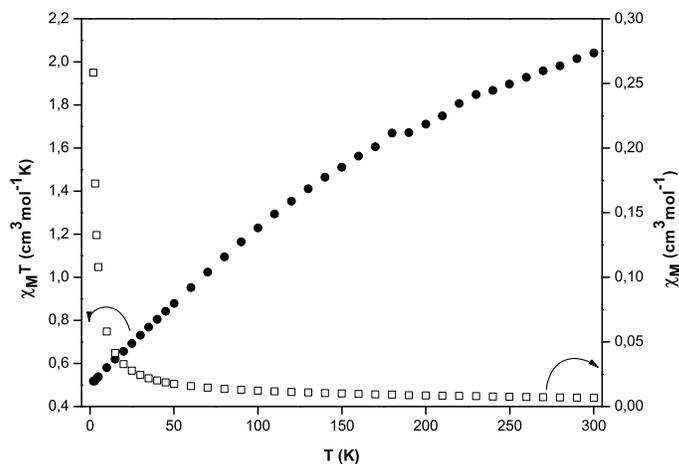


Figure 6.19: Plot of thermal dependence of χ_M (empty squares) and $\chi_M T$ product (black filled circles) for $[\text{Cu}(\text{OMesalen})\text{Eu}(\text{NO}_3(\text{Pyr}(\text{COO})_2)]_n \cdot (\text{DMF})_n$ (**30**) 1-D chain complex measured with an applied magnetic field of 2000 Oe.

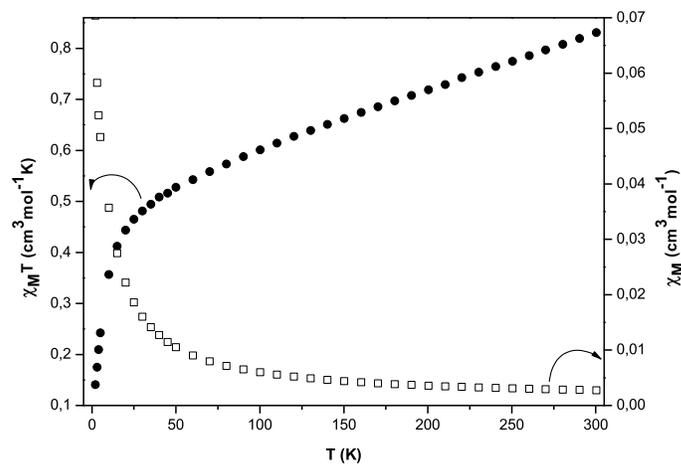


Figure 6.20: Plot of thermal dependence of χ_M (empty squares) and $\chi_M T$ product (black filled circles) for $[\text{Cu}(\text{OMesalen})\text{Sm}(\text{NO}_3)(\text{Pyr}(\text{COO})_2)]_n \cdot (\text{DMF})_n$ (**31**) 1-D chain complexes measured with an applied magnetic field of 2000 Oe.

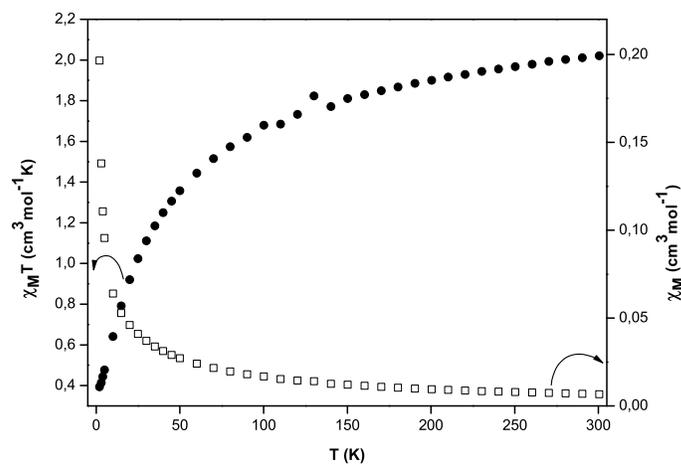


Figure 6.21: Plot of thermal dependence of χ_M (empty squares) and $\chi_M T$ product (black filled circles) for $[\text{Cu}(\text{OMesalen})\text{Pr}(\text{NO}_3)(\text{Pyr}(\text{COO})_2)]_n \cdot (\text{DMF})_n$ (**32**) 1-D chain complex measured with an applied magnetic field of 2000 Oe.

Kahn *et al.*^{323,339} proposed that for $4f^1$ to $4f^6$ electronic configuration of Ln(III) ions, the orbital and spin momenta are antiparallel and the ferromagnetic spin coupling will give rise to an overall antiferromagnetic interaction between the angular momenta.⁴⁰² Conversely, the orbital and spin momenta for $4f^8$ to $4f^{13}$ configurations are parallel and the ferromagnetic spin coupling will result in an overall ferromagnetic interaction. Regarding the interaction between Cu(II) - Ln(III) centers, Kahn *et al.*^{323,339} and Costes *et al.*³³⁸ reported antiferromagnetic interaction for lanthanides with less than half filled f-orbitals with the exception of Pr(III) and Eu(III) that were reported as noninteracting with the Cu(II) center. In agreement with these reports are the shape of the thermal variation of the magnetic susceptibility observed for $\text{Cu}^{\text{II}}\text{Ln}^{\text{III}}$ complexes with 4f orbital less than half-filled with electrons.

For the second series of $\text{Cu}^{\text{II}}\text{Ln}^{\text{III}}$ complexes with Ln(III) ion configuration $4f^{>7}$ the thermal variation of the $\chi_m T$ product are shown in Figure 6.22 for $[\text{Cu}(\text{OMesalen})\text{Tb}(\text{NO}_3)(\text{Pyr}(\text{COO})_2)]_n \cdot (\text{DMF})_n$ (**29**) and Figure 6.23 and Figure 6.24 for $[\text{Cu}(\text{OMesalen})\text{Dy}(\text{NO}_3)(\text{Pyr}(\text{COO})_2)]_n \cdot (\text{DMF})_n$ (**28**) complex. The $[\text{Cu}(\text{OMesalen})\text{Tb}(\text{NO}_3)(\text{Pyr}(\text{COO})_2)]_n \cdot (\text{DMF})_n$ (**29**) complex exhibits room temperature value of $\chi_m T$ of $13.75 \text{ cm}^3 \text{ mol}^{-1} \text{ K}$, much higher than expected $12.22 \text{ cm}^3 \text{ mol}^{-1} \text{ K}$ value for noninteracting Cu(II)-Tb(III) metal ions. The $\chi_m T$ value increases gradually on lowering the temperature presenting a maximum of $16.53 \text{ cm}^3 \text{ mol}^{-1} \text{ K}$ at 8 K. Below 8 K a slight decrease of the $\chi_m T$ value has been observed having a value of $11.28 \text{ cm}^3 \text{ mol}^{-1} \text{ K}$ at 2 K (Figure 6.22). The reciprocal magnetic susceptibility follows the Curie-Weiss equation:

$$\frac{1}{\chi} = \frac{T - \theta}{C} \quad (15)$$

with the Curie constant $C = 13.71 \pm 0.03$ and the Weiss constant $\theta = + 3.95 \pm 0.35 \text{ K}$ (Figure 6.22 - left plot). The increase of the $\chi_m T$ value on decreasing the temperature and positive Weiss constant indicate the ferromagnetic exchange coupling between Cu(II) and Tb(III) ions. On the other hand, the magnetization measurement performed at 2 K show an increase of the magnetization upon increasing the applied external magnetic field. The magnetization reaches a maxima of $4.5 N\beta$ at 50211 Oe, but does not reach the expected saturation value ($9 N\beta$ for Tb^{III} and $1 N\beta$ for Cu^{II}). This might be due to crystal field effect on Tb^{III} ion ($4f^8$, $J = 6$, $S = 3$, $L = 3$, 7F_6) that removes the degeneracy of the

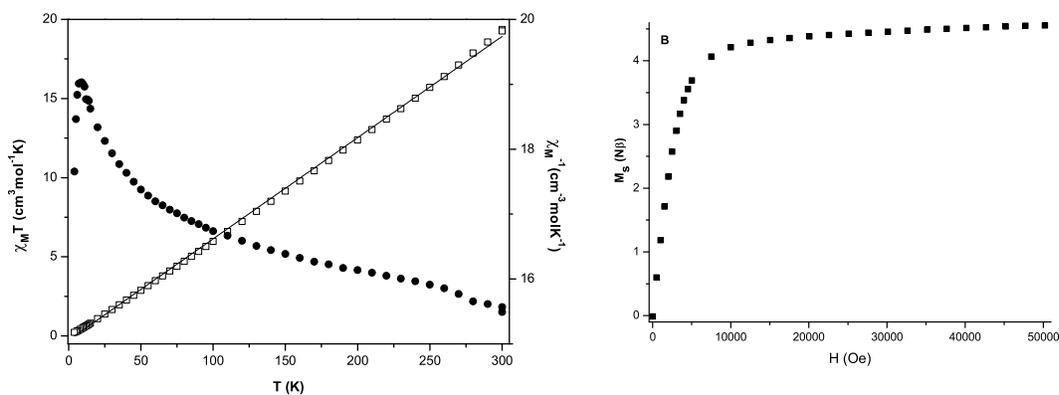


Figure 6.22: Plots of thermal dependence of $\chi_M T$ product (black filled circles) and $1/\chi_M$ (empty rhombus) for $[\text{Cu}(\text{OMesalen})\text{Tb}(\text{NO}_3)(\text{Pyr}(\text{COO})_2)]_n \cdot (\text{DMF})_n$ (**29**); the solid line represents the theoretical curve derived from Curie-Weiss law. The right picture (B inset) shows the field dependence of the magnetization expressed in $N\beta$ units for complex **29** measured at 2 K.

$^7\text{F}_6$ ground state. According to temperature-dependent magnetic susceptibility and field-dependent magnetization, the $[\text{Cu}(\text{OMesalen})\text{Tb}(\text{NO}_3)(\text{Pyr}(\text{COO})_2)]_n \cdot (\text{DMF})_n$ compound (**29**) exhibits ferromagnetic interaction. This is also sustained by existing reports in which the $\text{Cu}^{\text{II}}\text{-Tb}^{\text{III}}$ exchange interaction has been reported to be always ferromagnetic.³¹⁸ In general, Tb^{III} ion induce high magnetic anisotropy due to its orbital-angular momentum and alternating current susceptibility measurements are expected to bring more information.

For $[\text{Cu}(\text{OMesalen})\text{Dy}(\text{NO}_3)(\text{Pyr}(\text{COO})_2)]_n \cdot (\text{DMF})_n$ compound (**28**) a big difference has been observed for the thermal variation of $\chi_m T$ values measured at different magnetic fields, especially at low temperature values. At 300 K the $\chi_m T$ value is around $15.56 \text{ cm}^3 \text{ mol}^{-1} \text{ K}$ using a magnetic field of 2000 Oe and around $16.30 \text{ cm}^3 \text{ mol}^{-1} \text{ K}$ when a 5000 Oe magnetic field has been applied (Figure 6.23). Both values are much higher than theoretical $14.50 \text{ cm}^3 \text{ mol}^{-1} \text{ K}$ value expected for noninteracting $\text{Cu}(\text{II})\text{-Dy}(\text{III})$ metal ions, assuming $g_{\text{Cu}} = 2$ and $g_{\text{Dy}} = 1.33$.^{10,321} On lowering the temperature, the $\chi_M T$ values increase for both applied magnetic fields and reaches maximum of $19.03 \text{ cm}^3 \text{ mol}^{-1} \text{ K}$ at 9 K for 2000 Oe magnetic field and $23.37 \text{ cm}^3 \text{ mol}^{-1} \text{ K}$ at 4 K when 5000 Oe magnetic field has been used.

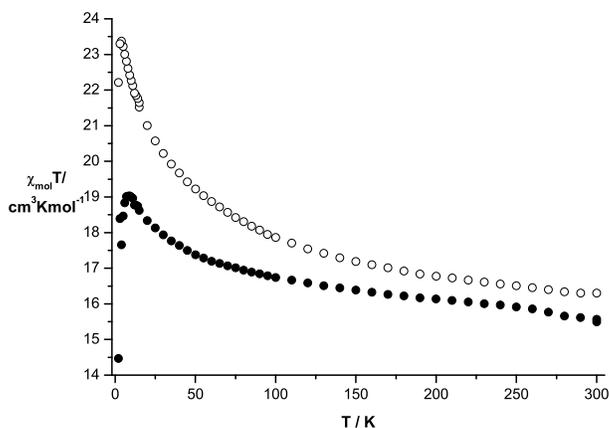


Figure 6.23: Plots of thermal dependence of $\chi_M T$ product at 2000 Oe (black filled circles) and 5000 Oe (empty circles) for $[\text{Cu}(\text{OMesalen})\text{Dy}(\text{NO}_3)(\text{Pyr}(\text{COO})_2)]_n \cdot (\text{DMF})_n$ (**28**).

The reciprocal magnetic susceptibility follows the Curie-Weiss law, resulting in a $\theta = 4.03 \pm 0.54$ K. The positive sign of Weiss constant and the shape of the temperature - dependent susceptibility measurements count for a ferromagnetic interaction between Cu^{II} - Dy^{III} metal ions. For $\text{Dy}(\text{III})$ as for $\text{Tb}(\text{III})$ ion, the anisotropy effect play a major role in determination of the Cu^{II} - Ln^{III} coupling constant. The $\text{Dy}(\text{III})$ has an ${}^6\text{H}_{15/2}$ ground state that is split in zero field by crystal field effects. The energy gaps induced by ligand - field effects are larger than kT at low temperatures, therefore the simulation of the magnetic data set must include ligand field effects, such as selective depopulation of the low - lying levels.

The ${}^6\text{H}_{15/2}$ ground state of $\text{Dy}(\text{III})$ atom is split into a set of Kramer doublets $|\pm M_J\rangle$, thus an anisotropic exchange model that involves both the orbital contribution and ligand field effect is required to interpret the magnetic behavior of $[\text{Cu}(\text{OMesalen})\text{Dy}(\text{NO}_3)(\text{Pyr}(\text{COO})_2)]_n \cdot (\text{DMF})_n$ (**28**) compound. The field dependence of magnetization for $[\text{Cu}(\text{OMesalen})\text{Dy}(\text{NO}_3)(\text{Pyr}(\text{COO})_2)]_n \cdot (\text{DMF})_n$ is shown in Figure 6.24 (right picture) as plot of the experimental values of $M(N\beta)$ versus H . On increasing the applied external magnetic field, the magnetization of **27** increases to $8.10 N\beta$ at 50000 Oe but does not reach an expected saturation value ($10 N\beta$ for $\text{Dy}(\text{III})$ ion and $1 N\beta$ for $\text{Cu}(\text{II})$ ion).

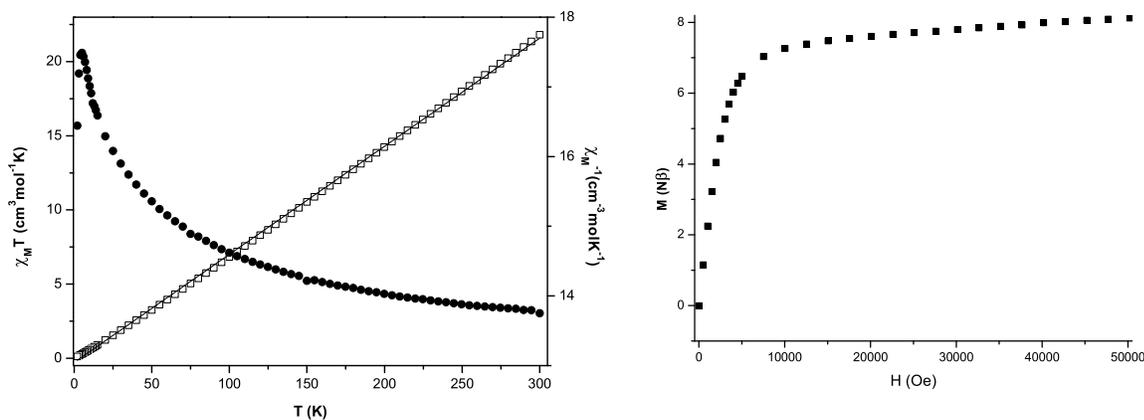


Figure 6.24: Plots of thermal dependence of $\chi_M T$ product (black filled circles at 5000 Oe) and $1/\chi_M$ (empty rhombus) for $[\text{Cu}(\text{OMesalen})\text{Dy}(\text{NO}_3)(\text{Pyr}(\text{COO})_2)]_n \cdot (\text{DMF})_n$ (**28**); the solid line represents the theoretical curve generated using the Curie-Weiss law (left picture). The right picture shows the field dependence of the magnetization expressed in $N\beta$ units for complex **28** measured at 2 K.

The experimental data sets for both complexes indicate a ferromagnetic interaction between Cu(II) and Ln(III) center, where Ln(III) is Tb(III) and Dy(III) ions. A quantitative fitting of the experimental data is not trivial due to the high anisotropy and spin-coupling interaction and it is an undergoing research. As anisotropy appears to be vital for synthesizing "single molecule magnets", the 1-D chains containing Dy(III) and Tb(III) ions are potentially exciting. Kahn *et al* reported a series of oxamido-bridged polymers of type $\text{Ln}_2[\text{CuL}]_3$ (L is ortho-phenylene-bis oxamato ligand) and for Tb and Dy-containing polymers a divergence in $\chi_M T$ product at low temperature was indicative of magnetic ordering interpreted as possible one-dimensional ferro- and ferrimagnets. Therefore the herein described $[\text{Cu}(\text{OMesalen})\text{Dy}(\text{NO}_3)(\text{Pyr}(\text{COO})_2)]_n \cdot (\text{DMF})_n$ and $[\text{Cu}(\text{OMesalen})\text{Tb}(\text{NO}_3)(\text{Pyr}(\text{COO})_2)]_n \cdot (\text{DMF})_n$ (**29**) one-dimensional chain compounds may show similar features and hence may represent rare examples of single chain magnets. The interchain separation is quite large and most likely no interchain interaction occurs (Figure 6.25). The Cu-Ln interchain separation range from around 810 pm to 1194 pm, whereas the Ln-Ln interchain separation falls within 1054-1082 pm limits. Therefore the countable magnetic interaction is the result of Cu-Ln ferromagnetic coupling within the constituent units of the chain and maybe antiferromagnetic intrachain Ln-

Ln interactions. Thus, the $[\text{Cu}(\text{OMesalen})\text{Dy}(\text{NO}_3)_3(\text{Pyr}(\text{COO})_2)]_n \cdot (\text{DMF})_n$ (**28**) and $[\text{Cu}(\text{OMesalen})\text{Tb}(\text{NO}_3)(\text{Pyr}(\text{COO})_2)]_n \cdot (\text{DMF})_n$ (**29**) one-dimensional chain compounds are potential candidates as single chain magnets.

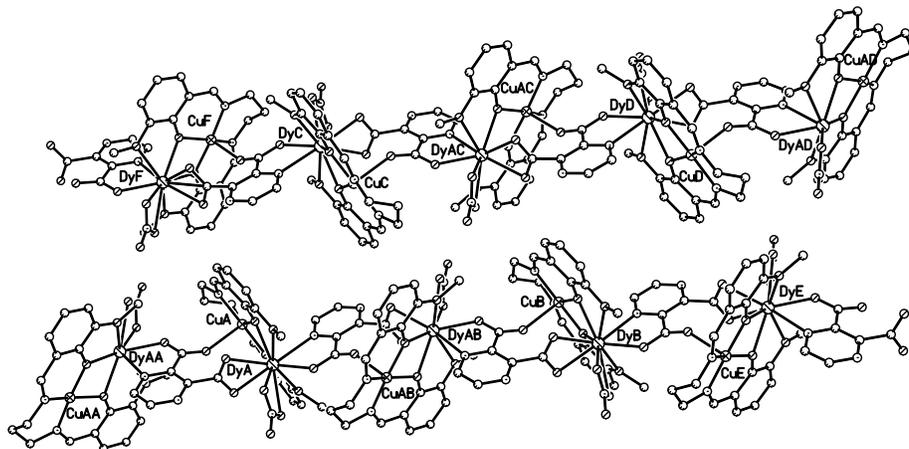


Figure 6.25: Packing diagram of $[\text{Cu}(\text{OMesalen})\text{Dy}(\text{NO}_3)_3(\text{Pyr}(\text{COO})_2)]_n \cdot (\text{DMF})_n$ (**28**) compound viewed along the b axis showing the separation of the constituent 1-D chains.

6.2 Trinuclear $\text{Cu}^{\text{II}}\text{-Ln}^{\text{III}}$ complexes

The design of new heteropolynuclear complexes has received considerable attention in the field of molecular magnetism.^{10,403} This has been stimulated by the search for molecular-based magnets and development of new models for investigations of the exchange interaction between the paramagnetic centers. The constituting metal centers have been found capable of interacting through extended bridging ligands, even if they are relatively well separated.¹⁰ The molecule-based magnetic materials are, in general formed by paramagnetic metal ions linked by organic framework. While the metal ions are the source of magnetic moments, the organic ligands are responsible for the exchange pathways between the magnetic centers. Changes in the exchange pathways produce modifications of the structural arrangement which in turn may affect the magnetic interaction.^{32,227,321,396,404} Lanthanide-containing exchanged-coupled system are versatile building blocks for molecule-based magnets due to large anisotropy associated with most lanthanide ions.^{227,321,405} Since the pioneering work started in 1985 by Gatteschi *et al.*,³⁰¹ a large number of polynuclear Cu-Ln complexes have been reported. However,

most of the studies have been focused on Cu^{II}-Gd^{III} couple where both ferromagnetic and antiferromagnetic interactions were observed, although the first is commonly observed.^{321,335} This illustrates the complexity of the system and the requirement to design more examples in order to investigate the magnetic mechanism. On the other hand, polynuclear complexes comprising other lanthanide ions have been purely investigated due to the vital role of their angular momentum in the interpretation of the magnetic properties.^{10,338} Clusters of higher nuclearity formed between d-transition metals and lanthanide ions^{363,386,388,389,391,392,394,406,407} have been also reported, and the magnetic behavior vary from weak antiferromagnetic/or ferromagnetic interaction to single molecular magnets behavior.^{386,392,394,407} The development of new complexes with d-f topology has been extended not only because of their interesting magnetic properties^{227,310,405,408} and potential application to luminescence materials,⁴⁰⁹ nonlinear optical materials⁴¹⁰ near infrared chiroptical sensors⁴¹¹ and MOCVD (single source precursor for metal organic vapor deposition).³¹⁵ The formation of oligo-dinuclear or trinuclear Cu^{II}-Ln^{III} complexes can be conducted by varying the ratio between Cu-salen precursor and the lanthanide salts, but the resulting magnetic exchange interaction is still difficult to be predicted.^{301,312,319,412} The reported approaches to synthesize trinuclear Cu₂Ln complexes is based on blocking the coordination sites of the lanthanide ion by the anions of the starting LnX₃·6H₂O salts, where X = NO₃⁻, Cl⁻, ClO₄⁻, trifluoroacetylacetonate and/or trifluoroacetate. In these complexes, the lanthanide ion is wrapped around by two Cu-salen moieties, whereas the anion establishes the connection between the d-metal ions and lanthanide center. The main magnetic interaction is described as ferromagnetic when gadolinium has been used as lanthanoid ion, whereas the Cu-Cu magnetic coupling range from antiferromagnetic, ferromagnetic to non-interacting d-d couple.^{301,319} While the Cu-Gd exchange interaction is ferromagnetic when *salen-type* ligands have been used as metallo-ligand, it has been reported that oxime-derivatives ligands led to an antiferromagnetic coupling between Cu(II) and Gd(III) paramagnetic centers.³¹² The intensity of the coupling constants is very much dependent upon used organic ligand and the bridging linker between Cu and Ln ions. Therefore, we purpose to scrutinize the influence of the d-f linker in trinuclear [Cu₂Ln] complexes by choosing salicylic acid as a bridge. This is based upon reports of ferromagnetic interaction between gadolinium(III) ions mediated by salicylic

acid in oligo- and coordination polymeric compounds.^{380,400} It is worth mentioning here, that the Gd–Gd magnetic exchange interaction is antiferromagnetic^{399,413} with few exceptions when the used ligand implies a weak ferromagnetic coupling among the lanthanoid ions.^{377,414} Thus, trinuclear $[\text{Cu}_2\text{Ln}]$ complexes have been isolated using salicylic acid as capping and bridging ligand. The $[\text{Cu}(\text{OMesalen})\text{H}_2\text{O}]$ precursor complex (**24**) (Figure 6.2) has been reacted in a 2:1 ratio with $\text{Ln}(\text{NO}_3)_3 \cdot 6\text{H}_2\text{O}$ salts, followed by addition of deprotonated salicylic acid solution. On going from pyrazine 2,3-dicarboxylic acid to salicylic acid, the polydentate nature of the ligand is reduced, and therefore the synthesis of oligotrinuclear complexes of type $[(\text{Cu}(\text{OMesalen}))_2\text{Ln}(\text{salCOO})_2]\text{NO}_3 \cdot \text{S}$ (S = solvent) has been possible. The molecular structure have been determined for Gd(III) (**34**), Sm(III) (**35**), Pr(III) (**36**) and La(III) (**37**) - containing complexes and are depicted in Figure 6.26 to Figure 6.29. Additionally, the corresponding Eu(III)-containing trinuclear $[(\text{Cu}(\text{OMesalen}))_2\text{Eu}(\text{salCOO})_2]\text{NO}_3 \cdot 3\text{MeOH} \cdot \text{H}_2\text{O}$ (**38**) have been spectroscopically characterized. Again the molecular structures within this series of compounds show isostructural features of crystallographically characterized complexes. Scrutinizing the structural data shows, that the most pertinent difference compared to previous herein described d-f complexes, concerns not only the nuclearity of the resulting complexes, but also the reactivity of the lanthanide (III) ions towards complex formation. In instance, by contrast to pyrazine 2,3-dicarboxylic acid bridge, the salicylic acid made possible the isolation of heterotrinuclear compounds only for lanthanide ions comprising lanthanum to gadolinium ions. Every attempt to synthesize the similar complexes with heavier lanthanide ions failed. This might be a consequence of smaller atomic radius for the last mentioned lanthanide ions and therefore their tendency to assume smaller coordination numbers. Another distinctive feature of these oligotrinuclear d-f complexes is that the trinuclear $[\text{Cu}_2\text{Ln}]$ entity is cationic with unbound distorted nitrate anion that compensate the positive charge of the triad $[\text{Cu}_2\text{Ln}]$ core. In addition, methanol and water lattice solvents have been found capable of establishing hydrogen bonding interactions between the trinuclear entities. The salicylic acid co-ligand coordinated to both copper and lanthanide centers only through carboxylate functionality, whereas the phenolate group is distorted and not involved in metal coordination, but instead establishes hydrogen bonding contacts intermediated by solvent molecules between the trinuclear entities.

The lanthanide atom is 10-coordinated and enclosed by two $[\text{Cu}(\text{OMesalen})\text{H}_2\text{O}]$ moieties. While the copper atoms conserve their classical positions in the inner N_2O_2 compartment of the *salen-type* ligand, the lanthanide atom is fixed in the molecule by two pairs of O_2O_2 donor sets of the compartmental methoxy-derivative *salen*-ligand. The lanthanide to oxygen atom bond lengths differ from previously described one-dimensional chain compounds and fall in the 236.3 - 288.2 pm region. Selected bond lengths and angles in complexes are listed in Table 6.10 to 6.13. The strength of the lanthanide to oxygen bond lengths differ among the two *Cu-salen* moieties and, namely is tighter embedded by Cu(2)-salen entity (Gd–O bond distances within 235.4-285.4 pm range) and weaker enclosed by Cu(1)-salen entity (Gd–O bond lengths within 236.3-288.2 pm range). The coordination sphere of the lanthanide ions is completed by the two salicylic acid molecules which function as capping and bridging ligands establishing two η^1, η^1, μ_2 -connections with copper atoms and the lanthanoid center.

The resulting structural motif consists of two copper atoms in square-pyramidal

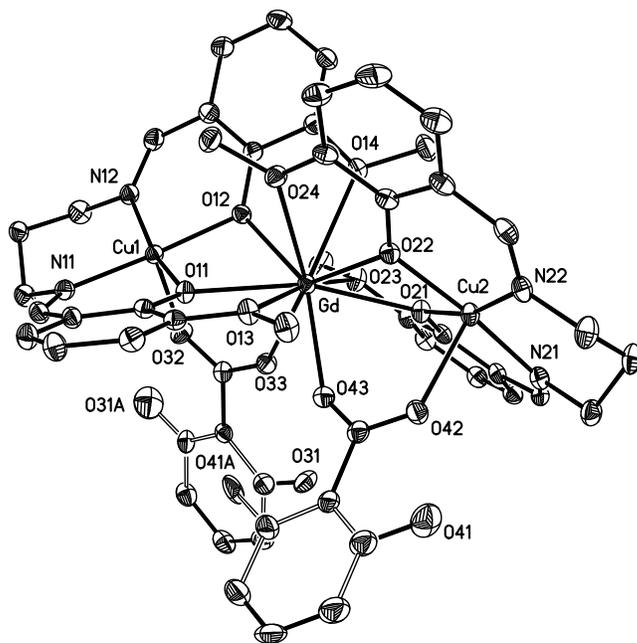


Figure 6.26: Molecular structure and numbering scheme atoms in $[(\text{Cu}(\text{OMesalen}))_2\text{Gd}(\text{salCOO})_2]\text{NO}_3 \cdot 2\text{MeOH} \cdot 0.25\text{H}_2\text{O}$ (**34**) complex. Thermal ellipsoids are drawn at 50% probability. Hydrogen atoms have been excluded for clarity.

Table 6.10: Selected bond lengths (pm) and angles ($^{\circ}$) for complex **34**.

Gd–O11	242.8(3)	Gd–O12	236.3(4)
Gd–O13	288.2(3)	Gd–O14	264.4(4)
Gd–O21	240.9(4)	Gd–O22	235.4(3)
Gd–O23	285.4(4)	Gd–O24	263.7(4)
Gd–O33	237.4(4)	Gd–O43	237.9(4)
Gd–Cu1	342.9(6)	Gd–Cu2	345.0(6)
Cu1–O11	198.1(4)	Cu1–O12	196.7(4)
Cu1–N11	196.8(5)	Cu1–N12	197.8(4)
Cu1–O32	219.9(4)	Cu2–O21	197.1(3)
Cu2–O22	197.8(4)	Cu2–N21	197.8(5)
Cu2–N22	199.2(4)	Cu2–O42	230.3(4)
O11–Gd–O12	64.71(12)	O11–Gd–O13	58.27(11)
O11–Gd–O14	118.93(12)	O11–Gd–O33	73.30(13)
O12–Gd–O13	113.95(12)	O12–Gd–O14	62.15(12)
O12–Gd–O33	82.33(13)	O13–Gd–O13	123.43(12)
O13–Gd–O33	108.86(13)	O14–Gd–O33	124.73(13)
O21–Gd–O22	63.46(12)	O21–Gd–O23	58.24(11)
O21–Gd–O24	120.26(12)	O21–Gd–O43	74.21(13)
O22–Gd–O23	112.99(12)	O22–Gd–O24	63.05(12)
O22–Gd–O43	83.47(13)	O23–Gd–O24	126.57(12)
O23–Gd–O43	108.41(13)	O24–Gd–O43	122.79(13)
O33–Gd–O43	68.97(14)	O11–Cu1–O12	81.01(15)
O11–Cu1–N11	91.94(17)	O11–Cu1–N12	162.17(18)
O11–Cu1–O32	99.22(15)	O12–Cu1–N11	170.01(18)
O12–Cu1–N12	90.14(17)	O12–Cu1–O32	96.05(15)
N11–Cu1–N12	94.68(19)	N11–Cu1–O32	92.04(17)
N12–Cu1–O32	97.08(18)	O21–Cu2–O22	78.77(14)
O21–Cu2–N21	92.18(17)	O21–Cu2–N22	164.74(19)
O21–Cu2–O42	100.25(15)	O22–Cu2–N21	170.61(16)
O22–Cu2–N22	91.67(17)	O22–Cu2–O42	92.11(15)
N21–Cu2–N22	97.70(19)	N21–Cu2–O42	87.03(17)

Table 6.11: Selected bond lengths (pm) and angles ($^{\circ}$) for complex **35**.

Sm–O11	244.6(4)	Sm–O12	238.8(5)
Sm–O13	285.4(5)	Sm–O14	266.7(6)
Sm–O21	243.7(5)	Sm–O22	238.8(4)
Sm–O23	282.3(5)	Sm–O24	266.1(5)
Sm–O33	239.7(5)	Sm–O43	239.2(6)
Sm–Cu1	345.9(8)	Sm–Cu2	347.2(9)
Cu1–O11	197.7(5)	Cu1–O12	198.0(5)
Cu1–N11	196.0(6)	Cu1–N12	198.3(6)
Cu1–O32	220.6(5)	Cu2–O21	195.8(5)
Cu2–O22	196.5(5)	Cu2–N21	196.8(6)
Cu2–N22	198.5(6)	Cu2–O42	230.9(6)
O11–Sm–O12	64.20(16)	O11–Sm–O13	58.62(14)
O11–Sm–O14	118.02(17)	O11–Sm–O33	72.36(16)
O12–Sm–O13	114.15(15)	O12–Sm–O14	61.44(16)
O12–Sm–O33	81.91(18)	O13–Sm–O14	124.23(16)
O13–Sm–O33	107.84(17)	O14–Sm–O33	124.48(19)
O21–Sm–O22	62.36(15)	O21–Sm–O23	58.41(15)
O21–Sm–O24	118.79(16)	O21–Sm–O43	73.09(18)
O22–Sm–O23	112.47(15)	O22–Sm–O24	62.40(16)
O22–Sm–O43	83.58(18)	O23–Sm–O24	127.19(18)
O23–Sm–O43	106.57(18)	O24–Sm–O43	123.47(18)
O33–Sm–O43	69.03(19)	O11–Cu1–O12	81.0(2)
O11–Cu1–N11	91.8(2)	O11–Cu1–N12	162.6(2)
O11–Cu1–O32	98.85(19)	O12–Cu1–N11	169.4(2)
O12–Cu1–N12	89.9(2)	O12–Cu1–O32	95.9(2)
N11–Cu1–N12	95.0(3)	N11–Cu1–O32	92.9(2)
N12–Cu1–O32	96.8(2)	O21–Cu2–O22	79.11(19)
O21–Cu2–N21	92.0(2)	O21–Cu2–N22	163.8(3)
O21–Cu2–O42	100.3(2)	O22–Cu2–N21	171.0(2)
O22–Cu2–N22	92.2(2)	O22–Cu2–O42	93.0(2)
N21–Cu2–N22	96.8(3)	N21–Cu2–O42	87.3(2)

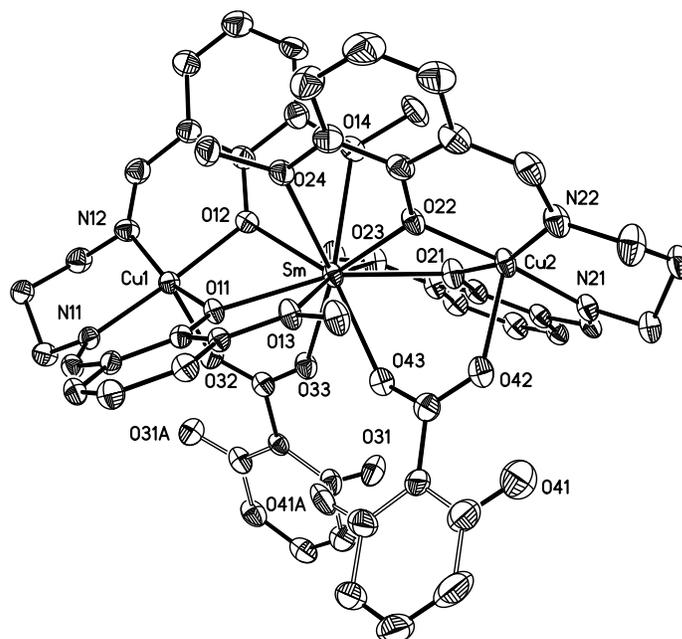


Figure 6.27: Molecular structure and numbering scheme atoms in $[(\text{Cu}(\text{OMesalen}))_2\text{Sm}(\text{salCOO})_2]\text{NO}_3 \cdot 2.5\text{MeOH} \cdot \text{H}_2\text{O}$ (**35**) complex. Thermal ellipsoids are drawn at 50% probability. Hydrogen atoms have been excluded for clarity.

environment with the carboxylate oxygen atoms of the co-ligand occupying the apical position and binds around 219.9 pm for Cu1–O32 bond length and 230.3 pm for Cu2–O42 bond distance, respectively. The remained carboxylate oxygen atom of each salicylic acid binds to the lanthanide center, with Ln–O bond distance of around 237.4–237.9 pm in the case of gadolinium(III)-containing complex **34**. A slight increase in the bond lengths have been observed on going from Gd(III) to La(III)-ion containing trinuclear $[(\text{Cu}(\text{OMesalen}))_2\text{Ln}(\text{salCOO})_2]\text{NO}_3 \cdot \text{S}$ compounds. Both copper(II) ions are five coordinated in a distorted square pyramidal geometries. The distortions from an ideal square pyramidal geometry²³⁹ is $\tau = 0.13$ for Cu1 center and $\tau = 0.09$ for Cu2 ion in $[(\text{Cu}(\text{OMesalen}))_2\text{Gd}(\text{salCOO})_2]\text{NO}_3 \cdot 2\text{MeOH} \cdot 0.25\text{H}_2\text{O}$ (**33**) complex. The distortion of the coordination geometry from the square pyramid remains similar for the series of $[(\text{Cu}(\text{OMesalen}))_2\text{Ln}(\text{salCOO})_2]\text{NO}_3 \cdot \text{S}$ complexes described herein, except for $[(\text{Cu}(\text{OMesalen}))_2\text{La}(\text{salCOO})_2]\text{NO}_3 \cdot 3.75\text{MeOH} \cdot 0.25\text{H}_2\text{O}$ (**37**) complex for which the τ parameter is around 0.10 for Cu1 ion and 0.07 for Cu2 ion. This τ value is defined as the difference between the two largest donor-metal-donor angles divided by 60 and

has a $\tau = 0$ value for an ideal square pyramid and $\tau = 1$ for the trigonal bipyramid.²³⁹ The copper ions form with the lanthanide ion an angle of 179.3° , very close to an linear Cu \cdots Gd \cdots Cu arrangement with Cu \cdots Cu separation of around 687.95 pm. The O11–Cu1–O12 and O11–Gd–O12 angles of 81.0 and 64.7° forms a dihedral angle of around 26.8° , whereas the O21–Cu2–O22 and O21–Gd–O22 angles are 63.4 and 78.7° , respectively that lead to a dihedral angle of 27.6° . The intramolecular Cu–Gd separation is around 345.0 pm for Cu1 \cdots Gd and 342.9 pm for Cu2 \cdots Gd separation. These dihedral angles specific for μ_2 -bridging mode of the phenoxy oxygen atoms of the compartmental *salen*-ligands showed no big difference from 1-D chain compounds to oligomeric trinuclear species. The Cu \cdots Gd separation within the [Cu₂Ln]-triad is smaller than corresponding intramolecular separation found in previous described one-dimensional [CuLn] complexes, but very close to corresponding intramolecular separation reported for trinuclear [Cu₂Ln]-complexes bridged by trifluoroacetate or amide-based Schiff base ligands.^{301,319}

The compounds crystallize in the P2₁/c monoclinic space group and have no crys-

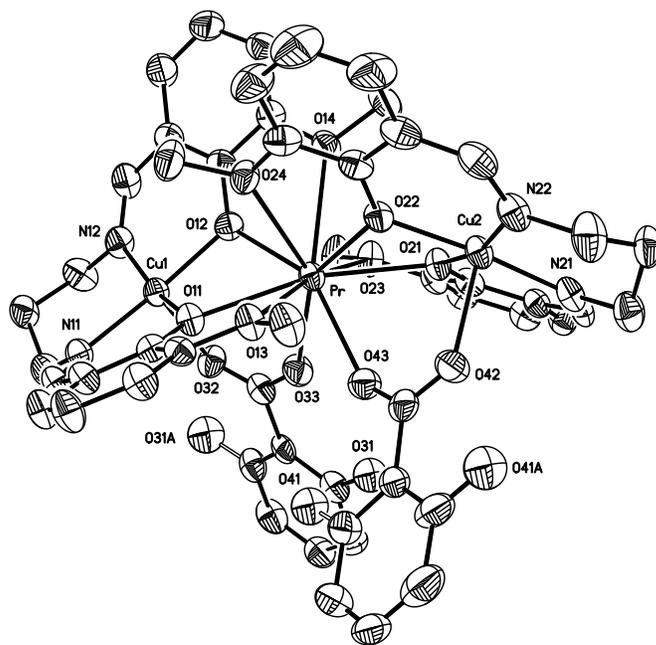


Figure 6.28: Molecular structure and numbering scheme atoms in [(Cu(OMesalen))₂Pr(salCOO)₂]NO₃·3MeOH·0.25H₂O (**36**) complex. Thermal ellipsoids are drawn at 50% probability. Hydrogen atoms have been excluded for clarity.

Table 6.12: Selected bond lengths (pm) and angles ($^{\circ}$) for complex **36**.

Pr–O11	248.9(4)	Pr–O12	248.0(4)
Pr–O13	285.4(4)	Pr–O14	270.0(5)
Pr–O21	243.9(4)	Pr–O22	243.4(4)
Pr–O23	280.0(6)	Pr–O24	268.4(5)
Pr–O33	243.9(5)	Pr–O43	244.6(5)
Pr–Cu1	349.8(8)	Pr–Cu2	352.0(8)
Cu1–O11	197.1(4)	Cu1–O12	197.2(5)
Cu1–N11	197.4(5)	Cu1–N12	197.1(6)
Cu1–O32	221.7(5)	Cu2–O21	194.9(4)
Cu2–O22	199.2(4)	Cu2–N21	198.2(6)
Cu2–N22	198.3(6)	Cu2–O42	232.8(5)
O11–Pr–O12	62.84(15)	O11–Pr–O13	57.95(13)
O11–Pr–O14	115.94(14)	O11–Pr–O33	71.41(16)
O12–Pr–O13	112.54(14)	O12–Pr–O14	60.54(14)
O12–Pr–O33	82.06(16)	O13–Pr–O14	124.32(14)
O13–Pr–O33	105.90(15)	O14–Pr–O33	125.10(16)
O21–Pr–O22	61.47(14)	O21–Pr–O23	58.53(13)
O21–Pr–O24	116.53(14)	O21–Pr–O43	73.23(15)
O22–Pr–O23	112.28(14)	O22–Pr–O24	61.05(14)
O22–Pr–O43	83.89(16)	O23–Pr–O24	127.52(15)
O23–Pr–O43	105.58(15)	O24–Pr–O43	123.52(16)
O33–Pr–O43	68.85(17)	O11–Cu1–O12	81.33(18)
O11–Cu1–N11	91.6(2)	O11–Cu1–N12	162.7(2)
O11–Cu1–O32	99.41(19)	O12–Cu1–N11	170.0(2)
O12–Cu1–N12	90.2(2)	O12–Cu1–O32	96.09(18)
N11–Cu1–N12	94.7(2)	N11–Cu1–O32	92.0(2)
N12–Cu1–O32	96.5(2)	O21–Cu2–O22	79.18(18)
O21–Cu2–N21	92.1(2)	O21–Cu2–N22	165.1(2)
O21–Cu2–O42	91.91(18)	O22–Cu2–N21	170.8(2)
O22–Cu2–N22	91.3(2)	O22–Cu2–O42	91.91(18)
N21–Cu2–N22	97.8(2)	N21–Cu2–O42	86.8(2)

Table 6.13: Selected bond lengths (pm) and angles ($^{\circ}$) for complex **37**.

La–O11	253.3(3)	La–O12	249.3(4)
La–O13	284.1(4)	La–O14	273.6(4)
La–O21	252.6(4)	La–O22	248.3(4)
La–O23	280.0(4)	La–O24	271.1(4)
La–O33	248.2(4)	La–O43	248.0(4)
La–Cu1	354.9(7)	La–Cu2	356.8(7)
Cu1–O11	196.9(4)	Cu1–O12	197.7(4)
Cu1–N11	197.4(5)	Cu1–N12	197.3(5)
Cu1–O32	221.4(4)	Cu2–O21	196.2(4)
Cu2–O22	198.7(4)	Cu2–N21	198.4(5)
Cu2–N22	198.2(5)	Cu2–O42	237.2(4)
O11–La–O12	61.61(12)	O11–La–O13	57.70(11)
O11–La–O14	114.10(12)	O11–La–O33	70.98(12)
O12–La–O13	111.91(11)	O12–La–O14	59.91(12)
O12–La–O33	81.24(13)	O13–La–O14	125.05(12)
O13–La–O33	104.67(12)	O14–La–O33	124.54(13)
O21–La–O22	60.64(12)	O21–La–O23	57.94(11)
O21–La–O24	115.19(12)	O21–La–O43	72.47(13)
O22–La–O23	111.53(11)	O22–La–O24	60.42(12)
O22–La–O43	83.62(13)	O23–La–O24	128.42(12)
O23–La–O43	103.68(13)	O24–La–O43	123.66(13)
O33–La–O43	69.03(14)	O11–Cu1–O12	81.43(15)
O11–Cu1–N11	91.62(17)	O11–Cu1–N12	163.18(19)
O11–Cu1–O32	99.27(16)	O12–Cu1–N11	169.33(18)
O12–Cu1–N12	89.84(18)	O12–Cu1–O32	96.49(15)
N11–Cu1–N12	94.76(19)	N11–Cu1–O32	92.61(18)
N12–Cu1–O32	95.96(19)	O21–Cu2–O22	79.62(15)
O21–Cu2–N21	91.96(17)	O21–Cu2–N22	166.52(22)
O21–Cu2–O42	99.44(15)	O22–Cu2–N21	170.93(17)
O22–Cu2–N22	91.43(18)	O22–Cu2–O42	91.85(15)
N21–Cu2–N22	97.40(22)	N21–Cu2–O42	86.17(18)

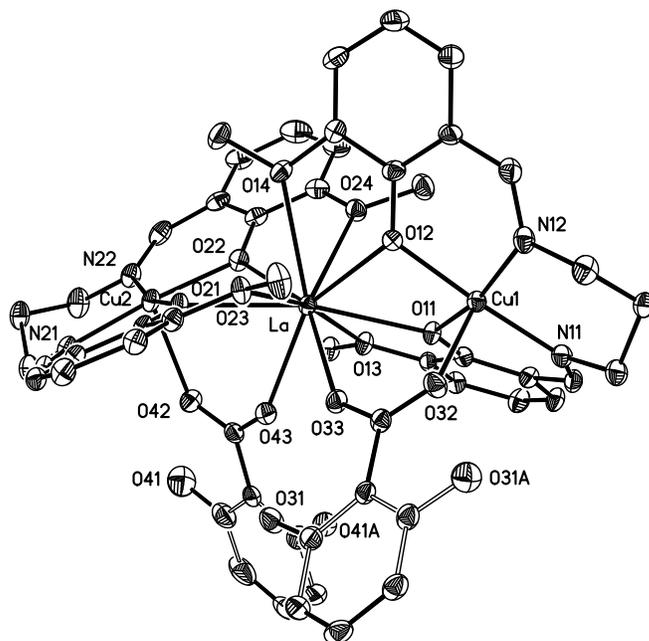


Figure 6.29: Molecular structure and numbering scheme atoms in $[(\text{Cu}(\text{OMesalen}))_2\text{La}(\text{salCOO})_2]\text{NO}_3 \cdot 3.75\text{MeOH} \cdot 0.25\text{H}_2\text{O}$ (**37**) complex. Thermal ellipsoids are drawn at 50% probability. Hydrogen atoms have been excluded for clarity.

tallographic symmetry. The $\text{Cu}(\text{O})_2\text{Ln}$ bridge is asymmetric and the bond lengths and angles of the two $[\text{Cu}(\text{OMesalen})\text{Gd}(\text{salCOO})]^+$ moieties show small differences. Nevertheless, each $[\text{Cu}(\text{OMesalen})\text{H}_2\text{O}]$ entity coordinates the central lanthanide ion in the same fashion, similarly to previously described one-dimensional chains. The major difference between the two bridging ligands, e.g. pyrazine 2,3-dicarboxylic acid and salicylic acid, resides from their coordination mode. In 1-D chain compounds, the polydentate ligand substitutes only two bidentate nitrate ligands of the classical $[\text{Cu}(\text{OMesalen})\text{Gd}(\text{NO}_3)_3]$ dinuclear complexes (Figure 6.5), whereas the salicylic acid co-ligand leads to a total replacement of the nitrate anion ligands but maintaining the dodecahedron arrangement of the lanthanoid center.

The formation of trinuclear complexes of type $[(\text{Cu}(\text{OMesalen}))_2\text{Ln}(\text{salCOO})_2]\text{NO}_3 \cdot 3\text{MeOH} \cdot \text{H}_2\text{O}$ is also confirmed by IR spectroscopy. Specific ligand stretching vibrations have been observed around 1626 cm^{-1} assigned to $\nu(\text{CH}=\text{N})$ bond. All the IR spectra exhibit broad band at 3420 cm^{-1} due to phenolic and methanol $\nu(\text{OH})$ stretching vibrations. Strong adsorption band has been detected at 1473 cm^{-1} assigned to symmetric stretching

vibrations of the carboxylate group of salicylic acid co-ligands. In addition, characteristic stretching vibration of the nitrate anion has been observed at 1384 cm^{-1} similarly to its stretching vibration in $[\text{Cu}(\text{OMesalen})\text{Ln}(\text{NO}_3)(\text{Pyr}(\text{COO})_2)]_n \cdot (\text{DMF})_n$ complexes when functions as bi-dentate ligand anion. The $[(\text{Cu}(\text{OMesalen}))_2\text{Eu}(\text{salCOO})_2]\text{NO}_3 \cdot 3\text{MeOH} \cdot \text{H}_2\text{O}$ (**37**) complex showed similar IR features.

6.2.1 Magnetic properties of $[\text{Cu}_2^{\text{II}}\text{-Ln}^{\text{III}}]$ trinuclear complexes

Owing to the difficulties in analyzing the magnetic properties of (CuLn) complexes involving a Ln^{3+} ion, which possesses a first-order orbital moment, the interpretation of the magnetic studies will concern the $[(\text{Cu}(\text{OMesalen}))_2\text{La}(\text{salCOO})_2]\text{NO}_3$ and $[(\text{Cu}(\text{OMesalen}))_2\text{Gd}(\text{salCOO})_2]\text{NO}_3$ complexes, for which a spin-only formalism can be applied. The $\text{La}(\text{III})$ ion has a $^1\text{S}_0$ ground state and is diamagnetic, while $\text{Gd}(\text{III})$ ion with a ground state $^8\text{S}_{7/2}$ is devoid of first-order angular momentum (see references for 1-D chain compounds described previously).

The thermal dependence of the $\chi_M T$ product for $[(\text{Cu}(\text{OMesalen}))_2\text{La}(\text{salCOO})_2]\text{NO}_3 \cdot 3.75\text{MeOH} \cdot 0.25\text{H}_2\text{O}$ (**37**) complex is plotted in Figure 6.30 (χ_M is the magnetic susceptibility corrected for diamagnetism).

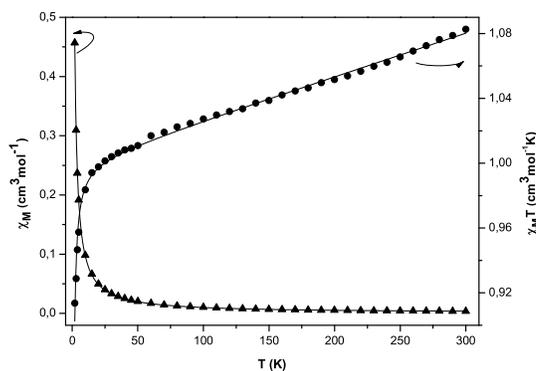


Figure 6.30: Plots of thermal dependence of $\chi_M T$ product (black filled circles) and χ_M (empty rhombus) for $[(\text{Cu}(\text{OMesalen}))_2\text{La}(\text{salCOO})_2]\text{NO}_3 \cdot 3.75\text{MeOH} \cdot 0.25\text{H}_2\text{O}$ (**37**) complex measured with an applied magnetic field of 2000 Oe; the solid line represents the theoretical curve derived from Bleaney Bowers equation for a pair of copper atoms.

The temperature dependence of $\chi_M T$ vs T is characteristic for a weak antiferromagnetic interaction between the two copper ions since no maximum was observed in the thermal variation of $\chi_M T$ over 300-2 K temperature range. A simulation of the magnetic data can be performed on the basis of a spin-only expression developed by Bleaney-Bowers for a pair of copper ions²⁵⁶ based on the spin Hamiltonian:

$$\hat{H} = -J_{CuCu} S_{Cu1} S_{Cu2}$$

$$\chi_M T = \frac{2N\beta^2 g^2}{kT} \frac{1}{3 + \exp(-J/kT)} + \chi_{TIP} \quad (13a)$$

where, χ_{TIP} is the temperature independent paramagnetism.

The resulting values of the parameters are: $J_{CuCu} = -0.50 \pm 0.01 \text{ cm}^{-1}$ for $g_{Cu} = 2.31 \pm 0.001$ with $\chi_{TIP} = 2.7 \cdot 10^{-4} \pm 6.4 \cdot 10^{-6} \text{ cm}^3 \text{ mol}^{-1}$ with a reliability factor $R^2 = 0.99369$. The small negative value of the coupling constant (J_{CuCu}) describes a very weak antiferromagnetic exchange interaction that occurs between the terminal copper ions at low temperature and it is illustrated by the decrease of $\chi_M T$ value from $1.08 \text{ cm}^3 \text{ mol}^{-1} \text{ K}$ at 300 K to around $0.91 \text{ cm}^3 \text{ mol}^{-1} \text{ K}$ at 2 K. This weak antiferromagnetic coupling is a consequence of large copper-copper interatomic separation of around 687.9 pm and, therefore the predominant magnetic interaction in trinuclear complexes of type $[(\text{Cu}(\text{OMesalen}))_2 \text{Ln}(\text{salCOO})_2] \text{NO}_3 \cdot \text{MeOH} \cdot \text{H}_2\text{O}$ is determined by magnetic coupling of the lanthanide ion with the two copper ions.

In the case of $[(\text{Cu}(\text{OMesalen}))_2 \text{Gd}(\text{salCOO})_2] \text{NO}_3 \cdot 2\text{MeOH} \cdot 0.25\text{H}_2\text{O}$ (**34**) complex, the temperature dependence of the $\chi_M T$ product is depicted in Figure 6.31 (χ_M is the magnetic susceptibility corrected for diamagnetism). The $\chi_M T$ value at 300 K is $9.72 \text{ cm}^3 \text{ mol}^{-1} \text{ K}$, which is higher than calculated value ($8.63 \text{ cm}^3 \text{ mol}^{-1} \text{ K}$) for three uncoupled ions (2 Cu^{II} with $S = 1/2$ and Gd^{III} with $S = 7/2$). On lowering the temperature, the $\chi_M T$ values increase constantly reaching a maximum of $13.05 \text{ cm}^3 \text{ mol}^{-1} \text{ K}$ at 5 K and drops to around $12.59 \text{ cm}^3 \text{ mol}^{-1} \text{ K}$ at 2 K. The maximum value observed at 5 K is indicative of ferromagnetic interaction between copper and gadolinium metal centers and it also confirms the ground state $S = 9/2$ of the $[\text{Cu}_2 \text{Gd}]$ triad, in which the local spins are aligned parallel (calculated $\chi_M T$ is $12.40 \text{ cm}^3 \text{ mol}^{-1} \text{ K}$).

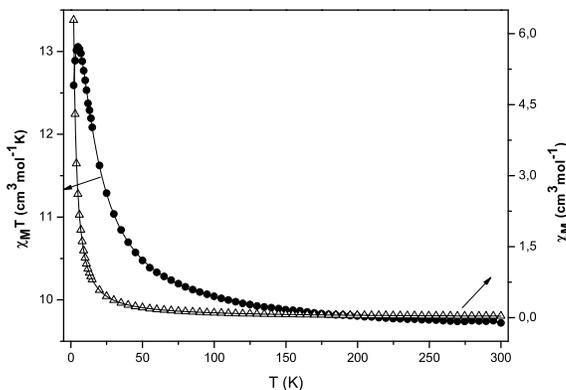


Figure 6.31: Plots of thermal dependence of $\chi_M T$ product (black filled circles) and χ_M (empty rhombus) for $[(\text{Cu}(\text{OMesalen}))_2\text{Gd}(\text{salCOO})_2]\text{NO}_3 \cdot 2\text{MeOH} \cdot 0.25\text{H}_2\text{O}$ (**34**) complex measured with an applied magnetic field of 2000 Oe; the solid line represents the theoretical curve derived from equation.

The analysis of the magnetic properties of $[(\text{Cu}(\text{OMesalen}))_2\text{Gd}(\text{salCOO})_2]\text{NO}_3 \cdot 2\text{MeOH} \cdot 0.25\text{H}_2\text{O}$ complex is based on the spin-only hamiltonian which takes into account the intramolecular interaction in the $[\text{Cu}_2\text{Gd}]$ triad and assuming that the two copper ions are equivalent for the sake of simplicity.

$$\hat{H} = -2J_{\text{CuGd}}S_{\text{Cu}}S_{\text{Gd}} - J'_{\text{CuCu}}S_{\text{Cu}}S_{\text{Cu}}$$

J_{CuGd} and J_{CuCu} describe the magnitude of the magnetic interaction between Cu^{II} - Gd^{III} and $\text{Cu}^{\text{I}}-\text{Cu}^{\text{II}}$. The energies $E(S, S')$ of low-lying spin states are expressed as: $E(9/2, 1) = 0$; $E(7/2, 1) = 4.5J_{\text{CuGd}}$, $E(7/2, 0) = 3.5J_{\text{CuGd}} + J'_{\text{CuCu}}$ and $E(5/2, 1) = 8J_{\text{CuGd}}$; where $(7/2, 1)$ and $(7/2, 0)$ refer to the states resulting from the coupling of S_{Gd} with $S' = 1$ and 0 as the intermediate spin obtaining by coupling of two S_{Cu} .

The resulting equation for the magnetic susceptibility as a function of T , the two J parameters, g and including a paramagnetic impurity (ρ) is the following:

$$\chi_M T = \frac{N\beta^2 g^2 T}{k(T - \theta)} \frac{A}{B} + \frac{63N\beta^2 g^2}{4kT} + \chi_{\text{TIP}} \quad (16)$$

$$A = 165 + 84\exp(-4.5J/kT) + 84\exp(-3.5J + J'/kT) + 35\exp(-8J/kT)$$

$$B = 5 + 4\exp(-4.5J/kT) + 4\exp(-3.5J + J'/kT) + 3\exp(-8J/kT)$$

J is J_{CuGd} and J' is J_{CuCu} coupling constants, g is the average of g_{Cu} and g_{Gd} value in order to avoid overparametrization and θ represents the Weiss constant which accounts for intermolecular coupling. The best fit of the experimental data has been obtained considering the $J_{CuCu} = 0 \text{ cm}^{-1}$, resulting the following values: $J_{CuGd} = 4.12 \pm 0.02 \text{ cm}^{-1}$ for $g_{av} = 2.12 \pm 0.0009$ with $\chi_{TIP} = 2.0 \cdot 10^{-6} \text{ cm}^3 \text{ mol}^{-1}$ for a paramagnetic impurity $\rho = 0.06 \pm 0.003$ and a Weiss constant $\theta = -0.15 \pm 0.002 \text{ K}$. The reliability factor $R^2 = 0.99996$ shows a good agreement between experimental and calculated values. If the data set is fitted varying also the J_{CuCu} parameter, the J_{CuGd} coupling constant varied little ($J_{CuGd} = 4.18 \pm 0.04 \text{ cm}^{-1}$) for a $J_{CuCu} = -0.58 \pm 0.33 \text{ cm}^{-1}$, value close to one found for the $[(\text{Cu}(\text{OMesalen}))_2\text{La}(\text{salCOO})_2]\text{NO}_3 \cdot 3.75\text{MeOH} \cdot 0.25\text{H}_2\text{O}$ (**37**) complex with the other parameters having the following values: $g_{av} = 2.11 \pm 0.002$, $\chi_{TIP} = 62.0 \cdot 10^{-5} \text{ cm}^3 \text{ mol}^{-1}$ for a paramagnetic impurity $\rho = 0.05 \pm 0.006$ and a Weiss constant $\theta = -0.15 \pm 0.003 \text{ K}$ ($R^2 = 0.99996$). The two sets of values do not differ very much, and owing to large Cu...Cu separation, the J_{CuCu} is very small and can be ignored. This is also in agreement with a Cu-Gd-Cu angle close to 180° , which is a structural parameter indicative of low magnitude magnetic interaction between the terminal copper centers.

Additional information may be gained from the magnetization measurements performed as field dependence at 2 K (Figure 6.32). The field dependence (H) of the magnetization (M) is similar to reported trinuclear $\text{Cu}_2^{\text{II}}\text{Gd}^{\text{III}}$ complexes with the [CuGd] pairs of the triad core coupled ferromagnetically. The best fit has been obtained using the Brillouin function for $g_{av} = 2$, resulting in a ground state $S_T = 4.61 \pm 0.002$, very close to expected $S_T = 9/2$.

The magnitude of the Cu-Gd magnetic interaction is close to magnetic interactions reported for similar trinuclear [Cu₂Gd] complexes when, the two copper ions are non-magnetically or weakly antiferromagnetically coupled.^{301,319} This may be a consequence of relatively large dihedral angle formed by two μ_2 -phenoxy bridged halves (i.e O-Cu-O

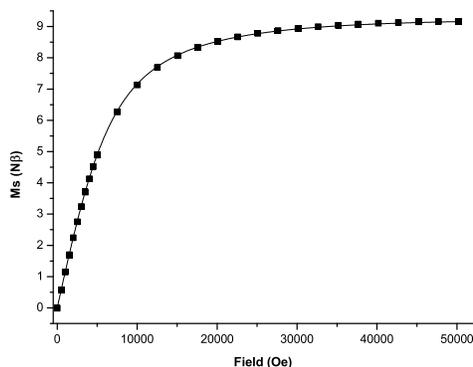


Figure 6.32: Field dependence of the magnetization of complex $[(\text{Cu}(\text{OMesalen}))_2\text{Gd}(\text{salCOO})_2]\text{NO}_3\cdot\text{MeOH}\cdot\text{H}_2\text{O}$ (**34**) complex measured at 2 K (black filled squares represent the experimental value; the solid line shows the theoretical curve generated using the Brillouin equation for $g_{av} = 2.00$ and $S = 4.614 \pm 0.002$).

and O–Gd–O) of around 27.6 and 26.8° . The bending of the CuO_2Gd core is similar to one found in the one-dimensional $[\text{CuGd}]$ chain and, it can be concluded that both bridging organic ligands cause a similar bending effect of the magnetic interacting core. The important role of this dihedral angle, as determinant of the magnitude of the magnetic interaction is well documented and it has been established that values larger than 40° change the Cu–Gd interaction from ferromagnetic to antiferromagnetic.³¹²

The cases of complexes $[(\text{Cu}(\text{OMesalen}))_2\text{Eu}(\text{salCOO})_2]\text{NO}_3\cdot\text{MeOH}\cdot\text{H}_2\text{O}$ (**38**) complex, $[(\text{Cu}(\text{OMesalen}))_2\text{Sm}(\text{salCOO})_2]\text{NO}_3\cdot 2.5\text{MeOH}\cdot\text{H}_2\text{O}$ (**35**) complex and $[(\text{Cu}(\text{OMesalen}))_2\text{Pr}(\text{salCOO})_2]\text{NO}_3\cdot 3\text{MeOH}\cdot 0.25\text{H}_2\text{O}$ (**36**) complexes are more complicated from a magnetic point of view. The magnetic properties of 3d-4f compounds, in which the lanthanide ion possesses first-order angular momentum are based on two phenomena: the thermal depopulation of the Stark sublevels of 4f ion and the exchange interaction between the constituent paramagnetic centers. For Pr(III) ion, the ground state is well separated from the first excited state and its contribution to the magnetic susceptibility in trinuclear $[(\text{Cu}(\text{OMesalen}))_2\text{Pr}(\text{salCOO})_2]\text{NO}_3\cdot 3\text{MeOH}\cdot 0.25\text{H}_2\text{O}$ complex is $1.60 \text{ cm}^3\text{mol}^{-1}\text{K}$ for $g_J = 4/5$.^{10,321} The thermal dependence of magnetic susceptibility in form of χ_M and $\chi_M T$ vs T plots are shown in Figure 6.33. At 300 K, the $\chi_M T$ value is around 2.70

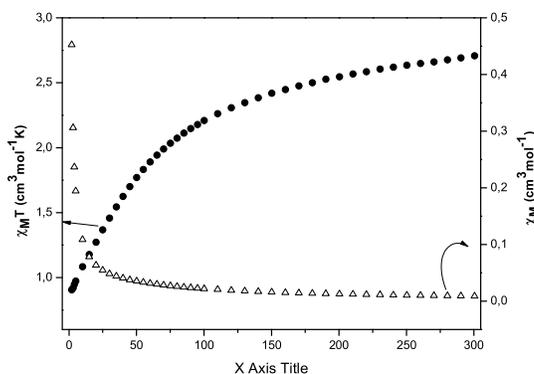


Figure 6.33: Plots of thermal dependence of $\chi_M T$ product (black filled circles) and χ_M (empty rhombus) for $[(\text{Cu}(\text{OMesalen}))_2\text{Pr}(\text{salCOO})_2]\text{NO}_3 \cdot 3\text{MeOH} \cdot 0.25\text{H}_2\text{O}$ (**36**) complex measured with an applied magnetic field of 2000 Oe.

$\text{cm}^3\text{mol}^{-1}\text{K}$, which is a little bit higher than calculated value ($2.35 \text{ cm}^3\text{mol}^{-1}\text{K}$). On lowering the temperature, the $\chi_M T$ decreases constantly reaching a value of $0.90 \text{ cm}^3\text{mol}^{-1}\text{K}$ at 2 K (Fig. 6.33).

In the case of Eu(III) and Sm(III) ions, the energy separation between the ground state and first excited state is very small (300 cm^{-1} for Eu(III) and 200 cm^{-1} for Sm(III)) and therefore, the first excited state is populated at room temperature. For Eu^{III} ion, the ground state ${}^7\text{F}_J$ is split by spin-orbit coupling into seven excited states and, thus the magnetic susceptibility of the ground state is a sum of orbital and spin contribution. the high-temperature limit $(\chi_m T)_{HT}$ would be according with the equation:

$$\chi_M T = \frac{N\beta^2 g^2}{3k} (g_L^2 L(L+1) + g_S^2 S(S+1)) \quad (g_L = 1, g_S = 2) \quad (17)$$

around $4.50 \text{ cm}^3\text{mol}^{-1}\text{K}$.¹⁰ The measured $\chi_M T$ value for $[(\text{Cu}(\text{OMesalen}))_2\text{Eu}(\text{salCOO})_2]\text{NO}_3 \cdot \text{MeOH} \cdot \text{H}_2\text{O}$ (**38**) complex is around $2.81 \text{ cm}^3\text{mol}^{-1}\text{K}$ at 300 K (Figure 6.34, top plot), much higher than expected one. Indeed, Kahn *et al* reported that high limit value of magnetic susceptibility is not to be reached in europium-containing complexes due to population of the three low-lying states at high temperature. The decrease of temperature values cause an almost linear decrease of the $\chi_M T$ values reaching a value of $1.14 \text{ cm}^3\text{mol}^{-1}\text{K}$ at 3 K.

Similar situation was observed for magnetic data sets for $[(\text{Cu}(\text{OMesalen}))_2\text{Sm}(\text{salCOO})_2]\text{NO}_3 \cdot 2.5\text{MeOH} \cdot \text{H}_2\text{O}$ (**35**) complex (Figure 6.34, bottom plot). The χ_T values are decreasing constantly on lowering the temperature from $1.45 \text{ cm}^3\text{mol}^{-1}\text{K}$ at 300 K to $0.69 \text{ cm}^3\text{mol}^{-1}\text{K}$ at 2 K. Sm(III) ion with a $6\text{H}_{5/2}$ ground state has a magnetic susceptibility contribution of around $0.09 \text{ cm}^3\text{mol}^{-1}\text{K}$ ($g_J = 2/7$) and this value is reached only at very low temperatures. This peculiarity is observed for the magnetic behavior of $[(\text{Cu}(\text{OMesalen}))_2\text{Sm}(\text{salCOO})_2]\text{NO}_3 \cdot 2.5\text{MeOH} \cdot \text{H}_2\text{O}$ (**35**) complex for which a linear decrease of $\chi_M T$ value is observed from 300 K to 20 K ($\chi_M T = 1.02 \text{ cm}^3\text{mol}^{-1}\text{K}$ at 20 K) and abruptly below this temperature.

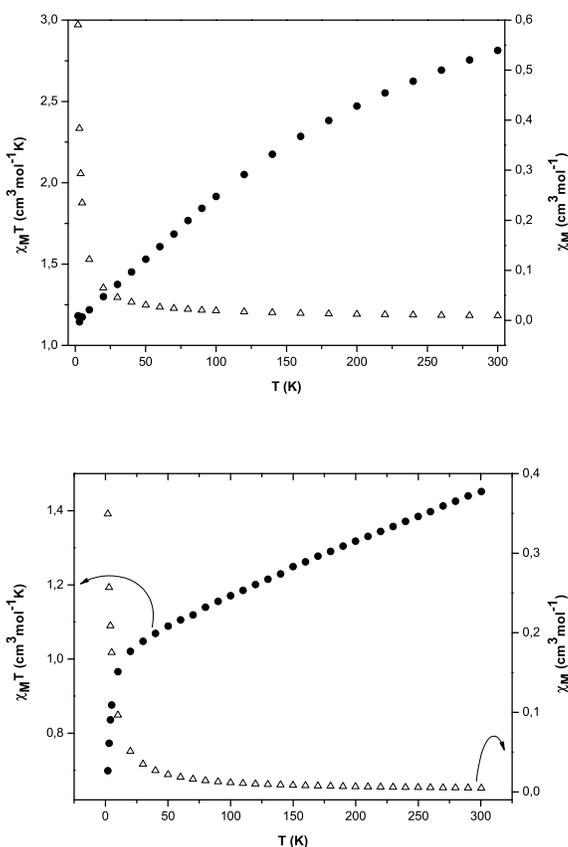


Figure 6.34: Plots of thermal dependence of $\chi_M T$ product (black filled circles) and χ_M (empty rhombus) for $[(\text{Cu}(\text{OMesalen}))_2\text{Eu}(\text{salCOO})_2]\text{NO}_3 \cdot \text{MeOH} \cdot \text{H}_2\text{O}$ (**38**) complex (top plot) and $[(\text{Cu}(\text{OMesalen}))_2\text{Sm}(\text{salCOO})_2]\text{NO}_3 \cdot 2.5\text{MeOH} \cdot \text{H}_2\text{O}$ (**35**) complex (bottom plot) measured with an applied magnetic field of 2000 Oe.

6.3 Conclusions and future perspectives

In conclusion, one-dimensional chains and oligo-trinuclear heterometallic complexes could be isolated using Cu-*salen type* precursor as "complex-ligand". The structural studies show that μ_2 -phenoxo bridged [CuLn] core is successful building block for synthesizing polymeric coordination compounds. Due to high anisotropy associated with the majority of the lanthanide ions, such d-f topologies are most appealing for constructing extended architectures with interesting magnetic properties. Trinuclear [Cu₂Ln] complexes have been isolated using salicylic acid as capping and bridging ligand, whereas 1-D chains were isolated in the case of pyrazine 2,3-dicarboxylic acid co-ligand. The major difference between the two bridging ligands, e.g. pyrazine 2,3-dicarboxylic acid and salicylic acid, resides from their coordination mode. In 1-D chain compounds, the polydentate ligand substitutes only two bidentate nitrate ligands of the classical [Cu(OMesalen)Gd(NO₃)₃] dinuclear complexes, whereas the salicylic acid co-ligand leads to a total replacement of the nitrate anion ligands but maintaining the decahedron arrangement of the lanthanoid center. Polymeric 1-D chains have been isolated for lanthanide ions placed before and after gadolinium ion in the periodical table and by contrast, the salicylic acid made possible the isolation of heterotrinary compounds only for lanthanide ions comprising lanthanum to gadolinium ions. For both types of d-f coordination compounds, the magnetic behavior was found to be very similar, owing to close value of the dihedral angle formed by the phenoxy-bridged copper(II)-lanthanide(III) planes. One-dimensional [CuLn] chains formed with polydentate pyrazine 2,3-dicarboxylic acid as bridging ligand represent rare examples of such extended architectures with d-f topology. The resulting polymers of type [Cu(OMesalen)Ln(NO₃)(Pyr(COO)₂)]_n·(DMF)_n are formed by alternating pairs of Cu···Ln and Ln···Ln through polydentate bridging ligand yielding an infinite zigzag chain. The magnetic properties of these 1-D chains are determined by the Cu–Ln magnetic coupling of the constituting heterodinuclear entities. On the other hand, the magnitude of the magnetic interaction is strongly dependent upon the bending of the CuO₂Gd core (see equation 10), namely the dihedral angle formed by O–Cu–O and O–Gd–O halves. Therefore, the spacer of the starting compartmental *salen-type* ligand plays a key role in inducing a stronger magnetic coupling between the param-

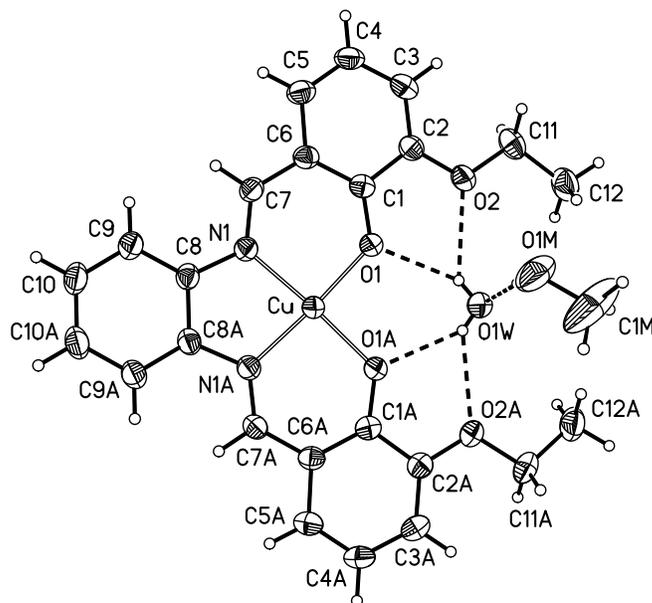


Figure 6.35: Molecular structure and numbering scheme atoms in $[\text{Cu}(\text{o-OEtPhsalph})]\cdot\text{H}_2\text{O}\cdot\text{MeOH}$ (**39**) complex. Thermal ellipsoids are drawn at 50% probability. Dashed lines represent hydrogen bonding interactions.

agnetic centers. Aromatic frameworks are known as best mediators of the magnetic interaction and magnetic exchange interaction through extended π -conjugated aromatic system is well documented. Organic frameworks that contain a π -conjugated spacers have been reported able of mediating the magnetic interaction between the paramagnetic centers, even when the constituting metal ions are very well separated. Therefore, the Cu-*salen* type precursor $[\text{Cu}(\text{o-OEtPhsalph})]\cdot\text{H}_2\text{O}\cdot\text{MeOH}$ (**39**) (Figure 6.35) might be a good starting material for designing 1-D polymeric chains with d-f topology. The copper ions maintain the classical O_2N_2 position in the inner compartment of the bis(2-hydroxy-3-ethoxy-benzylidene)-o-phenylene diamine ligand in a square-planar environment. The mean deviation of the copper atom from the ligand plane is only 10 pm, which shows a good planarity. The complex crystalize with a water molecule as solvent of crystallization that is hosted in the outer compartment of the *salen*-type ligand by hydrogen bonding interaction with both pairs of phenoxy and ethoxy oxygen atoms ($\text{O1w}\cdots\text{O1}$ 279.8 pm and $\text{O1w}\cdots\text{O2}$ 287.5 pm). In addition, methanol as cocrystallized solvent completes the hydrogen bonding network establishing hydrogen bonding contacts with the water molecule through the hydroxyl group ($\text{O1w}\cdots\text{O1M}$ 278.2 pm).

Table 6.14: Selected bond lengths (pm) and angles ($^{\circ}$) for complex **39**.

Cu–O1	192.72(16)	Cu–N1	195.3(2)
O1–Cu–O1A	90.89(10)	O1–Cu–N1	93.04(8)
O1–Cu–N1A	175.91(7)	O1A–Cu–N1	175.91(7)
O1–Cu–N1	93.04(8)	N1–Cu–N1	83.04(12)

The relevance of this *Cu-salen type* precursor in constructing extended architectures with d-f topology is supported by reports of discrete heterodinuclear [CuGd] complex which confirm this supposition.³²⁹ The dihedral angle formed by the two halves is around 4.1° , one of the smallest bending of CuO_2Gd core reported up to now in heterometallic [CuLn] complexes. Kahn et al. proposed that the exchange coupling reaches a maximum value for the Cu(II)-Gd(III) exchange interaction in co-planar arrangement of the O–Cu–O and O–Gd–O planes.³¹⁷ Therefore, the magnetic interaction within the constituting entities of the polymeric chains are expected to be increased when such an organic framework is used.

Owing to the difficulties in analyzing the magnetic properties of heterometallic d-f complexes that involve Ln(III) ions, other than gadolinium ion, an empirical approach has been developed.⁴¹⁵ This is based on comparison of the magnetic susceptibilities of [Cu^{II}Ln^{III}] complexes with isostructural [Ni^{II}Ln^{III}] complexes which involves diamagnetic Ni^{II} ions and assuming the Ln^{III}-Ln^{III} negligible. Therefore, the isostructural Ni^{II}-salen type precursor -[Ni(o-OEtPhsalph)]·H₂O (**40**) has also been isolated. The molecular structure determination is shown in Figure 6.36 and shows a square-planar environment for Ni^{II} ion, accommodated in the inner pocket of the salen-type ligand, similarly to copper ion in [Cu(o-OEtPhsalph)] (**39**) complex. Selected bond lengths and angles for complex **40** are listed in Table 6.15.

The mean deviation of the Ni^{II} from the ligand plane is around 9 pm, similarly to corresponding copper(II) ion in isostructural copper complex **39**. Complex **40** crystallizes with a water molecule as solvent of crystallization, which as previously described is hosted by hydrogen bonding interactions in the outer O₂O₂ shell of the compart-

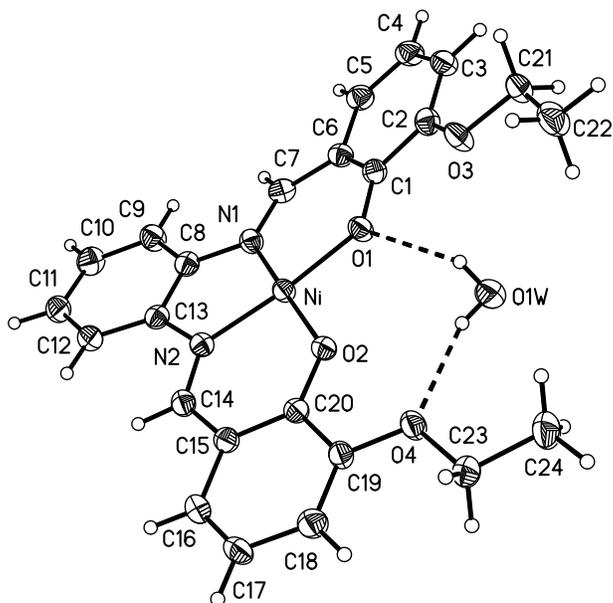


Figure 6.36: Molecular structure and numbering scheme atoms in $[\text{Ni}(\text{o-OEtPhsalph})]\cdot\text{H}_2\text{O}$ (**40**) complex. Thermal ellipsoids are drawn at 50% probability. Dashed lines represent hydrogen bonding interactions.

mental bis(2-hydroxy-3-ethoxy-benzylidene)-o-phenylene diamine ($\text{O1w}\cdots\text{O1}$ 300.2 pm, $\text{O1w}\cdots\text{O4}$ 292 pm). Nevertheless, when polydentate bridging ligands are used to construct coordination polymers, the Zn^{II} -containing precursor is more appropriate. This is because, according to the nature of the bridging units, modification of the coordination geometry of Ni^{II} ion in the precursor changes its magnetic properties.

Table 6.15: Selected bond lengths (pm) and angles ($^\circ$) for complex **40**.

Ni–O1	185.78(14)	Ni–O2	184.87(14)
Ni–N1	186.11(18)	Ni–N2	185.74(17)
O2–Ni–O1	85.13(6)	O2–Ni–N1	174.75(7)
O2–Ni–N2	94.96(7)	O1–Ni–N1	94.95(7)
N2–Ni–O1	172.87(7)	N2–Ni–N1	85.61(8)

The design of polynuclear complexes with predictable magnetic interaction is still a challenging area for inorganic chemists. Ferromagnetic interaction, caused by a parallel alignment of the electrons, has been rationalized to be created by orthogonal orientation of the magnetic orbitals and/or by spin-polarization effects.^{10,416,417} The spin polarization mechanism appears when the metal ions are linked by a meta-substituted aromatic system. In this case, the intramolecular ferromagnetic interaction can be propagated throughout molecule due to topologically networked $d\pi$ spins to the ligand $p\pi$ orbitals.^{416,417,417} Thus, substituted m-phenylene ligands have been reported as ferrocouplers between first-row transition metals. Therefore, salen-type ligand based on m-phenylene diamine spacer might show interesting features. On going from ortho-phenylene diamine spacer to meta-phenylene derivatives, the bis(2-hydroxy-3-methoxy-benzylidene)-m-phenylene diamine salen-type ligand yield a dinuclear copper(II) complex **41** (Figure 6.37). The *salen-type* ligand bridges and accommodates two Cu^{II} ions, resulting in a centrosymmetric $[\text{Cu}(\text{m-OMePhsalph})]_2 \cdot 2\text{H}_2\text{O}$ complex. Each Cu^{II} ion has an N_2O_2 environment in a square-planar geometry (N1-Cu-O1 94.34° and O1-Cu-O3 90.09°). The intramolecular $\text{Cu} \cdots \text{Cu}$ separation is around 741.63 pm, similar with corresponding separation reported for dinuclear $\text{Cu}(\text{II})$ complexes bridged by m-phenylene derivatives. The two m-phenylene rings are ideally parallel to each other with the average interplanar separation 294.6 pm.

An important role is determining the nature of ferro- or antiferro-magnetic interaction between the two copper(II) ions is played by the orientation of the copper basal planes to the benzene rings of the m-phenylene diamine spacer.⁴¹⁶ In complex **41**, the dihedral angle between this two planes is around 47.66° with the two m-phenylene rings in anti-orientation with no π - π interaction (Figure 6.39). Selected bond lengths and angles in complex **41** are listed in Table 6.16. Complex **41** crystallizes with two water molecules as solvents of crystallization which are again hosted through hydrogen bonding interactions in the outer compartment of the bis(2-hydroxy-3-methoxy-benzylidene)-m-phenylene diamine *salen-type* ligand ($\text{O1w} \cdots \text{O1}$ 289.0 pm, $\text{O1w} \cdots \text{O3A}$ 290.4, $\text{O1w} \cdots \text{O2}$ 307.9 pm and $\text{O1w} \cdots \text{O4A}$ 296.8 pm). This hydrogen bonding network is completed by co-crystallized methanol molecules ($\text{O1M} \cdots \text{O1w}$ 111 pm), resulting in a one-dimensional polymer constructed throughout the direction in which the shortest $\text{Cu} \cdots \text{Cu}$ intermolec-

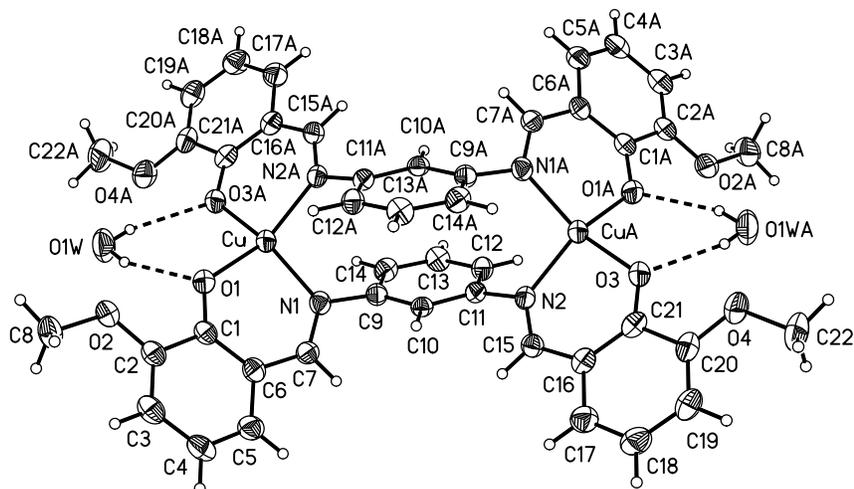


Figure 6.37: Molecular structure and numbering scheme atoms of $[\text{Cu}(\text{m-OMePhsalph})]_2 \cdot 2\text{H}_2\text{O}$ (**41**) complex. Thermal ellipsoids are drawn at 50% probability level. Dashed lines represent hydrogen bonding interactions.

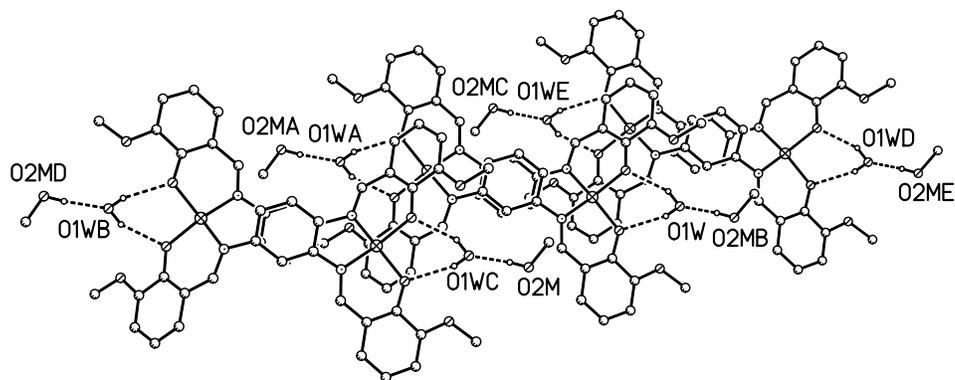


Figure 6.38: Hydrogen bonding interaction in complex **41** showing the formation of the 2-D polymer build up by hydrogen bonding contacts among the solvent molecules. Dashed lines represent hydrogen bonding interactions. Only the heteroatoms of the solvent molecules are numbered.

ular separation is larger than 700 pm (Figure 6.38).

Such a dinuclear copper-precursor may be used to design one-dimensional chains with a $[\text{Cu}_2\text{Ln}_2]$ topology. The magnetic interaction within the constituent entities will take place between the $[\text{CuLn}]$ dimers and, in addition between the copper centers. According with the existing reports for similar dinuclear copper complexes, it seems that such an *anti*-orientation of the two *m*-phenylene rings will mediate a weak antiferromagnetic

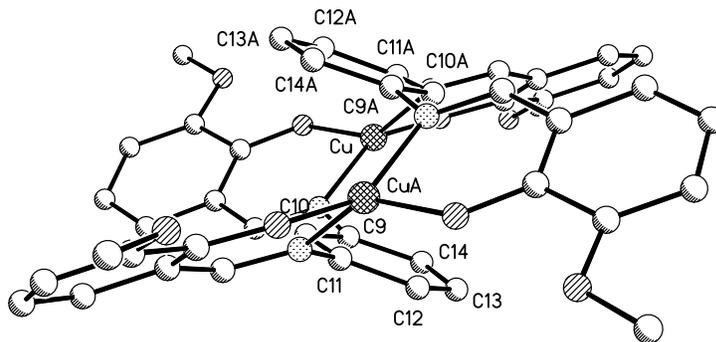


Figure 6.39: Perspective view of molecular structure of complex $[\text{Cu}_2(\text{m-OMe-Phsalen})]_2 \cdot 2\text{H}_2\text{O}$ showing the anti-orientation of the m-phenylene rings. Only the numbering scheme for m-phenylene carbon atoms is shown.

interaction between the copper ions. The orientation of the magnetic orbitals on each metal center relative to the m-phenylene rings plays the crucial role in establishing the final exchange interaction.⁴¹⁸ The ferromagnetic coupling of the copper centers will be favored by a *syn* orientation of the m-phenylene rings which are parallel to each other and π - π stacked (Figure 6.40). Such orientation of the phenylene rings has been found in oxamide-type m-phenylene derivatives with the copper ions coupled ferromagnetically in the 14.56 cm^{-1} to 16.8 cm^{-1} range.^{416,417} An *anti*-orientation of the phenylene rings (Figure 6.39) shadows the spin-polarization effect and leads to an antiferromagnetic coupling of the copper centers.^{416,418}

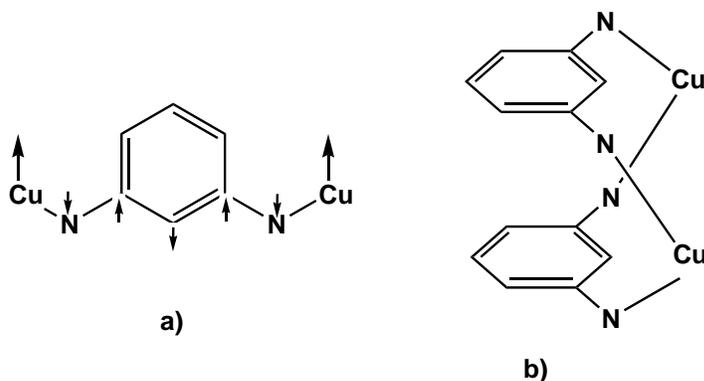


Figure 6.40: Schematic representation of spin polarization effect (inset a) and *syn*-orientation of the m-phenylene rings (inset b) in m-phenylene diamine derivatives copper complexes as sum of effects responsible for ferromagnetic coupling of copper sites.

Table 6.16: Selected bond lengths (pm) and angles ($^{\circ}$) for complex **41**.

Cu–O1	189.7(3)	Cu–O3	190.5(2)
Cu–N1	196.1(3)	Cu–N2	197.2(3)
O1–Cu–O3	90.09(11)	O1–Cu–N1	94.34(11)
O1–Cu–N2	144.56(11)	O3–Cu–N1	150.17(12)
O3–Cu–N2	93.14(11)	N1–Cu–N2	99.98(12)

The "complex as ligand" approach is so far the best strategy to design heteronuclear compounds. The precursor-complex should contain potential donor groups able of binding another metal ion. Besides, salen-type ligands, bis(2-pyridylcarbonyl)amine ligand (Hbpca) is a versatile organic framework for isolation of heteronuclear species and/or supramolecular assemblies.^{159,204,205} The Cu-precursor complex is isolated by hydrolysis of 2,4,6-tris-2-pyridin s-triazine ligand^{157–162} by $\text{Cu}(\text{NO}_3)_2 \cdot 3\text{H}_2\text{O}$ when through one-pot reaction, mononuclear Cu-complex of type $[\text{Cu}(\text{bcpa})(\text{OH}_2)_2]\text{NO}_3 \cdot \text{MeOH}$ is obtained (see Figure 6.41). This anionic copper complex has been used to design a large variety of molecular assemblies that range from oligo-heteronuclear species to one-dimensional coordination polymers with d-d topology.^{159,204,205} The copper ion is five-coordinated in a distorted trigonal bipyramidal geometry. The N1–Cu–N2 and N1–Cu–O2w angles are around 163.9 and 157.5 $^{\circ}$ with the Cu–N bond distances within the 193.9–199.7 pm range (see table 6.17).

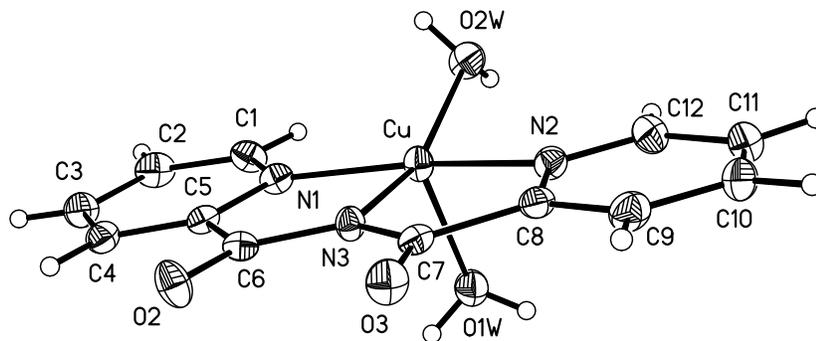


Figure 6.41: Molecular structure and numbering scheme atoms in anionic complex $[\text{Cu}(\text{bcpa})(\text{OH}_2)_2]\text{NO}_3 \cdot \text{MeOH}$ (**42**).

Table 6.17: Selected bond lengths (pm) and angles ($^{\circ}$) for complex **42**.

Cu–N1	199.73(18)	Cu–N2	199.49(18)
Cu–N3	193.96(17)	Cu–O1W	224.05(17)
Cu–O2W	196.79(17)	-	-
N1–Cu–N2	163.89(7)	N1–Cu–N3	81.87(7)
N1–Cu–O1W	90.63(7)	N1–Cu–O2W	98.56(7)
N3–Cu–N2	82.04(7)	N3–Cu–O1W	110.48(7)
N3–Cu–O2W	157.53(8)	N2–Cu–O1W	95.64(7)
N2–Cu–O2W	96.04(7)	O1W–Cu–O2W	91.99(8)

The interesting feature of this complex is represented by labile coordination positions of the copper centers which are occupied by solvent molecules and may be used towards isolation of new molecular assemblies. In instance, salicylic acid co-ligand substitutes one of the solvent molecule yielding the copper-precursor [Cu(bcpa)(salCOO)H₂O] (**43**) (Figure 6.42). The copper ion maintains the N₃O₂ environment with Cu–N and Cu–O bond lengths that range from 193.2 to 231.7 pm, comparable to bond distances reported in analogous Cu–bpca complexes. Selected bond lengths and angles in complex **43** are given in Table 6.18. The salicylic acid is involved in intra- and inter-molecular hydrogen bonding interaction, whereas the enolized amide and carbonyl functionalities create a hydrogen bonded dimeric structure (Figure 6.43). This new precursor has two dissimilar cavities, resulting in a rich oxygen-donor environment appropriate to accommodate lanthanide ions due to their known oxophilicity. Lanthanide ions can be accommodate by the salicylic acid and the two carbonyl-type groups resulting, most likely in polymeric assemblies. On the other hand, taking advantage of the presence of dissimilar cavities, complex **43** may be used as molecular brick in design of coordination polymers containing two or three different metal ions. In addition, the magnetic interaction between Cu(II)-Ln(III) ions is expected to be stronger if the lanthanide ion is coordinated *via* bidentate chelating carbonyl sites, due to the magnetic orbital of the copper ion placed on its basal plane.

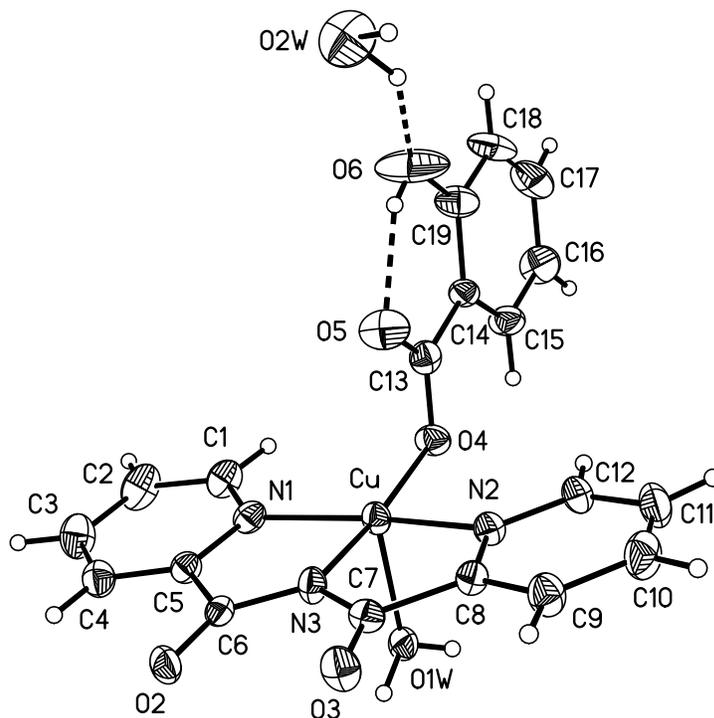


Figure 6.42: Molecular structure and numbering scheme atoms in complex **43**. Dashed lines represent intramolecular hydrogen bonding interactions.

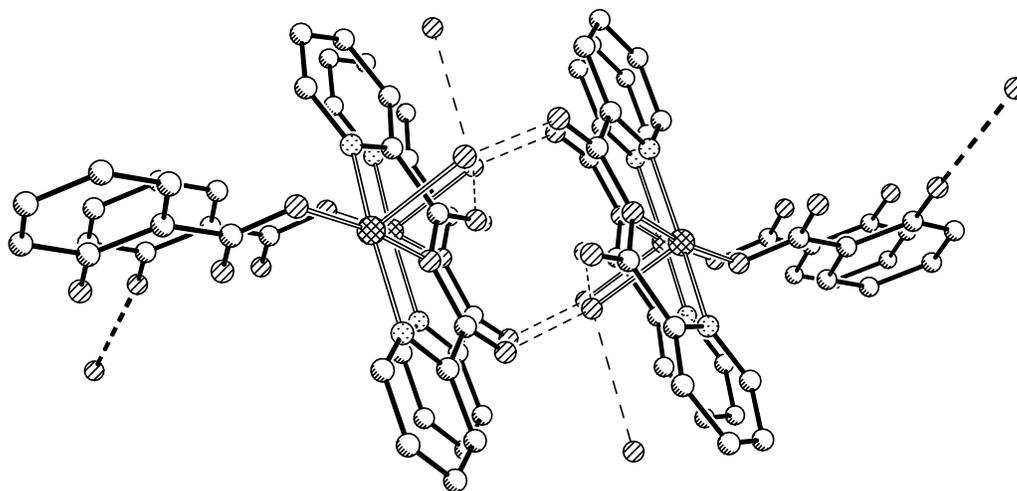


Figure 6.43: Hydrogen bonding interaction in complex **43** as viewed along the b axis. Dashed lines represent hydrogen bonding interactions.

Replacement of the diamine spacer of the compartmental salen-type ligands with inexpensive hydrazine affords diazine ligands with an =N–N= bridging fragment. Due to the twisting around the single N–N bond, metalhelicates can be isolated as models

Table 6.18: Selected bond lengths (pm) and angles ($^{\circ}$) for complex **43**.

Cu–N1	201.2(2)	Cu–N2	201.6(2)
Cu–N3	193.2(2)	Cu–O4	195.11(18)
Cu–O1W	231.7(2)	O5–C13	125.7(3)
N1–Cu–N2	1623.68(9)	N1–Cu–N3	81.41(9)
N1–Cu–O4	98.90(9)	N1–Cu–O1W	87.77(9)
N3–Cu–N2	81.97(9)	N3–Cu–O4	171.77(9)
N3–Cu–O1W	96.37(9)	N2–Cu–O1W	98.90(9)
O4–Cu–N2	96.84(9)	O4–Cu–O1W	91.85(8)

to understand the helical self-organization processes that occur in nature. The compartmental diazine ligand - N,N'-bis (3-methoxy-salicylidene) hydrazine - has been reacted with $\text{Fe}(\text{NO}_3)_3 \cdot \text{H}_2\text{O}$ salt in methanol solution, using NEt_3 as base yielding the dinuclear iron complex $[\text{Fe}_2(\mu\text{-valhy})_3] \cdot 4\text{DMF}$ (**44**).⁴¹⁹ The molecular structure, shown in Figure 6.44 contains two octahedral Fe(III) centers connected by three diazine =N–N= bridges. Each of the three ligands coordinates the metal center through two phenolate-O and two imine-N atoms, resulting in an N_3O_3 coordination environment for each iron ion. The Fe···Fe separation is around 399.05 pm, value that compares well with intramolecular Fe···Fe separation in analogous complexes.⁴¹⁹ The dinuclear complex is neutral with Fe–O bond distances in the 191.3–193.1 pm range consistent with the 3+ oxidation state of the iron metal. Selected bond lengths and angles in complex **44** are listed in Table 6.19. The complex crystallizes in the triclinic P-1 space group with the asymmetric unit containing one full complex molecule with a triple-helicate motif. The helical twist along the N–N bond differs in three ligand moieties with dihedral angles of 50.7, 66.1 and 40.4 $^{\circ}$ and, therefore not identical, hence not an ideal D_{3h} symmetry characteristic for a perfect triple helicate. The complex crystallizes with four DMF molecules which are involved in hydrogen bonding interaction with the donor atoms of the diazine ligands. Complex **44** may be a potential candidate as precursor to synthesize $\text{Fe}_2^{\text{III}}\text{-Ln}^{\text{III}}$ complexes, due to additional free sites able of accommodating lanthanide ions, namely the $-\text{OCH}_3$ arms of the aromatic supporting ligand.

Table 6.19: Selected bond lengths (pm) and angles ($^{\circ}$) for complex **44**.

FeA–O1A	191.4(3)	FeA–O1B	191.7(3)
FeA–O1C	192.3(3)	FeA–N1A	219.5(3)
FeA–N1B	217.6(4)	FeA–N1C	219.0(4)
FeB–O2A	193.1(3)	FeB–O2B	191.3(3)
FeB–O2C	192.5(3)	FeB–N2A	219.9(4)
FeB–N2C	217.6(4)	FeB–N2B	2179.(4)
O1A–FeA–O1B	97.44(13)	O1A–FeA–O1C	95.25(14)
O1A–FeA–N1A	84.00(13)	O1A–FeA–N1B	97.25(14)
O1A–FeA–N1C	168.30(13)	O1B–FeA–O1C	97.18(13)
O1B–FeA–N1B	83.98(13)	O1B–FeA–N1A	169.00(13)
O1B–FeA–N1C	94.21(13)	O1C–FeA–N1A	93.53(13)
O1C–FeA–N1B	167.19(13)	O1C–FeA–N1C	84.27(13)
N1B–FeA–N1A	85.03(13)	N1B–FeA–N1C	82.93(14)
N1C–FeA–N1A	84.36(13)	O2A–FeB–N2A	84.07(13)
O2A–FeB–N2B	166.26(14)	O2A–FeB–N2C	90.85(14)
O2B–FeB–O2A	100.20(13)	O2B–FeB–O2C	96.23(13)
O2B–FeB–N2A	92.91(13)	O2B–FeB–N2B	84.41(13)
O2B–FeB–N2C	168.67(14)	O2C–FeB–O2A	100.26(13)
O2C–FeB–N2A	169.00(13)	O2C–FeB–N2B	92.03(13)
O2C–FeB–N2C	84.14(13)	N2B–FeB–N2A	82.76(13)
N2C–FeB–N2A	85.70(13)	N2C–FeB–N2B	84.26(13)

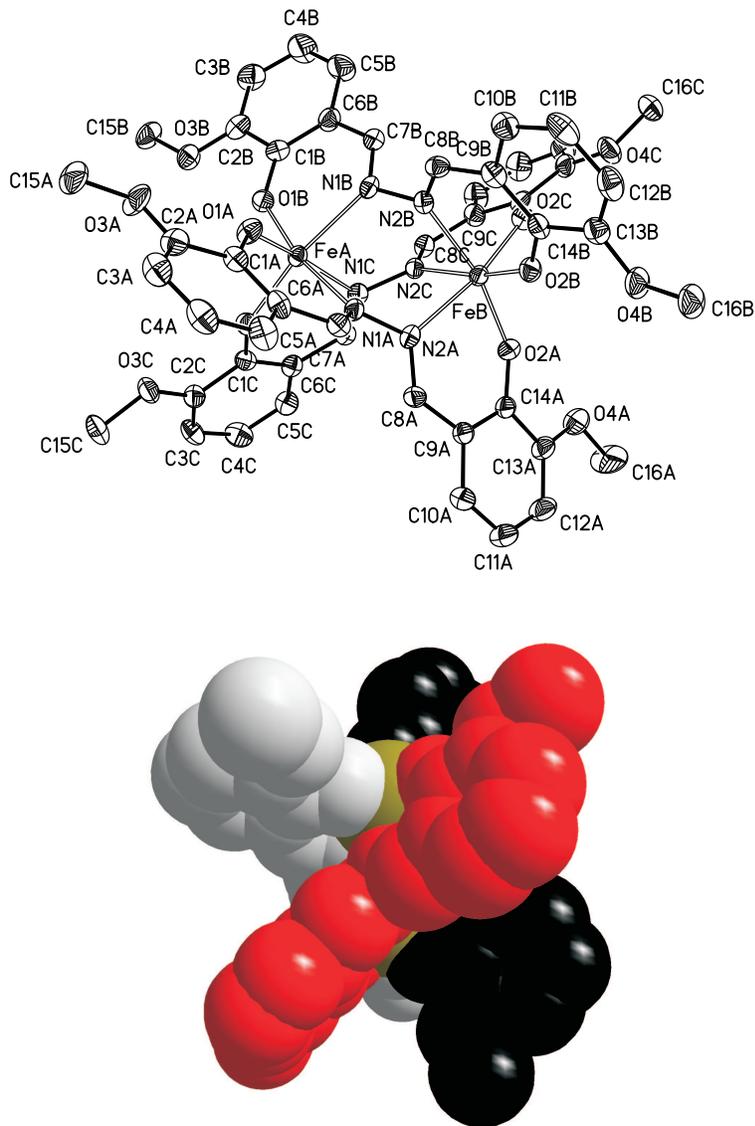


Figure 6.44: Molecular structure and numbering scheme atoms in complex $[\text{Fe}_2(\mu\text{-valhy})_3]\cdot 4\text{DMF}$ (**44**) (up) with hydrogen atoms omitted for clarity and all atoms represented using 50% thermal ellipsoids. The bottom picture shows the space-filling representation of the triple helical structure.

The magnetic behavior of dinuclear iron complex **44** in the 300-2 K temperature range is shown in Figure 6.45 as χ_M and $\chi_M T$ vs. T plots. The high temperature $\chi_M T$ is around $6.80 \text{ cm}^3 \text{ mol}^{-1} \text{ K}$, value higher than expected for two uncoupled high-spin Fe(III) ions. On lowering the temperature, the $\chi_M T$ product decreases gradually reaching a value close to zero at 2 K. The shape of the thermal variation of the $\chi_M T$ product indicates an

antiferromagnetic between the iron ions. Simulation of the magnetic data set has been achieved using the isotropic spin exchange hamiltonian:

$$\hat{H} = -J_{FeFe}S_{Fe1}S_{Fe2}$$

with $S_1=S_2=5/2$.

Considering the energies of the low-lying states and taking into account paramagnetic impurities, the magnetic susceptibility was calculated using equation 6, previously discussed in Chapter 4.

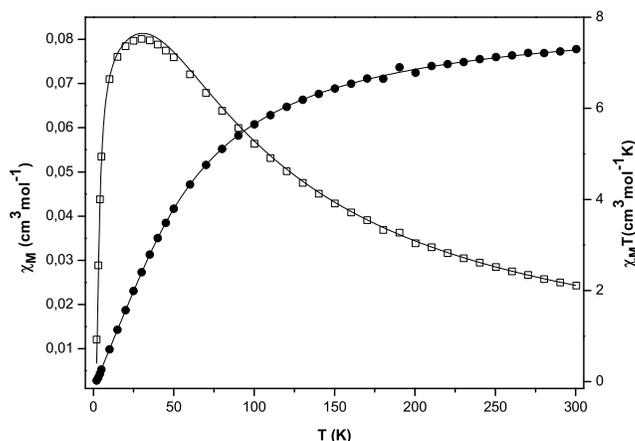


Figure 6.45: Plots of thermal dependence of $\chi_M T$ product (black filled circles) and χ_M (empty squares) for $[\text{Fe}_2(\mu\text{-valhy})_3]\cdot 4\text{DMF}$ (**44**) measured with an applied magnetic field of 2000 Oe. Solid lines represent the simulation of the data set using equation for a pair of iron atoms.

The best fit was obtained for $\chi_M T$ vs T experimental data points and led to $g = 1.93 \pm 0.001$, $J = -7.59 \pm 0.04 \text{ cm}^{-1}$ for a paramagnetic impurity $\rho = 0.002 \pm 0.001$ with reliability factor $R^2 = 0.99988$. The calculated data curve (solid line in Figure 6.45) matches well the experimental magnetic data. The magnitude of the antiferromagnetic interaction is smaller than previous described dinuclear Fe(III) complexes (Chapter 4), but of the same range order with similar homodinuclear iron(III) complexes.⁴¹⁹

It can be concluded that all d-transition metal complexes briefly described herein can be used as precursors to isolate one-dimensional polymers and or oligo-heteropolynuclear

complexes with d-f topology. The most interesting complexes are the Cu(II)-complexes based on bis(2-hydroxy-3-OR-benzylidene)-(o/m)-phenylene diamine ligands, where a small bending of the CuO₂Gd fragment has been reported. Such a polymeric chains are expected to contain a higher magnitude of the magnetic coupling between the copper(II)-lanthanide(III) constituting units. On the other hand, other bridging organic linkers (Figure 6.46) may be successful candidates to replace the pyrazine 2,3-dicarboxylic acid used herein to design coordination polymers.

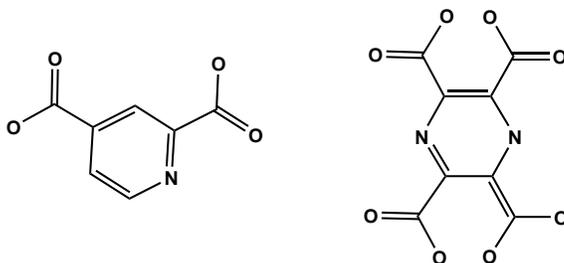


Figure 6.46: Proposed new organic linker compounds able to generate one-dimensional chain with d-f topology.

6.4 Experimental Part

Synthesis of [[Cu(OMesalen)H₂O] precursor (24)

The *salen-type* precursor **23** have been prepared following similar reported procedures: to the *in situ* formed Schiff base ligands (prepared following typical synthesis procedures by condensation of o-vanillin (3.04 g, 0.02 mol) with alkyl-diamine derivatives (0.01 mol) in 2:1 ratio) in methanol solution was added M(II) acetate salt (0.01 mol), followed by addition of water. The resulting solution was stirred at room temperature overnight.[?] Yield: 3.2 g (7.0 mmol, 76.0%). *Anal.* Calc. for C₁₉H₂₂N₂O₅Cu (421.93): C 56.49, H 4.99, N 6.94. Found: C 56.22, H 5.02, N 6.78. Selected IR data (cm⁻¹): 3435 (br, H₂O), 1629 (s, -CH=N).

Synthesis of [Cu(OMesalen)Na(H₂O)]NO₃ (25) complex

To [Cu(OMesalen)H₂O](105 mg, 0.25 mmol) precursor suspended in MeOH (5 mL) was added an aqueous solution (5 mL) of NaNO₃ (21.0 mg, 0.25 mmol), followed by addition of DMF (5 mL) for a total dissolution of reaction components. The resulting solution was stirred at room temperature for 15 minutes, filtered and let standing for slow evaporation of the solvent mixture. Yield: 70.0 mg (0.13 mmol, 52.0%). *Anal.* Calc. for C₂₁H₂₆N₃O₈CuNa (534.98): C 47.15, H 4.90, N 7.85. Found: C 46.66, H 4.27, N 9.10. Selected IR data (cm⁻¹): 3420 (br, H₂O), 1630, 1613 (s, -CH=N), 1384 (s, NO₃).

[Cu(MeOH)(OMesalen)Gd(NO₃)₃] (26) complex

To [Cu(OMesalen)H₂O](210 mg, 0.50 mmol) precursor suspended in MeOH (10 mL) was added a methanol solution of Gd(NO₃)₃·6H₂O (110 mg, 0.25 mmol) followed by addition of a methanol (10 mL) solution formed by salicylic acid (75 mg, 0.50 mmol) and NEt₃ (1.0 mL 1 N methanol solution). The resulting solution was stirred at room temperature for 15 minutes and allowed to stand undisturbed for slow evaporation of the solvent. Crystals suitable for X-ray analyze are obtain within four hours. Yield: 145.0 mg (0.18 mmol, 72.0%). *Anal.* Calc. for C₂₂H₂₈N₅O₁₄CuGd (807.27): C 32.73, H 3.50, N 8.68. Found: C 32.72, H 3.20, N 8.61.

General synthesis pathway used to isolate [Cu(OMesalen)Ln(NO₃)-(Pyr(COO)₂)]_n·(DMF)_n complexes

To a suspension of [Cu(OMesalen)H₂O] precursor complex (105 mg, 0.25 mmol) in MeOH (10 mL) was added stepwise a methanolic solution (5 mL) of Ln(NO₃)₃·6H₂O (0.25 mmol) followed by addition of a methanol (10 mL) solution formed by pyrazine 2,3-dicarboxylic (42 mg, 0.25 mmol) and NEt₃ (0.5 mL 1 N methanol solution). The resulting solution was stirred at room temperature with a precipitate formed within the first 5 minutes of reaction. This was redissolved by addition of DMF (5 mL) and the reaction has been continued for other 10 minutes. After filtration the light green filtrate was allowed to stand at room temperature for slow evaporation of the solvent. Suitable crystals for X-Ray measurement were obtained within a week. Selected IR data (cm⁻¹): 1671 (s, -C=O),

1633 (s, -CH=N), 1569 (s, -CH=N_{pyrazine}), 1384 (s, NO₃).

[Cu(OMesalen)Gd(NO₃)(Pyr(COO)₂)]_n·(DMF)_n (27)

Yield: 137.0 mg (0.16 mmol, 63.4%). *Anal.* Calc. for C₂₈H₃₀N₆O₁₂CuGd (863.36): C 38.95, H 3.50, N 9.73. Found: C 38.69, H 3.52, N 9.85.

[Cu(OMesalen)Dy(NO₃)(Pyr(COO)₂)]_n·(DMF)_n (28)

Yield: 127.0 mg (0.14 mmol, 58.0%). *Anal.* Calc. for C₂₈H₃₀N₆O₁₂CuDy (868.61): C 38.72, H 3.48, N 9.68. Found: C 38.30, H 3.13, N 9.67.

[Cu(OMesalen)Tb(NO₃)(Pyr(COO)₂)]_n·(DMF)_n (29)

Yield: 105.0 mg (0.12 mmol, 48.0%). *Anal.* Calc. for C₂₈H₃₀N₆O₁₂CuTb (865.03): C 38.88, H 3.50, N 9.72. Found: C 38.52, H 3.22, N 9.79.

[Cu(OMesalen)Eu(NO₃)(Pyr(COO)₂)]_n·(DMF)_n (30)

Yield: 109.0 mg (0.13 mmol, 50.8%). *Anal.* Calc. for C₂₈H₃₀N₆O₁₂CuEu (858.07): C 38.19, H 3.52, N 9.79. Found: C 39.09, H 3.47, N 9.95.

[Cu(OMesalen)Sm(NO₃)(Pyr(COO)₂)]_n·(DMF)_n (31)

Yield: 110.0 mg (0.13 mmol, 51.0%). *Anal.* Calc. for C₂₈H₃₀N₆O₁₂CuSm (856.46): C 39.27, H 3.53, N 9.81. Found: C 39.25, H 3.50, N 9.89.

[Cu(OMesalen)Pr(NO₃)(Pyr(COO)₂)]_n·(DMF)_n (32)

Yield: 96.0 mg (0.11 mmol, 45.0%). *Anal.* Calc. for C₂₈H₃₀N₆O₁₂CuPr (847.02): C 39.70, H 3.57, N 9.92. Found: C 39.65, H 3.53, N 10.05.

[Cu(OMesalen)La(NO₃)(Pyr(COO)₂)]_n·(DMF)_n (33)

Yield: 117.0 mg (0.14 mmol, 55.3%). *Anal.* Calc. for C₂₈H₃₀N₆O₁₂CuLa (845.02): C 39.80, H 3.58, N 9.95. Found: C 39.08, H 3.55, N 9.83. Selected IR data (cm⁻¹): 1671 (s, -C=O), 1633 (s, -CH=N), 1569 (s, -CH=N_{pyrazine}), 1384 (s, NO₃).

General synthesis pathway used to isolate trinuclear [(Cu(OMesalen))₂-Ln(salCOO)₂]NO₃·3MeOH·H₂O complexes

To a suspension of [Cu(OMesalen)H₂O] precursor complex (105 mg, 0.25 mmol) in MeOH (10 mL) was added stepwise a methanolic solution (5 mL) of Ln(NO₃)₃·6H₂O (0.125 mmol) followed by addition of a methanol (10 mL) solution formed by salicylic acid (34.5 mg, 0.25 mmol) and NEt₃ (0.5 mL 1 N methanol solution). The resulting solution was stirred at room temperature for 10 minutes. After filtration the green filtrate was allowed to stand at room temperature for slow evaporation of the solvent. Suitable crystals for X-Ray measurement were obtained within a week. Selected IR data (cm⁻¹): 3420 (br, OH_{ass}), 1627 (s, -CH=N), 1473 (s, COO), 1384 (s, NO₃).

[(Cu(OMesalen))₂Gd(salCOO)₂]NO₃·2MeOH·0.25H₂O (34)

Yield: 120.0 mg (0.08 mmol, 68.0%). *Anal.* Calc. for C₅₄H₆₃N₅O₂₁Cu₂Gd (1402.43): C 46.25, H 4.53, N 4.99. Found: C 46.56, H 3.89, N 5.14 ([Cu(OMesalen))₂Gd(salCOO)₂]NO₃·3MeOH·H₂O).

[(Cu(OMesalen))₂Sm(salCOO)₂]NO₃·2.5MeOH·H₂O (35)

Yield: 100.0 mg (0.07 mmol, 57.0%). *Anal.* Calc. for C₅₃H₅₇N₅O₁₉Cu₂Sm (1345.52) ([Cu(OMesalen))₂Sm(salCOO)₂]NO₃·2MeOH): C 46.48, H 4.55, N 5.02. Found: C 47.15, H 4.00, N 5.01.

[(Cu(OMesalen))₂Pr(salCOO)₂]NO₃·3MeOH·0.25H₂O (36)

Yield: 110.0 mg (0.08 mmol, 63.0%). *Anal.* Calc. for C₅₄H_{63.5}N₅O_{21.25}Cu₂Pr (1390.63): C 46.64, H 4.60, N 5.04. Found: C 46.51, H 4.00, N 5.07.

[(Cu(OMesalen))₂La(salCOO)₂]NO₃·3.75MeOH·0.25H₂O (37)

Yield: 114.0 mg (0.08 mmol, 64.0%). *Anal.* Calc. for C₅₄H₆₃N₅O₂₁Cu₂La ([Cu(OMesalen))₂La(salCOO)₂]NO₃·3MeOH·H₂O) (1384.09): C 46.86, H 4.59, N 5.05. Found: C 46.40, H 4.38, N 4.87.

$[(\text{Cu}(\text{OMesalen}))_2\text{Eu}(\text{salCOO})_2]\text{NO}_3 \cdot 3\text{MeOH} \cdot \text{H}_2\text{O}$ (38**)**

Yield: 112.0 mg (0.08 mmol, 62.0%). *Anal.* Calc. for $\text{C}_{54}\text{H}_{63}\text{N}_5\text{O}_{21}\text{Cu}_2\text{Eu}$ (1397.14): C 46.42, H 4.54, N 5.01. Found: C 46.05, H 4.25, N 5.10.

Synthesis of d-transition metal precursor complexes

To a solution of 3-alkoxy-2-hydroxy-benzaldehyde (0.01 mol) and the corresponding phenylene-diamine (350 mg, 5.0 mmol) in methanol (10 mL) was added stepwise a methanolic solution (5 mL) of $\text{M}(\text{OAc})_2 \cdot n\text{H}_2\text{O}$ (5.0 mmol) followed by addition of DMF (5 mL). The resulting clear solution was stirred overnight at room temperature, then filtered and let to stand at room temperature for slow evaporation of the solvents mixture.

$[\text{Cu}(\text{o-OEtPhsalph})] \cdot \text{H}_2\text{O} \cdot \text{MeOH}$ (39**) complex**

This complex has been prepared *in situ* by reaction between 2-hydroxy-3-ethoxy-benzaldehyde (166 mg, 0.01 mol) with o-phenylene diamine copper acetate (1 g, 5 mmol) in methanol, followed by addition of DMF (5 mL) when a clear dark-blue solution is formed. Yield: 1.8 g (4.44 mmol, 88.8%). *Anal.* Calc. for $\text{C}_{18}\text{H}_{20}\text{N}_2\text{O}_5\text{Cu}$ (407.90): C 53.00, H 4.94, N 6.87. Found: C 54.99, H 5.61, N 6.34. Selected IR data (cm^{-1}): 3509 (s, H_2O , MeOH), 1606 (s, $-\text{CH}=\text{N}$).

$[\text{Ni}(\text{o-OEtPhsalph})] \cdot \text{H}_2\text{O}$ (40**) complex**

This complex has been prepared similarly to copper precursor **38**, using nickel acetate (5.0 mmol) in methanol/DMF solution and it has been isolated as red crystals. Yield: 1.4 g (2.92 mmol, 58.4%). *Anal.* Calc. for $\text{C}_{24}\text{H}_{24}\text{N}_2\text{O}_5\text{Ni}$ (479.16): C 60.16, H 5.05, N 5.85. Found: C 60.05, H 5.13, N 5.76. Selected IR data (cm^{-1}): 3552, 3508 (s, H_2O), 1606 (s, $-\text{CH}=\text{N}$).

$[\text{Cu}(\text{m-OMePhsalph})]_2 \cdot 2\text{H}_2\text{O}$ (41**) complex**

Complex **40** has been prepared following the reaction pathway described for complex **38** using -m-phenylene diamine A precipitate relative impure is obtained, whereas 100 mg (0.09 mmol) are isolated as pure material. *Anal.* Calc. for $\text{C}_{48}\text{H}_{56}\text{N}_4\text{O}_{14}\text{Cu}_2$ (1040.06):

C 55.43, H 5.43, N 5.39. Found: C 55.67, H 4.61, N 5.86. Selected IR data (cm^{-1}): 3447 (br, H_2O), 1610 (s, $-\text{CH}=\text{N}$).

[Cu(bcpa)(OH₂)₂]NO₃·MeOH (42) complex

This complex has been prepared by one-pot hydrolysis and complexation of 2,4,6-tris(2-pyridyl)-1,3,5-triazine (78.0 mg, 0.25 mmol) dissolved in MeOH (10 mL) and $\text{Cu}(\text{NO}_3)_2 \cdot 6\text{H}_2\text{O}$ (0.25 mmol), followed by addition of methanol-water solution formed by salicylic acid (34 mg, 0.25 mmol) and NaOH (0.5 mL aqueous solution) when there were obtained 70.0 mg (0.18 mmol, 72.0%).

[Cu(bcpa)(Hsal-COO)(OH₂)]NO₃·MeOH (43) complex

To a methanol solution of complex **41** (96 mg, 0.25 mol) was added $\text{Gd}(\text{NO}_3)_3 \cdot 6\text{H}_2\text{O}$ (110 mg, 0.25 mmol) and the resulting mixture was reflux for 30 minutes, then filtered and allowed to stand at room temperature for slow evaporation. Yield: 45.0 mg (0.10 mmol, 40.0%). *Anal.* Calc. for $\text{C}_{19}\text{H}_{17}\text{N}_3\text{O}_7\text{Cu}$ (462.89): C 49.30, H 3.70, N 9.08. Found: C 50.07, H 3.66, N 9.36. Selected IR data (cm^{-1}): 3418 (br, OH hydrogen bonded), 1715 (s, $-\text{C}=\text{O}$), 1635, 1604 (s, $\text{C}=\text{N}$, amide and pyridine rings), 1384 (s, NO_3).

[Fe₂(μ -valhy)₃]₄·DMF (44) complex

To a suspension of bis(2-hydroxy-3-methoxy-benzylidene)-hydrazide ligand (75 mg, 0.25 mmol) in MeOH (10 mL) was added $\text{FeCl}_3 \cdot 6\text{H}_2\text{O}$ (78 mg, 0.16 mmol) dissolved in MeOH (5 mL), followed by addition of NEt_3 (0.5 mL 1N methanol solution). A precipitate is formed in the first minutes of reaction which was partly redissolved by addition of DMF (5 mL) and the reaction mixture has been stirred for 15 minutes. The precipitate was filtered and the clear filtrate solution allowed to stand at room temperature. Yield: 40.0 mg pure compound (0.03 mmol). *Anal.* Calc. for $\text{C}_{48}\text{H}_{42}\text{N}_6\text{O}_{12}\text{Fe}_2 \cdot 4\text{DMF}$ (1056.48): C 55.48, H 5.43, N 10.78. Found: C 55.06, H 4.88, N 9.52. Selected IR data (cm^{-1}): 1695 (s, DMF), 1615 (s, $-\text{CH}=\text{N}$).

Chapter 7

Conclusions

In summary, a small contribution to the field of molecular magnetism has been achieved. The thesis comprises a collection of molecular assemblies with various nuclearity and magnetic behaviors, going from d-block metal complexes to mixed d-f molecular compounds. Easy accessible organic ligands have been employed as supporting organic framework, which according with their polydentate character determined the topology of the resulting polynuclear complexes.

Chapter 2 describes a series of self-assembled azametalla crown iron(III) complexes with the structural topology enabled by the N-imidazol-2-yl salicyloyl-hydrazide Schiff base ligand. This organic framework made possible isolation of three neutral trinuclear iron complexes with mixed ligand composition. Each iron atom is six-coordinated with the dianionic pentadentate ligand fulfilling five of the coordination sites of the metal center, whereas monodentate chelate coligands such as chloride, azide and isothiocyanate occupy the remained vacant position of the metal center. The structural core is based on [Fe–N–N]₃ linkage which led to a 9-membered aza-ring motif. These complexes represent rare example of azametallacrown compounds based on Fe(III) metal ion and in addition the first examples of trinuclear iron(III) complexes in which the presence of μ_3 -bridged mode of oxygen atom is not present. Interesting structural feature have been found for the isothiocyanate derivative of type [Fe(imsalhy)(NCS)]₃ which presupposes the *host-guest* concept, encapsulating nitrate anion in the cavity of the Fe₃-ring. Moreover, this compound supports an ring expansion leading to a tetranuclear Fe(III) complex with the structural core based on 12-membered aza-ring motif which can be regarded as [2+2] grid

compound. Changing from iron to nickel metal ion, a different coordination mode of the hydrazide Schiff base ligand has been observed. While for iron(III) ion coordination, the organic ligand functioned as *bis*-nucleating pentadentate system, in the case of nickel ion, two ligand moieties wrap around the same metal center, resulting in mononuclear nickel(II) complex formation. It can be concluded, based on the results described herein and also according with existing reports that, azametalla-crown topology is characteristic for d-metal ions in 3+ oxidation state. The magnetic behavior of the Fe(III) series of complexes is antiferromagnetic, with the magnitude of interaction determined by Fe···Fe interatomic separation and Fe–N–N–Fe torsion angles (see Table 7.1).

Table 7.1: Magnetostructural parameters for iron(III) aza-crown complexes.

	Fe···Fe interatomic separation (pm)	Fe–N–N–Fe angles torsion angles (°)	J (cm ⁻¹)
[Fe(imsalhy)(Cl)] ₃ ·3CH ₃ OH (1)	509.8	150.0	-9.28±0.06
[Fe(imsalhy)(N ₃)] ₃ ·3.5DMF (2)	506.5-510.9	148.1-152.7	-7.68±0.03
[Fe(imsalhy)(NCS)] ₃ ·(H ₃ imsalhy)·(NO ₃)·0.5H ₂ O·4.25CH ₃ OH (3)	502.2-507.1	149.7-151.2	-8.95±0.03
[Fe(imsalhy)(NCS)] ₄ ·4CH ₃ OH (4)	512.3	165	-6.15±0.14

Chapter 3 makes the change from self-assembly process to a rational strategy to design polynuclear complexes. This is sustained by use of threefold chelating organic framework of type 5-bromo- and 3-methoxy- tris(salicylidene)triaminoguanidine ligands. With these organic ligands, trinuclear Ni(II) complexes have been isolate using 2,2'-bipyridine and 2,4,6-tris(2-pyridyl)-1,3,5-triazine as coligands. The topology of the Ni₃^{II} triad is very similar among these series of complexes and it consists of octahedral nickel ions linked by three diazine bridges. The aromatic co-ligand systems are involved in π - π -stacking interaction which completes various supramolecular arrangements in addition to hydrogen bonding interactions formed by lattice anions and solvent molecules. The influence of anions in the self-organization of the oligomeric trinuclear Ni(II) units have been also studied. Using 5-bromo-substituted triaminoguanidine-based Schiff ligands and 2,2'-bipyridine coligand, the presence of anion vary from coordinated chloride

ligand to lattice nitrate anion which contributes to hydrogen bonding channels formed between sheets of trinuclear Ni(II)-entities. Changing the co-ligand system to 2,4,6-tris(2-pyridyl)-1,3,5-triazine coligand, the terpyridine-coordination mode of this capping ligand made possible the isolation of cationic trinuclear nickel(II) complexes. Nevertheless, in both coligand systems case, the trinuclear Ni(II) complexes are reorganized to yield a pentanuclear Ni(II)-complex. The structural feature of these high-nuclearity Ni(II) complexes is described as two triangular units hold together by a common nickel(II) center. On the other hand, the 3-methoxy- tris(salicylidene)triaminoguanidine derivative ligand was involved in isolation of cationic trinuclear Ni(II) complexes using 2,4,6-tris(2-pyridyl)-1,3,5-triazine as coligand. The influence of the lattice anion, i.e nitrate and chloride have been also investigating. Different crystal packing diagram are formed in these two cases, with hydrogen bonding interactions observed in both cases. The interesting feature of the self-organization of trinuclear Ni(II) units was observed in presence of chloride anion. This unbounded anion forms pillared chains *via* Cl $\cdot\cdot$ HC (aromatic ring from co-ligand) hydrogen bonding interactions. These supramolecular interactions are complementary to π - π stacking interactions between molecules of 2,4,6-tris(2-pyridyl)-1,3,5-triazine coligand to yield a honeycomb two-dimensional architectures with void channels along the crystallographic a axis.

The magnetism of these series of Ni(II) complexes is described as antiferromagnetic coupled metal ions. Again, the magnitude of the exchange coupling within the Ni₃-triad is determined by interatomic Ni $\cdot\cdot$ Ni separation and Ni-N-Ni torsion bridging angles (Table 7.2). From the magnetic behavior point of view, this polydentate system with C₃ symmetry was expected to yield trinuclear metal-complexes with a resulting non-zero spin ground state. A non-diamagnetic ground-state has been found in the case of [Ni₃L^{Br}(bipy)₃(DMF)₂Cl]·2DMF·4CH₃CN·2MeOH·0.5H₂O (**7**) where the magnetization *vs* field measurement fits the Brillouin function for S = 1. In this case, the magnitude of the antiferromagnetic interaction is instead smaller than in the other trinuclear Ni(II) complexes, due to a more obtuse torsion Ni-N-Ni bridging angle (see Table7.2).

It has been established that the ground state is determined not by the absolute values of J and J' but by their ratio, $\rho = J'/J$. For $\rho = 1/2$, the ground state is E(1,2), and for $\rho = 2$, the ground state is E(1,0). On the other hand for $1/2 \leq \rho \leq 2$, the ground state

is E(0,1). As a whole, the situation may be described as follows : the antiferromagnetic interaction between Ni1···Ni2 and Ni1···Ni3 polarizes the spins around Ni2 and Ni3 in a ferromagnetic fashion. Any antiferromagnetic interaction along Ni2···Ni3 opposes this effect. When $|J'|$ is small enough ($\rho \leq 1/2$), the ferromagnetic polarization takes over. When $|J'|$ is large enough ($\rho \geq 2$), the antiferromagnetic interaction takes over. When the ferromagnetic polarization and the antiferromagnetic interaction are of the same order of magnitude, the system looks for a compromise. The spin vectors around Ni2 and Ni3 are neither parallel nor antiparallel and the spin takes an intermediate value $S' = 1$.

Table 7.2: Magnetostructural parameters for iron(III) aza-crown complexes.

	Ni···Ni interatomic separation (pm)	Ni–N–Ni angles torsion angles (°)	J (cm ⁻¹)
[Ni ₃ L ^{Br} (bipy) ₃ (OH ₂) ₃]NO ₃ ·S (6)	499.0	168.7	-30.99±0.58
[Ni ₃ L ^{Br} (bipy) ₃ (DMF) ₂ Cl]·S (7)	497.7-501.3	173.6-179.9	-19.88±1.30 -12.84±1.14
[Ni ₃ L ^{Br} (tptz) ₃]NO ₃ ·S (9)	482.0	154.0	-27.06±0.31
[Ni ₃ L ^{Br} (tptz) ₃]Cl·S (10)	-	-	-28.55±0.39
[Ni ₃ L ^{Br} (tptz) ₃]ClO ₄ ·S (11)	-	-	-30.88±0.29
[Ni ₃ L ^{OMe} (tptz) ₃]NO ₃ ·S (13)	493.8-493.7	160.5-177.7	-33.55±0.72
[Ni ₃ L ^{OMe} (tptz) ₃]Cl·S (14)	497.2-498.2	173.9-179.4	-31.17±0.62
[Ni ₃ L ^{OMe} (tptz) ₃]ClO ₄ ·S (15)	-	-	-31.45±0.45

S = solvent molecules

A diamagnetic Co(III) complex has been also isolated using tris(3-methoxy-salicylidene)triaminoguanidine ligand *via* in situ oxidation of cobalt(II) starting material. In addition, the 2,4,6-tris(2-pyridyl)-1,3,5-triazine coligand was also hydrolyzed to bis(2-pyridylcarbonyl)amine capping ligand. The capability of this hydrolyzed co-ligand system to function as bis-nucleating bridge is well documented and, hence the ability of this trinuclear Co(III) complex to function as molecular brick to construct magnetic dendrimers when is beforehand reduced to anisotropic cobalt(II) ions.

Chapter 4 describes the magnetostructural characterization of homonuclear Fe(III) and Cu(II) complexes. Homodinuclear iron(III) complexes have been isolated using *salen*-

type-N,N'-ethylene-bis(pyridoxylideneiminato) ligand and N-salicylidene-2-bis(2-hydroxyethyl)amino)ethylamine ligand. The salen-type ligand yields a neutral oxo-bridged dinuclear Fe(III) complex, whereas the N-salicylidene-2-bis(2-hydroxyethyl)amino)ethylamine ligand yielded an hydroxy-bridge cationic dinuclear iron(III) complex. Both these complexes are organized through hydrogen bonding interaction between donor groups of the supporting ligands into one-dimensional polymers. The magnetic coupling of the iron(III) ions has been found to be antiferromagnetic, stronger in the case of oxo-bridged dinuclear Fe(III) complex, whereas a weak antiferromagnetic interaction has been mediated by N-salicylidene-2-bis(2-hydroxyethyl)amino)ethylamine ligand.

The second part of this chapter describes different nuclearity of copper(II) complexes resulting from self-assembly reaction between [2-(2-dimethylamino-ethylimino)-methyl]phenol and its methoxy-derivative ligands with $\text{Cu}(\text{ClO}_4)_2$ salt in presence of different outer metal salts. The homotrimeric copper(II) complex present a partial cubane-like structural core formed by $[\text{Cu}_3\text{L}_3(\mu_3\text{-OH})]^{2+}$ cation which can be simply formulated as Cu_3O_4 -motif. The organic framework enforced, in this case an accidental orthogonality orientation of the magnetic orbital of the three copper(II) ions, resulting in a ferromagnetic interaction between the metal centers of $J = 8.50 \text{ cm}^{-1}$ magnitude. Instead, the homodinuclear copper(II) complex comprises only one phenoxo-bridged Cu-O(Ph)-Cu moiety with an obtuse bridging angle, most likely responsible for the antiferromagnetic exchange pathway between the copper(II) ions.

Chapter 5 is focused on dinucleating oximate-type ligand that was successfully used to isolate heteropolynuclear complexes following the "complex as ligand" strategy. The easy accessible N-(2-dimethylamino-ethyl)-oxalamide ligand has been employed to isolate a mononuclear anionic Cu(II) complex. The ligand undergoes "template" hydrolysis to N-(2-dimethylamino-ethyl)-oxalamic acid organic framework upon copper(II) coordination. This coordination compound is capable of bridging Co(II) ion *via* oxamate oxygen atoms, yielding a trinuclear $[\text{Cu}_2\text{Co}]$ -complex. Due to the presence of high anisotropic Co(II) ion, for which the spin-orbit coupling has to be considered in the magnetic behavior interpretation, a quantitative analysis of the magnetic data is not available. Nevertheless, the thermal variation of the magnetic susceptibility in $\chi_M T$ vs T plot is characteristic of an overall ferrimagnetic behavior.

Chapter 6 is focused on copper(II)-lanthanide(III) heteronuclear complexes with topologies ongoing from one-dimensional chain compounds to oligomeric trinuclear heterometallic d-f complexes. These coordination compounds have been isolated using *Cu-salen type* precursor following "complex as ligand" strategy. The structural studies show that μ_2 -phenoxy bridged [CuLn] core is successful building block for synthesizing polymeric coordination compounds. Due to high anisotropy associated with the majority of the lanthanide ions, such d-f topologies are most appealing for constructing extended architectures with interesting magnetic properties. Trinuclear [Cu₂Ln] complexes have been isolated using salicylic acid as capping and bridging ligand, whereas 1-D chains were isolated in the case of pyrazine 2,3-dicarboxylic acid co-ligand. The major difference between the two bridging ligands, e.g. pyrazine 2,3-dicarboxylic acid and salicylic acid, resides from their coordination mode. In 1-D chain compounds, the polydentate ligand substitutes only two bidentate nitrate ligands of the classical [Cu(OMesalen)Gd(NO₃)₃] dinuclear complexes, whereas the salicylic acid co-ligand leads to a total replacement of the nitrate anion ligands but maintaining the decahedron arrangement of the lanthanoid center. Polymeric 1-D chains have been isolated for lanthanide ions placed before and after gadolinium ion in the periodical table and by contrast, the salicylic acid made possible the isolation of heterotrinuclear compounds only for lanthanide ions comprising lanthanum to gadolinium ions. For both types of d-f coordination compounds, the magnetic behavior was found to be very similar, owing to close values of the dihedral angle formed by the phenoxy-bridged copper(II)-lanthanide(III) planes. One-dimensional [CuLn] chains formed with polydentate pyrazine 2,3-dicarboxylic acid as bridging ligand represent rare examples of such extended architectures with d-f topology. The resulting polymers of type [Cu(OMesalen)Gd(NO₃)(Pyr(COO)₂)_n·(DMF)_n are formed by alternating pairs of Cu···Ln and Ln···Ln through polydentate bridging ligand yielding an infinite zigzag chain. The magnetic properties of [Cu(OMesalen)Gd(NO₃)(Pyr(COO)₂)_n·(DMF)_n (**27**) compound, showed that the ferromagnetism of these 1-D chains is determined by the Cu–Gd magnetic coupling ($J = 4.72 \text{ cm}^{-1}$) of the constituting heterodinuclear entities. For the heterotrinuclear [(Cu(OMesalen))₂Gd(salCOO)₂]NO₃·3MeOH·H₂O (**34**), the ferromagnetic [Cu–Gd] interaction in the [Cu₂Gd]-triad was found to be $J = 4.12 \text{ cm}^{-1}$, with similar order of magnitude as in the 1-D chain compounds. This is caused by the well

established dependence of the ferromagnetic interaction upon dihedral Cu- μ_2 phenoxy-Gd angle, which was found to be very similar within the two series of d-f coordination compounds.

It can be summarized that various exchange-coupled systems have been described on traversing the periodic table of elements from pure d-block transition metals to combined d-f topologies. The *conclusion and future perspective* section of each chapter demonstrate that this thesis is the "small-step" for constructing high-nuclear high-spin molecular magnetic materials.

Bibliography

- [1] W. Plass. *Chem. unserer Zeit* **1998**. 32, 323.
- [2] G. L. Verschuur. Oxford University Press, Oxford **1993**.
- [3] W. Gillbert. In *De Magnete*. Dover Publications Inc., New York **1958** .
- [4] A. H. Murrish. In *The physical principles of Magnetism*. Jhon Wiley and Sons, New York **1980** .
- [5] R. L. Carlin. In *Magnetochemistry*. Spring Verlag, New York **1986** .
- [6] J. S. Miller. *Inorg. Chem.* **2000**. 39, 4392.
- [7] B. Pilawa. *Ann. Phys.* **1999**. 8, 191.
- [8] J. S. Miller, A. J. Epstein. *Ang. Chem. Int. Ed.* **1994**. 33, 385.
- [9] D. Gatteschi, R. Sessoli. *Angew. Chem., Int. Ed.* **2003**. 42, 268 and references therein.
- [10] O. Kahn. In *Molecular Magnetism*. Wiley-WCH Inc., Weinheim **1993** 211.
- [11] O. Kahn. *Adv. Inorg. Chem.* **1996**. 179.
- [12] J. S. Miller. *Adv. Mater.* **1992**. 4, 298.
- [13] J. M. Rawson, F. Palacio. In *Structure and Bonding; π -Electron Magnetism: From Molecules to Magnetic Materiales*. Springer-Verlag, Heidelberg **2001** 94.
- [14] J. J. Novoa, M. Deumal. In *Structure and Bonding; π -Electron Magnetism: From Molecules to Magnetic Materiales*. Springer-Verlag, Heidelberg **2001** 33.
- [15] A. Caneschi, D. Gatteschi, N. Lalioti, C. Sangregorio, R. Sessoli, G. Venturi, A. Vindigni, A. Rettori, M. G. Pini, M. A. Novak. *Angew. Chem.* **2001**. 113, 1810.
- [16] L. Bogani, C. Sengregorio, R. Sessoli, D. Gatteschi. *Angew. Chem.* **2005**. 117, 5967.
- [17] J. Manriquez, J. T. Yee, R. S. McLean, A. J. Epstein, J. S. Miller. *Science* **1991**. 252, 1415.
- [18] G. A. Candela, L. J. Swartzendruber, J. S. Miller, M. J. J. Rice. *J. Am. Chem. Soc.* **1979**. 101, 2755.
- [19] S. Ferlay, T. Mallah, R. Ouahes, P. Veillet, M. Verdaguer. *Nature* **1995**. 378, 701.
- [20] H. U. Guedel, H. Stucki, A. Ludi. *Inorg. Chim. Acta* **1973**. 7, 121.

- [21] M. Verdaguer, G. S. Girolami. In *Magnetism: Molecules and materiales IV*. Wiley-WCH Inc., Weinheim **2005** 283.
- [22] R. Lescouézec, J. Veissermann, C. Ruiz-Perez, F. Lloret, R. Carrasco, M. Julve, M. Verdaguer, Y. Dromze, D. Gatteschi, W. Vernsdorfer. *Angew. Chem.* **2003**. *115*, 1521.
- [23] R. Sessoli, H. L. Tsai, A. R. Schake, S. Sheyi, J. B. Vincent, K. Folting, D. Gatteschi, G. Christou, D. N. Hendrickson. *J. Am. Chem. Soc.* **1993**. *115*, 1804.
- [24] R. Sessoli, D. Gatteschi, A. Caneschi, M. A. Novak. *Nature* **1993**. *365*, 141.
- [25] T. Lis. *Acta Crystallogr.* **1980**. *B36*, 2042.
- [26] D. Gatteschi, R. Sessoli, A. Cornia. *Chem. Commun.* **2000**. 725 and references therein.
- [27] A. Caneschi, D. Gatteschi, L. Pardi, R. Sessoli. *Science* **1994**. *265*, 1054.
- [28] J. Larionova, S. A. Chavan, J. V. Yakhmi, A. G. Froystein, J. Sletten, C. Sourisseau, O. Kahn. *Inorg. Chem.* **1997**. *36*, 6374.
- [29] O. Kahn, J. Larionova, J. V. Yakhmi. *Chem. Eur. J.* **1999**. *5*, 3443.
- [30] V. L. Pecoraro, A. J. Stemmler, B. R. Gibney, J. J. Bodwin, H. Wang, J. W. Kampf, A. Barwinski. *Prog. Inorg. Chem.* **1997**. *45*, 83.
- [31] R. D. Cannon, R. P. White. *Prog. Inorg. Chem.* **1988**. *36*, 195.
- [32] L. K. Thompson. *Cord. Chem. Rev* **2002**. *233-234*, 193.
- [33] S. Castro, W. E. Streib, J.-S. Sun, G. Christou. *Inorg. Chem.* **1996**. *35*, 4462.
- [34] M. S. Ray, S. Chattopadhyay, M. G. B. Drew, A. Figuerola, J. Ribas, C. Diaz, A. Ghosh. *Eur. J. Inorg. Chem.* **2005**. 4562.
- [35] C. E. Anson, J. P. Bourke, R. D. Cannon, U. A. Jayasooriya, M. Molinier, A. K. Pawell. *Inorg. Chem.* **1997**. *36*, 1265.
- [36] S. Ferre, F. Lloret, I. Bertomeu, G. Alzuet, J. Borrás, S. Garcia-Granda, M. Liu-Gonzales, J. G. Haasnoot. *Inorg. Chem.* **2002**. *41*, 5821.
- [37] J. Yoon, L. M. Mirica, T. D. P. Stack, E. I. Solomon. *J. Am. Chem. Soc.* **2004**. *126*, 12586.
- [38] B. Cage, F. Cotton, N. S. Dalal, E. A. Hillard, B. Rakvin, C. M. Ramsey. *J. Am. Chem. Soc.* **2003**. *125*, 5270.
- [39] E. Brechin. *Chem. Commun.* **2005**. 5141.
- [40] A. Zharkouskaya. *Merkernige Übergangsmetallkomplexe als Basis für neue Klassen magnetischer Materialien*. Ph.D. thesis, Fridrich-Schiller Universität Jena, Jena, Germany **2006**.
- [41] O. Kahn. *Chem. Phys. Lett.* **1997**. *265*, 109.
- [42] K. Kambe. *J. Phys. Soc., Jpn.* **1950**. *48*, 15.

- [43] J. M. Lehn. In *Supramolecular Chemistry: Concepts and Perspectives*. VCH, Weinheim **1995** .
- [44] M. Ruben, J. Rojo, F. J. Romero-Salguero, L. H. Upadine, J. M. Lehn. *Angew. Chem.* **2004**. *116*, 3728.
- [45] S. Leininger, B. Olenyuk, P. J. Stang. *Chem. Rev.* **2000**. *100*, 853.
- [46] C. Piguet, G. Bernardinelli, G. Hopfgartner. *Chem. Rev.* **1997**. *97*, 2005.
- [47] P. N. W. Baxter, J. M. Lehn, G. Baum, D. Fenske. *Chem. Eur. J.* **1989**. *5*, 102.
- [48] P. N. W. Baxter, J. M. Lehn, B. O. Kaasel, G. Baum, D. Fenske. *Chem. Eur. J.* **1999**. *5*, 113.
- [49] W. Huang, S. Gou, D. Hu, S. Chantrapromma, H. K. Fun, Q. Meng. *Inorg. Chem.* **2001**. *40*, 1712.
- [50] P. N. W. Baxter, G. S. Hanan, J. M. Lehn. *Chem. Commun.* **1996**. 2019.
- [51] P. Ceroni, A. Credi, V. Balzani, S. Campagna, G. S. Hanan, C. R. Arana, J. M. Lehn. *Eur. J. Inorg. Chem* **1999**. 1409.
- [52] L. Zhao, Z. Xu, L. K. Thompson, S. L. Heath, D. O. Miller, M. Ohba. *Angew. Chem.* **2000**. *39*, 3114.
- [53] O. Waldmann, J. Hassmann, P. Müller, G. S. Hanan, D. Volkmer, U. S. Schubert, J. M. Lehn. *Phys. Rev. Lett.* **1997**. *78*, 3390.
- [54] L. K. Thompson, L. Zhao, Z. Xu, D. O. Miller, W. M. Reiff. *Inorg. Chem.* **2003**. *42*, 128.
- [55] M. Ruben, E. Breuning, M. Barboiu, J. P. Gisselbrecht, J. M. Lehn. *Chem. Eur. J.* **2003**. *9*, 291.
- [56] R. V. Slone, K. D. Benkstein, S. Bélanger, J. T. Hupp, I. A. Guzei, A. L. Rheingold. *Coord. Chem. Rev.* **1998**. *171*, 221.
- [57] M. Fujita, Y. J. Kwon, S. Washizu, K. Ogura. *J. Am. Chem. Soc.* **1994**. *116*, 1151.
- [58] Y. Bai, D. Dang, C. Duan, Y. Song, Q. Meng. *Inorg. Chem.* **2005**. *44*, 5972.
- [59] H. Chen, M. F. Maestre, R. H. Fish, Y. Song, Q. Meng. *J. Am. Chem. Soc.* **1995**. *117*, 3631.
- [60] H. Chen, S. Ogo, R. H. Fish. *J. Am. Chem. Soc.* **1996**. *118*, 4993.
- [61] J. J. Bodwin, V. L. Pecoraro. *Inorg. Chem.* **2000**. *39*, 3434.
- [62] M. Moon, I. Kim, M. S. Lah. *Inorg. Chem.* **2000**. *39*, 2710.
- [63] A. C. C.-V. Hood, J. W. Kampf, V. L. Pecoraro. *Angew. Chem. Int. Ed.* **2002**. *41*, 4668.
- [64] V. L. Pecoraro. *Inorg. Chim. Acta* **1989**. *155*, 171.
- [65] M. S. Lah, V. L. Pecoraro. *Polyhedron* **1989**. *111*, 7258.
- [66] M. Fujita. *Chem. Rev.* **1998**. *27*, 417.

- [67] R. Koch, O. Waldmann, P. Müller, U. Reimann, R. W. Saalfrank. *Phys. Rev. B* **2003**. *67*, 0944407.
- [68] R. Frank, S. Trummer, U. Reimann, M. M. Chowdhri, F. Hampel, O. Waldmann. *Angew. Chem.* **2000**. *112*, 3634.
- [69] J. A. Johnson, J. W. Kampf, V. L. Pecoraro. *Angew. Chem. Int. Ed.* **2003**. *42*, 546.
- [70] C. J. Matthews, S. T. Onions, G. Morata, L. J. Davis, S. L. Heath, D. J. Price. *Angew. Chem. Int. Ed.* **2003**. *42*, 3166.
- [71] R. W. Saalfrank, A. Dresel, V. Seitz, S. Trummer, F. Hampel, M. Teichert, D. Stalke, C. Stadler, J. Daub, V. Schunemann, A. X. Trautwein. *Chem. Eur. J.* **1997**. *3*, 2058.
- [72] R. W. Saalfrank, V. Seitz, D. L. Caulder, K. N. Raymond, M. Teichert, D. Stalke. *Eur. J. Inorg. Chem.* **1998**. 1313.
- [73] V. J. Catalano, M. A. Malwitz. *Inorg. Chem.* **2002**. *41*, 6553.
- [74] P. D. Beer, A. G. Cheetham, M. G. B. Drew, O. D. Fox, E. J. Hayes, T. D. Rolls. *Dalton Trans.* **2003**. 603.
- [75] H. Rauter, E. C. Hillgeris, A. Erxleben, B. Lippert. *J. Am. Chem. Soc.* **1994**. *116*, 616.
- [76] M. J. Rauterkus, B. Krebs. *Angew. Chem. Int. Ed.* **2004**. *43*, 1300.
- [77] C. Dendrinou-Samara, C. M. Zaleski, A. Evagorou, J. W. Kampf, V. L. Pecoraro. *Chem. Commun.* **2003**. 2668.
- [78] C. Dendrinou-Samara, M. Alexoiu, C. M. Zaleski, J. W. Kampf, M. L. Kirk, D. P. Kessissoglou, V. L. Pecoraro. *Angew. Chem.* **2003**. *115*, 3893.
- [79] G. Psomas, A. J. Stemmler, C. Dendrinou-Samara, J. J. Bodwin, M. Scheider, M. Alexoiu, J. W. Kampf, D. P. Kessissoglou, V. L. Pecoraro. *Inorg. Chem.* **2001**. *40*, 1562.
- [80] M. S. Lah, M. L. Kirk, W. Hatfield, V. L. Pecoraro. *Chem. Commun.* **1989**. 1606.
- [81] B. R. Gibney, A. J. Stemmler, S. Pilotek, J. W. Kampf, V. L. Pecoraro. *Inorg. Chem.* **1993**. *32*, 6008.
- [82] B. R. Gibney, D. P. Kessissoglou, J. W. Kampf, V. L. Pecoraro. *Inorg. Chem.* **1994**. *33*, 4840.
- [83] D. Gaynor, Z. A. Starikova, S. Ostrovsky, W. Haase, K. B. Nolan. *Chem. Commun.* **2002**. 506.
- [84] A. J. Stemmler, J. W. Kampf, M. L. Kirk, B. H. Atasi, V. L. Pecoraro. *Inorg. Chem.* **1999**. *38*, 2807.
- [85] M. S. Lah, V. L. Pecoraro. *J. Amer. Chem. Soc.* **1989**. *111*, 7258.
- [86] Y. Agnus, R. Louis, B. Metz, C. Boudon, J. P. Gisselbrecht, M. Gross. *Inorg. Chem.* **1991**. *30*, 3155.
- [87] B. R. Gibney, H. Wang, J. W. Kampf, V. L. Pecoraro. *Inorg. Chem.* **1996**. *35*, 6184.
- [88] S. Koizumi, M. Nihei, M. Nakano, H. Oshio. *Inorg. Chem.* **2005**. *44*, 1208.

- [89] S. X. Liu, S. Lin, B. Z. Lin, C. C. Lin, J. Q. Huang. *Angew. Chem.* **2001.** *113*, 1118.
- [90] S. Liu, S. X. Liu, Z. Chen, B. Z. Lin, S. Gao. *Inorg. Chem.* **2004.** *43*, 2222.
- [91] D. Moon, J. Song, B. J. Kim, B. J. Suh, M. S. Lah. *Inorg. Chem.* **2004.** *43*, 4320.
- [92] R. P. John, K. Lee, M. S. Lah. *Chem. Commun.* **2004.** 2660.
- [93] L. K. Thompson, O. Waldmann, Z. Xu. In *Magnetism: Molecular to Materials 3*. Wiley-WCH, Weinheim **2000** 173.
- [94] L. K. Thompson. *Coord. Chem. Rev.* **2002.** *233-234*, 193.
- [95] L. K. Thompson, C. J. Matthews, L. Zhao, C. Wilson, M. A. Leech, A. Michael, J. A. K. Howard. *Dalton Trans.* **2001.** 2258.
- [96] Z. Xu, L. K. Thompson, D. O. Miller. *Chem. Commun.* **2001.** 1170.
- [97] Z. Xu, S. White, L. K. Thompson, D. O. Miller. *Dalton Trans.* **2000.** 1751.
- [98] B. Kwak, H. Rhee, S. Park, M. S. Lah. *Inorg. Chem.* **1998.** *35*, 3599.
- [99] B. Kwak, H. Rhee, M. S. Lah. *Polyhedron* **2000.** 1985.
- [100] S. Lin, S. X. Liu, B. Z. Lin. *Inorg. Chim. Acta* **2002.** 328.
- [101] S. Liu, S. X. Liu, J. Q. Huang, C. C. Lin. *Dalton Trans.* **2002.** 1595.
- [102] S. S. Tandon, L. K. Thompson, M. E. M. and J. N. Bridson. *Inorg. Chem.* **1994.** *33*, 5555.
- [103] A. W. Addison, R. J. Butcher, Z. Homonnay, V. V. Pavlishchuk, M. J. Prushan, L. K. Thompson. *Eur. J. Inorg. Chem.* **2005.** 2404.
- [104] G. Spocrates. In *Infrared and Raman Characteristic Group Frequencies*. John Wiley and Sons Ltd., Weinheim **2001** .
- [105] R. P. John, K. Lee, B. J. Kim, B. J. Suh, H. Rhee, M. S. Lah. *Inorg. Chem.* **2005.** *44*, 7109.
- [106] Y. Zhang, W. A. Hallows, W. J. Ryan, J. C. Jones, G. B. Carpenter, D. A. Sweigart. *Inorg. Chem.* **1994.** *33*, 3306.
- [107] K. R. Reddy, M. W. Rajasekharan, J. P. Tuchagues. *Inorg. Chem.* **1998.** *37*, 5978.
- [108] A. Ozarowski, Y. Shunzhong, B. McGarvey, A. Mislankar, J. E. Drake. *Inorg. Chem.* **1991.** *30*, 3167.
- [109] A. Mukherjee, M. Nethaji, A. R. Chakravarty. *Chem. Commun.* **2003.** 2978.
- [110] B. Kwak, H. Rhee, S. Park, M. S. Lah. *Inorg. Chem.* **1998.** *37*, 3599.
- [111] K. Dunbar, R. Heintz. *Prog. Inorg. Chem.* **1997.** *45*, 283.
- [112] V. Marvard, C. Decroix, A. Sculler, F. T. C. Guyard-Duhayon, J. Vaissermann, J. Marrot, F. Gonnet, M. Verdager. *Chem. Eur. J.* **2003.** *9*, 1692.

- [113] V. Marvaud, J. M. Herrera, T. Barilero, F. Tuyeras, R. Garde, A. Sculler, C. Decroix, M. Cantuel, C. Depsplanches. *Monatsh. Chem.* **2003**. *134*, 149.
- [114] S. M. Holmes, G. S. Girolami. *J. Am. Chem. Soc.* **1999**. *121*, 5593.
- [115] R. H. Holm, E. I. Solomon. *Chem. Rev.* **1996**. *96*.
- [116] A. L. Feig, S. J. Lippard. *Chem, Rev.* **1994**. *94*, 759.
- [117] A. Ardzzioia, M. A. Angarconi, G. LaMonica, F. Cariati, S. Cenini, M. Moret, N. Masciocci. *Inorg. Chem.* **91**. *30*, 43.
- [118] S. Parsons, J. M. Rawson, D. Reed, R. E. P. Winpenny. *J. Chem. Soc. Dalton Trans.* **1995**. 63.
- [119] B. Moulton, M. Zaworotko. *Chem. Rev.* **2001**. *101*, 1629.
- [120] R. Robson. *J. Chem. Soc. Dalton Trans.* **2000**. 3735.
- [121] C. Janiak. *Dalton Trans.* **2003**. 2781.
- [122] D. Braga, F. Grepioni. *Acc. Chem. Rev.* **2000**. 601.
- [123] S. L. James. *Chem. Soc. Rev.* **2003**. *32*, 276.
- [124] N. Rosi, J. Kim, M. Edaoudi, B. Chen, M. O'Keeffe, O. M. Yaghi. *J. Am. Chem. Soc.* **2005**. 1504.
- [125] T. D. Hamilton, L. R. MacGilliverray. *Crystal Growth Design* **2004**. *4*, 419.
- [126] S. Kitagawa, R. Kitaura, S. Noro. *Angew. Chem.* **2004**. *116*, 2388.
- [127] M. Wesolek, D. Meyer, J. A. Osborn, A. D. Cian, J. Fisher, A. Derory, P. Logoll, M. Drillon. *Angew. Chem. Int. Ed. Engl.* **1994**. *33*, 1592.
- [128] A. J. Amoroso, J. C. Jefferey, P. L. Jones, J. A. McCleverty, P. Thornton, M. D. Ward. *Angew. Chem. Int. Ed. Engl.* **1995**. *34*, 1443.
- [129] J. E. Létard, P. Guionneau, E. Coudjovi, O. Lavastre, G. Bravic, D. Chasseau, O. Kahn. *J. Am. Chem. Soc.* **1997**. *119*, 10861.
- [130] J. E. Létard, P. Guionneau, L. Rabardel, J. A. K. Howard, A. E. Goeta, D. Chasseau, O. Kahn. *Inorg. Chem.* **1998**. *37*, 4432.
- [131] F. A. Cotton, C. Lin, C. A. Murillo. *PNAS* **2002**. *99*, 4810.
- [132] S. L. James. *Chem. Soc. Rev.* **2003**. *32*, 276.
- [133] G. R.W, B. H. R. Robson. *J. Chem. Soc. Chem. Commun.* **1990**. 1677.
- [134] H. Roesky, M. Andruh. *Coord. Chem. Rev.* **2003**. *236*, 91.
- [135] D. L. Long, A. J. Blake, N. R. Champness, C. Wilson, M. Schöder. *Chem. Eur. J.* **2002**. *8*, 2026.
- [136] T. Glaser, M. Gerenkamp, R. Fröhlich. *Angew. Chem.* **2002**. *114*, 3984.
- [137] T. Glaser, M. Heidemeier, S. Grimme, E. Bill. *Inorg. Chem* **2004**. *43*, 5192.

- [138] Z. Wang, V. C. Kravtsos, M. J. Zaworotko. *Angew. Chem.* **2005.** *117,* 2937.
- [139] M. Pascu, F. Lloret, N. Avarvari, M. Julve, M. Andruh. *Inorg. Chem.* **2004.** *43,* 5189.
- [140] W. Zhang, S. B. and C. P. Landee, J. L. Parent, M. M. Turnbull. *Inorg. Chim. Acta* **2003.** *342,* 193.
- [141] M. J. Plater, M. R. S. J. Foreman, E. Coronado, C. J. Gomez-Garcia, A. M. Z. J. Slawin. *J. Chem. Soc. Dalton Trans.* **1999.** 4209.
- [142] S. O. H. Gutschke, M. Molinier, A. K. Powell, R. Winpenny, P. T. Wood. *Chem. Commun.* **1996.** 823.
- [143] I. M. Müller, D. Möllner, C. A. Schalley. *Angew. Chem.* **2005.** *117,* 485.
- [144] I. Müller, D. Möller. *Eur. J. Inorg. Chem.* **2005.** 257.
- [145] I. M. Müller, D. Möller. *Angew. Chem.* **2005.** *117,* 3029.
- [146] I. M. Müller. *Angew. Chem. Int. Ed.* **2000.** *39,* 4357.
- [147] I. M. Müller, R. Robson, F. Separovic. *Angew. Chem. Int. Ed.* **2001.** *40,* 4385.
- [148] I. M. Muler, S. Spillmann, H. Franck, R. Pietshnig. *Chem. Eur. J.* **2004.** *10,* 2207.
- [149] A. Zharkouskaya, A. Buchholz, W. Plass. *Eur. J. Inorg. Chem.* **2005.** 4875.
- [150] P. Gütligh, V. Ksenofontov, A. Gaspar. *Coord. Chem. Rev* **2005.** *249,* 1811.
- [151] J. F. Letard, P. Guionneau, O. Nguyen, J. S. Costa, S. Marcen, G. Chastanet, M. Marchivie, L. Goux-Capes. *Chem. Eur. J.* **4582.** *11,* 2005.
- [152] T. Glaser, T. Lügger, R. Fröhlich. *Eur. J. Inorg. Chem.* **2004.** 394.
- [153] B. H. Ye, M. L. Tong, X. M. Chen. *Coord. Chem. Rev.* **2005.** *249,* 545.
- [154] T. J. Podesta, A. G. Orpen. *Crystal Growth Design* **2005.** *5,* 681.
- [155] W. L. Jorgensen, D. L. Severance. *J. Am. Chem. Soc.* **1990.** *112,* 4768.
- [156] C. Janiak. *Dalton Trans.* **2000.** 3885.
- [157] E. I. Lerner, S. J. Lippard. *J. Am. Chem. Soc.* **1976.** *98,* 5397.
- [158] E. I. Lerner, S. J. Lippard. *Inorg. Chem.* **1977.** *16,* 1546.
- [159] A. Canarero, J. M. Amigo, J. Faus, M. Julve, T. Debaerdemaeker. *Dalton Trans.* **1988.** 2033.
- [160] J. Faus, M. Julve, J. M. A. T. Debaerdemaeker. *Dalton Trans.* **1989.** 1681.
- [161] T. Kajiwara, A. Kamiyama, T. Ito. *Chem. Commun.* **2002.** 1256.
- [162] A. Kamiyama, T. Noguchi, T. Kajiwara, T. Ito. *Inorg. Chem.* **2002.** *41,* 507.
- [163] R. L. Paul, Z. R. Bell, J. C. Jeffery, J. A. McCleverty, M. D. Ward. *PNAS* **2002.** *99,* 4883.

- [164] R. Winpenny. *J. Chem. Soc. Dalton Trans* **2002**. 1.
- [165] C. S. Campos-Fernandez, R. Clerac, J. M. Koomen, D. R. Russel, K. R. Dunbar. *J. Am. Chem. Soc* **2001**. 123, 773.
- [166] J. J. R. F. da Silva, R. J. P. Williams. In *The biological chemistry of the elements. The inorganic chemistry of life*. Oxford University Press, Oxford, U.K. **2001** .
- [167] H. Anders, R. Basler, A. J. Blake, C. Cadiou, G. Chaboussant, G. M. G. H.-U. M. Murrie, S. Parsons, C. Paulsen, F. Semandini, V. Villar, W. Wersdorfer, R. Winpeny. *Chem. Eur. J.* **2002**. 8, 4867.
- [168] E.-C. Yang, D. Hendrickson, W. Wernsdorfer, M. Nakano, L. V. Zakharov, R. D. Sommer, A. L. Rheingold, M. Ledezma-Gairaud, G. Christou. *J. Appl. Phys.* **2002**. 91, 7382.
- [169] C. Benelli, A. J. Blake, E. Brechin, S. J. Coles, A. Graham, S. G. Harris, S. Mayers, A. Parkin, S. Parsons, A. M. Seddon, R. E. P. Winpenny. *Chem. Eur. J.* **2000**. 6, 883.
- [170] A. Caneschi, D. Gatteschi, N. Lalioti, R. Sessoli, L. Sorace, V. Tangoulis, A. Vindigni. *Chem. Eur. J.* **2002**. 8, 286.
- [171] D. V. Yazigi, J. Cano, S. Alvares. *J. Chem. Soc. Dalton Trans.* **2006**. 2643.
- [172] M. Murrie, S. J. Teat, H. Stoeckli-Evans, H. Güdel. *Angew. Chem.* **2003**. 115, 4801.
- [173] M. Moragues-Canovas, M. Helliwell, L. Ricard, E. Riviere, W. Wernsdorfer, E. Brechin, T. Mallah. *Eur. J. Inorg. Chem.* **2004**. 2219.
- [174] S. K. Ghosh, P. K. Bharadwaj. *Inorg. Chem.* **2004**. 43, 6887.
- [175] F. Keutsch, J. Ctuzan, R. Saykelly. *Chem. Rev.* **2002**. 103, 2533.
- [176] T. Weyhermüller, R. Wagner, S. Khanra, P. Chaudhuri. *Dalton. trans.* **2005**. 2539.
- [177] J. Cano, G. D. Munno, F. lloret, M. Julve. *Inorg. Chem.* **2000**. 39, 1611.
- [178] R. CLerac, F. A. Cotton, K. R. Dubnar, C. A. Murrillo. *Inorg. Chem.* **1998**. 38, 2655.
- [179] M. Arnold, D. A. Brown, O. Deeg, W. Errington, W. Hasse, T. J. Kemp, H. Nimir, R. Werner. *Inorg. Chem.* **1998**. 37, 2970.
- [180] K. K. Nanda, A. W. Addison, N. Paterson, E. Sinn, L. K. Thompson, U. Sakaguchi. *Inorg. Chem.* **1998**. 37, 1028.
- [181] A. Escuer, I. Castro, F. Mautner, M. S. E. Fallah, R. Vicente. *Inorg. Chem.* **1997**. 36, 4633.
- [182] S. Mohamta, K. K. Nanda, R. Werner, W. Haase, A. K. Mukherjee, S. K. Dutta, K. Nag. *Inorg. Chem.* **1997**. 36, 4656.
- [183] A. Escuer, R. Vicente, S. R. Kumar, X. Solanas, M. Front-Bardia, A. Caneshi. *Inorg. Chem.* **1996**. 35, 3094.
- [184] L. Antolini, A. C. Fabretti, D. Gatteschi, A. Giusti, R. Sessoli. *Inorg. Chem.* **1990**. 29, 143.
- [185] A. P. Cinsenberg, R. L. Martin, R. C. Sherwood. *Inorg. Chem.* **1968**. 7, 932.

- [186] Z. Xu, L. K. Thompson, D. O. Miller. *Inorg. Chem.* **1997**. *36*, 3985.
- [187] Z. Xu, L. K. Thompson, V. A. Milway, L. Zhao, T. Kelly, D. O. Miller. *Inorg. Chem.* **2003**. *42*, 2950.
- [188] J. H. Herrera, V. Marvaud, M. Verdaguer, J. Marrot, M. Kalisz, C. Mathoniere. *Angew. Chem.* **2004**. *116*, 5584.
- [189] E. Breuning, U. ziener, J. M. Lehn, E. Wegelius, K. Rissanen. *Eur. J. Inorg. Chem.* **2001**. 155.
- [190] Z. Qin, M. C. Jennings, R. J. Puddephatt. *Chem. Commun.* **2001**. 1676.
- [191] A. Lavalette, F. Tuna, G. Clarkson, N. W. Alcock, M. J. Hannon. *Chem. Commun.* **2003**. 2666.
- [192] M. Munakata, J. Dai, M. Maekawa, T. Kuroda-Sowa, J. Fukui. *Chem. Commun.* **1994**. 2331.
- [193] C. He, B. G. Zhang, C. Y. Duan, J. H. Li, Q. J. Meng. *Eur. J. Inorg. Chem.* **2000**. 2549.
- [194] P. Gomez, P. D. Hong, O. Roubeau, M. Lutz, W. L. Driessen, A. L. Speck, J. Reedijk. *Chem. Commun.* **2002**. 1488.
- [195] B. K. Saha, R. K. R. Jetti, S. Reddy, S. Aitipamula, A. Nangia. *Crystal Growth Design* **2005**. *5*, 887.
- [196] J. C. A. Kerckhoffs, F. W. B. van Leeuwen, A. L. Speck, H. Kooijman, M. Crego-Calama, D. N. Reinhoudt. *Angew. Chem.* **2003**. *115*, 5895.
- [197] C. R. L. P. N. Jeukens, P. Jonkheijm, F. J. P. Wijnen, J. C. Gielen, P. C. M. Cristianen, A. P. J. Schenning, E. W. Meijer, J. C. Man. *J. Am. Chem. Soc.* **2005**. *127*, 8280.
- [198] P. de Hoog, P. G. amd M. Lüken, O. Roubeau, B. Krebs, J. Reedijk. *Inorg. Chim. Acta* **2004**. *357*, 213.
- [199] S. Demeshko, G. Leibelng, S. Dechert, F. Meyer. *Dalton. Trans.* **2004**. 3782.
- [200] S. Demeshko, S. Dechert, F. Meyer. *J. Am. Chem. Soc.* **2004**. *126*, 4508.
- [201] H. Oshio, H. Ichida. *J. Phys. Chem.* **1995**. *99*, 3294.
- [202] S. P. Foxon, G. R. Torres, O. Walter, J. Z. Pederson, H. Toftlund, M. Hüber, K. Falk, W. Haase, J. Cano, F. Lloret, M. Julve, S. Schindler. *Eur. J. Inorg. Chem.* **2004**. 335.
- [203] T. T. Luo, Y. H-Liu, H. L. Tsai, C. C. Su, C. H. Ueng, K. L. Lu. *Eur. J. Inorg. Chem.* **2004**. 4253.
- [204] A. Kamiyama, T. Noguchi, T. Kajiwara, T. Ito. *Inorg. Chem.* **2002**. *42*, 507.
- [205] A. Kamiyama, T. Noguchi, T. Kajiwara, T. Ito. *CrystEngCommun.* **2003**. *5*, 231.
- [206] B. F. Abrahams, S. R. Batten, H. Hamit, B. Hoskins, R. Robson. *Angew. Chem. Int. Ed.* **1996**. *35*, 1690.
- [207] B. F. Abrahams, S. R. Batten, H. Hamit, B. Hoskins, R. Robson. *Chem. Commun.* **1996**. 1313.

- [208] S. R. Batten, B. Hoskins, R. Robson. *J. Am. Chem. Soc.* **1995**. *117*, 5385.
- [209] B. F. Abrahams, S. R. Batten, M. J. Grannas, H. Hamit, B. Hoskins, R. Robson. *Angew. Chem. Int. Ed.* **1999**. *38*, 1475.
- [210] M. I. J. Polson, N. J. Taylor, G. S. Hanan. *Chem. Commun.* **2002**. 1356.
- [211] A. Powell, S. L. Heath, D. Gatteschi, L. Pardi, R. Sessoli, G. Spina, F. D. Giallo, F. Pieralli. *J. Am. Chem. Soc.* **1995**. *117*, 2491.
- [212] A. L. Barra, A. Caneschi, A. Cornia, F. F. de Biani, D. Gatteschi, C. Sangregorio, R. Sessoli, L. Sorace. *J. Am. Chem. Soc.* **1999**. *121*, 5302.
- [213] C. Benelli, J. Cano, Y. Journaux, R. Sessoli, G. A. Solan, R. E. P. Winpenny. *Inorg. Chem.* **2001**. *40*, 188.
- [214] C. Wilson, B. B. Iversen, J. Overgaard, F. K. Larsen, G. Wu, S. P. Palli, G. A. Timco, N. V. Gerbeleu. *J. Am. Chem. Soc.* **2000**. *122*, 11370 and references herein.
- [215] G. J. Long, W. T. Robinson, W. P. Tappmeyer, D. L. Bridges. *Dalton Trans.* **1973**. 573.
- [216] H. R. Chang, K. Folting, J. C. Huffmann, G. Christou, D. N. Hendrickson. *J. Am. Chem. Soc.* **1987**. *109*, 5703.
- [217] R. D. Cannon, R. P. White. *Prog. Inorg. Chem.* **1988**. *36*, 195.
- [218] D. M. Kurtz. *Chem. Rev.* **1990**. *90*, 585.
- [219] R. E. Stenkamp. *Chem. Rev.* **1994**. *94*, 715.
- [220] D. T. Logan, X. D. Su, A. aberg, K. Regnstrom, J. Hajdu, H. Eklund, P. Nordlung. *Structure* **1996**. *4*, 1053.
- [221] A. C. Rosenzweig, C. A. Frederick, S. J. Lippard, P. Nordlund. *Nature* **1993**. *366*, 537.
- [222] B. J. Wallar, J. D. Lipscomb. *Chem Rev.* **1996**. *96*, 2625.
- [223] T. Klabunde, N. Sträter, B. krebs, H. Witzel. *FEBS Lett.* **1995**. *367*, 56.
- [224] E. I. Solomon, T. C. Brunold, M. I. Davis, J. N. Kemsley, S. K. Lee, N. Leanert, F. Neese, A. J. Skulan, Y. S. Zhou. *Chem. Rev.* **2000**. *100*, 235.
- [225] M. Costas, K. Chen, L. Que. *Coord. Chem. Rev.* **2000**. *517*, 200.
- [226] R. H. Holm, P. Kennepohl, E. I. Solomon. *Chem. Rev.* **1996**. *96*, 2239.
- [227] O. Kahn. *Acc. Chem. Res.* **2000**. *33*, 647.
- [228] H. H. T. Nguyen, A. K. Shiemke, S. J. Jacobs, B. J. Hales, M. E. Linstrom, S. I. Chan. *J. Biol. Chem.* **1994**. *269*, 14995.
- [229] A. Mukherjee, R. Raghunathan, M. K. Saha, M. Nethaji, S. Ramasesha, A. R. Chakravarty. *Chem. Eur. J.* **2005**. *11*, 3087.
- [230] N. S. Venkataramanan, G. Kuppuraj, S. Rajagopal. *Coord. Chem. Rev.* **2005**. *249*, 1249.
- [231] W. Plass. *Z. Anorg. Allg. Chem.* **1997**. *623*, 997.

- [232] W. Plass. *Inorg. Chim. Acta* **1996**. *224*, 221.
- [233] W. Plass. *Z. Anorg. Allg. Chem.* **1997**. *623*, 461.
- [234] W. Plass, A. Pohlmann, J. Rautengarten. *Angew. Chem.* **2001**. *113*, 4333.
- [235] W. Plass. *Angew. Chem.* **1996**. *108*, 699.
- [236] W. Plass. *Inorg. Chem.* **1997**. *36*, 2200.
- [237] W. Plass, G. Fries. *Z. Anorg. Allg. Chem.* **1997**. *623*, 1205.
- [238] I. Correia, J. C. Pessoa, M. T. Duarte, T. R. Henriques, M. F. M. Piedade, M. Fatima, L. F. Veiros, J. Tamas, T. Kiss, A. Doernyei, M. C. A. M. Margarida, F. C. G. G. Castro, F. Avecilla. *Chem. Eur. J.* **2004**. *10*, 2301.
- [239] A. W. Addison, T. N. Rao, J. Reedijk, J. van Rijn, G. C. Verschoor. *Dalton Trans.* **1984**. 1349.
- [240] K. S. Murray. *Coord. Chem. Rev.* **1974**. *12*, 1.
- [241] S. J. Lippard. *Angew. Chem., Int. Ed.* **1988**. *27*, 344.
- [242] R. E. Norman, R. C. Holz, S. Menage, C. J. O'Connor, J. H. Zhang, L. Q. Jr. *Inorg. Chem.* **1990**. *20*, 4629.
- [243] R. G. Wollman, D. N. Hendrickson. *Inorg. Chem.* **1977**. *16*, 723.
- [244] D. M. Collins, R. Countryman, J. L. Hoard. *J. Am. Chem. Soc.* **1972**. *94*, 2066.
- [245] J. L. Hoard, G. H. Cohen, M. D. Glick. *J. Am. Chem. Soc.* **1967**. *89*, 1992.
- [246] W. R. Scheidt, K. J. Haller, K. Hatano. *J. Am. Chem. Soc.* **1980**. *102*, 3017.
- [247] H. Masuda, T. Taga, K. Osaki, H. Sugimoto, Z. Yoshira, H. Ogoshi. *Inorg. Chem.* **1980**. *19*, 950.
- [248] B. J. Kennedy, K. S. Murray, P. R. Zwack, H. Hamborg, W. Kalz. *Inorg. Chem.* **1986**. *25*, 2539.
- [249] S. C. H. Wu, G. R. Rossman, H. B. Gray, G. S. Hammond, H. J. Schugar. *Inorg. Chem.* **1972**. *11*, 990.
- [250] S. M. Gorun, S. J. Lippard. *Inorg. Chem.* **1991**. *30*, 1625.
- [251] F. L. Gall, F. F. de Biani, A. Caneschi, P. Cinelli, A. Cornia, A. C. Fabretti, D. Gatteschi. *Inorg. Chim. Acta* **1998**. *262*, 2870.
- [252] F. Tuna, L. Patron, Y. Journaux, M. Andruh, W. Plass, J. C. Trombe. *Dalton Trans.* **1999**. 539.
- [253] H. D. Bian, J. Y. Xu, W. Gu, S. P. Yan, P. Cheng, D. Z. Liao, Z. H. Jiang. *Polyhedron* **2003**. *22*, 2927.
- [254] K. Isele, P. Franz, C. Ambrus, G. Bernardinelli, S. Decurtins, A. F. Williams. *Inorg. Chem.* **2005**. *44*, 3896.

- [255] Y. M. Li, J. J. Zhang, R. B. Fu, S. C. Xiang, T. L. Sheng, D. Q. Yuan, X. H. Huang, X. T. Wu. *Polyhedron* **2006**. *25*, 1618.
- [256] B. Bleaney, K. D. Bowers. *Proc. Roy. Soc. (London) Ser.A* **1952**. *214*, 451.
- [257] L. K. Thompson, S. K. Mandal, S. S. T. J. N. Bridson, M. K. Park. *Inorg. Chem.* **1996**. *35*, 3117.
- [258] C. L. M. Pereira, E. P. Pedroso, H. O. Strumpf, M. A. Novak, L. Ricard, R. Ruiz-Garcia, E. Rivière, Y. Journaux. *Angew. Chem.* **2004**. *116*, 973.
- [259] O. Kahn, Y. Pei, M. Verdaguer, J. P. Renard, J. Sletten. *J. Am. Chem. Soc.* **1988**. *11*, 782.
- [260] J. P. Costes, J. P. Laurent, J. M. Sanchez, J. S. Varela, M. Ahlgren, M. Sundberg. *Inorg. Chem.* **1997**. *36*, 4641.
- [261] H. O. Stumpf, Y. Pei, O. Kahn, J. Sletten, J. P. Renard. *J. Am. Chem. Soc.* **1993**. *115*, 6738.
- [262] D. Ranganathan, N. K. Vaish, G. Chandramouli, B. Varghese, R. Bose, P. Manoharan. *J. Am. Chem. Soc* **1995**. *117*, 1643.
- [263] M. Fettouhi, L. Ouahab, A. Boukhari, O. Cador, C. Mathoniere, O. Kahn. *Inorg. Chem.* **1996**. *35*, 4932.
- [264] I. Unamuno, J. M. Gutierrez-Zorrilla, A. Luque, P. Roman, L. Lezema, R. Calvo, T. Rojo. *Inorg. Chem.* **1998**. *37*, 6452.
- [265] H.-X. Zhang, B. S. Kang, A. w. Xu, Z.-N. Chen, Z.-Y. Zhou, A. Chan, K.-B. Yu, C. Ren. *J. Chem. Soc. Dalton Trans.* **2001**. 2559.
- [266] J. L. Sanz, B. Cervera, R. Ruiz, C. Bois, J. Faus, F. Lloret, M. Julve. *J. Chem. Soc. Dalton Trans* **1996**. 1359.
- [267] C. Surville-Barland, R. Ruiz, A. Aukauloo, Y. Journaux, I. Castro, B. Cervera, M. Julve, F. Lloret, F. Sapina. *Inorg. Chim. Acta* **1998**. *278*, 159.
- [268] J. Tercero, C. Diaz, J. Ribas, E. Ruiz, J. Mahia, M. Maestro. *Inorg. Chem.* **2002**. *41*, 6780.
- [269] Y.-Q. Sun, m. Liang, W. Dong, G.-M. Yang, D.-Z. Liao, Z. H. Jiang, S.-P. Yan, P. Cheng. *Eur. J. Inorg. Chem.* **2004**. 1514.
- [270] S. b. Wang, G. m. Yang, Y. f. Wang, D. z. Liao. *Eur. J. Inorg. Chem.* **2004**. 4907.
- [271] Z. N. Cheng, H. X. Zhang, K. B. Yu, K. C. Zheng, H. Cai, B. S. Kang. *Dalton Trans.* **1998**. 1133.
- [272] M. G. F. Vaz, L. M. M. Pinhero, H. O. Stumpf, A. F. C. Alcantara, S. Golhen, L. Ouahab, L. Ouahab, O. Cador, C. Mathoniere, O. Kahn. *Chem. Eur. J.* **1999**. *5*, 1486.
- [273] O. Kahn, Y. Pei, M. Verdaguer, J. P. Renard, J. Sletten. *J. Am. Chem. Soc.* **1988**. *110*, 782.

- [274] K. Nakatani, J. Y. Carriat, Y. Journaux, O. Kahn, F. Lloret, J. P. Renard, Y. Pei, J. Sletten, M. Verdaguer. *J. Am. Chem. Soc.* **1989**. *111*, 5739.
- [275] F. Lloret, M. Julve, J. Faus, Y. Journaux, M. P.-L. Y. Jeannin. *Inorg. Chem.* **1989**. *28*, 3702.
- [276] Y. Pei, O. Kahn, K. Nakatani, E. Coddjovi, C. Mathoniere, J. Sletten. *J. Am. Chem. Soc.* **1991**. *113*, 6558.
- [277] K. Nakatani, P. Bergerat, E. Coddjovi, C. Mathonière, Y. Pei, O. Kahn. *Inorg. Chem.* **1991**. *30*, 3978.
- [278] V. Baron, B. Guillon, J. Sletten, C. Mathoniere, E. Coddjovi, O. Kahn. *Inorg. Chim. Acta* **1995**. *235*, 69.
- [279] S. Turner, O. Kahn, L. Rabardel. *J. Am. Chem. Soc.* **1996**. *118*, 6428.
- [280] V. Baron, B. Gillon, A. Cousson, C. Mathonière, O. Kahn, A. Grand, L. Öhrström, B. delley, M. Bonnet, J. X. Boucherle. *J. Am. Chem. Soc.* **1997**. *119*, 3500.
- [281] O. Cadour, C. Mathoniere, O. Khan. *Inorg. Chem.* **2000**. *39*, 3799.
- [282] R. Ruiz, J. Faus, F. Lloret, M. Julve, Y. Journaux. *Coord. Chem. Rev.* **1999**. *193-195*, 1069.
- [283] J. Rrocero, c. Diaz, J. Ribas, M. Maestro, J. Mahia, H.S.-Evans. *Inorg. Chem.* **2003**. *42*, 3366.
- [284] L. Zhang, S.-B. Wang, G.-M. Yang, J. k Tang, D.-Z. Liao, Z.-H. Jiang, S.-P. Yan, P.Cheng. *Inorg. Chem.* **2003**. *42*, 1462 and references therein.
- [285] E.-Q. Gao, Q.-H. Zhao, J.-K. Tang, D.-Z. Liao, Z.-H. Jiang, S.-P. Yan. *J. Chem. Soc. Dalton Trans* **2001**. 1537.
- [286] F. Lloret, M. Julve, J. A. Real, J. Faus, R. Ruiz, M. Mollar, I. Castro, C. Bois. *Inorg. Chem.* **1992**. *31*, 2956.
- [287] F. Lloret, M. Julve, J. Faus, R. Ruiz, I. Castro, M. Mollar, M. Philoche-Levisalles. *Inorg. Chem.* **1992**. *31*, 784.
- [288] E. Q. Gao, J.-K. Tang, D.-Z. Liao, Z.-H. J. S.-P. Yan, G.-L. Wang. *Inorg. Chem.* **2001**. *40*, 3134.
- [289] Y. Pei, Y. Journaux, O. Khan. *Inorg. Chem.* **1988**. *27*, 399.
- [290] O. Gouillou, O. Khan, R. L. Oushoorn, K. Boubekour, P. Batail. *Inorg. Chim. Acta* **1992**. *198-200*, 119.
- [291] O. Kahn, J. Galy, Y. Journaux, J. Jaud, I. Morgenstern-Badarau. *J. Am. Chem. Soc.* **1982**. *104*, 2165.
- [292] Y. Journaux, O. Kahn, J. Zarembowitch, J. Galy, J. Jaud. *J. Am. Chem. Soc.* **1983**. *105*, 7585.
- [293] R. Ruiz, C. Surville-Barland, A. Aukauloo, E. Anxolabehere-Mallart, Y. Journaux, J. Cano, M. C. Munoz. *Dalton Trans.* **1997**. 745.

- [294] B. Cervera, J. L. Sanz, M. J. I. nez, G. Vila, F. Lloret, M. Julve, R. Ruiz, X. Ottenwaelder, A. Aukauloo, S. Poussereau, Y. Journaux, M. C. M. noz. *Dalton Trans.* **1998**. 781.
- [295] J. A. Real, R. Ruis, J. Faus, F. Lloret, M. Julve, Y. Journaux, M. Philoche-Levisalles, C. Bois. *Dalton Trans.* **1994**. 3769.
- [296] C. Mathonière, J. P. Sutter, J. V. Yakhmi. In *Magnetism: Molecules and materiales IV*. Wiley-WCH Inc., Weinheim **2005** 1.
- [297] D. Cooper, R. A. Plane. *Inorg. Chem.* **1966**. 5, 1677.
- [298] E. G. Cox, W. Wardlaw, K. C. Webster. *J. Chem. Soc.* **1936**. 775.
- [299] D.-H. Kim, J.-e, C. S. Oh, Y. Do. *Inorg. Chem.* **2005**. 44, 4383.
- [300] E. Sinn, C. M. Harris. *Coord. Chem. Rev.* **1969**. 391.
- [301] A. Bencini, C. Benelli, A. Caneschi, R. L. Carlin, A. Dei, D. Gatteschi. *J. Am. Chem. Soc.* **1985**. 107, 8128.
- [302] P. A. Vigato, S. Tamburini. *Coord. Chem. Rev.* **2004**. 248, 1717.
- [303] P. G. Cozzi. *Chem. Soc. Rev.* **2004**. 33, 410.
- [304] J. A. McCleverty, M. D. Ward. *Acc. Chem. Res.* **1998**. 31, 842.
- [305] A. Bencini, C. Benelli, A. Caneschi, A. Dei, D. Gatteschi. *Inorg. Chem.* **1986**. 25, 572.
- [306] C. Benelli, A. Caneschi, D. G. abd O. Guillou, L. Pardi. *Inorg. Chem.* **1990**. 29, 1750.
- [307] U. Casellato, P. Guerriero, S. Tamburini, S. Sitran, P. A. Vigato. *Dalton Trans.* **1991**. 2145.
- [308] I. Ramade, O. K. Y. Jeannini, F. Robert. *Inorg. Chem.* **1997**. 26, 930.
- [309] M. Sasaki, K. Manseki, H. Horiuchi, M. Kumagai, M. Sakamoto, H. Sakiyama, Y. Nishida, M. Sakai, Y. Sadaoka, M. Ohba, H. Okawa. *Dalton Trans.* **2000**. 259.
- [310] M. Sakamoto, K. Manseki, H. Ōkawa. *Coord. Chem. Rev.* **2001**. 219-221, 379.
- [311] J. P. Costes, f. Dahan, G. Novitchi, V. Arion, S. Shova, J. Lipkowski. *Eur. J. Inorg. Chem.* **2004**. 1530.
- [312] J. Costes, F. Dahan, A. Depuis. *Inorg. Chem.* **2000**. 39, 5994.
- [313] J. Costes, F. Dahan, A. Depuis, J. P. Laurent. *Inorg. Chem.* **1997**. 36, 3429.
- [314] J. Costes, F. Dahan, A. Depuis, J. P. Laurent. *New. J. Chem.* **1998**. 1525.
- [315] A. Gleizes, M. Julve, N. Kuzmina, A. Alikhanyan, F. Lloret, I. Malcherova, J. L. Sanz, F. Senocq. *Eur. J. Inorg. Chem.* **1998**. 1169.
- [316] A. Seminara, S. Giuffrida, A. Musumeci, I. Fragala. *Inorg. Chim. Acta* **1984**. 95, 201.
- [317] I. Ramade, O. Khan, Y. Jeannin, F. Robert. *Inorg. Chem.* **97**. 36, 930.
- [318] J. P. Costes, F. Dahan, W. Wernsdorfer. *Inorg. Chem.* **2006**. 45, 5.

- [319] G. Novitchi, S. Shova, A. Caneschi, J. P. Costes, M. Gdniec, N. Stanica. *Dalton Trans.* **2004.** 1194.
- [320] M. Ryazanov, V. Nikivorov, F. Lloret, M. Julve, N. Kuzmina, A. Gleizes. *Inorg. Chem.* **2002.** *41*, 1816.
- [321] C. Benelli, D. Gatteschi. *Chem. Rev.* **2002.** *102*, 2369.
- [322] C. Kollmar, O. Kahn. *Acc. Chem. Res.* **1993.** *26*, 259.
- [323] M. Andruh, I. Ramade, E. Codjovi, O. Guillou, O. Kahn, J. C. Trombe. *J. Am. Chem. Soc.* **1993.** *115*, 1822.
- [324] Y. Aratake, M. Koikawa, H. Ōkawa, S. Kida. *Inorg. Chim. Acta* **1991.** *190*, 85.
- [325] J. Costes, F. Dahan, A. Dupuis, J. P. Laurent. *Inorg. Chem.* **1997.** *36*, 3429.
- [326] J. P. Costes, F. Dahan, A. Dupuis, J. P. Laurent. *Inorg. Chem.* **1996.** *35*, 2400.
- [327] J. Costes, F. Dahan, A. Dupuis, J. P. Laurent. *Inorg. Chem.* **1997.** *36*, 4284.
- [328] J. P. Costes, M. Auschel, F. Dahan, V. Peyrou, S. Shova, W. Wernsdorfer. *Inorg. Chem.* **2006.** *45*, 1924.
- [329] R. Koner, G. Lee, Y. Wang, H. Wei, S. Mohanta. *Eur. J. Inorg. Chem.* **200.** 1500.
- [330] J. P. Costes, S. Shova, J. M. C. Juan, N. Suet. *Dalton Trans.* **2005.** 2830.
- [331] J. P. Costes, A. Dupuis, J. P. Laurent. *Eur. J. Inorg.* **1998.** 1543.
- [332] J. P. Costes, G. Novitchi, S. Shova, F. Dahhan, B. Donnadieu, J. P. Tuchagues. *Inorg. Chem.* **2004.** *43*, 7792.
- [333] J. P. Costes, J. M. Clemente-Juan, F. Dahan, J. Milon. *Inorg. Chem.* **2004.** *43*, 8200.
- [334] J. Costes, F. Dahan, A. Dupuis. *Inorg. Chem.* **2000.** *39*, 165.
- [335] J. Costes, F. Dahan, A. Dupuis, J. P. Laurent. *Inorg. Chem.* **2000.** *39*, 169.
- [336] R. Gheorghe, M. Andruh, A. Muller, M. Schmidtman. *Inorg. Chem.* **2002.** *41*, 5314.
- [337] D. Cunningham, P. McArdle, M. Mitchell, N. N. Chonchubhair, M. O'Gara, F. Franceschi, C. Floriani. *Inorg. Chem.* **2000.** *39*, 1639.
- [338] J. Costes, F. Dahan, A. Dupuis, J.-P. Laurent. *Chem. Eur. J.* **1998.** *4*, 1616.
- [339] M. L. Kahn, C. Mathoniere, O. Kahn. *Inorg. Chem.* **1999.** *38*, 3692.
- [340] S. Leininger, B. Olenyuk, P. J. Stang. *Chem. Rev.* **2000.** *100*, 853.
- [341] H. W. Roesky, M. Andruh. *Coord. Chem. Rev.* **2003.** *236*, 91.
- [342] M. Fujita, Y. J. Kwon, S. Washizu, K. Ogura. *J. Am. Chem. Soc.* **1994.** *116*, 1151.
- [343] O. R. Evans, H. L. Ngo, W. Lin. *J. Am. Chem. Soc.* **2001.** *123*, 10395.
- [344] Y. Matuura, S. Matsushima, M. Sakamoto, Y. Sadaoka. *J. Mater. Chem.* **1993.** *3*, 767.

- [345] M. Sakamoto, K. Matsuki, R. Oshumi, Y. Nakayama, A. Matsumoto, H. Okawa. *Bull. Chem. Soc. Jpn.* **1992**. *65*, 2278.
- [346] J. Yang, Q. Yue, G.-D. Li, J.-J. Cao, G.-H. Li, J.-S. Chen. *Inorg. Chem.* **2006**. *45*, 2857.
- [347] O. Kahn. *Acc. Chem. Res.* **2000**. *33*, 647.
- [348] S. Ueki, Y. Kobayashi, T. Ishida, T. Nogami. *Chem. Commun* **2005**. 5223.
- [349] R. Gheorge, P. Cucos, M. Andruh, J. P. Costes, B. Donnadiou, S. Shova. *Chem. Eur. J.* **2005**. *11*, 1.
- [350] R. Gheorge, M. Andruh, J. P. Costes, B. Donnadiou. *Chem. Commun.* **2003**. 2778.
- [351] P. Przychodzen, K. Lewinski, R. Pelka, M. Balanda, K. Tomola, B. Sicklucka. *Dalton Trans.* **2006**. 625.
- [352] A. Figuerola, C. Diaz, J. Ribas, V. Tangoulis, J. Granell, F. lloret, J. Mahaia, M. Maestro. *Inorg. Chem.* **2003**. *42*, 641.
- [353] A. Figuerola, C. Diaz, M. E. Fallah, J. Ribas, M. Maestro, J. Mahia. *Chem. Commun.* **2001**. 1240.
- [354] O. Kahn, J. Larionova, L. Ouahab. *Chem. Commun.* **1998**. 945.
- [355] S. Tanase, M. Andruh, a. Muller, M. Schmidtman, C. Mathoniere. *Chem. Commun.* **2001**. 1084.
- [356] H.-Z. Kou, S. Gao, C. h Li, D.-Z. Liao, B.-C. Zhou, R.-J. Wang, Y. Li. *Inorg. Chem.* **2002**. *41*, 4756.
- [357] A. Figuerola, C. Diaz, J. Ribas, V. Tangoulis, C. Sangregorio, D. Gatteschi, M. Maestro, J. Mahia. *Inorg. Chem* **2003**. *42*, 5274.
- [358] H.-Z. Kou, B. C. Zhoun, S. Gao, J. Wang. *Angew. Chem.* **2003**. *115*, 3410.
- [359] H.-Z. Kou, B. C. zhou, R.-J. Wang. *Inorg. Chem.* **2003**. *42*, 7658.
- [360] G. Novitchi, J. P. Costes, B. Donnadiou. *Eur. J. Inorg. Chem.* **2004**. 1808.
- [361] A.-Q. Wu, F.-K. Zheng, W.-T. Chen, G.-C. Guo, J.-S. Huang, Z.-C. Dong, Y. Takano. *Inorg. Chem.* **2004**. *43*, 4839.
- [362] Y. Kobayashi, S. Ueki, T. Ishida, T. Nogami. *Chem. Physics Lett.* **2003**. *378*, 337.
- [363] J.-K. Tang, Y. z Li, Q.-L. Wang, E.-Q. Gao, D.-Z. Liao, Z. H. Jiang, S.-P. Yan, P. Cheng, L.-F. Wang, G.-L. Wang. *Inorg. Chem.* **2002**. *41*, 2188.
- [364] C. Daiguebone, N.Kerbellec, K. Bernot, Y. Gerault, O. Guillou. *Inorg. Chem.* **2006**. *45*, 5399.
- [365] Q. Yue, G. Li, G. Li, W. Xu, J. Chen, S. Wang. *Inorg Chem.* **2005**. *44*, 5241.
- [366] A. Dimos, D. Tsaousis, A. Michelides, S. Skoulika, S. Golhen, L. Ouahab, C. D. A. Aubry. *Chem. Mater.* **02**. *14*, 2002.

- [367] Z. Zhang, Y. Song, T. Okamura, Y. Hasegawa, W. Sun, N. Ueyama. *Inorg. Chem.* **2006**. *44*, 2887.
- [368] S. Zang, Y. Su, Y. Li, H. Zhu, Q. Meng. *Inorg. Chem.* **2006**. *45*, 2972.
- [369] W. Shi, X.-Y. Chen, Y.-N. Zhao, B. Zhao, P. Cheng, A. Yu, H. Song, H. Wang, D. Liao, S. Yan, Z. Jiang. *Chem. Eur. J.* **2005**. *11*, 5031.
- [370] D. Jhon, W. Urland. *Eur. J. Inorg. Chem.* **2005**. 4486.
- [371] S. Thushari, J. A. K. Cha, H. H. Y. Sung, S. S. Y. C. A. L.-F. Leung, Y.-F. Yen, I. D. Williams. *Chem. Commun.* **2005**. 5515.
- [372] P. Mahata, G. Sankar, G. Madras, S. Natarajan. *Chem. Commun.* **2005**. 5787.
- [373] Q. Yue, J. Yang, G.-H. Li, G. D. Li, W. Xu, J. S. Chen, S. N. Wang. *Inorg. Chem.* **2005**. *44*, 5241.
- [374] S. Ghosh, P. Bharadwaj. *Eur. J. Inorg. Chem.* **2005**. 4886.
- [375] Q. Liu, L. Xu. *Eur. J. Inorg. Chem.* **2005**. 3458.
- [376] J. Zhang, T. L. Sheng, S. Q. Xia, G. Leibelling, F. Mayer, S. Hu, R. Fu, S. Xiang, X. Weu. *Inorg. Chem.* **2004**. *43*, 5472.
- [377] M. H. Molina, C. Ruiz-Perez, T. Lopes, F. Lloret, M. Julve. *Inorg. Chem.* **2003**. *42*, 5446.
- [378] S. T. Hatscher, W. Urland. *Angew. Chem.* **2003**. *115*, 2969.
- [379] B. Zhao, P. Cheng, Y. Dai, C. Cheng, D. Z. Liao, S.-P. Yan, Z.-H. Jiang, G. L. Wang. *Angew. Chem.* **2003**. *115*, 964.
- [380] J. P. Costes, J. M. Clemente-Juan, F. Dahan, F. Nicodeme, M. Verelst. *Angew. Chem.* **2002**. *114*, 333.
- [381] X.-J. Zheng, L. P. Jin, S.-Z. Lu. *Eur. J. Inorg. Chem.* **2002**. 3356.
- [382] A. Rizzi, R. Baggio, R. Calvo, M. T. Garland, O. Pena, M. Perec. *Inorg. Chem.* **2001**. *40*, 3623.
- [383] Y. Liang, R. Cao, W. Su, M. Hong, W. Zhang. *Angew. Chem.* **2000**. *112*, 3442.
- [384] L. Pan, X. Huang, J. Liand, Y. Wu, N. Zheng. *Angew. Chem.* **2000**. *112*, 537.
- [385] Y. Cui, G. Chen, J. Rin, Y. Quian, J. Huang. *Inorg. Chem.* **2000**. *39*, 4165.
- [386] C. Aronica, G. Pilet, G. Chastanet, W. Wernsdorfer, J.-F. Jaquot, D. Luneau. *Angew. Chem.* **2006**. *118*, 4775.
- [387] N. Ishikawa, S. Otsuka, Y. Kaizu. *Angew. Chem.* **2004**. *116*, 2.
- [388] T. Kido, Y. Ikuta, Y. Sanatsuki, Y. Ogawa, N. Matsumoto. *Inorg. Chem.* **2003**. *42*, 398.
- [389] J. Tang, I. Hewitt, N. T. G. Chasanet, W. Wernsdorfer, C. E. Anson, C. Benelli, R. Sessoli, A. K. Powell. *Angew. Chem.* **2006**. *118*, 1761.

- [390] N. Ishikawa, M. Sugita, W. Wernsdorfer. *Angew. Chem.* **2005.** *117,* 2991.
- [391] A. Mishara, W. Wernsdorfer, K. A. Abboud, G. Cristou. *J. Am. Chem. Soc.* **2004.** *126,* 15648.
- [392] C. M. Zeleski, E. Depperman, J. W. Kampf, M. L. Kirk, V. C. Pecoraro. *Angew. Chem.* **2004.** *116,* 4002.
- [393] N. Ishikawa, M. Sugita, T. Ishikawa, S. Y. Kóshihara, Y. Kaizu. *J. Am. Chem. Soc.* **2003.** *125,* 8694.
- [394] A. Mishra, W. Wernsdorfer, S. Parson, G. Christou, E. Brecin. *Chem. Commun.* **2005.** 2086.
- [395] L. Thomas, F. Lioni, R. Ballou, D. Gatteschi, R. Sessoli, B. Barbara. *Nature* **1996.** *383,* 145.
- [396] D. Gatteschi, R. Sessoli. *Angew. Chem.* **2003.** *115,* 278.
- [397] S. Noro, H. Miyasaka, S. Kitagawa, T. Okubo, M. Yamashita, T. Mitani. *Inorg. Chem.* **2005.** *44,* 133.
- [398] J. Sutter, M. Kahn. In *Magnetism: Molecules and materials V.* Wiley-WCH Inc., Weinheim **2005** 161.
- [399] F. Avecilla, C. Platas-Iglesias, R. Rodriguez-Cortinas, G. Guillemont, J.-C. Bunzeli, C. D. Brondino, C. Geraldes, T. Rodrigues-Blas. *Dalton Trans.* **2002.** 4658.
- [400] J. P. Costes, J. Clemente-juan, F. Dahan, F. Nicodeme. *Dalton Trans.* **2003.** 1272.
- [401] A. Figuerola, J. Ribas, M. Llunell, D. Casanova, M. Maestro, S. Alvares, C. Diaz. *Inorg. Chem.* **2005.** *44,* 6939.
- [402] J. Paulovic, F. Cimpoesu, M. Fierbinteanu, K. Hirao. *J. Am. Chem. Soc.* **2004.** *3126,* 3321.
- [403] C. Christou, D. Gatteschi, D. N. Hendrickson, R. Sessoli. *MRS. Bull.* **2000.** *25,* 66.
- [404] J. McCleverty, M. Ward. *Acc. Chem. Res.* **1998.** *31,* 842.
- [405] R. Winpenny. *Chem. Soc. Rev.* **1998.** *27,* 447.
- [406] Y. Yukawa, G. Aromi, S. Igarashi, J. Ribas, S. A. Zvyagin, J. Krzystek. *Angew. Chem.* **2004.** *117,* 2033.
- [407] S. Osa, T. Kido, N. Matsumoto, N. Re, A. Pochaba, J. Mrozinski. *J. Am. Chem. Soc.* **2004.** *126,* 420.
- [408] J.-C. Bünzli. *Acc. Chem. Rev.* **2006.** *39,* 53.
- [409] S. Torelli, D. Imbert, M. Cantuel, G. Bernardinelli, S. Delahage, A. Hauser, J.-C. Bünzeli, C. Piquet. *Chem. E. J.* **2005.** *11,* 3228.
- [410] O. Margeat, P. G. Lacroix, J. Costes, B. Donnadiou, C. Lepetit. *Inorg. Chem.* **2004.** *43,* 4743.
- [411] H. Tsukube, S. Shinoro. *Chem. Rev.* **2002.** *102,* 2389.

- [412] S. Akine, T. Matsumoto, T. Taniguchi, T. Nebeshima. *Inorg. Chem.* **2005.** *44,* 3270.
- [413] J. P. Costes, F. Dahan, F. Nicodeme. *Inorg. Chem.* **2004.** *42,* 6556.
- [414] R. Boggio, R. Calvo, M. Garland, O. Pena, M. Pereg, A. Rizzi. *Inorg. Chem.* **2005.** *44,* 8979.
- [415] T. Shiga, M. Ohba, H. Okawa. *Inorg. Chem.* **2004.** *43,* 4435.
- [416] A. R. Paital, T. Mitra, D. Ray, W. T. Wong, J. Ribas-Arino, J. J. Novoa, J. Ribas, G. Aromí. *Chem. Commun.* **2005.** 5172.
- [417] I. Fernández, R. Ruiz, J. Faus, M. Julve, F. Lloret, J. Cano, X. Ottenwaelder, Y. Journaux, M. C. Munoz. *Angew. Chem.* **2001.** *113,* 3129.
- [418] A. Bencini, D. Gatteschi, F. Totti, D. N. Sanz, J. A. McCleverty, M. D. Ward. *J. Phys. Chem. A* **1998.** *102,* 10545.
- [419] S. G. Sreerama, S. Pal. *Inorg. Chem.* **2005.** *44,* 6299.

Characterization techniques

Carbon, hydrogen and nitrogen contents were determined at the "Institut für Organische und Makromolekulare Chemie", Friedrich-Schiller University, Jena using LECO CHN/932 and VARIO EL III elemental analyzers.

Spectrophotometric measurements in solution - Varian Cary 5000 UV/Vis/NIR spectrophotometer equipped with dual cell peltier accessory. Additionally, spectrophotometric measurements in solid state on BaSO₄ diluted samples were performed using Varian Cary 5E UV/Vis/NIR spectrophotometer.

IR spectra were recorded on Bruker IFS55/Equinox spectrometer on samples prepared as KBr pellets.

Thermogravimetric analysis were carried out using NETZSCH STA 409PC/PG instrument. The samples were placed in a heating block, with a heating rate of 20 K/min, under nitrogen atmosphere

¹H, ¹³C, NMR, ¹H{¹H} COSY and ¹H{¹³C} heteronuclear correlation NMR spectra were recorded on Bruker Avance 200 and 400 MHz spectrometers.

Mass spectroscopy analysis were conducted on a MATSSQ-710 Bruker instrument as FAB measurements.

Electronic paramagnetic resonance measurements were performed on a Bruker ESP 300E using X-Band (9 GHz).

Variable temperature magnetic data were obtained using Quantum Design MPMSR-55-SQUID Magnetometer with a magnet of 5 Tesla in the temperature range 2-300 K. Fitting of the experimental magnetic data sets were performed using ORIGIN Programm based

on non-linear described equations.

The crystallographic data were collected on a Nonius KappaCCD diffractometer, using graphite-monochromated Mo-K α radiation of 71.073 pm. A summary of crystallographic data and data collection for all complexes is given in the last part of the thesis. The structures were solved by direct methods (SHELXL-97, G. Sheldrick, Göttingen University, 1997) and subsequent least square refinement. All non-hydrogen atoms were refined by using anisotropic displacement parameters, while the hydrogen atoms were fixed and refined including their isotropic displacement parameters. Additionally, small sized crystals were measured using synchrotron-radiation at the European Synchrotron Radiation Facility, Grenoble, France.

Summary of crystallographic data for complex **1** [Fe(imsalhy)(Cl)]₃·3CH₃OH.

Formula	C ₃₆ H ₃₆ N ₁₂ Cl ₃ O ₉ Fe ₃
Formula weight	1054.67
Crystal size (mm)	0.03 x 0.03 x 0.02
Crystal system	rhombohedral
Space group	R3c
Lattice parameters	
a (pm)	1511.04(2), α 90.00
b(pm)	1511.04(2), β 90.00
c (pm)	4104.54(6), γ 120.00
Cell volume (10 ⁶ pm ³)	8116.09(19)
Z	6
Temperature (K)	183(2)
Δ_{calc} (g cm ⁻³)	1.295
F(000)	3222
μ (Mo K α)(mm ⁻¹)	0.996
Data collection range (°)	3.08 ≤ Θ ≤ 27.87
Index range	-17 ≤ h ≤ 19 19 ≤ k ≤ -53 -53 ≤ l ≤ 52
Reflection measured	
total	4282
unique	4012 (R_{int} = 0.0332)
Goodness-of-fit	1.100
R ₁	0.0456
wR ₂	0.1352

Summary of crystallographic data for complex **1·3EtOH** [Fe(imsalhy)(Cl)]₃·3EtOH.

Formula	C ₄₀ H ₃₆ N ₁₂ Cl ₃ O ₁₀ Fe ₃
Formula weight	1124.04
Crystal size (mm)	0.02 x 0.02 x 0.02
Crystal system	rhombohedral
Space group	R3c
Lattice parameters	
a (pm)	14.6253(2), α 90.00
b(pm)	14.6253(2), β 90.00
c (pm)	80.1913(13), γ 120.00
Cell volume (10 ⁶ pm ³)	14854.8(4)
Z	12
Temperature (K)	293(2)
Δ_{calc} (g cm ⁻³)	1.508
F(000)	6860
μ (Mo K α)(mm ⁻¹)	1.095
Data collection range (°)	2.89 ≤ Θ ≤ 27.48
Index range	-13 ≤ h ≤ 18 -18 ≤ k ≤ 14 -81 ≤ l ≤ 103
Reflection measured	
total	15062
unique	2856 ($R_{int} = 0.0338$)
Goodness-of-fit	1.029
R ₁	0.0387
wR ₂	0.1031

Summary of crystallographic data for complex **2** [Fe(imsalhy)(N₃)₃·3.5DMF

Formula	C _{43.50} H _{48.50} N _{24.50} O _{9.50} Fe ₃
Formula weight	1234.12
Crystal size (mm)	0.03 x 0.03 x 0.02
Crystal system	triclinic
Space group	P-1
Lattice parameters	
a (pm)	13.2723(3), α 114.065
b(pm)	13.8547(3), β 93.6130
c (pm)	16.3576(13), γ 90.4740
Cell volume (10 ⁶ pm ³)	2739.10
Z	2
Temperature (K)	183(2)
Δ_{calc} (g cm ⁻³)	1.496
F(000)	1270
μ (Mo K α)(mm ⁻¹)	0.861
Data collection range (°)	2.50 ≤ Θ ≤ 27.49
Index range	-17 ≤ h ≤ 15 -17 ≤ k ≤ 17 -18 ≤ l ≤ 21
Reflection measured	
total	18219
unique	9250 (R_{int} = 0.0356)
Goodness-of-fit	1.055
R ₁	0.0650
wR ₂	0.1634

Summary of crystallographic data for complex **3**
 $[[\text{Fe}(\text{imsalhy})(\text{NCS})]_3 \cdot (\text{H}_3\text{imsalhy}) \cdot (\text{NO}_3) \cdot 0.5\text{H}_2\text{O} \cdot 4.25\text{CH}_3\text{OH}]$

Formula	$\text{C}_{47}\text{H}_{35.50}\text{N}_{20}\text{O}_{11}\text{S}_3\text{Fe}_3 \cdot 0.5\text{H}_2\text{O} \cdot 4.25\text{CH}_3\text{OH}$
Formula weight	1465.37
Crystal size (mm)	0.03 x 0.03 x 0.02
Crystal system	triclinic
Space group	P-1
Lattice parameters	
a (pm)	11.7463(6), α 97.764
b (pm)	16.0107(7), β 96.029
c (pm)	18.6462(9), γ 96.910
Cell volume (10^6pm^3)	2739.10
Z	2
Temperature (K)	183(2)
$\Delta_{calc}(\text{g cm}^{-3})$	1.422
F(000)	1506
$\mu(\text{Mo K}\alpha)(\text{mm}^{-1})$	0.794
Data collection range ($^\circ$)	$2.22 \leq \Theta \leq 27.50$
Index range	$-15 \leq h \leq 12$ $-20 \leq k \leq 19$ $-20 \leq l \leq 24$
Reflection measured	
total	22248
unique	8171 ($R_{int} = 0.0587$)
Goodness-of-fit	1.075
R_1	0.0981
wR_2	0.2149

Summary of crystallographic data for complex **1a** [Fe(imsalhy)(Cl)]₃·CH₃OH·3DMF

Formula	C ₄₃ H ₄₉ N ₁₅ O ₁₀ Cl ₃ Fe ₃
Formula weight	1209.87
Crystal size (mm)	0.04 x 0.03 x 0.03
Crystal system	triclinic
Space group	P-1
Lattice parameters	
a (pm)	13.8168(2), α 63.4410(10)
b(pm)	15.0960(3), β 73.4850(10)
c (pm)	15.1955(3), γ 69.6010(10)
Cell volume (10 ⁶ pm ³)	2625.85(8)
Z	2
Temperature (K)	183(2)
Δ_{calc} (g cm ⁻³)	1.530
F(000)	1242
μ (Mo K α)(mm ⁻¹)	1.040
Data collection range (°)	2.02 ≤ Θ ≤ 27.46
Index range	-17 ≤ h ≤ 17 -19 ≤ k ≤ 19 -19 ≤ l ≤ 19
Reflection measured	
total	18958
unique	8858 (R_{int} = 0.0277)
Goodness-of-fit	1.013
R ₁	0.0411
wR ₂	0.0919

Summary of crystallographic data for complex 4 [Fe(imsalhy)(NCS)]₄·4CH₃OH

Formula	C ₅₂ H ₄₈ N ₂₀ O ₁₂ S ₄ Fe ₄
Formula weight	1496.74
Crystal size (mm)	0.03 x 0.03 x 0.02
Crystal system	tetragonal
Space group	P4(2)/n
Lattice parameters	
a (pm)	15.3263(3), α 90
b(pm)	15.3263(3), β 90
c (pm)	13.5603(3), γ 90
Cell volume (10 ⁶ pm ³)	3185.4(1)
Z	2
Temperature (K)	183(2)
Δ_{calc} (g cm ⁻³)	1.561
F(000)	1828
μ (Mo K α)(mm ⁻¹)	1.099
Data collection range (°)	2.01 ≤ Θ ≤ 27.48
Index range	-19 ≤ h ≤ 19 -19 ≤ k ≤ 19 -17 ≤ l ≤ 16
Reflection measured	
total	22313
unique	2756(R_{int} = 0.0549)
Goodness-of-fit	1.014
R ₁	0.0409
wR ₂	0.1063

Summary of crystallographic data for complex **5** [Ni(imsalhy)₂] \cdot 4CH₃CN

Formula	C ₂₆ H ₂₄ N ₁₀ O ₄ Ni
Formula weight	599.26
Crystal size (mm)	0.03 x 0.03 x 0.02
Crystal system	monoclinic
Space group	C2/c
Lattice parameters	
a (pm)	18.9168(5), α 90
b(pm)	9.3221(2), β 101.642(1)
c (pm)	15.1112(5), γ 90
Cell volume (10 ⁶ pm ³)	2609.9(1)
Z	4
Temperature (K)	183(2)
Δ_{calc} (g cm ⁻³)	1.525
F(000)	1240
μ (Mo K α)(mm ⁻¹)	0.798
Data collection range (°)	2.20 \leq Θ \leq 27.47
Index range	-20 \leq h \leq 24 -11 \leq k \leq 12 -17 \leq l \leq 19
Reflection measured	
total	8167
unique	2501(R_{int} = 0.0352)
Goodness-of-fit	1.030
R ₁	0.0477
wR ₂	0.1344

Summary of crystallographic data for complex **6**
 $[\text{Ni}_3\text{L}^{\text{Br}}(\text{bipy})_3(\text{OH}_2)_3]\text{NO}_3 \cdot 8\text{H}_2\text{O} \cdot 1.5\text{DMF} \cdot 2.25\text{MeOH}$

Formula	$\text{C}_{58.50}\text{H}_{42.25}\text{N}_{13.50}\text{O}_{21.50}\text{Br}_3 \text{Ni}_3$
Formula weight	1694.17
Crystal size (mm)	0.06 x 0.06 x 0.04
Crystal system	hexagonal
Space group	P6(3)/m
Lattice parameters	
a (pm)	21.9299(4), α 90.00
b(pm)	21.9299(4), β 90.00
c (pm)	21.9961(4), γ 120.00
Cell volume (10^6pm^3)	9161.1(3)
Z	4
Temperature (K)	183(2)
$\Delta_{\text{calc}}(\text{g cm}^{-3})$	1.250
F(000)	3510
$\mu(\text{Mo K}\alpha)(\text{mm}^{-1})$	1.982
Data collection range ($^\circ$)	$2.62 \leq \Theta \leq 27.47$
Index range	$-22 \leq h \leq 28$ $-28 \leq k \leq 27$ $-26 \leq l \leq 23$
Reflection measured	
total	7092
unique	5088 ($R_{\text{int}} = 0.0524$)
Goodness-of-fit	1.063
R_1	0.0700
wR_2	0.2088

Summary of crystallographic data for complex **7**
 $[\text{Ni}_3\text{L}^{\text{Br}}(\text{bipy})_3(\text{DMF})_2\text{Cl}]\cdot\text{DMF}\cdot 2\text{CH}_3\text{CN}\cdot\text{MeOH}\cdot\text{H}_2\text{O}$

Formula	$\text{C}_{71}\text{H}_{79}\text{N}_{19}\text{O}_9\text{Br}_3 \text{Ni}_3$
Formula weight	1793.84
Crystal size (mm)	0.06 x 0.06 x 0.04
Crystal system	Triclinic
Space group	P-1
Lattice parameters	
a (pm)	12.5258(4), α 70.691(2)
b(pm)	18.0165(7), β 73.096(2)
c (pm)	20.8704(9), γ 84.678(2)
Cell volume (10^6pm^3)	4252(3)
Z	2
Temperature (K)	183(2)
$\Delta_{\text{calc}}(\text{g cm}^{-3})$	1.401
F(000)	1832
$\mu(\text{Mo K}\alpha)(\text{mm}^{-1})$	2.159
Data collection range ($^\circ$)	$2.10 \leq \Theta \leq 27.45$
Index range	$-16 \leq h \leq 15$ $-23 \leq k \leq 22$ $-22 \leq l \leq 27$
Reflection measured	
total	27941
unique	10975 ($R_{\text{int}} = 0.0479$)
Goodness-of-fit	1.012
R_1	0.0699
w R_2	0.1643

Summary of crystallographic data for complex **8**
 $[\text{Ni}_5(\text{L}^{Br})_2(\text{bipy})_4(\text{OH}_2)_4(\text{DMF})] \cdot 1.5\text{MeOH} \cdot 6\text{DMF} \cdot 4.75\text{H}_2\text{O}$

Formula	$\text{C}_{106.50}\text{H}_{129}\text{N}_{27}\text{O}_{22.25}\text{Br}_6 \text{Ni}_5$
Formula weight	2916
Crystal size (mm)	0.04 x 0.04 x 0.03
Crystal system	monoclinic
Space group	P2(1)/n
Lattice parameters	
a (pm)	16.1787(4), α 90.00
b(pm)	28.8422(8), β 92.335
c (pm)	26.7712(5), γ 90.00
Cell volume (10^6pm^3)	4252(3)
Z	4
Temperature (K)	183(2)
$\Delta_{calc}(\text{g cm}^{-3})$	1.552
F(000)	5940
$\mu(\text{Mo K}\alpha)(\text{mm}^{-1})$	2.737
Data collection range ($^\circ$)	$1.89 \leq \Theta \leq 27.54$
Index range	$-18 \leq h \leq 20$ $-25 \leq k \leq 37$ $-34 \leq l \leq 32$
Reflection measured	
total	70758
unique	13375 $R_{int} = 0.1063$)
Goodness-of-fit	0.995
R_1	0.0724
w R_2	0.1462

Summary of crystallographic data for complex **9** $[\text{Ni}_3\text{L}^{\text{Br}}(\text{tptz})_3]\text{NO}_3 \cdot 6.75\text{MeOH} \cdot 4\text{H}_2\text{O}$

Formula	$\text{C}_{82}\text{H}_{67.50}\text{N}_{25.50}\text{O}_{15.75}\text{Br}_3 \text{Ni}_3$
Formula weight	2077.98
Crystal size (mm)	0.05 x 0.05 x 0.05
Crystal system	rhombohedral
Space group	R-3c
Lattice parameters	
a (pm)	22.2156(10), α 90.00
b(pm)	22.2156(10), β 90.00
c (pm)	66.798(3), γ 120.00
Cell volume (10^6pm^3)	28550(2)
Z	12
Temperature (K)	183(2)
$\Delta_{\text{calc}}(\text{g cm}^{-3})$	1.450
F(000)	12636
$\mu(\text{Mo K}\alpha)(\text{mm}^{-1})$	1.921
Data collection range ($^\circ$)	$1.93 \leq \Theta \leq 27.44$
Index range	$-26 \leq h \leq 26$ $-25 \leq k \leq 28$ $-80 \leq l \leq 86$
Reflection measured	
total	7831
unique	2002 $R_{\text{int}} = 0.0301$)
Goodness-of-fit	1.048
R_1	0.0642
wR_2	0.1934

Summary of crystallographic data for complex **12** $[\text{Ni}_5(\text{L}^{Br})_2(\text{tptz})_4] \cdot 7.5\text{H}_2\text{O} \cdot 6\text{MeOH}$

Formula	$\text{C}_{122}\text{H}_{62}\text{N}_{36}\text{O}_{19.50}\text{Br}_6 \text{Ni}_5$
Formula weight	3117.09
Crystal size (mm)	0.05 x 0.05 x 0.05
Crystal system	triclinic
Space group	P-1
Lattice parameters	
a (pm)	16.5193(4), α 101.4240(10)
b(pm)	16.7116(3), β 98.0740(10)
c (pm)	27.7661(7), γ 110.4630(10)
Cell volume (10^6pm^3)	6853.3(2)
Z	2
Temperature (K)	183(2)
$\Delta_{calc}(\text{g cm}^{-3})$	1.511
F(000)	3104
$\mu(\text{Mo K}\alpha)(\text{mm}^{-1})$	2.499
Data collection range ($^\circ$)	$1.72 \leq \Theta \leq 27.49$
Index range	$-20 \leq h \leq 21$ $-21 \leq k \leq 18$ $-36 \leq l \leq 31$
Reflection measured	
total	43988
unique	15819 $R_{int} = 0.0410$)
Goodness-of-fit	1.022
R_1	0.0888
wR_2	0.2165

Summary of crystallographic data for complex **13**
 $[\text{Ni}_3\text{L}^{\text{OMe}}(\text{tptz})_3]\text{NO}_3 \cdot 4.5\text{H}_2\text{O} \cdot 1.5\text{MeOH}$

Formula	$\text{C}_{80}\text{H}_{71}\text{N}_{24}\text{O}_{12.50}\text{Ni}_3$
Formula weight	1735.72
Crystal size (mm)	0.04 x 0.04 x 0.04
Crystal system	monoclinic
Space group	C2/c
Lattice parameters	
a (pm)	36.2147(12), α 90.00
b (pm)	21.9674(10), β 116.964(3)
c (pm)	23.6433(7), γ 90.00
Cell volume (10^6pm^3)	16764.5(11)
Z	8
Temperature (K)	183(2)
$\Delta_{\text{calc}}(\text{g cm}^{-3})$	1.375
F(000)	7180
$\mu(\text{Mo K}\alpha)(\text{mm}^{-1})$	0.741
Data collection range ($^\circ$)	$2.24 \leq \Theta \leq 27.47$
Index range	$-44 \leq h \leq 46$ $-27 \leq k \leq 28$ $-29 \leq l \leq 30$
Reflection measured	
total	19106
unique	8997 ($R_{\text{int}} = 0.1154$)
Goodness-of-fit	1.034
R_1	0.0995
wR_2	0.2642

Summary of crystallographic data for complex **14** $[\text{Ni}_3\text{L}^{OMe}(\text{tptz})_3]\text{Cl}\cdot 2\text{DMF}$

Formula	$\text{C}_{85}\text{H}_{71}\text{N}_{26}\text{O}_8\text{ClNi}_3$
Formula weight	1796.26
Crystal size (mm)	0.06 x 0.06 x 0.05
Crystal system	triclinic
Space group	P-1
Lattice parameters	
a (pm)	13.3675(12), α 61.939(2)
b(pm)	21.1969(10), β 80.478(3)
c (pm)	21.2212(7), γ 82.461(2)
Cell volume (10^6pm^3)	5223.2(3)
Z	2
Temperature (K)	183(2)
$\Delta_{calc}(\text{g cm}^{-3})$	1.142
F(000)	1856
$\mu(\text{Mo K}\alpha)(\text{mm}^{-1})$	0.620
Data collection range ($^\circ$)	$1.95 \leq \Theta \leq 27.47$
Index range	$-17 \leq h \leq 15$ $-24 \leq k \leq 27$ $-26 \leq l \leq 27$
Reflection measured	
total	33741
unique	16873 ($R_{int} = 0.1783$)
Goodness-of-fit	1.130
R_1	0.1783
wR_2	0.4491

Summary of crystallographic data for complex **16** [Co₃L^{OMe}(bcpa)₃]NO₃·6DMF

Formula	C ₇₉ H ₈₇ N ₂₂ O ₂₁ Co ₃
Formula weight	1857.50
Crystal size (mm)	0.05 x 0.05 x 0.04
Crystal system	hexagonal
Space group	P6(3)
Lattice parameters	
a (pm)	13.3675(6), α 90.00
b(pm)	21.1969(6), β 90.00
c (pm)	21.2212(4), γ 12.00
Cell volume (10 ⁶ pm ³)	5223.2(3)
Z	2
Temperature (K)	183(2)
Δ_{calc} (g cm ⁻³)	1.411
F(000)	1928
μ (Mo K α)(mm ⁻¹)	0.645
Data collection range (°)	1.94 \leq Θ \leq 27.49
Index range	-25 \leq h \leq 21 -25 \leq k \leq 25 -16 \leq l \leq 17
Reflection measured	
total	26903
unique	5081 (R_{int} = 0.1047)
Goodness-of-fit	1.067
R ₁	0.0592
wR ₂	0.1469

Summary of crystallographic data for complex **17** [Fe(pyren)]₂O·3H₂O

Formula	C ₂₀ H ₂₆ N ₂ O ₆ Fe
Formula weight	446.28
Crystal size (mm)	0.03 x 0.03 x 0.02
Crystal system	triclinic
Space group	P-1
Lattice parameters	
a (pm)	11.4913(3), α 82.753(1)
b(pm)	13.5531(4), β 70.651(1)
c (pm)	13.7025(3), γ 75.181(1)
Cell volume (10 ⁶ pm ³)	1944.56(9)
Z	4
Temperature (K)	120(2)
Δ_{calc} (g cm ⁻³)	1.524
F(000)	936
μ (Mo K α)(mm ⁻¹)	0.431
Data collection range (°)	2.45 ≤ Θ ≤ 21.33
Index range	-16 ≤ h ≤ 16 -19 ≤ k ≤ 19 -19 ≤ l ≤ 19
Reflection measured	
total	89199
unique	9655R _{int} = 0.0497)
Goodness-of-fit	1.064
R ₁	0.0494
wR ₂	0.1399

Summary of crystallographic data for complex **18**

[$\{\text{Fe}(\text{sabhea})\}_2\{\text{Fe}(\text{Hsabhea})\}_2\text{ClO}_4\cdot 2\text{DMF}$]	
Formula	$\text{C}_{29}\text{H}_{42}\text{N}_5\text{O}_{11}\text{ClFe}$
Formula weight	783.83
Crystal size (mm)	0.10 x 0.09 x 0.07
Crystal system	triclinic
Space group	P-1
Lattice parameters	
a (pm)	10.1527(10), α 99.800(7)
b (pm)	10.8739(13), β 96.303(8)
c (pm)	16.131(2), γ 97.142(9)
Cell volume (10^6pm^3)	1725.6(3)
Z	2
Temperature (K)	183(2)
$\Delta_{calc}(\text{g cm}^{-3})$	1.509
F(000)	816
$\mu(\text{Mo K}\alpha)(\text{mm}^{-1})$	0.982
Data collection range ($^\circ$)	$4.04 \leq \Theta \leq 27.58$
Index range	$-12 \leq h \leq 13$ $-14 \leq k \leq 13$ $-19 \leq l \leq 20$
Reflection measured	
total	9488
unique	4613 ($R_{int} = 0.0407$)
Goodness-of-fit	1.076
R_1	0.0712
w R_2	0.1794

Summary of crystallographic data for complex **19** [(CuL)₃(μ₃-OH)](ClO₄)₂·H₂O

Formula	C ₃₃ H ₄₇ N ₆ O ₁₃ Cl ₂ Cu ₃
Formula weight	997.29
Crystal size (mm)	0.35 x 0.30 x 0.30
Crystal system	monoclinic
Space group	P2(1)/c
Lattice parameters	
a (pm)	10.9180(3), α 90.00
b (pm)	29.3790(7), β 106.459(1)
c (pm)	13.0608(3), γ 90.00
Cell volume (10 ⁶ pm ³)	4017.71(17)
Z	4
Temperature (K)	183(2)
Δ _{calc} (g cm ⁻³)	1.649
F(000)	2048
μ(Mo K _α)(mm ⁻¹)	1.777
Data collection range (°)	1.39 ≤ Θ ≤ 27.44
Index range	-14 ≤ h ≤ 14 -33 ≤ k ≤ 38 -13 ≤ l ≤ 16
Reflection measured	
total	26943
unique	6288 (R _{int} = 0.0545)
Goodness-of-fit	1.019
R ₁	0.0476
wR ₂	0.1002

Summary of crystallographic data for complex **20** [(CuL)₂](ClO₄)₂·0.5H₂O

Formula	C ₂₇ H ₄₄ N ₅ Cl ₂ O _{14.50} Cu ₂
Formula weight	868.65
Crystal size (mm)	0.04 x 0.04 x 0.03
Crystal system	monoclinic
Space group	C2/c
Lattice parameters	
a (pm)	13.8570(2), α 90.00
b(pm)	16.0675(3), β 95.3050(10)
c (pm)	32.4670(6), γ 90.00
Cell volume (10 ⁶ pm ³)	7197.7(2)
Z	8
Temperature (K)	183(2)
Δ_{calc} (g cm ⁻³)	1.603
F(000)	3592
μ (Mo K α)(mm ⁻¹)	1.403
Data collection range (°)	2.61 ≤ Θ ≤ 27.49
Index range	-17 ≤ h ≤ 17 -20 ≤ k ≤ 20 -42 ≤ l ≤ 25
Reflection measured	
total	21120
unique	5625 (R_{int} = 0.0418)
Goodness-of-fit	1.014
R ₁	0.0508
wR ₂	0.1274

Summary of crystallographic data for complex **21** ($[\text{Cu}(\text{dmae-oximate})(\text{OH}_2)(\text{NCS})]\text{K}\cdot\text{H}_2\text{O})_n$

Formula	$\text{C}_7\text{H}_{14}\text{N}_4\text{O}_3\text{SCuK}$
Formula weight	344.92
Crystal size (mm)	0.03 x 0.02 x 0.02
Crystal system	monoclinic
Space group	P2/c
Lattice parameters	
a (pm)	14.5388(10), α 90.00
b (pm)	6.5248(4), β 101.723(4)
c (pm)	13.4028(6), γ 90.00
Cell volume (10^6pm^3)	1244.91
Z	4
Temperature (K)	183(2)
$\Delta_{calc}(\text{g cm}^{-3})$	1.840
F(000)	704
$\mu(\text{Mo K}\alpha)(\text{mm}^{-1})$	2.263
Data collection range ($^\circ$)	$2.86 \leq \Theta \leq 27.47$
Index range	$-18 \leq h \leq 18$ $-8 \leq k \leq 8$ $-17 \leq l \leq 17$
Reflection measured	
total	8430
unique	2482 ($R_{int} = 0.0488$)
Goodness-of-fit	1.113
R_1	0.1261
wR_2	0.3756

Summary of crystallographic data for complex **22** [(Cu(dmae-oximate)(MeOH)(NCS)₂Co(MeOH)₂)]

Formula	C ₁₈ H ₃₆ N ₆ O ₁₀ S ₂ Cu ₂ Co
Formula weight	746.66
Crystal size (mm)	0.05 x 0.05 x 0.04
Crystal system	monoclinic
Space group	C2/c
Lattice parameters	
a (pm)	33.8518(11), α 90.00
b (pm)	6.8944(3), β 114.469(3)
c (pm)	14.3780(7), γ 90.00
Cell volume (10 ⁶ pm ³)	3054.3(2)
Z	4
Temperature (K)	183(2)
Δ_{calc} (g cm ⁻³)	1.624
F(000)	1532
μ (Mo K α)(mm ⁻¹)	2.109
Data collection range (°)	4.20 \leq Θ \leq 27.47
Index range	-42 \leq h \leq 43 -8 \leq k \leq 8 -18 \leq l \leq 18
Reflection measured	
total	10164
unique	2988 (R_{int} = 0.0519)
Goodness-of-fit	0.821
R ₁	0.0436
wR ₂	0.1245

Summary of crystallographic data for complex **24** [Cu(OMesalen)H₂O]

Formula	C ₁₉ H ₂₁ N ₂ O ₅ Cu
Formula weight	420.19
Crystal size (mm)	0.03 x 0.03 x 0.03
Crystal system	orthorhombic
Space group	Pnma
Lattice parameters	
a (pm)	10.6368(5), α 90.00
b(pm)	22.5964(6), β 90.00
c (pm)	7.4372(4), γ 90.00
Cell volume (10 ⁶ pm ³)	2625.85(8)
Z	4
Temperature (K)	183(2)
Δ_{calc} (g cm ⁻³)	1.564
F(000)	872
μ (Mo K α)(mm ⁻¹)	1.256
Data collection range (°)	$3.46 \leq \Theta \leq 27.47$
Index range	$-13 \leq h \leq 13$ $-29 \leq k \leq 25$ $-9 \leq l \leq 8$
Reflection measured	
total	11556
unique	1653 ($R_{int} = 0.0590$)
Goodness-of-fit	1.073
R ₁	0.0447
wR ₂	0.1129

Summary of crystallographic data for complex **25** [Cu(OMesalen)Na(H₂O)]NO₃

Formula	C ₂₁ H ₂₆ N ₃ O ₈ CuNa
Formula weight	534.98
Crystal size (mm)	0.04 x 0.04 x 0.04
Crystal system	monoclinic
Space group	P2(1)/c
Lattice parameters	
a (pm)	12.8067(9), α 90.00
b(pm)	11.7256(8), β 109.283(4)
c (pm)	15.9778(8), γ 90.00
Cell volume (10 ⁶ pm ³)	2264.7(2)
Z	4
Temperature (K)	183(2)
Δ_{calc} (g cm ⁻³)	1.569
F(000)	110
μ (Mo K α)(mm ⁻¹)	1.037
Data collection range (°)	2.20 ≤ Θ ≤ 27.46
Index range	-16 ≤ h ≤ 16 -15 ≤ k ≤ 13 -20 ≤ l ≤ 18
Reflection measured	
total	14558
unique	3678(R_{int} = 0.0965)
Goodness-of-fit	1.030
R ₁	0.0526
wR ₂	0.1269

Summary of crystallographic data for complex **26** [Cu(MeOH)(OMesalen)Gd(NO₃)₃]

Formula	C ₂₂ H ₂₈ N ₅ O ₁₄ CuGd
Formula weight	807.28
Crystal size (mm)	0.09x 0.09 x 0.06
Crystal system	triclinic
Space group	P-1
Lattice parameters	
a (pm)	8.6555(3), α 79.769(2)
b(pm)	12.9676(4), β 77.109(2)
c (pm)	13.4356(3), γ 71.385(7)
Cell volume (10 ⁶ pm ³)	1383.84(7)
Z	2
Temperature (K)	183(2)
Δ_{calc} (g cm ⁻³)	1.937
F(000)	800
μ (Mo K α)(mm ⁻¹)	3.223
Data collection range (°)	2.42 ≤ Θ ≤ 27.43
Index range	-11 ≤ h ≤ 11 -15 ≤ k ≤ 16 -17 ≤ l ≤ 17
Reflection measured	
total	9784
unique	5574(R_{int} = 0.0240)
Goodness-of-fit	0.842
R ₁	0.0281
wR ₂	0.0670

Summary of crystallographic data for complex **27**
 $[\text{Cu}(\text{OMesalen})\text{Gd}(\text{NO}_3)_3(\text{Pyr}(\text{COO})_2)]_n \cdot (\text{DMF})_n$

Formula	$\text{C}_{29}\text{H}_{27}\text{N}_5\text{O}_{12}\text{CuGd}$
Formula weight	858.38
Crystal size (mm)	0.03x 0.03 x 0.02
Crystal system	orthorhombic
Space group	Pbcn
Lattice parameters	
a (pm)	16.4218(5), α 90.00
b(pm)	19.0802(6), β 90.00
c (pm)	19.0423(6), γ 90.00
Cell volume (10^6pm^3)	5966.5(3)
Z	8
Temperature (K)	183(2)
$\Delta_{calc}(\text{g cm}^{-3})$	1.911
F(000)	3400
$\mu(\text{Mo K}\alpha)(\text{mm}^{-1})$	2.992
Data collection range ($^\circ$)	$1.95 \leq \Theta \leq 27.54$
Index range	$-21 \leq h \leq 18$ $-24 \leq k \leq 24$ $-22 \leq l \leq 24$
Reflection measured	
total	38827
unique	4462($R_{int} = 0.1171$)
Goodness-of-fit	0.993
R_1	0.460
w R_2	0.0877

Summary of crystallographic data for complex **28**
 $[\text{Cu}(\text{OMesalen})\text{Dy}(\text{NO}_3)_3(\text{Pyr}(\text{COO})_2)]_n \cdot (\text{DMF})_n$

Formula	$\text{C}_{29}\text{H}_{27}\text{N}_5\text{O}_{12}\text{CuDy}$
Formula weight	863.60
Crystal size (mm)	0.03x 0.03 x 0.02
Crystal system	orthorhombic
Space group	Pbcn
Lattice parameters	
a (pm)	16.3723(4), α 90.00
b(pm)	19.0764(4), β 90.00
c (pm)	19.0394(4), γ 90.00
Cell volume (10^6pm^3)	5946.5(2)
Z	8
Temperature (K)	183(2)
$\Delta_{calc}(\text{g cm}^{-3})$	1.929
F(000)	3416
$\mu(\text{Mo K}\alpha)(\text{mm}^{-1})$	3.285
Data collection range ($^\circ$)	$1.96 \leq \Theta \leq 27.49$
Index range	$-20 \leq h \leq 21$ $-24 \leq k \leq 24$ $-24 \leq l \leq 24$
Reflection measured	
total	40430
unique	4905($R_{int} = 0.0887$)
Goodness-of-fit	1.005
R_1	0.0375
w R_2	0.0826

Summary of crystallographic data for complex **29**
 $[\text{Cu}(\text{OMesalen})\text{Tb}(\text{NO}_3)_3(\text{Pyr}(\text{COO})_2)]_n \cdot (\text{DMF})_n$

Formula	$\text{C}_{29}\text{H}_{27}\text{N}_5\text{O}_{12}\text{CuTb}$
Formula weight	863.02
Crystal size (mm)	0.03x 0.03 x 0.02
Crystal system	orthorhombic
Space group	Pbcn
Lattice parameters	
a (pm)	16.3859(3), α 90.00
b(pm)	19.0320(3), β 90.00
c (pm)	19.0368(3), γ 90.00
Cell volume (10^6pm^3)	5936.75(17)
Z	8
Temperature (K)	183(2)
$\Delta_{calc}(\text{g cm}^{-3})$	1.924
F(000)	3408
$\mu(\text{Mo K}\alpha)(\text{mm}^{-1})$	3.156
Data collection range ($^\circ$)	$1.96 \leq \Theta \leq 27.48$
Index range	$-21 \leq h \leq 20$ $-24 \leq k \leq 20$ $-24 \leq l \leq 24$
Reflection measured	
total	40974
unique	4497($R_{int} = 0.1179$)
Goodness-of-fit	1.004
R_1	0.0423
wR_2	0.0864

Summary of crystallographic data for complex **30**
 $[\text{Cu}(\text{OMesalen})\text{Eu}(\text{NO}_3)_3(\text{Pyr}(\text{COO})_2)]_n \cdot (\text{DMF})_n$

Formula	$\text{C}_{29}\text{H}_{27}\text{N}_5\text{O}_{12}\text{CuEu}$
Formula weight	853.06
Crystal size (mm)	0.06x 0.05 x 0.04
Crystal system	orthorhombic
Space group	Pbcn
Lattice parameters	
a (pm)	16.4654(4), α 90.00
b(pm)	19.0767(5), β 90.00
c (pm)	19.0704(4), γ 90.00
Cell volume (10^6pm^3)	5990.1(2)
Z	8
Temperature (K)	183(2)
$\Delta_{calc}(\text{g cm}^{-3})$	1.892
F(000)	3392
$\mu(\text{Mo K}\alpha)(\text{mm}^{-1})$	2.860
Data collection range ($^\circ$)	$1.95 \leq \Theta \leq 27.47$
Index range	$-18 \leq h \leq 21$ $-24 \leq k \leq 24$ $-21 \leq l \leq 24$
Reflection measured	
total	38817
unique	5281 ($R_{int} = 0.0843$)
Goodness-of-fit	1.110
R_1	0.0489
w R_2	0.1063

Summary of crystallographic data for complex **31**
 $[\text{Cu}(\text{OMesalen})\text{Sm}(\text{NO}_3)_3(\text{Pyr}(\text{COO})_2)]_n \cdot (\text{DMF})_n$

Formula	$\text{C}_{29}\text{H}_{27}\text{N}_5\text{O}_{12}\text{CuSm}$
Formula weight	851.45
Crystal size (mm)	0.05x 0.05 x 0.04
Crystal system	orthorhombic
Space group	Pbcn
Lattice parameters	
a (pm)	16.5885(5), α 90.00
b(pm)	19.0857(5), β 90.00
c (pm)	19.1195(5), γ 90.00
Cell volume (10^6pm^3)	6053.3(3)
Z	8
Temperature (K)	183(2)
$\Delta_{calc}(\text{g cm}^{-3})$	1.869
F(000)	3384
$\mu(\text{Mo K}\alpha)(\text{mm}^{-1})$	2.698
Data collection range ($^\circ$)	$1.63 \leq \Theta \leq 27.54$
Index range	$-21 \leq h \leq 21$ $-19 \leq k \leq 24$ $-24 \leq l \leq 24$
Reflection measured	
total	39513
unique	4632($R_{int} = 0.1047$)
Goodness-of-fit	1.015
R_1	0.0434
wR_2	0.1015

Summary of crystallographic data for complex **32**
 $[\text{Cu}(\text{OMesalen})\text{Pr}(\text{NO}_3)_3(\text{Pyr}(\text{COO})_2)]_n \cdot (\text{DMF})_n$

Formula	$\text{C}_{29}\text{H}_{27}\text{N}_5\text{O}_{12}\text{CuPr}$
Formula weight	842.01
Crystal size (mm)	0.04x 0.04 x 0.04
Crystal system	orthorhombic
Space group	Pbcn
Lattice parameters	
a (pm)	16.5811(4), α 90.00
b(pm)	19.1032(3), β 90.00
c (pm)	19.1237(3), γ 90.00
Cell volume (10^6pm^3)	6057.5(2)
Z	8
Temperature (K)	183(2)
$\Delta_{calc}(\text{g cm}^{-3})$	1.847
F(000)	3360
$\mu(\text{Mo K}\alpha)(\text{mm}^{-1})$	2.336
Data collection range ($^\circ$)	$1.94 \leq \Theta \leq 27.48$
Index range	$-21 \leq h \leq 21$ $-22 \leq k \leq 24$ $-23 \leq l \leq 24$
Reflection measured	
total	39477
unique	5436($R_{int} = 0.0524$)
Goodness-of-fit	1.000
R_1	0.0311
w R_2	0.0758

Summary of crystallographic data for complex **34**
 $[(\text{Cu}(\text{OMesalen}))_2\text{Gd}(\text{salCOO})_2]\text{NO}_3 \cdot 2\text{MeOH} \cdot 0.25\text{H}_2\text{O}$

Formula	$\text{C}_{54}\text{H}_{55}\text{N}_5\text{O}_{19.25}\text{Cu}_2\text{Gd}$
Formula weight	1366.36
Crystal size (mm)	0.06x 0.05 x 0.05
Crystal system	monoclinic
Space group	P2(1)/c
Lattice parameters	
a (pm)	13.3094(2), α 90.00
b(pm)	24.9063(3), β 101.2200(10)
c (pm)	18.4808(2), γ 90.00
Cell volume (10^6pm^3)	6009.07(13)
Z	4
Temperature (K)	183(2)
$\Delta_{calc}(\text{g cm}^{-3})$	1.510
F(000)	2760
$\mu(\text{Mo K}\alpha)(\text{mm}^{-1})$	1.866
Data collection range ($^\circ$)	$1.98 \leq \Theta \leq 27.49$
Index range	$-17 \leq h \leq 17$ $-32 \leq k \leq 27$ $-22 \leq l \leq 23$
Reflection measured	
total	42535
unique	10069($R_{int} = 0.0459$)
Goodness-of-fit	1.072
R_1	0.0529
wR_2	0.1464

Summary of crystallographic data for complex **35**
 $[(\text{Cu}(\text{OMesalen}))_2\text{Sm}(\text{salCOO})_2]\text{NO}_3 \cdot 2.5\text{MeOH} \cdot \text{H}_2\text{O}$

Formula	$\text{C}_{54.50}\text{H}_{60}\text{N}_{4.50}\text{O}_{19}\text{Cu}_2\text{Sm}$
Formula weight	1359.50
Crystal size (mm)	0.05x 0.05 x 0.04
Crystal system	monoclinic
Space group	P2(1)/c
Lattice parameters	
a (pm)	13.3826(3), α 90.00
b(pm)	25.0093(5), β 101.5740(10)
c (pm)	18.4583(3), γ 90.00
Cell volume (10^6pm^3)	6052.2(2)
Z	4
Temperature (K)	183(2)
$\Delta_{calc}(\text{g cm}^{-3})$	1.492
F(000)	2762
$\mu(\text{Mo K}\alpha)(\text{mm}^{-1})$	1.727
Data collection range ($^\circ$)	$1.91 \leq \Theta \leq 27.40$
Index range	$-17 \leq h \leq 16$ $-32 \leq k \leq 31$ $-23 \leq l \leq 23$
Reflection measured	
total	41784
unique	8763($R_{int} = 0.0614$)
Goodness-of-fit	1.040
R_1	0.0671
w R_2	0.1904

Summary of crystallographic data for complex **36**
 $[(\text{Cu}(\text{OMesalen}))_2\text{Pr}(\text{salCOO})_2]\text{NO}_3 \cdot 3\text{MeOH} \cdot 0.25\text{H}_2\text{O}$

Formula	$\text{C}_{55}\text{H}_{62}\text{N}_5\text{O}_{20.25}\text{Cu}_2\text{Pr}$
Formula weight	1385.09
Crystal size (mm)	0.04x 0.04 x 0.04
Crystal system	monoclinic
Space group	P2(1)/c
Lattice parameters	
a (pm)	13.2615(3), α 90.00
b(pm)	24.9953(7), β 101.252(2)
c (pm)	18.4631(4), γ 90.00
Cell volume (10^6pm^3)	6003.0(3)
Z	4
Temperature (K)	183(2)
$\Delta_{calc}(\text{g cm}^{-3})$	1.533
F(000)	2824
$\mu(\text{Mo K}\alpha)(\text{mm}^{-1})$	1.578
Data collection range ($^\circ$)	$1.92 \leq \Theta \leq 27.48$
Index range	$-14 \leq h \leq 17$ $-32 \leq k \leq 28$ $-23 \leq l \leq 23$
Reflection measured	
total	35308
unique	8497($R_{int} = 0.0684$)
Goodness-of-fit	1.023
R_1	0.0664
wR_2	0.1653

Summary of crystallographic data for complex **37**
 $[(\text{Cu}(\text{OMesalen}))_2\text{Sm}(\text{salCOO})_2]\text{NO}_3 \cdot 3.75\text{MeOH} \cdot 0.25\text{H}_2\text{O}$

Formula	$\text{C}_{55.75}\text{H}_{65}\text{N}_5\text{O}_{21}\text{Cu}_2\text{La}$
Formula weight	1407.12
Crystal size (mm)	0.06x 0.04 x 0.04
Crystal system	monoclinic
Space group	P2(1)/c
Lattice parameters	
a (pm)	13.33138(2), α 90.00
b(pm)	25.1553(4), β 101.3860(10)
c (pm)	18.5120(3), γ 90.00
Cell volume (10^6pm^3)	6077.88(17)
Z	4
Temperature (K)	183(2)
$\Delta_{calc}(\text{g cm}^{-3})$	1.538
F(000)	2870
$\mu(\text{Mo K}\alpha)(\text{mm}^{-1})$	1.462
Data collection range ($^\circ$)	$2.25 \leq \Theta \leq 27.48$
Index range	$-17 \leq h \leq 15$ $-32 \leq k \leq 27$ $-21 \leq l \leq 24$
Reflection measured	
total	39919
unique	8800($R_{int} = 0.0662$)
Goodness-of-fit	1.032
R_1	0.0577
wR_2	0.1421

Summary of crystallographic data for complex **39** [Cu(o-OEtPhsalph)]·H₂O·MeOH

Formula	C ₂₆ H ₃₂ N ₂ O ₇ Cu
Formula weight	548.08
Crystal size (mm)	0.08x 0.06x 0.05
Crystal system	monoclinic
Space group	I2/a
Lattice parameters	
a (pm)	12.1967(8), α 90.00
b(pm)	14.3541(9), β 97.869(10)
c (pm)	14.5512(9), γ 90.00
Cell volume (10 ⁶ pm ³)	2523.5(3)
Z	4
Temperature (K)	183(2)
Δ_{calc} (g cm ⁻³)	1.443
F(000)	1148
μ (Mo K α)(mm ⁻¹)	0.914
Data collection range (°)	2.84 ≤ Θ ≤ 27.49
Index range	-14 ≤ h ≤ 15 -18 ≤ k ≤ 17 -18 ≤ l ≤ 18
Reflection measured	
total	8834
unique	2201(R _{int} = 0.0540)
Goodness-of-fit	1.016
R ₁	0.0460
wR ₂	0.1029

Summary of crystallographic data for complex **40** [Ni(o-OEtPhsalph)]·H₂O

Formula	C ₂₄ H ₂₄ N ₂ O ₅ Ni
Formula weight	479.16
Crystal size (mm)	0.06x 0.06x 0.04
Crystal system	monoclinic
Space group	P2(1)/c
Lattice parameters	
a (pm)	9.8384(4), α 90.00
b(pm)	12.1761(5), β 91.643(3)
c (pm)	17.2134(6), γ 90.00
Cell volume (10 ⁶ pm ³)	2061.20
Z	4
Temperature (K)	183(2)
Δ_{calc} (g cm ⁻³)	1.544
F(000)	1000
μ (Mo K α)(mm ⁻¹)	0.982
Data collection range (°)	2.94 ≤ Θ ≤ 27.48
Index range	-12 ≤ h ≤ 12 -15 ≤ k ≤ 15 -22 ≤ l ≤ 22
Reflection measured	
total	14438
unique	3462(R_{int} = 0.0539)
Goodness-of-fit	1.017
R ₁	0.0384
wR ₂	0.0841

Summary of crystallographic data for complex **41** [Cu(m-OMePhsalph)]₂·2H₂O

Formula	C ₄₈ H ₅₆ N ₄ O ₁₄ Cu ₂
Formula weight	1040.05
Crystal size (mm)	0.10x 0.10x 0.03
Crystal system	rhombohedral
Space group	R-3
Lattice parameters	
a (pm)	34.6690(12), α 90.00
b(pm)	34.6690(12), β 90.00
c (pm)	10.6742(6), γ 120.00
Cell volume (10 ⁶ pm ³)	11110.9(8)
Z	9
Temperature (K)	183(2)
Δ_{calc} (g cm ⁻³)	1.399
F(000)	4878
μ (Mo K α)(mm ⁻¹)	0.930
Data collection range (°)	3.10 ≤ Θ ≤ 27.55
Index range	-37 ≤ h ≤ 45 -42 ≤ k ≤ 45 -13 ≤ l ≤ 13
Reflection measured	
total	14490
unique	3321(R_{int} = 0.1059)
Goodness-of-fit	1.023
R ₁	0.0520
wR ₂	0.1125

Summary of crystallographic data for complex **42** [Cu(bcpa)(OH₂)₂]₂NO₃·MeOH

Formula	C ₁₂ H ₁₆ N ₄ O ₉ Cu
Formula weight	423.83
Crystal size (mm)	0.03x 0.03x 0.02
Crystal system	triclinic
Space group	P-1
Lattice parameters	
a (pm)	6.7180(2), α 88.9740(10)
b(pm)	10.1788(3), β 82.8450(10)
c (pm)	11.9929(4), γ 89.9160(10)
Cell volume (10 ⁶ pm ³)	11110.9(8)
Z	2
Temperature (K)	183(2)
Δ_{calc} (g cm ⁻³)	1.730
F(000)	434
μ (Mo K α)(mm ⁻¹)	1.401
Data collection range (°)	2.66 ≤ Θ ≤ 27.47
Index range	-8 ≤ h ≤ 8 -13 ≤ k ≤ 13 -14 ≤ l ≤ 15
Reflection measured	
total	5521
unique	3121(R_{int} = 0.0232)
Goodness-of-fit	1.050
R ₁	0.0335
wR ₂	0.0707

Summary of crystallographic data for complex **43** [Cu(bcpa)(salCOO)H₂O]

Formula	C ₁₉ H ₁₇ N ₃ O ₇ Cu
Formula weight	462.90
Crystal size (mm)	0.03x 0.03x 0.02
Crystal system	monoclinic
Space group	P2(1)/n
Lattice parameters	
a (pm)	15.0150(4), α 90.00
b(pm)	7.0474(2), β 112.055(2)
c (pm)	19.7873(7), γ 90.00
Cell volume (10 ⁶ pm ³)	1940.61(10)
Z	4
Temperature (K)	183(2)
Δ_{calc} (g cm ⁻³)	1.584
F(000)	984
μ (Mo K α)(mm ⁻¹)	1.174
Data collection range (°)	2.14 ≤ Θ ≤ 27.48
Index range	-18 ≤ h ≤ 19 -9 ≤ k ≤ 8 -24 ≤ l ≤ 25
Reflection measured	
total	11363
unique	2979(R_{int} = 0.0514)
Goodness-of-fit	1.019
R ₁	0.0440
wR ₂	0.0902

Summary of crystallographic data for complex **44** $[\text{Fe}_2(\mu\text{-valhy})_3]\cdot 4\text{DMF}$

Formula	$\text{C}_{30}\text{H}_{35}\text{N}_5\text{O}_8\text{Fe}_2$
Formula weight	649.48
Crystal size (mm)	0.12x 0.12x 0.09
Crystal system	triclinic
Space group	P-1
Lattice parameters	
a (pm)	12.7581(6), α 77.475(3)
b(pm)	13.5769(5), β 77.473(3)
c (pm)	19.9528(9), γ 66.753(3)
Cell volume (10^6pm^3)	3066.6(2)
Z	4
Temperature (K)	183(2)
$\Delta_{calc}(\text{g cm}^{-3})$	1.407
F(000)	1360
$\mu(\text{Mo K}\alpha)(\text{mm}^{-1})$	0.550
Data collection range ($^\circ$)	$1.06 \leq \Theta \leq 27.48$
Index range	$-16 \leq h \leq 15$ $-17 \leq k \leq 17$ $-25 \leq l \leq 24$
Reflection measured	
total	13278
unique	8208($R_{int} = 0.0518$)
Goodness-of-fit	1.045
R_1	0.0767
wR_2	0.1773

Selbständigkeitserklärung

Ich erkläre, dass ich die vorliegende Arbeit selbständig und unter Verwendung der angegebenen Hilfsmittel, persönlichen Mitteilungen und Quellen angefertigt habe.

Ort, Datum

Unterschrift des Verfassers/der Verfasserin

Curriculum Vitae

Personal Details

Name	Adrian Eugeniu Ion
Address	Am Herrenberge 11, App. 417, Jena, 07745, Germany
Sex	Male
Marital status	Single
Nationality	Romanian
Telephone	
mobile	01795457171
office	03641948138
Date of birth	July 31 st 1977
e-mail	adrian.ion@uni-jena.de

Academic Career and Education

1995 - 1999	Chemistry studies at Faculty of Chemistry from University of Bucharest, Romania
June 1999	Bachelor of Science in organic chemistry
1999 - 2001	Master of Science studies in Organic Chemistry at Faculty of Chemistry from University of Bucharest, Romania
June 2001	Master of Science in organic chemistry
January. 2003 - present	Ph. D. student in Magnetochemistry at Friedrich-Schiller University, Jena, Germany

Professional Experience

1999-2003	Analytical Chemist at Laboratory of Environmental Chemistry and Toxicology of S. C. PETROM S.A. company Bucharest, Romania
-----------	-----------------------------------------------------------------------------------------------------------------------------------

Place, Date

Signature